2009

JAEA R&D Review

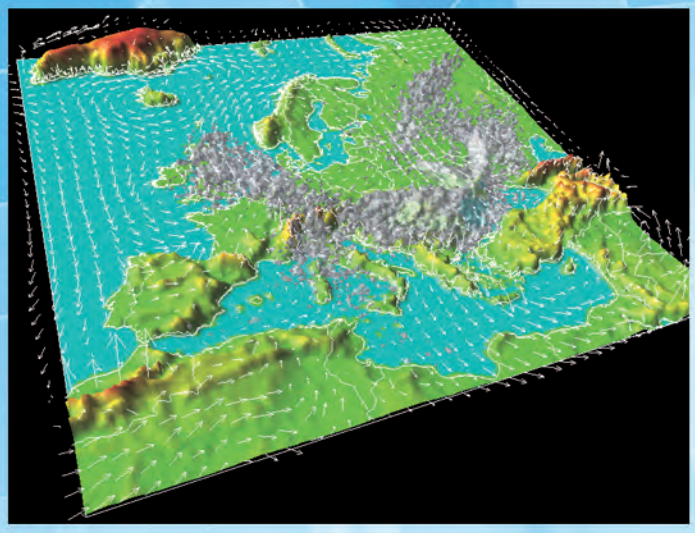

3D Image of WSPEEDI-II

JAEA Horonobe Underground Research Center

Message from the President

岡崎俊雄

President Toshio Okazaki

Welcome to the fourth issue of the "JAEA R&D Review", which will inform you of the current R&D activities of the Japan Atomic Energy Agency (JAEA).

Energy security and measures to stop global warming have become recognized in recent years as being of great importance to the entire world. The important role of nuclear energy in solving these problems has been realized, and the positions of all nations with regard to nuclear energy have changed significantly. JAEA was established in 2005 as the sole comprehensive R&D institute for nuclear energy in Japan. Since then, JAEA has promoted a wide range of research and development, including establishment of nuclear fuel cycle technology and basic research aiming at technological innovation and creating industries related to nuclear energy. We are now at a very important stage, concluding the R&D activities dictated in our first mid-term plan.

In the field of Fast Breeder Reactor (FBR) cycle technology, designated as a "Key Technology of National Importance" by the government of Japan, JAEA has been making great efforts to restart "MONJU" (a prototype FBR). In R&D for utilization of applied quantum beams, JAEA started the operation of J-PARC (high-intensity proton accelerator project) which utilizes the most advanced quantum beam technologies. In the field of fusion energy, JAEA is strongly pursuing the ITER Project and Broader Approach Project, and our advances here attract world-wide attention. Furthermore, JAEA is constructing two underground research laboratories where R&D projects for disposal of high-level radioactive waste are being undertaken. In addition, JAEA is steadily and safely executing decommissioning of our own nuclear facilities and disposal of radioactive wastes which are generated by our research facilities.

The mission of JAEA is to improve the quality of life for all people by innovative advancements in nuclear energy. I strongly believe that JAEA will achieve this goal and become one of the world's most authoritative and comprehensive institutes, what we call a Center of Excellence (COE), for creative and reliable nuclear energy R&D.

This publication constitutes a review of our achievements in the fiscal year 2008. It provides you with a look at some of the work that has been carried out, and also invites you to check the references listed and contact the researchers if there are any topics that you wish to learn more about. I would be most gratified if I could hear from you with any comments on this publication.

I hope that you enjoy this publication. Thank you very much for your interest.

JAEA R&D Review 2009

1 Research and Development of Advanced Nuclear System

2 Research and Development on Geological Disposal of High-Level Radioactive Waste

3 Nuclear Fusion Research and Development

4 Quantum Beam Science Research

5 Nuclear Safety Research

6 Advanced Science Research

7 Nuclear Science and Engineering Research

Toward the Commercialization of Fast Reactor Cycle Systems
—Plans for Innovative FBR Cycle Technology Development—

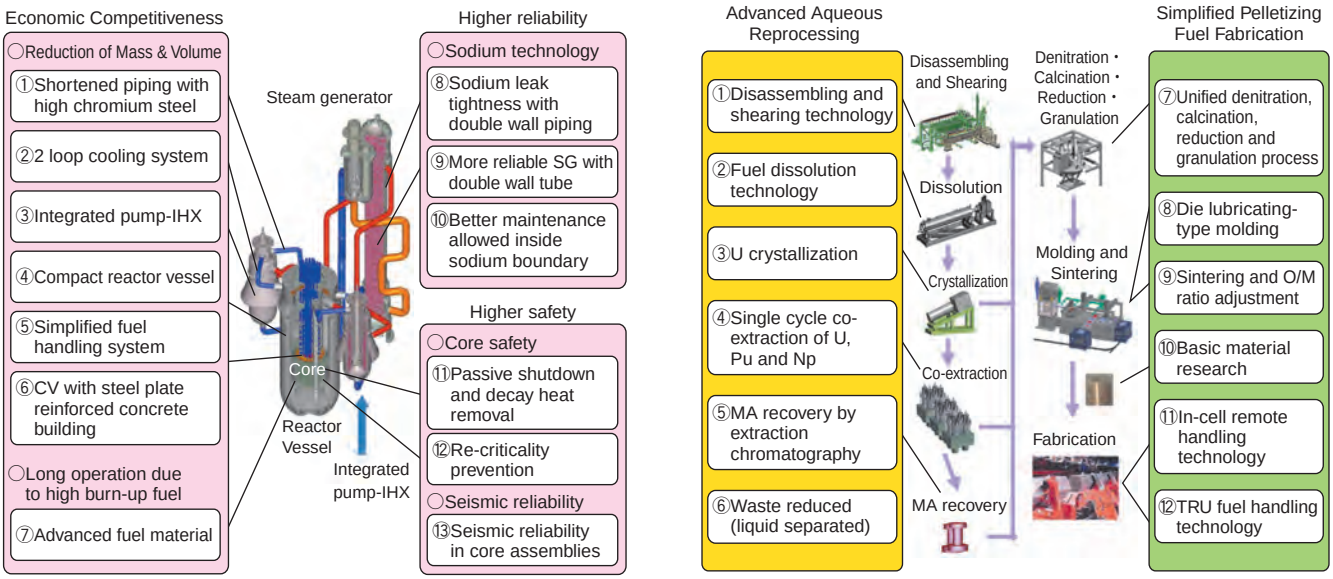

(a) Innovative reactor system technologies

(b) Innovative fuel cycle system technologies

Fig.1-1 Innovative FBR cycle technologies

(a) In plans for innovative technology development in the reactor system, development of 13 new technologies is proposed in the fields of reduction of mass and volume, core fuel material, sodium technology, core safety, and seismic reliability, from the viewpoint of economy, safety and reliability.

(b) In plans for innovative technology development in the fuel cycle system, there are priorities such as sustainability and nuclear non-proliferation in addition to economy and safety, and 12 new technologies are proposed in the fields of the reprocessing spent fuel and the fuel fabrication.

Aiming for the start-up of a demonstration fast breeder reactor (FBR) around 2025 and its introduction on a commercial basis before 2050, we are now promoting the "Fast Reactor Cycle Technology Development (FaCT)" project, with the collaboration of electric utilities and manufacturers.

In the FaCT project, we are developing a combination of the sodium-cooled FBR cycle system utilizing oxide fuel, advanced aqueous reprocessing, and simplified pelletizing fuel fabrication. The FaCT project will decide on which of the innovative technologies (Fig.1-1) to adopt by 2010 and present conceptual designs of commercial and demonstration FBR cycle facilities along with development plans to realize them by 2015. In FY2008, three years after the start of the FaCT project, an interim report of the current results and future plans were made in preparation for the technology selection in 2010. Here is a summary of each topic shown after the following pages:

As part of the development of the FBR system, research into the demonstration reactor and the commercial reactor systems will be promoted, and a general conception of the nuclear reactor plant will be decided upon (Topic 1-1). In the development of core fuel, to lessen the environmental burden, a core fuel that contains Minor Actinide (Topic 1-2) and irradiation tests of core integrity (Topic 1-3) will be developed. To make the reactor vessel compact and to reduce the construction cost, 3-dimensional analyses that clarify the thermal striping phenomenon in the reactor core internal structure were developed (Topic 1-4), and we presented a rationalized design which meets new, higher standards for structures and components (Topic 1-5). For reliability improvement, a sensor monitoring the wall thinning of the high-temperature piping during operation is being developed (Topic 1-6), and the oxidation mechanism of sodium combustion, basic knowledge for sodium leakage prevention technology, has been clarified (Topic 1-7). For the improvement of safety, a reasonable building design that can endure a huge earthquake is being sought, and for this, valuable data on the process leading to the breakage of a seismic isolation device was obtained (Topic 1-8).

For the fuel cycle system, highly effective dissolution technology in the reprocessing system is being developed (Topic 1-9). In the solvent extraction processes, U-Pu-Np co-extraction has become possible (Topic 1-10). In studies of fuel fabricating processes, the mechanism of microwave heating denitration is being elucidated (Topic 1-11).

1-1 Commercial Fast Reactor Concept with Improved Economy
—R&D of Innovative Technologies and Their Application to Plant Design—

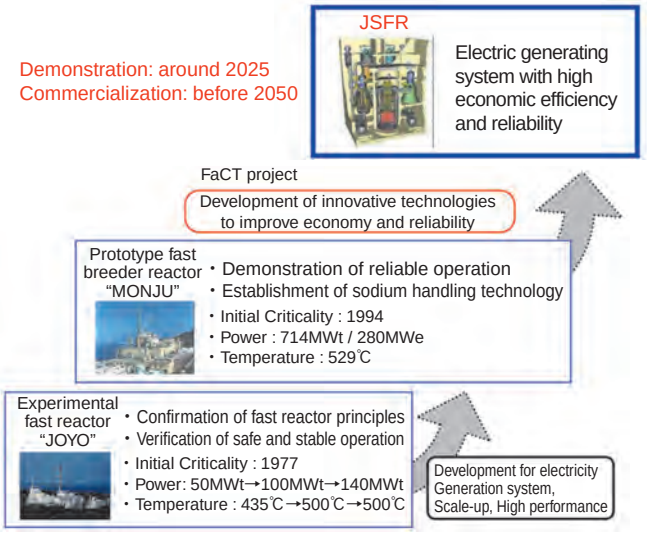

Fig.1-2 Steps to commercialization of Fast Reactor in Japan
We aim to commercialize fast reactors step by step, introducing innovative technologies to realize high economic efficiency and reliability, based on the experience accumulated through designs, construction, and operation of the experimental fast reactor "JOYO" and the prototype fast breeder reactor "MONJU".

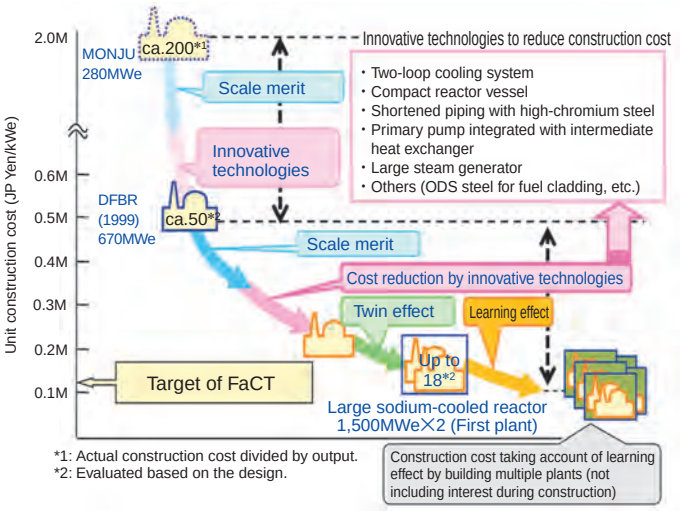

Fig.1-3 Approaches to reduce construction cost
We are achieving considerable reduction of construction cost for the commercialization of fast reactors, by adopting innovative technologies including a simplified cooling system (two-loop, shortened high-chromium steel piping, primary pump integrated with intermediate heat exchanger) and a compact reactor vessel, and taking a twin plant configuration and the learning effect into account.

In the FaCT project, we are carrying out a design study of an advanced loop-type sodium-cooled fast reactor (FR), namely the Japan Sodium-cooled Fast Reactor (JSFR), and related research and development (R&D), aiming for it to be economically competitive with future light water reactors by taking advantages of the loop-type reactor's merits in maintenance, repair, fabrication and construction.

Japan is aiming to commercialize FRs by utilizing experience accumulated through the design, construction, and operation of the experimental fast reactor "JOYO" and the prototype fast breeder reactor "MONJU", and attempting to apply to JSFR innovative technologies to improve economic efficiency and reliability (Fig.1-2).

Fig.1-3 shows approaches to reduce construction cost. In the JSFR design, the cooling system is simplified by a two-loop configuration satisfying the high flow velocity conditions in large-diameter pipes with electricity generation of 1,500MWe, as well as by piping shortened with high-chromium steel. Efforts to realize a compact reactor vessel (RV) are made by, for example, removing the space conventionally provided for refueling in the upper internal structure (UIS), and moving this inside the RV. These innovative technologies are attempted to reduce the commodity. We are pursuing considerable reduction of construction cost by scale merits, a twin plant configuration and the learning effect.

Enhancement of safety is always required at all development stages, and JSFR is equipped with safety systems to accomplish the rapid reactor shut down and the secure decay heat removal in emergencies. We are developing innovative technologies using only passive safety functions to avoid core disruptive accidents (CDAs), and, to contain the consequences of a CDA within the RV. We are also pursuing higher reliability by adopting a double boundary concept for the piping to strengthen the design measure against sodium leaks, and a reactor system of simple configuration with shorter welding lines which make inspection targets easy to access and reduce inspection load.

We have carried out experimental studies to elucidate various thermal-hydraulic phenomena induced by high flow velocity of sodium in a compact RV, so that the effectiveness of the design measures against these phenomena is confirmed. Full scale tests of the fuel handling machine moving fuel in a slit made in the UIS to eliminate the space needed for transferring the UIS during refueling, as well as development of equipment to test the reactor internal structural elements in sodium, are being carried out, and the obtained results are being steadily applied to the plant design.

We will steadily continue the design study and the development of elemental technologies, aiming toward the commercialization of FRs around 2050.

Reference

Uto, N. et al., Conceptual Design for Japan Sodium-Cooled Fast Reactor (1) : Current Status of System Design for JSFR, Proceedings of 2009 International Congress on Advances in Nuclear Power Plants (ICAPP '09), Tokyo, Japan, 2009, paper 9298, 11p., in CD-ROM.

1-2 Improvement in Environmental Burden Reduction of Advanced FBR
—Core and Fuel Design Study for Minor Actinide Containing Oxide Fuel—

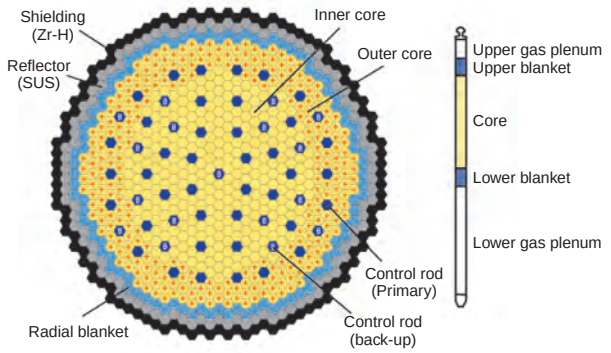

Fig.1-4 Configuration of core and fuel pin for commercial JSFR

Table 1-1 Major specification and design targets of commercial JSFR

Specification	Core power	1500MWe
	Core outlet/inlet coolant temperature	823/668K
Design target	Average Burn-up	150GWd/t
	Breeding ratio	~1.1
	Cycle length	> 24months
	Na void reactivity	< 6$

We are developing an advanced FBR named "Japan Sodium-cooled Fast Reactor (JSFR)", with development targets on safety and reliability, sustainability (environmental burden reduction, efficient utilization of resources, etc.), economic competitiveness and nuclear non-proliferation. The core and fuel design studies of JSFR with oxide fuel containing minor actinide (MA) have been performed.

JSFR is required to burn MA mainly from the viewpoint of reduction of environmental burden. The amount of MA contained in the fuel changes depending on the number of years after the introduction of FBR. When all the reactors are replaced by FBR many years after the FBR introduction, spent fuels from FBRs will be recycled, and MA content of the fuel is estimated to become around 1wt% after multiple recycling in FBRs. On the other hand, during the period when the light water reactors (LWRs) are in operation along with FBRs, spent fuels from LWRs, which contain much more MA, will be recycled and tend to increase the MA content in the fuel. Therefore, the core and fuel of JSFR must be designed to be able to accept MA-containing fuel with a certain variation range in content.

Although it is known that MA has influence on the core and fuel design, necessary information such as the material properties of MA-containing fuel is limited, and hence, relatively large design margins were taken corresponding to this situation. Therefore, we have tried to accumulate necessary fuel data, and by fully utilizing them the core and fuel design of the commercial JSFR has been performed, as presented in Fig.1-4 and Table 1-1. On the MA content, a fuel composition case for LWR spent fuel with the MA content of 3wt% is tentatively considered as well as a case for the multiple-recycled FBR.

Table 1-2 Major characteristics of commercial JSFR for two fuel compositions of multiple-recycled FBR and LWR spent fuels

	FBR multiple-recycled SF composition	LWR SF composition
MA content (wt%)	0.9 (IC) 1.0 (OC)	3.0 (IC) 3.0 (OC)
Pu enrichment (wt%)	18.3 (IC) 20.9 (OC)	19.6 (IC) 22.1 (OC)
Core height (cm)	100	100
Axial blanket length (m)	20 (upper) 20 (lower)	15 (upper) 20 (lower)
Na void reactivity ($)	5.3	5.9
Doppler coefficient (Tdk/dT)	-0.0057	-0.0045
Max. linear heat rate (W/cm)	398 (IC) 396 (OC)	411 (IC) 395 (OC)
Max. linear heat rate limitation (W/cm)	442 (IC) 438 (OC)	435 (IC) 433 (OC)
Lower gas plenum length (cm)	110	115

SF : Spent fuel, IC : Inner core, OC : Outer core

As shown in Table 1-2, the effects of increased MA content are recognized in the core design as increased sodium void reactivity and also in the fuel design as extended gas plenum length and as reduced linear heat rate limitation, which are due to increased He gas generation caused by α-decay of MA and due to decreased melting point and thermal conductivity, respectively. However, it has been indicated that MA can be acceptable without serious effects on the core and fuel design specifications for the assumed MA content range of 1 to 3wt%.

It is planned to conduct further investigation of the recycle scenario of LWR spent fuels as well as to promote accumulation of necessary data on MA-containing fuel, which will be reflected in the core and fuel design.

Reference

Naganuma, M. et al., Development of Advanced Loop-Type Fast Reactor in Japan, (6) Minor Actinide Containing Oxide Fuel Core Design Study for the JSFR, Proceedings of 2008 International Congress on Advances in Nuclear Power Plants (ICAPP '08), Anaheim, CA, USA, 2008, paper 8082, p.526-535, in CD-ROM.

1-3 Investigation of Irradiation Behavior of Future FBR Fuel
—Short-Term Irradiation Behavior of Am-Containing MOX Fuel—

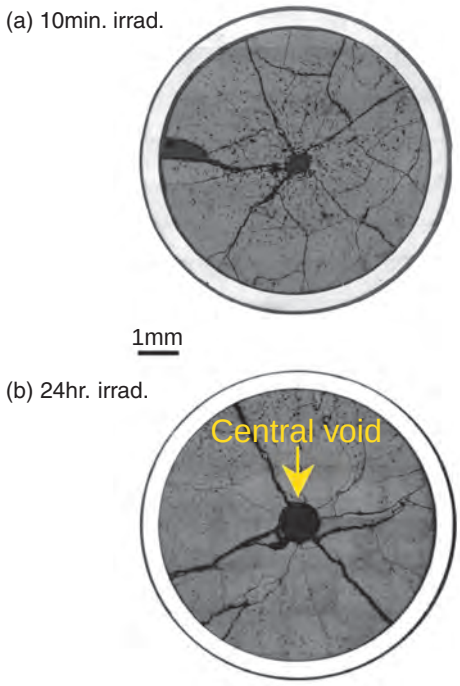

Fig.1-5 Ceramograph of irradiated 5% Am-MOX fuel
The ceramography results showed that restructuring started early, within the first 10 min of irradiation, and that the central void developed after 24 hour of irradiation.

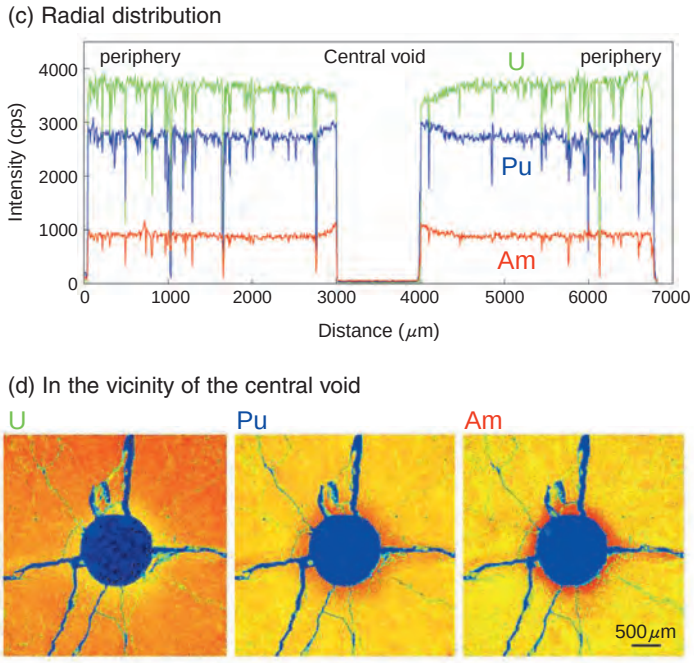

Fig.1-6 The elemental distribution of 5%Am-MOX fuel irradiated for 24 hour
The concentration of Pu and Am increased in the vicinity of the central void (The red in Fig.1-6 (d) indicates high concentration).

MOX fuels containing several percent concentrations of minor actinides (MA) and fission products (FP) are promising candidates for a closed nuclear cycle system based on a fast reactor. Cycle management of MA such as Am, Np and Cm is of crucial importance from the viewpoint of reduction of environmental burden, effective use of natural resources, and enhancement of nuclear nonproliferation. For evaluating the irradiation performance of the fuel, it is indispensable to understand irradiation behavior, such as Am redistribution and fuel cladding chemical interaction.

In order to confirm the effect of MA addition on irradiation behavior of MOX fuel pellets, an irradiation program named “Am-1” is being conducted in JAEA. The Am-1 program consists of two short-term irradiation tests of 10-minutes and 24 hours, and a steady-state irradiation test. The two short-term irradiation tests have been successfully completed. After the reactor power was raised continuously to the targeted peak linear heating rate of 430W/cm and kept there for 10 min, the power was manually shut down. The second irradiation test was performed with almost the same power history up to the targeted peak heating rate of 430W/cm and held for 24 hours.

Post irradiation examinations such as ceramography and electron probe microanalysis (EPMA) have been conducted in order to evaluate the irradiation behavior of the fuel.

No sign of fuel melting was found in any of the specimens taken from the Am-MOX fuel pins irradiated for 10 min and 24 hour. This implied that the thermal design had a sufficient safety margin for these test conditions. The configuration of the microstructure after 10 min irradiation was similar to that of conventional oxide fuels irradiated for a short time at a high linear heating rate (Fig.1-5(a)). After the 24 hour irradiation, a central void developed, and the change in structure seen at the beginning of irradiation was completed (Fig.1-5(b)).

The results of EPMA revealed that Am migrated to the radial center of the fuel pellet up the temperature gradient during the initial stage of irradiation. This tendency is similar to that of Pu (Fig.1-6).

It has been reported that the melting point temperature is decreased by the addition of a large amount of Am, which leads to a smaller design margin for fuel melting. The present EPMA results indicated that careful consideration must be given to the redistribution behavior of Am as well as that of Pu for evaluating its impact on the thermal performance of Am-MOX fuels.

The irradiation behavior at a high linear heat rate observed in the Am-1 program will be useful for the modeling and design study of Am-containing MOX fuel.

Reference

Tanaka, K. et al., Microstructure and Elemental Distribution of Americium-Containing Uranium Plutonium Mixed Oxide Fuel under a Short-Term Irradiation Test in a Fast Reactor, Journal of Nuclear Materials, vol.385, issue 2, 2009, p.407-412.

1-4 Numerical Simulation of Time-Dependent Thermal Interaction between Fluid and Structure

—Thermal Mixing in T-Junction Piping System—

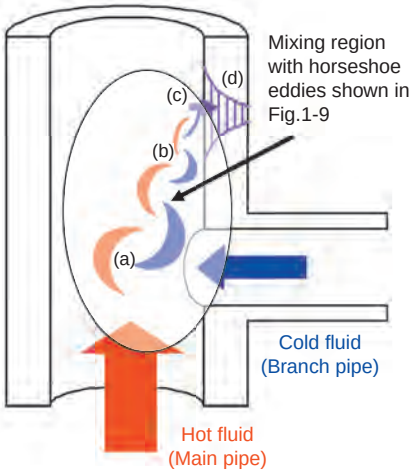

Fig.1-7 Thermal striping in a T-junction piping system

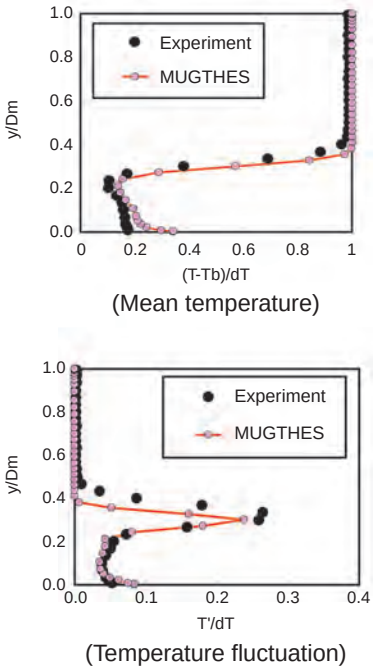

Fig.1-8 Radial profiles of fluid temperature
0.5Dm downstream from mixing point

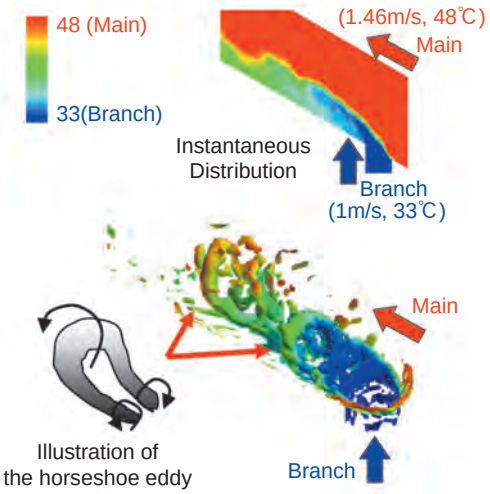

Fig.1-9 Horseshoe eddies showing Iso-Surfaces of rotating flow strength
Color gradation shows fluid temperature

Fig.1-7 illustrates the thermal striping phenomenon in a T-junction piping system (T-pipe) where cold fluid through the branch pipe mixes with hot fluid in the main pipe (a). If the temperature fluctuation caused by the mixing (b) is transmitted to structure surface (c), high cycle thermal stress may be induced on the surface (d) and may cause crack initiation and propagation according to the frequency and the amplitude of the temperature fluctuation. Therefore, thermal striping is recognized as an important issue in plant safety because of its threat to structural integrity.

We have developed the numerical simulation program "MUGTHES" in order to clarify the nature of thermal striping and to establish an estimation method for high cycle thermal fatigue in structure. MUGTHES is designed to calculate thermal interaction between unsteady thermal-hydraulic phenomena and unsteady heat conduction in a structure, utilizing a conjugate heat transfer model. The Boundary Fitted Coordinate (BFC) system and the Large Eddy Simulation (LES) approach are employed to simulate complicated geometry and turbulent flow phenomena, respectively. To improve the computation efficiency, a new matrix solver for pressure equations is established and parallel computation technique is used.

Numerical simulation of thermal striping in T-pipe was carried out to confirm the applicability of MUGTHES and to determine the mixing mechanism in T-pipe. From Fig.1-8, it was confirmed that the numerical results could reproduce experimental results well in fluid temperature profiles. Moreover, the contribution of horseshoe eddies generated in the mixing region to temperature fluctuation generation in T-pipe could be predicted as shown in Fig.1-9.

Numerical simulations of thermal interaction experiments are expected to validate the physical models in MUGTHES. Through this V&V (Verification and Validation) process, MUGTHES will be applied to the thermal striping in upper plenum of JSFR (Japan Sodium-cooled Fast Reactor).

Reference

Tanaka, M. et al., Thermal Mixing in T-Junction Piping System Concerned with High-Cycle Thermal Fatigue in Structure, The 6th Japan-Korea Symposium on Nuclear Thermal Hydraulics and Safety (NTHAS 6), Okinawa, Japan, 2008, PN6P1039, 8p., in USB flash drive.

1-5 Sophisticated Design Concept for FBR Components
—Evaluation of Creep Design Region by Negligible Creep Curve—

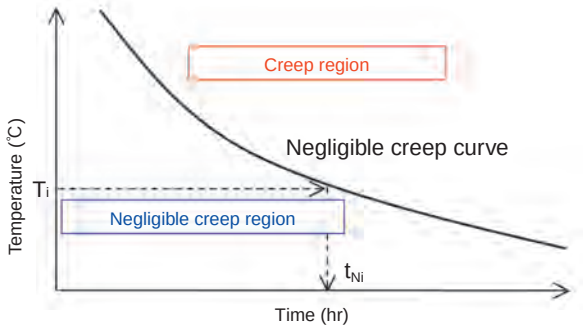

Fig.1-10 Illustration of negligible creep concept

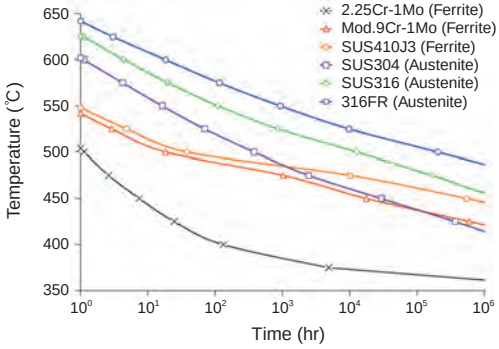

Fig.1-11 Proposed negligible creep curves for each material

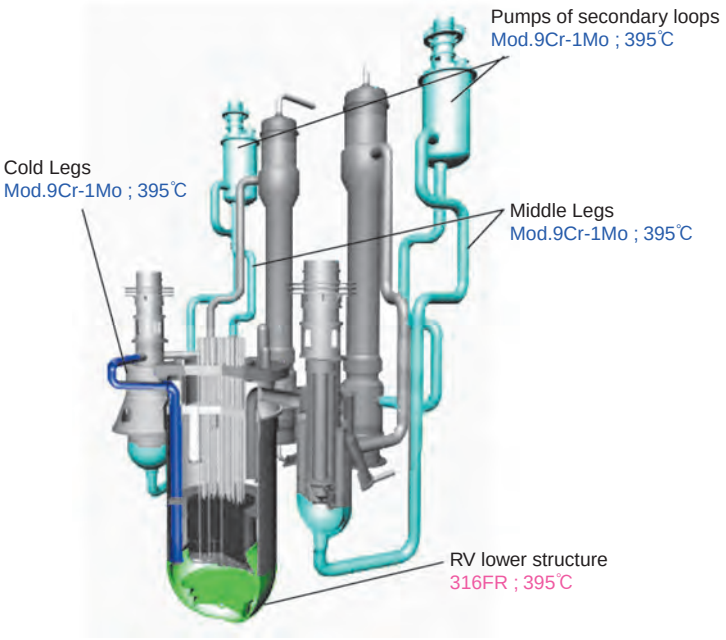

Fig.1-12 Components with negligible creep effect in design

The main components in FBR are used at elevated temperature (about 550°C). Therefore, the design evaluation method and standard should consider the influence of creep behavior. The current structural design standard for FBR is divided into those for a elevated temperature design region and for a normal temperature design region, according to whether creep needs to be considered. This division rule is based on the 100,000hr creep properties of 2.25Cr-1Mo and SUS304, because these materials were standard structural materials when the current evaluation method was under development. As a result, a uniform temperature limit was standardized for each steel type, but regardless of the exposed time. These were 375°C for ferrite steel and 425°C for austenite steel. Design considering creep is required for components used over this temperature limit.

However, materials with superior strength at elevated temperature such as 316FR and Mod. 9Cr-1Mo have been developed for FBR structures. The creep rupture strength of Mod. 9Cr-1Mo at 100,000hr is over twice as large as that of 2.25Cr-1Mo, although both materials are categorized as ferrite steel. Conventional classification by steel type and the uniform temperature limit regardless of the exposed time provides a too conservative design evaluation for components made of high creep strength material. Thus, a reasonable division rule for the temperature limit based on creep strength of each material was needed, and we have developed one.

Fig.1-10 shows the proposed concept of the negligible creep curve. It means the effect of creep can be negligible in component design, if the following equation (1) is satisfied.

$$\sum_{i=1}^{n}\left(t_i / t_{Ni}\right) \le 1 \qquad \cdots\cdots(1)$$

Where the t_i is exposure time at which temperature T_i is reached, t_{Ni} is maximum exposure time to reach T_i for creep to be negligible, and n is the number of temperatures considered.

Negligible creep curves proposed for each material are shown in Fig.1-11.

These negligible creep curves, developed independently by us, allow all the rules considering creep of a component to be ignored in a design (Fig.1-12) if the length of operation at a given high temperature falls under the curve. This negligible creep curve concept simplifies the design procedure and allows adequate component design. This means that this concept reduces design costs and widens the design range of FBR components.

Reference

Ando, M. et al., A Comparative Study of Negligible Creep Curves for Rational Elevated Temperature Design, Proceedings of the 2009 ASME Pressure Vessels and Piping Division Conference (PVP 2009), Prague, Czech, 2009, paper PVP2009-77232, in CD-ROM.

1-6 Efforts to Improve Monitoring of High Temperature Piping
－Development of Pipe Wall Thinning Sensor－

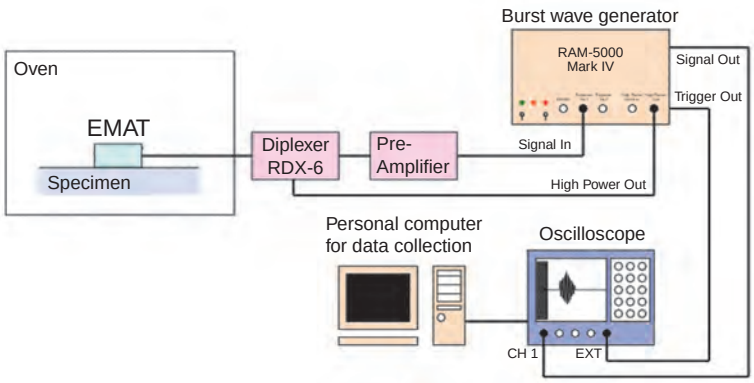

Fig.1-13 Measurement system

Table 1-3 Development target

Max. Temp.	200℃
Durability	200hour
Limit of detection	≦4mm
Accuracy	≦±0.3mm
Material	SS400

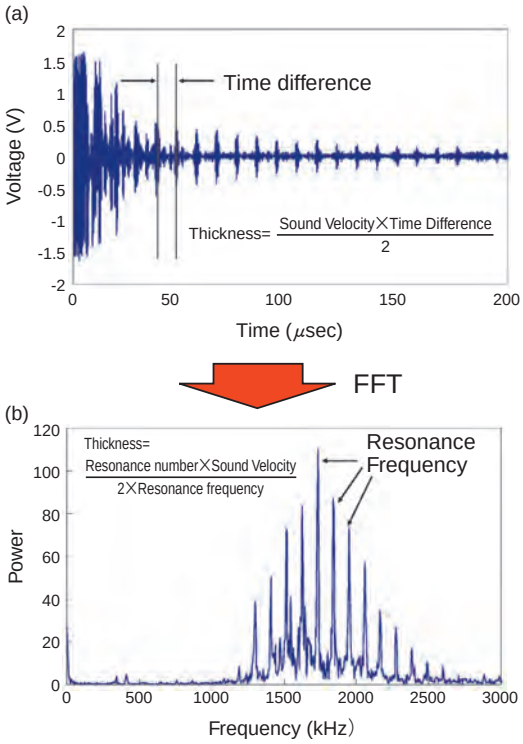

Fig.1-14 Measured Data
Until now, the method used the resonance frequency decided after sweeping through the resonates. In the actual method, it is used the ultrasonic wave transmitted on a wide frequency band. After the analysis of the received waveforms the resonance frequency is determined. The measured time is shortened using this method.

In nuclear power plants in Japan a periodical inspection has been carried out once every 13 months. However, maintenance activities and inspections are concentrated during plant shut down periods and tend to be fragmented. Also, there were indications that the required inspection interval was too long in some cases. To deal with these problems, a new inspection code (maintenance program) was carried out in 2009, in which the checking intervals have a scientific rationale.

Many of the past studies had focused on the condition-monitoring technique of active components such as a motor. However, there is also a high interest in the condition monitoring of passive components, such as a piping. For their monitoring, it is necessary to install a sensor with high temperature durability under the thermal insulator. Also, the sensor should be able to be manufactured with a low cost price.

In this present study an electromagnetic acoustic transducer (EMAT) composed of a permanent magnet and a coil were used. The sensor was specifically developed for a piping monitor. It excels in durability because EMAT has a simple structure, and also thus has a low price. Moreover, it is possible to attach it to the pipe using a permanent magnet. The pipe wall thinning monitoring sensor was developed to meet the targets described in Table 1-3. The data received from EMAT are taken to a computer as shown in Fig.1-13.

The sensor is detects multiple ultrasonic wave reflections in a wall, and thickness is calculated from the intervals between them (Fig.1-14(a)). The frequency composition of the reception signal can be analyzed to find resonance frequencies, which are used together with sound speed to calculate thickness (Fig.1-14(b)).

It was difficult to measure the thickness of thinner wall by the reflection time difference. It was also difficult to measure the thickness of a thick wall using the resonance frequency. This study was able to properly measure the wall thickness using different techniques applied to the same received data. By this method a 2mm board thickness was measured with±0.1mm accuracy, which is much better then the development target of 4mm±0.3mm. The sensor was confirmed to be usable at high temperature (200℃). In the future, it will be possible to enhance the safety of piping by installing these sensors on them.

Reference

Tagawa, A. et al., Investigation of the On-line Monitoring Sensor for a Pipe Wall Thinning with High Accuracy, E-Journal of Advanced Maintenance vol.1, no.1, 2009, p.52-62.

1-7 Oxidation in Sodium Combustion Process
—Role of Sodium Oxide Generated on Liquid Sodium—

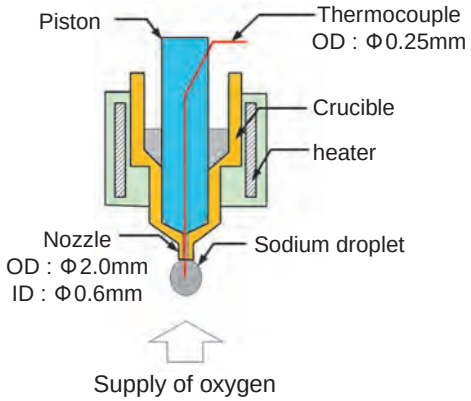

Fig.1-15 Experimental apparatus of sodium combustion

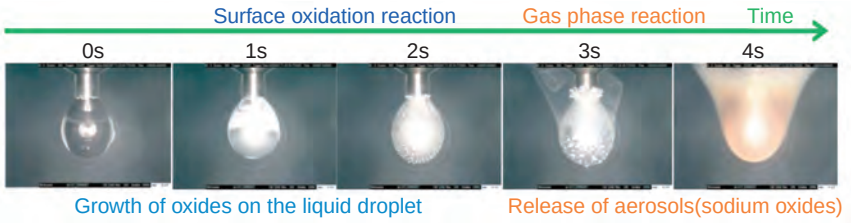

Fig.1-16 Event transition of sodium combustion 20%O_2
At first, "surface oxidation reaction" occurs accompanied with a temperature rise due to the reaction heat. Then, the vapor pressure rises. As a result, sodium vapor reacts with the oxygen in the air, and the so called "gas phase reaction" occurs.

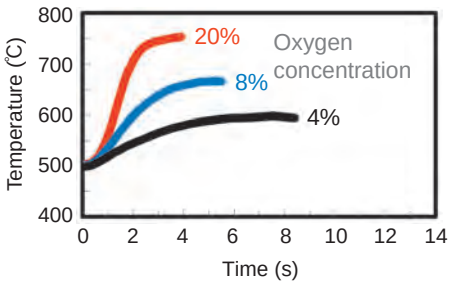

Fig.1-17 Internal temperature of the liquid droplet

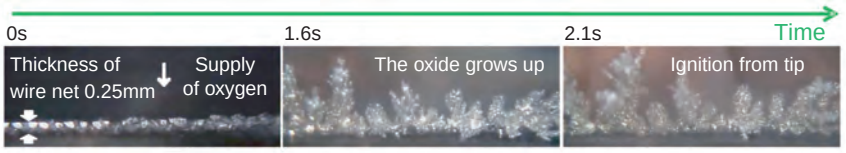

Fig.1-18 Growth of the columnar oxides
The columnar oxides independently grow up toward the direction of oxygen supply in the surface reaction.

The Fast Breeder Reactor (FBR) is being designed so that the consequences from accidents are mitigated. In case of the coolant (sodium) leakage from the secondary loop, sodium reacts with oxygen in the air and begins to burn at high temperature. Such sodium fire can be extinguished by cooling or oxygen cutoff using nitrogen gas injection.

The FBR plant must be designed to maintain safety even if a sodium fire accident happens. Thus, it is necessary to clarify the combustion process of sodium in detail to evaluate the consequences of the accident. A simple test device as shown in Fig.1-15 was set in a glove box and operated to observe the reaction interface easily. In the device, a sodium droplet was reacted with oxygen supplied from below. Visualization using a high speed camera and measurement of the internal temperature of the liquid sodium droplet were done simultaneously.

This simultaneous measurement enables us to know the correlation between the sodium internal temperature and the surface oxide growth. The combustion of sodium starts with the surface oxidization reaction, and changes to the gas phase reaction gradually (Fig.1-16).

The sodium temperature increased rapidly, reaching a value at which with heat radiation balanced the reaction heat, this value being influenced by the oxygen concentration (Fig.1-17). During the transition to the gas phase reaction from the surface oxidization reaction, it was observed that unique columnar oxides formed and grew on the surface of sodium which was covered by the white thin film oxide. This columnar oxide grew up greatly when the temperature of sodium was low or the oxygen concentration was low. To observe the growth of the columnar oxide in detail, the sodium was set on a wire net and reacted by supplying oxygen; up-close photos were taken by the high-speed camera. From these observations, it was clarified that the columnar oxide supplied sodium to the reactive interface, and the combustion continued as a result (Fig.1-18).

This research contributes to progress in combustion analysis technique by elucidating the mass shift mechanism and the growth mechanism in the sodium oxidation reaction. We hope to clarify the combustion mechanism based on this basic understanding gained here, because understanding of the sodium reaction phenomenon in a variety of plant environments is desired.

Reference

Nishimura, M. et al., Oxidation Behavior of Liquid Sodium Droplet before Combustion : Dependency of Initial Temperature and Oxygen Fraction, The 7th International Topical Meeting on Nuclear Reactor Thermal Hydraulics, Operation and Safety (NUTHOS-7), Seoul, Korea, 2008, paper 230, 12p., in CD-ROM.

1-8 Ultimate Behavior of Seismically Isolated FBR Plants in Huge Earthquake
—Large Shaking Table Test of Horizontal Isolation System—

Fig.1-19 Horizontal isolation system test apparatus
Shaking table tests for the breaking of the laminated rubber bearing were performed on a scale as large as any in the world. The response reduction function in a tentative model of ground motion was confirmed, and the ultimate behavior data of the system in response to ground motion four times greater than the model were measured.

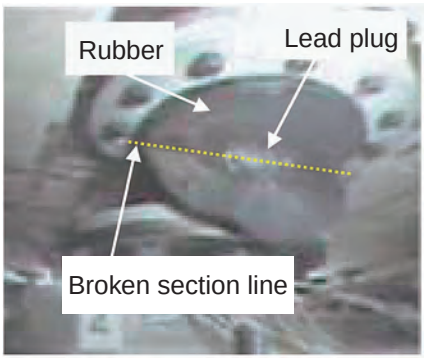

Fig.1-20 Moment that laminated rubber bearing broke
This photograph taken with a video camera shows the moment that a laminated rubber bearing broke. Breaking started from the edge of the rubber, and pieces of the lead plug were ejected when the bearing broke.

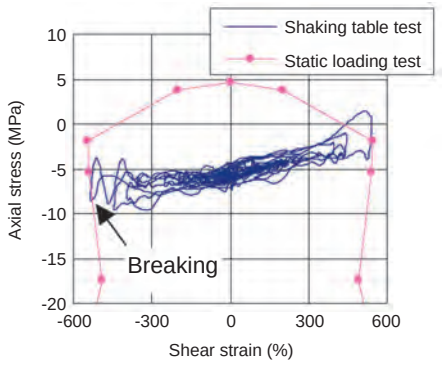

Fig.1-21 Breaking strain of laminated rubber bearing
The solid line shows the relation between the axial stress and the shear strain during a shaking table test where the laminated rubber broke. The pink line plots the breaking conditions, based on a static loading test. The breaking strain measured in the shaking table test was almost the same value as that of the static loading test.

Seismic isolation technology is to be introduced into fast breeder reactor plants of the next generation in order to reduce the seismic load subjected to components. To grasp the ultimate behavior of a base isolated plant in a huge earthquake of a level higher than that considered in the design, we made ultimate behavior tests of seismically isolated FBR plants with a large shaking table, in cooperation with Central Research Institute of Electric Power Industry.

A seismic isolation effect is achieved by setting up soft springs (laminated rubber bearings) under the building so that the building may shake slowly. The relation between the load and the displacement of the rubber bearing is almost linear in the range where the load is small. A seismic isolation system is designed so that the building may also respond linearly to the seismic intensity. When the seismic load is large, the seismic isolation effect is lost because of the hardening of the rubber, which then may break. In this test, data concerning the loss of the isolation effect and the breaking behavior of rubber were obtained.

One of the world's largest three-dimensional shaking tables, "E-Defense" of National Research Institute for Earth Science and Disaster Prevention, was used to observe actual behavior of the isolation system. Fig.1-19 shows the shaking table test apparatus. The test specimen was composed of a superstructure of about 600 tons and six rubber bearings of 505mm outside diameter (about 1/3 the size of the prototype). There was seismic isolation of the ground motion on the scale considered in the design. After motion was increased, non-linear response in the hardening range and breaking of the rubber were observed. When the ground motion was amplified from 4.0 to 4.8 times the design level, some laminated rubber bearings broke (Fig.1-20). The breaking strains were from 550 to 600%, which agreed with the breaking conditions observed in static loading tests (Fig.1-21).

This breaking test of the laminating rubber bearing of a diameter of 505mm that are 1/3 of the prototype bearing was done on a scale without precedent. The risk evaluation method of seismically isolated plants will be developed based on these data in the future.

Reference

Kitamura, S. et al., Shaking Table Tests with Large Test Specimens of Seismically Isolated FBR Plants Part1: Response Behavior of Test Specimen under Design Ground Motions, Proceedings of the 2009 ASME Pressure Vessels and Piping Division Conference (PVP 2009), Prague, Czech, 2009, paper PVP2009-77614, 8p., in CD-ROM.

1-9 Effectively Dissolving Spent Fuels

—Development of Rotary Drum Type Continuous Dissolver for FBR Fuel Reprocessing—

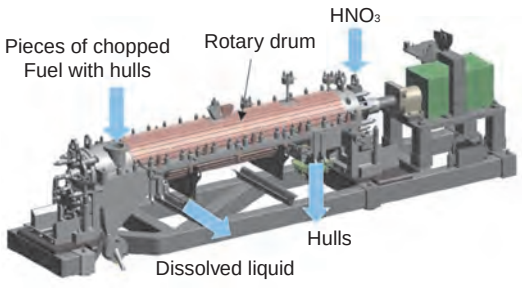

Fig.1-22 Rotary Drum Type Continuous Dissolver
Fuel dissolution is performed inside drum which receives chopped spent fuel with hulls at one side of the drum and fresh nitric acid at the other side, and then is swinging slowly. The inside of the drum has the form of a screw, and the drum rotation moves the undissolved hulls to the far end where they are expelled.

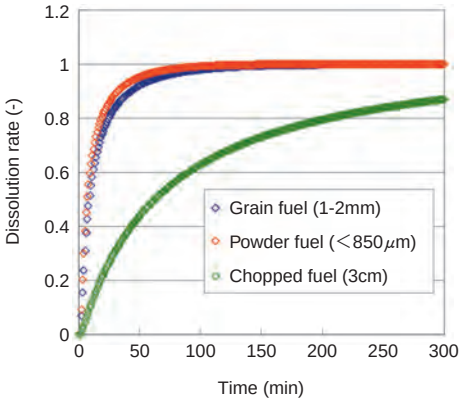

Fig.1-23 Result of irradiated fuels dissolution test
Dissolution speeds of powder fuel and 3cm length chopped fuel were distinctly different. It was confirmed that making fuel grains smaller than 2mm reduced dissolution time.

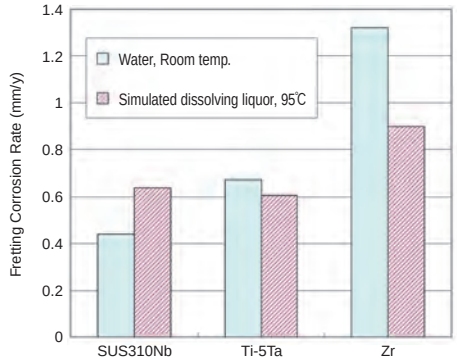

Fig.1-24 Result of fretting corrosion speed
The test showed that the fretting corrosion resistance of Ti-5Ta and SUS310Nb was higher than that of Zr in simulated solution conditions, the opposite of static corrosion results.

We have been developing a rotary drum type continuous dissolver for FBR spent fuel reprocessing in favor of ensuring criticality safety for the fuel of high Pu concentration. The apparatus has a screw structure with several meters long, and is designed to dissolve spent fuels well and exhaust hulls effectively not only by means of counter-flow contact between chopped spent fuels and fresh nitric acid, receiving spent fuels from one end of the drum and fresh nitric acid from the other end, but also by means of rocking the drum to accelerate dissolution and rotating the drum for transferring the hulls (Fig.1-22).

The advanced aqueous reprocessing system (NEXT) adopts a crystallization process for recovering uranium from dissolver solution. In this process, a high concentration of heavy metal solution is required to get a high rate of recovery. Hence, pins are sheared to shorter lengths so that the fuel is more powderized for better dissolution. Fig.1-23 shows the dependency of the dissolution rate on the grain size of irradiated MOX fuel. It was confirmed that the dissolution rate of powder fuel is higher than that of 3cm chopped fuel, and also confirmed that a grain size of 2mm or less could achieve sufficient shortening of time for completing a high rate of dissolution.

As for the corrosion resistance, the thickness of the drum structure should be chosen to have an appropriate safety margin against fretting corrosion, since the material might be worn away by hulls rubbing back and forth on the drum surface during swinging and rotation as well as static wet corrosion caused by high temperature (95ºC) and high concentration of nitric acid (max12N). We therefore evaluated the fretting corrosion rate of Zr,Ti-5Ta and SUS310Nb, well known anti-corrosion materials used in reprocessing plants, in a corrosion test composed by a special apparatus that contained hulls(SUS316) and that simulated actual nitric acid solution and swing motion conditions. As a result, the fretting corrosion rate of Zr was faster than the others, although Zr was more resistant to static corrosion (Fig.1-24). The fretting corrosion rates of Ti-5Ta and SUS310Nb were almost same in the simulated solution, while the abrasion in water conditions depended on the hardness of the materials, which indicates the necessity of material selection considering the combined effect of static corrosion and wear of re-passivized surface film by friction.

We are now developing a 50t/y capacity dissolver, and with integration of all the above knowledge, e.g. drum bearing characteristics, will plan development of a 200tHM/y dissolver.

Reference

Katsurai, K. et al., Development of Highly Effective Dissolution Technology for FBR MOX Fuels, The Nuclear Fuel Cycle: Sustainable Options & Industrial Perspectives (GLOBAL 2009), Paris, France, 2009, paper 9219, p.108-112, in CD-ROM.

1-10 Simple Control of Valence of Actinide Element
—Development of U-Pu-Np Co-Extraction Process—

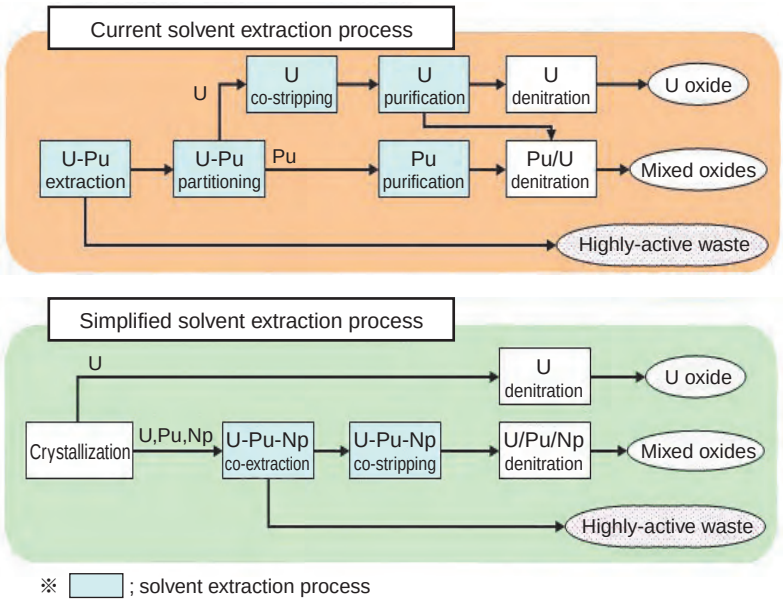

Fig.1-25 Comparison of current extraction process and simplified extraction process
In the current process, U and Pu are extracted by TBP, then Pu is reduced in order to partition U and Pu, and U is finally stripped from the TBP phase by dilute nitric acid. In the advanced aqueous process, U, Pu and Np are collectively recovered after U crystallization process.

Table 1-4 Valence states and their extractabilities
◎, most stable ions in nitric acid medium; ○, valence states observed in nitric acid medium. The extractability of actinide elements mainly depends on their valence state.

		Element					Extractability
		U	Np	Pu	Am	Cm	
Valence state	+3			○	◎	◎	low
	+4	○	○	◎			high
	+5		◎				low
	+6	◎	○	○			high

A simplified solvent extraction process to recover Uranium (U), Plutonium (Pu) and Neptunium (Np) collectively is one of the advanced aqueous reprocessing technologies being developed (Fig.1-25). Utilizing a crystallization process, the nuclear fuel material to be treated in the simplified solvent extraction process is quantitatively less than that in the conventional reprocessing process. Moreover, the construction of the extraction process where Pu is made to co-exist with U etc. in all reprocessing steps (i.e. Pu is never isolated alone) is made possible by the deletion of the U/Pu distribution process. It is expected that the new process will generate less waste, reduce costs, and enhance nuclear proliferation resistance.

The extractability of actinide elements to tributyl phosphate (TBP) mainly depends on their valence state (Table 1-4). In the current reprocessing process, U and Pu are extracted by TBP in their extractable valence states, U(VI) and Pu(IV). Then, Pu is reduced by a reducing reagent from Pu(IV) to Pu(III) and is stripped from the TBP phase while U(VI) remains in the TBP phase. Finally, U(VI) is stripped from the TBP phase by dilute nitric acid. In the advanced aqueous process, U(VI) and Pu(IV) in the TBP phase are collectively stripped by diluted nitric acid because a certain part of U is separated beforehand utilizing U crystallization. As for Np, it can exist as extractable Np(IV), Np(VI) or inextractable Np(V) in the solvent extraction system, their behavior can be controlled by their valence state adjustment. The use of redox reagent, however, makes the adjustment of the chemical condition of the process complex, increasing the number of reagents to be used. We are studying the control of Np valence state simply by changing the concentration of nitric acid, for U-Pu-Np co-extraction process development.

The experimental studies on the U-Pu-Np co-extraction process are being done at the Chemical Processing Facility (CPF). The CPF type centrifugal contactor we designed was used as a counter current extraction device. The demonstrations have shown that U, Pu and Np can be collectively extracted and recovered by simple control of valence state through adjustment of the nitric acid concentration.

Reference

Nakahara, M., Sano, Y., Nomura, K. et al., Uranium, Plutonium and Neptunium Co-Recovery with Irradiated Fast Reactor MOX Fuel by Single Cycle Extraction Process, Proceedings of 3rd International ATALANTE Conference (ATALANTE 2008), Monpellier, FRANCE, 2008, 5p., in CD-ROM.

1-11 Toward the Commercialization of MOX Fuel Production by Simplified Pelletizing
—Mechanism of Boiling Step in Innovative De-Nitration, Its Effect on Vessel Design—

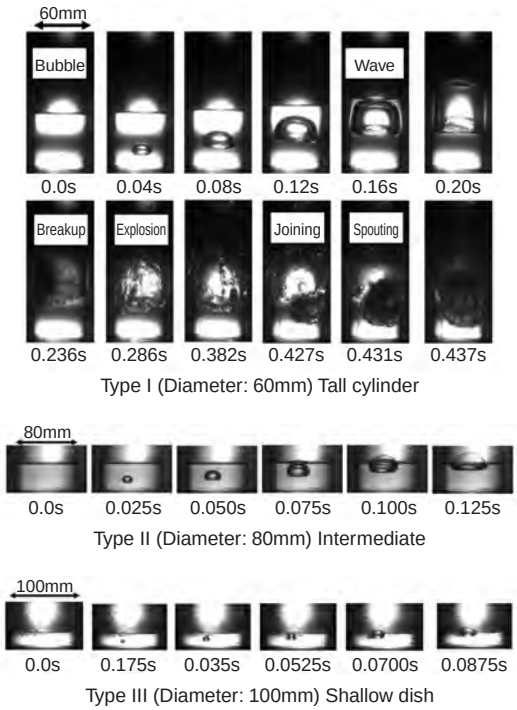

Fig.1-26 Observation of spouting caused by MH
(Type I, II, III): water 150mℓ constant

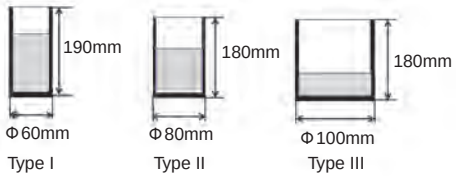

Fig.1-27 Experimental vessel (3 types)

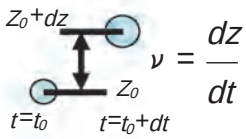

Fig.1-28 Method for estimation of bubble surfacing velocity

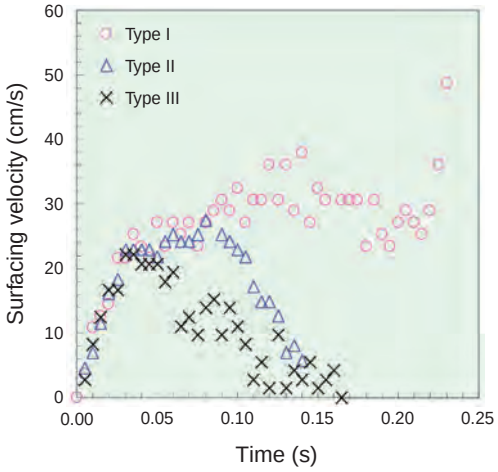

Fig.1-29 Surfacing velocity of bubble (Different vessels)

It is absolutely necessary for practical realization of FBR to decrease the cost as well as increase the speed and volume of production of MOX fuel to be burned in the reactor. A turn table system which employs a cylindrical vessel for the de-nitration was proposed as one of the design candidates for these purposes in the Project Phase II which was finished in 2004. It became necessary to quantitatively compare this idea to the former proposals employing a shallow dish, and to judge their feasibility

So, the fundamental sequential mechanism from micro-scale boiling, expansion with surfacing, explosion, and spouting, which causes the de-nitration, was observed by "particle image velocimetry" (PIV) in water subjected to microwave heating (MH). In case of familiar heating like a gas range, a tiny bubble appears at micro flaws on the heated surface and then the water boils at 100℃. This process is called boiling based on "non-uniform nucleation". If the surface of vessel is perfectly smooth, however, no tiny bubble is generated until the water is heated up to 300℃. This phenomenon is called super heating. After this bubble generation, boiling suddenly starts, this phenomenon being called flushing or explosion. This process is called the boiling based on the "uniform nucleation".

On the other hand, in case of MH, the boiling occurs at 100℃ with a little super heating. This is due to the peculiar property of energy supplied by the microwave irradiation; namely, micro boiling can start anywhere in the water, being independent of the condition of vessel's surface. This peculiar property of MH was made clear through joint research between JAEA and University of Tsukuba, for the first time anywhere in the world.

It can be seen from Fig.1-26 that the nature of the steam explosion is considerably different according to the configuration of the vessels shown in Fig.1-27. In Type I vessel (tall cylinder), a single micro bubble is generated and surfaces due to the energy stored underneath the bubble as it expands. When the head of the bubble reaches the water surface, break of the bubble and violent spouting occur simultaneously. This sequential action is repeated by following micro bubbles.

In Type II vessel (intermediate), the phenomena from generation of a micro bubble to its expansion is almost the same, but the head of the bubble rises much higher than water surface. When it breaks, a violent explosion occurs and many large size secondary bubbles are generated at the water surface, resulting in violent waves, but no spouting occurs. In type III (shallow dish), the amplitude of the waves remains low and no spouting occurs.

In summary, the tall cylinder causes spouting, while the shallow dish and intermediate type are free from spouting. This fact clarifies the essence of spouting, that the energy accumulated underneath the bubble, which becomes the driving power, increases with the surfacing path length, i.e. the water depth, demonstrating the superiority of the shallow dish.

Fig.1-29 shows the surfacing velocity of a bubble calculated by the method shown in Fig.1-28. As is clear from this, the surfacing velocity is 20cm/s in a shallow dish, and 50cm/s in a tall cylinder. We are now attempting to analyze the relation between surfacing velocity and spouting height.

As the next step in this development work, we are constructing de-nitration apparatuses for Pu/U mixed nitrate solution, to decide which has the best performance on samples with different physical characteristics.

Reference

Hori, S., Abe, Y., Suzuki, M. et al., On the Nucleation Behavior of the Solution by the Microwave Direct Heating, Proceedings of 17th International Conference on Nuclear Engineering (ICONE 17), Brussels, Belgium, 2009, ICONE17-75653, 5p., in CD-ROM.

R&D Supporting the Technology and Reliability of Geological Disposal in Japan

In essence, geological disposal aims to isolate high-level radioactive wastes (hereafter, HLW), which are produced by nuclear power generation, from human environments for a long time. In Japan, spent fuel from power reactors is reprocessed to extract re-useable uranium and plutonium for power generation purposes. The liquids separated from the spent fuel during chemical reprocessing are solidified into a stable glass form. In the Japanese concept, vitrified wastes are encapsulated in a thick steel overpack, which is surrounded by highly compacted bentonite and then placed in a stable geological environment at a depth below 300m (Fig.2-1).

Geological disposal of HLW will be a long-term project of more than one hundred years from site selection to repository construction and operation, followed by post-closure monitoring. To launch repository operation in the late 2030s, the Nuclear Waste Management Organization of Japan (NUMO), which has the responsibility for geological disposal of HLW, is now calling for volunteer municipalities for preliminary investigations of their area as a site for the repository. It is thus of much significance that the project should be promoted efficaciously, as a national responsibility, by continuously reinforcing the technical base and enhancing public confidence. To this end, we have made and will continue to make steady progress in research and development in various fields, *e.g.* geoscientific research, engineering technology and safety assessment, taking advantage of developments in these fields to improve the technology and reliability of geological disposal in Japan.

A particular focus of our research and development (R&D) at present involves projects at two Underground Research Laboratories (URLs) to establish techniques for characterising the geological environment: one at Mizunami in crystalline rocks and the other at Horonobe in sedimentary formations (Fig.2-2). Surface-based investigations (Phase I) have been completed at both URLs. Investigations during tunnel excavation (Phase II) are currently ongoing, which will verify the reliability of the surface-based investigation techniques. Underground tunnels will serve as a place for the public to experience deep geological environments first-hand and appreciate our R&D activities. In addition, study of the long-term stability of geological environments has progressed, which involves the development of new techniques for, *e.g.* investigating the presence of hidden magmas in the crust and simulating the topographical evolution.

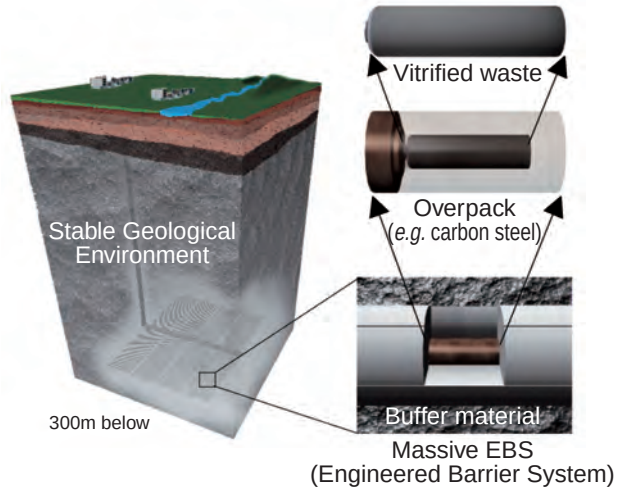

Fig.2-1 Basic concept of geological disposal of HLW in Japan

In parallel with such geoscientific research, we are conducting an extensive laboratory programme at the Tokai R&D Center to improve the geological disposal technology. Studies have been carried out over a wide range, *e.g.* performance assessment of multi-barrier systems and experiments on engineered barrier systems and long-term chemical and migration behaviour of radionuclides under actual geological conditions. These studies are linked with the geological environment data obtained from URLs. In 2008, a database for steel overpack corrosion was preliminarily developed based on long-term experimental data, and the world's first attempt was made to develop a radionuclide sorption database in which the reliability of each value was clearly categorised, which represented a notable advance.

Based on such R&D activities, we have now been working intensively on the development of the next generation knowledge management system (KMS) to systematically manage multiple lines of evidence and the R&D results relevant to safety in the form of a knowledge base.

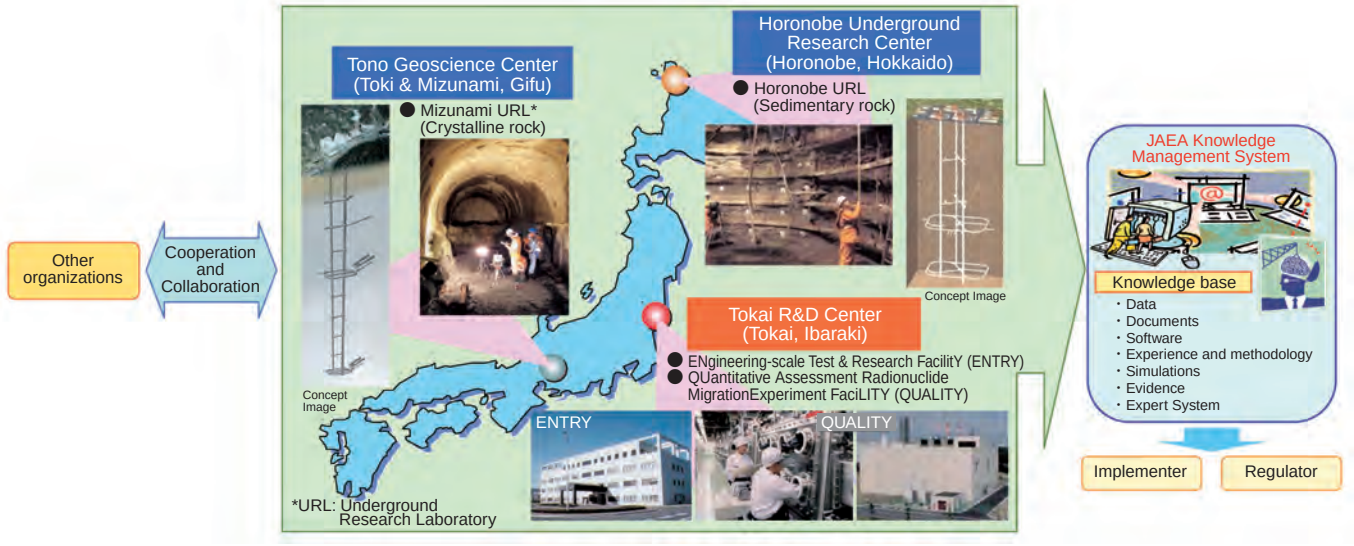

Fig.2-2 JAEA's R&D activities

2-1 Structuring Knowledge on Geological Disposal Technology
—Development of a Knowledge Management System—

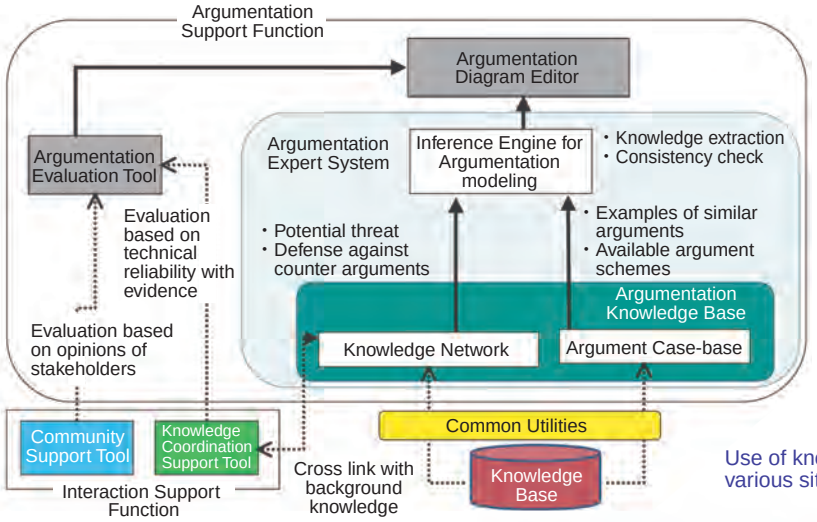

Fig.2-3 Overview of the knowledge management system

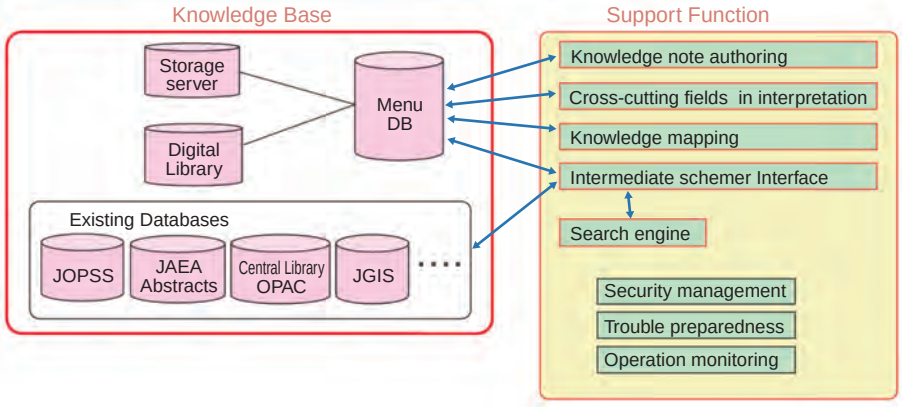

Fig.2-4 Knowledge base and user support function

"Knowledge" of geological disposal technology consists of many different types, ranging from "explicit knowledge", such as databases, literature and software, to "tacit knowledge", such as experience and know-how stored in the brains of experts. This knowledge will continue to increase during a repository development program spanning several decades. In order to show throughout the program that the demonstration of safety is sufficiently reliable, it is necessary to make full use of all this knowledge. It is not sufficient to compile individual items of knowledge from a range of sources - this knowledge has to be positioned within the context of a safety case, providing an innovative platform that allows knowledge to be shared among the users concerned. JAEA is developing a knowledge management system for the purpose of appropriately managing key knowledge on geological disposal technology. This is challenging work that cannot be done using traditional search tools and needs to utilize, to the maximum extent, state-of-the-art information technology and the latest knowledge engineering methodology.

Fig.2-3 provides an overview of the knowledge management system. The main elements of this system are the knowledge base and the management function. Data, software, information and knowledge that have been obtained through research and development work are structured and the tacit knowledge of experts is externalized in the form of expert systems and stored in a knowledge base. The main part of the management function is the argumentation support function, which shows how the knowledge stored in the knowledge base is used in the demonstration of safety. The argumentation model expresses the logic for the demonstration of a certain argument, for example the long-term safety of geological disposal, with a chain of "arguments" and "counter-arguments".

As shown in Fig.2-4, a user support function is extended in order to make the system accessible to a wide range of users, not only disposal implementers and regulators but also politicians and the general public. Two examples are a powerful and efficient search engine constructed with optimum use of the newest technology and the "cross-cutting interpretation support function", which interprets the differences in technical terms in different fields and extracts the relevant knowledge effectively.

To make the knowledge management system common intellectual property, JAEA is planning to make a prototype publicly available in 2010.

Reference

Hioki, K., Development of Knowledge Management System, Genshiryoku eye, vol.54, no.7, 2008, p.31-33 (in Japanese).

2-2 Study of Hydraulic Behavior in Rock Fractures
—Quantitative Measurement of Flow in a Fracture by Optical Method—

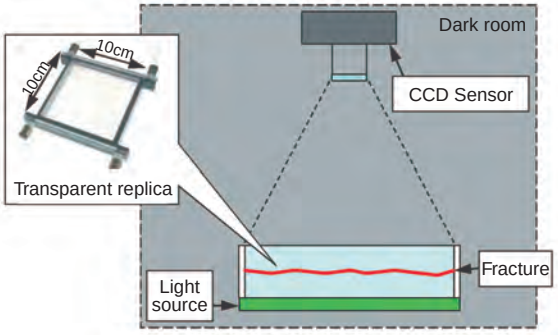

Fig.2-5 Concept of optical measurement of a fracture
Attenuation of transmitted light passing through a fracture is measured by CCD sensor.

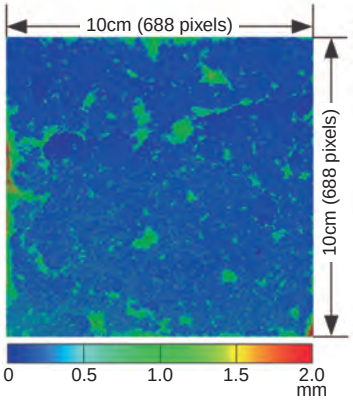

Fig.2-6 Example of fracture aperture measurement
The spatial resolution of aperture measurement is dependent on the resolution of CCD sensor.

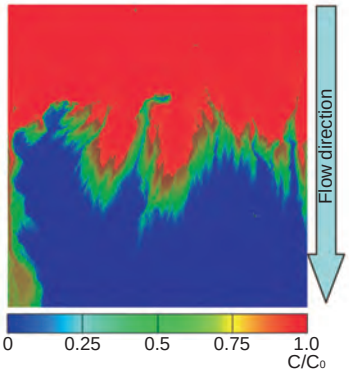

Fig.2-7 Example of measured dye tracer concentration
The dye concentration after injecting a dye tracer from upper boundary at a constant flow rate, normalized to inlet concentration.

Safety assessment of radioactive waste disposal is mainly based on scenarios in which moving groundwater provides pathways for radionuclide migration from a waste repository to the surface environment. To evaluate groundwater flow and nuclide migration, an appropriate model capable of describing the characteristics of the host rock should be used. In the case of hard rock with low porosity such as granite, fractures and/or faults carry nearly all of the groundwater flow. A single fracture is usually approximated by a parallel plate fracture model. Natural fractures, however, exhibit in-plane heterogeneity in terms of its variable aperture, and furthermore a huge number of heterogeneously distributed fractures constitute a network of water flow paths. A model with multiple parallel plate fractures is often used to represent the fracture network to evaluate the heterogeneous flow paths in rock mass. In such a fracture model, one of the key issues to be solved is the method for defining the representative values of hydraulic and transport properties of the parallel plate model used for modeling natural fractures with its in-plane heterogeneity.

We have, therefore, developed a laboratory experiment system that can measure quantitatively both the fracture aperture distribution and the groundwater flow within a fracture, under the same conditions (Fig.2-5). The system consists of a transparent replica of a single fracture and a transmitted-light optical measurement system. The fracture replica is made by duplicating a fracture that has been artificially generated in 10cm scale of rock block with transparent resin. The optical measurement system consists of a light source of constant intensity and a high resolution and sensitivity CCD (Charge Coupled Device) sensor to measure the transmitted light intensity through the transparent replica perpendicular to its plane. The light intensity is attenuated depending on the light absorbance of the dye, the dye concentration, and thickness of the gap filled with dye. When the transmitted light attenuation is measured after the fracture replica is filled with a constant-concentration dye tracer, the quantitative degree of fracture aperture at each point can be obtained (Fig.2-6). After getting the aperture distribution, the dye can be replaced with water, the dye tracer flowing in from one side. Thus, it is possible to use the optical system for visualizing dye tracer migration and also for measuring dye concentration distribution and time dependent concentration change at every point, quantitatively (Fig.2-7).

The experimentally obtained high spatial resolution quantitative data for both aperture distribution and tracer migration in the fracture plane is valuable to validate results of previous studies by numerical simulations of virtual fractures. The data obtained in this study have been published. In the future, we shall continue our experiments to get additional data on fractures with various patterns of in-plane heterogeneity, to understand flow and transport in a fracture, and determine the representative flow and transport parameters for these fractures.

Reference

Sato, H., Sawada, A., Study on Flow and Mass Transport Property Evaluation Method by Optically Measured Data in a Single Fracture, JAEA-Research 2008-067, 2008, 32p.(in Japanese).

2-3 Impact of a Fault Movement Across a HLW Repository
—Observed and Calculated Barrier Shear Due to Fault Movements—

Fig.2-8 Laboratory 1:20 scale simulation test equipment

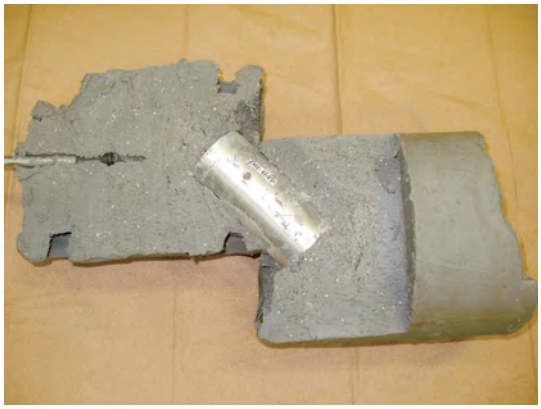

Fig.2-9 Sheared sample after test

Table 2-1 Shear test cases and experimental conditions

Shear rate	Shear displacement (ratio to thickness of buffer)	Test case. (two times for reproducibility)
0.1m/s	40mm（80%）	Case-1/Case-2
0.01m/s	70mm（140%）	Case-3/Case-4

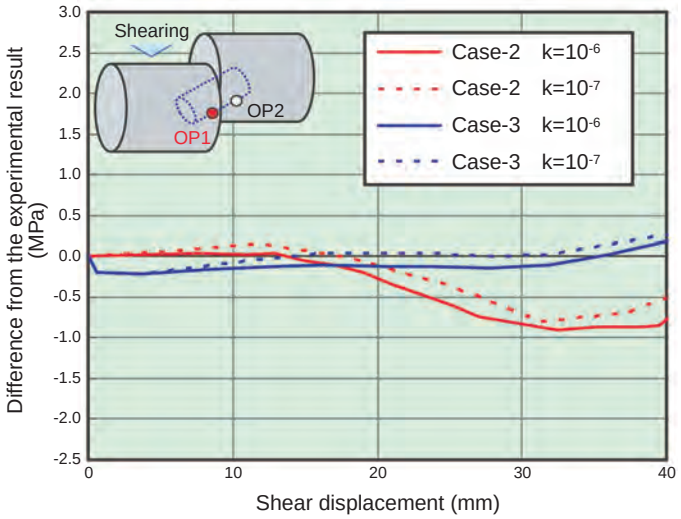

Fig.2-10 Comparison of calculated and observed data: total pressure against shear displacement
(k: hydraulic conductivity value (m/s) used for calculation)

In the Japanese repository concept, high-level radioactive waste (HLW) is encapsulated in a steel overpack, which is surrounded by a bentonite clay buffer. The overpack is required to completely isolate the waste from human and his environment for at least 1,000 years.

In accordance with Japanese law, site selection of a HLW repository is being implemented in three steps. Currently, the national R&D program for HLW disposal is aiming to realize the 2nd phase, in which the Detailed Investigation Area will be selected based on a surface-based investigation, paying special care to avoid areas affected by fault movements. However, minor faults are difficult to identify and characterize from the surface, especially if they are at some depth. Thus, the size of impact a fault movement could have if it intersects the HLW repository is of great concern.

JAEA is now conducting experiments using laboratory 1:20 scale simulation test equipment (Fig.2-8). Based on previous hidden faults, the present study focused on fault movements with a displacement less than 1m and shear rates less than 1m/s. Due to the mechanical limits of the test equipment, the tests have to be conducted an order of magnitude below these values. It was therefore necessary to develop a numerical model in order to extrapolate results to the critical range.

Four test cases carried out under the conditions given in Table 2-1 resulted in no visible damage to or deformation of the overpack, although it rotated within the buffer (Fig.2-9). Numerical analysis was conducted with a three-dimensional, non-linear, finite element model. Through comparison with experimental results, it was found that the current numerical model can only estimate the impact on the system caused by fault movement displacement up to half of the buffer thickness (~20mm) (Fig.2-10). This showed the limitations of the finite element mesh model used. It is therefore crucial to further improve the model for confident extrapolation into the critical range, e.g. a model that includes contacting elements, which generate friction in sliding.

Reference

Naito, M. et al., Experimental Study on the Effects of Fault Movement on the Engineered Barrier System, Journal of Power & Energy Systems, vol.3, no.1, 2009, p.158-169, (http://www.jstage.jst.go.jp/article/jpes/3/1/3_158/_article/-char/ja/).

2-4 Development of Radionuclide Migration Database
－Update of Sorption/Diffusion Database Categorized by QA－

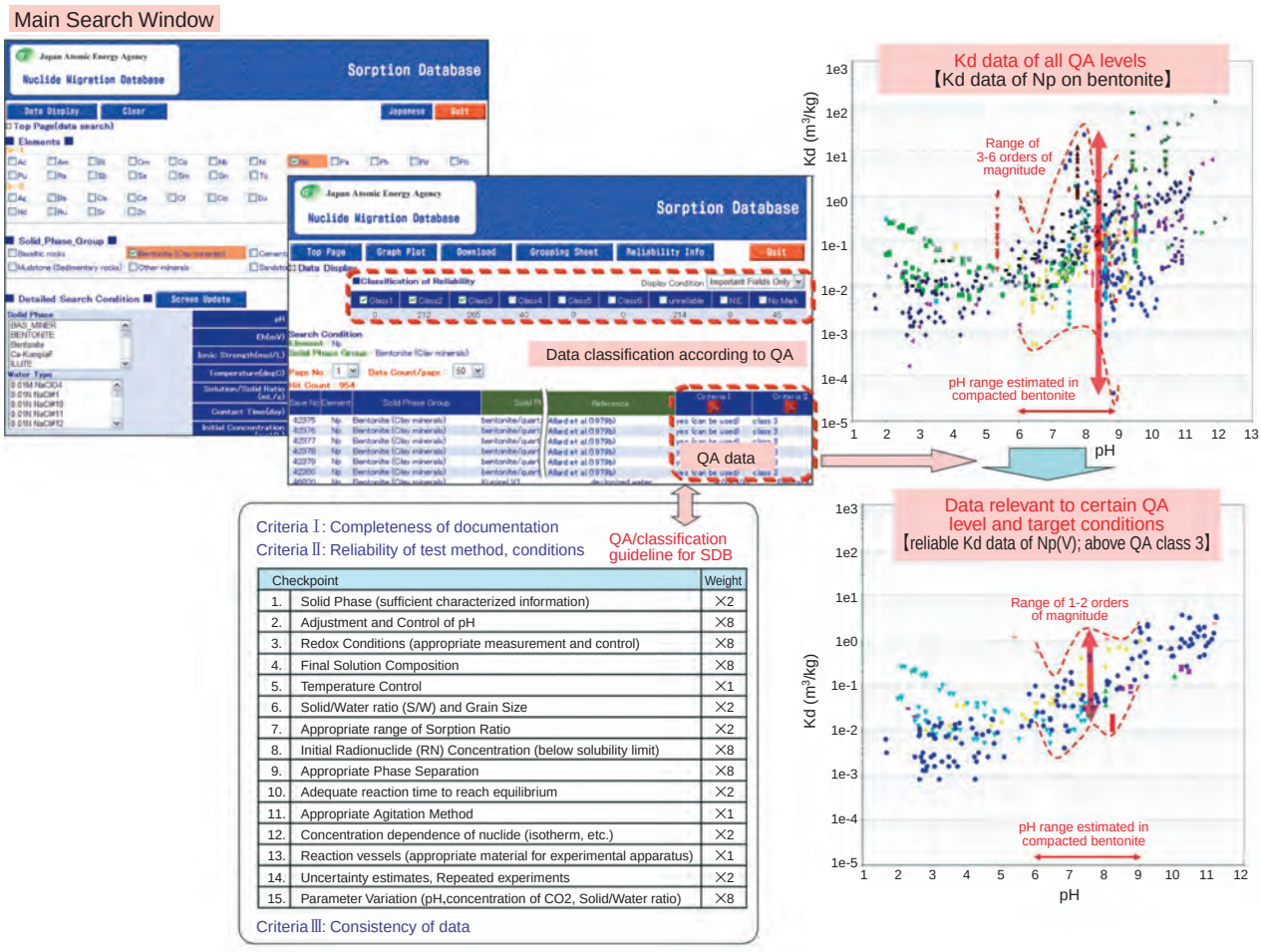

Checkpoint		Weight
1.	Solid Phase (sufficient characterized information)	×2
2.	Adjustment and Control of pH	×8
3.	Redox Conditions (appropriate measurement and control)	×8
4.	Final Solution Composition	×8
5.	Temperature Control	×1
6.	Solid/Water ratio (S/W) and Grain Size	×2
7.	Appropriate range of Sorption Ratio	×2
8.	Initial Radionuclide (RN) Concentration (below solubility limit)	×8
9.	Appropriate Phase Separation	×8
10.	Adequate reaction time to reach equilibrium	×2
11.	Appropriate Agitation Method	×1
12.	Concentration dependence of nuclide (isotherm, etc.)	×2
13.	Reaction vessels (appropriate material for experimental apparatus)	×1
14.	Uncertainty estimates, Repeated experiments	×2
15.	Parameter Variation (pH,concentration of CO2, Solid/Water ratio)	×8

Fig.2-11 The new web-based JAEA-SDB - Examples of search, extraction of data relevant to QA level

Sorption and diffusion of radionuclides in buffer materials (bentonite) and rocks are key processes to be considered in the safe geological disposal of radioactive waste. Sorption and diffusion databases have been developed as an important basis for the H12 performance assessment (PA) of high-level radioactive waste disposal in Japan. We have developed a practical and reliable sorption and diffusion database (JAEA-SDB/DDB), improving the existing SDB/DDB in view of potential future data utilization, e.g. attaining a desired quality assurance (QA) level and setting migration parameters for geological environments.

The updated SDB/DDB includes 24,000 Kd values (distribution coefficients) and 3,000 De/Da values (diffusion coefficients) and related experimental information from many different sources. The following functions are key improved points;

(1) Consistency and linkage between SDB and DDB
(2) Quality assurance evaluation method, utilization of QA results
(3) Estimating of parameters and graphing of relation between parameters
(4) Compiling sources and making data summary charts

The SDB includes a great variety of Kds of different reliability levels which were obtained with various conditions and methods. Accordingly, a QA evaluation method for sorption data has been developed in order to evaluate the reliability of each Kd. The QA guideline consists of three main criteria; I: completeness of documentation, II: reliability of test methods and conditions, III: consistency of data. The reliability of Kd data in the SDB was evaluated based on the guideline, and the QA results were added to the SDB. As shown in Fig.2-11, this QA scheme makes it possible to extract reliable data for parameter-setting in an effective, traceable and transparent manner.

The new web-based JAEA-SDB/DDB have Japanese/English versions and are provided free on the web (http://migrationdb.jaea.go.jp/).

Reference

Tachi, Y., Tochigi, Y., Suyama, T. et al., Development of the Sorption and Diffusion Database System for Safety Assessment of Geological Disposal, JAEA-Data/Code 2008-034, 2009, 36p. (in Japanese).

2-5 Past Geological Events Discovered with 1mg of Carbon

—Development of Dating Method with an Accelerator Mass Spectrometer—

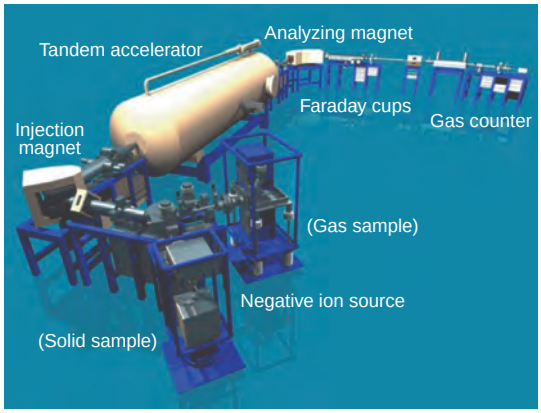

Fig.2-12 Outline of pelletron dating instrument
A tandem accelerator mass spectrometer (maximum voltage: 5.0MV, maximum current: 1μA). More than 800 samples are measured per year.

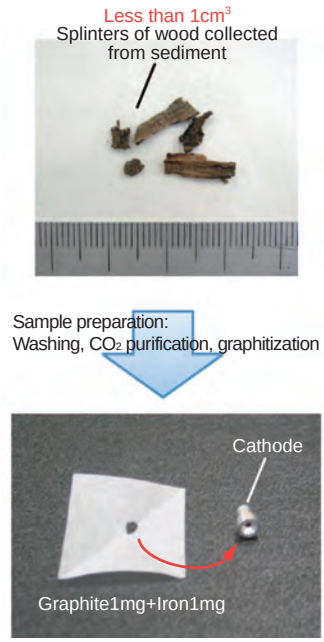

Fig.2-13 Preparation of a measuring sample
A sample such as a wood chip collected in sediment was pretreated and then was mixed with iron powder to make a measuring sample. A hole (1mm) in a cathode was filled with the sample. The cathode was loaded into the spectrometer.

Fig.2-14 Gravel beds at the upper reaches of Azusa River and sample collection place
Fossil wood collected from the beds was measured. Age taken to be the average of results of 4 samples.

Radiometric dating method is used to study when past geological events such as earthquake and volcanic activity occurred. The method using radiocarbon is based on the rate of decay of ^{14}C ($T_{1/2}$=5730 y), which is formed through the effect of cosmic ray neutrons upon ^{14}N. This method is one of the most powerful methods of dating from modern times back to about 60,000 years ago. As plants and animals utilize carbon for photosynthesis or respiration during their lifetimes, they exist in equilibrium with the concentrations of carbon isotopes (^{12}C, ^{13}C and ^{14}C) of the atmosphere. After the plants or animals die, ^{14}C in them only decay. A measurement of the ^{14}C content of a sample can provide a determination of the sample's age.

By using an accelerator mass spectrometer installed at the Tono Geoscience Center (Fig.2-12), the number of ^{14}C atoms in 1mg of a carbon sample can be measured. The advantage of the AMS method is that a smaller amount of the sample is sufficient for dating than with radioactivity measurement. For example, a few hundred liters of groundwater was required to measure ^{14}C by the radioactivity measurement. On the other hand, measurement of about 1 liter of the sample by the AMS method can provide the same level of precision. Therefore, utilization of the AMS method enables us lighten our burden of sample collection and measure a small sized sample.

In the prediction of future changes in a geological environment being considered for geological disposal, it is necessary to understand their history of geological events. For example, in studies of formational process of river terrace and plain, and development process of an active fault, carbon in 1cm^3 of a wood chip or a shell collected in sediment was measured to determine depositional age (Fig.2-13). We studied the terrace along the Azusa River between Matsumoto and Kamikouchi in Nagano. Concentrations of ^{14}C in fossils of wood chips collected at gravel beds were measured. These results indicated that these beds were deposited 48,000 years ago (Fig.2-14). This accurate formation age of this terrace is basic information needed to understand changes in the flow upstream of the Azusa River and the evolutional history of geographical features around this area.

Radiocarbon dating by the accelerator mass spectrometer can be used to measure geological sample containing carbon such as wood chips, bones and ground water. We have made use of this method to get an understanding past geological events, which we need for the prediction of a future changes in the geological environment. Moreover, we will develop dating method of ^{10}Be etc.

References

Ishimaru, T. et al., The Current Condition and Utilization of JAEA-AMS-TONO, JAEA-Conf 2008-003, 2008, p.17-20 (in Japanese).

Oikawa, T., Sasao, E. et al., Re-^{14}C Dating of Wood Fossils from the Gravel Bed at Sebadani, the Upper Reaches of Azusa River, Central Japan, Dai-4-Ki Kenkyu, vol.47, no.6, 2008, p.425-431 (in Japanese).

2-6 Effective Groundwater Flow Modeling and Analysis

— Development of Efficient Modeling and Analysis System for Complicated Groundwater Flow —

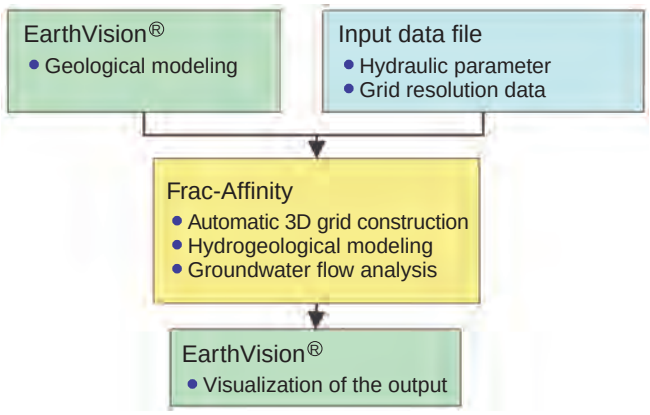

Fig.2-15 Working flow of GEOMASS system
The GEOMASS system creates a 3D geological model using a commercial system (EarthVision®), efficiently and flexibly integrating hydrogeological modeling (Frac-Affinity) results.

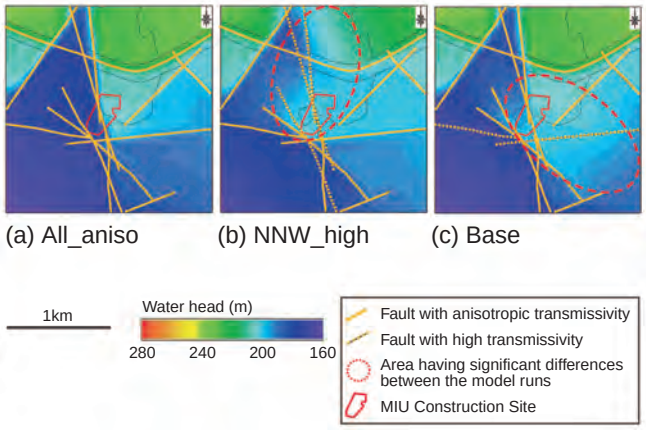

Fig.2-16 Hydraulic head distribution based on result of sensitivity analysis
Several sensitivity cases are set with different fault transmissivity values.
(a) All faults are modeled with anisotropic transmissivity.
(b) Only NNW faults (shown by yellow dashed lines) have high transmissivity.
(c) Only E-W faults (shown by yellow dashed lines) have high transmissivity.

For research and development of geological disposal of high-level radioactive waste, it is important to improve the methods of evaluating groundwater flow deep underground. For characterization of groundwater flow, modeling of faults and fractures are particularly essential because these geological features have a significant effect on the groundwater flow in the rock mass. However, significant time and effort is also required for modeling and analysis as the complexity of the geological and hydrogeological environment increases. To deal with this problem, the GEOMASS (Geological Modelling Analysis and Simulation Software) system has been under development since 1997. A simplified work flow diagram of the GEOMASS system is shown in Fig.2-15. In the system, 3D geological models development by EarthVision® are integrated with automatic numerical analysis, including groundwater flow simulations and hydrogeological grid generation, by Frac-Affinity.

In the MIU Project (Mizunami Underground Research Laboratory Project), based on the results of the surface-based investigation, and construction phases, geological and hydrogeological models have been revised and groundwater flow simulations have been carried out using the GEOMASS system.

Sensitivity analyses using the revised models were carried out to evaluate the impact of the hydraulic properties of faults on groundwater flow in many simulation cases varying the permeability of faults. Examples of the results are shown in Fig.2-16. It is clear that hydraulic head distribution is significantly influenced by permeability of faults and therefore, that faults are a major influence on groundwater flow in the deep underground. The GEOMASS system provides users with important and uncertain factors, after which the main issues for further investigation can be identified through modeling and simulation work.

Moreover, groundwater flow analysis can be carried out to predict the inflow rate of groundwater into the shafts and galleries as excavation progresses and thus can provide a comparison between predicted and measured inflow rates. These results can rapidly and effectively be input into the design of shafts, galleries, water treatment facility, and so on.

The GEOMASS system allows users to reduce time and effort for geological and hydrogeological modeling, groundwater flow simulations, and modification of models. This capability of the GEOMASS system enables the integration of the investigations and the construction of the geological environment models during shaft excavations. Confirmation of the applicability and accuracy of the GEOMASS system for site characterization will continue, and modifications will be made to this system according to need.

Reference

Ohyama, T. et al., GEOMASS : The Application to Characterizations of Groundwater Flow in the Mizunami Underground Research Laboratory Project in Tono Area, Proceedings of 36th International Association of Hydrogeologists Congress (IAH 2008), Toyama, Japan, 2008, p.807-815, in CD-ROM.

2-7 Searching for the Spatial Distribution of Rock Fractures
—Modeling of Fracture Density Based on Geological Interpretation—

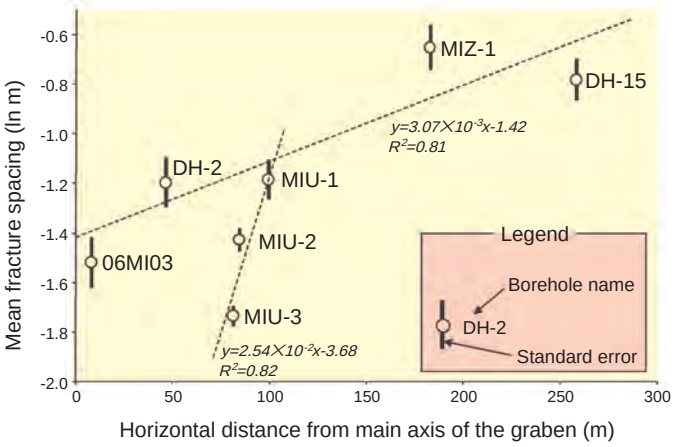

Fig.2-17 Scattergram between mean fracture spacing and horizontal distance from the main axis of a graben

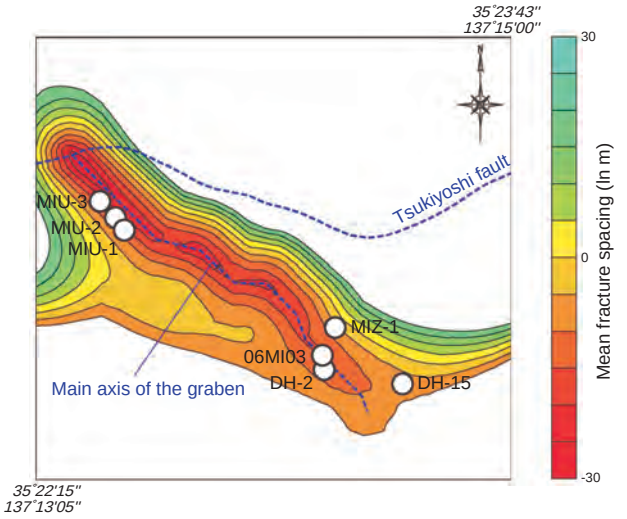

Fig.2-18 Contour map of estimated fracture density distribution (Tsukiyoshi fault line and the main axis line of a graben show trace lines on unconformity)

Since it has long been recognized that fractures in rock influence the distribution of groundwater flow and stress in the bedrock, determining the spatial distribution of fractures is important for deeper understanding of the characteristics of the bedrock. When extrapolations of the spatial distribution of rock fractures from limited borehole data are made, the extrapolation may be supported in areas with no data by empirical interpretations that geological engineers or researchers have made with information from previous investigations and the literature documenting the properties of similar geological environments. However, because empirical interpretation depends on knowledge, experience and capabilities of the geoscientists, it often lacks certainty. In this study, we attempted to develop an objective estimation method of distribution of fracture density applied to the Tono region (in Gifu prefecture, Central Japan), paying attention to the relative fracture density and distribution of geological structures (Tsukiyoshi fault and a graben on unconformity) determined by empirical interpretation. We established the following two working hypotheses on the assumption that the distribution of fracture density is related to the distribution of geological structures: (1) the fracture density increases with proximity to a fault and, (2) the fracture density increases with proximity to the intersection between faults. Secondarily, with the aim of confirming the working hypotheses, we examined the relationship between the horizontal distance from the geological structure to each borehole and the mean fracture spacing which was calculated from the distribution of fractures at each individual borehole and which was adopted as the index of fracture density.

As a result of this examination, we confirmed that there is a positive correlation between the mean fracture spacing and the horizontal distance from the geological structure to each borehole (Fig.2-17), and recognized that this correlation supports working hypothesis No.1. Moreover, working hypothesis No.2 is also supported, since the mean fracture spacing of boreholes (MIU-1 to 3) located close to the intersection of the Tsukiyoshi fault and the main axis of a graben is smaller than other boreholes, indicating that the distribution of fracture density is heterogeneous according to the distribution of geological structures. Such a heterogeneous structure of fracture density can be visualized as a contour map (Fig.2-18) reflecting the empirical interpretation, approximated as a trend surface by a first order polynomial function, allocating mean fracture spacing to geometrically calculated arbitrary points by entering the horizontal distance from the geological structures in the trend surface function.

The results of this study suggest that the geological phenomena which have been judged subjectively or uniquely by empirical interpretation can be represented objectively. Therefore, we consider that the analysis in this study is an effective method for extrapolation from limited spatial data to the heterogeneous distribution of characteristics of fractured rock such as fracture density.

Reference

Kurihara, A. et al., Characterization and Tectonic Significance of Low-Angle Fracture Distribution in the Upper Part of a Granite Body: New Insight from the Toki Granite around the Mizunami Underground Research Laboratory (MIU), Central Japan, Journal of MMIJ, vol.124, no.12, 2008, p.710-718 (in Japanese).

2-8 Estimation of Fracture Connectivity from One-Borehole Data
－Fracture Investigation of Sedimentary Rocks－

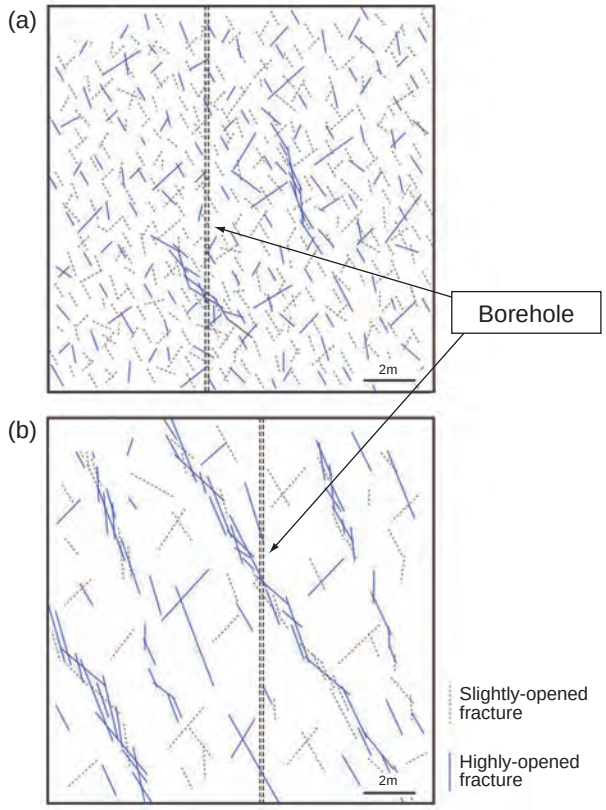

Fig.2-19 Conceptual model for connectivity of fractures
(a) Koetoi Fm: open fractures do not connect
(b) Wakkanai Fm: open fractures connect relatively often

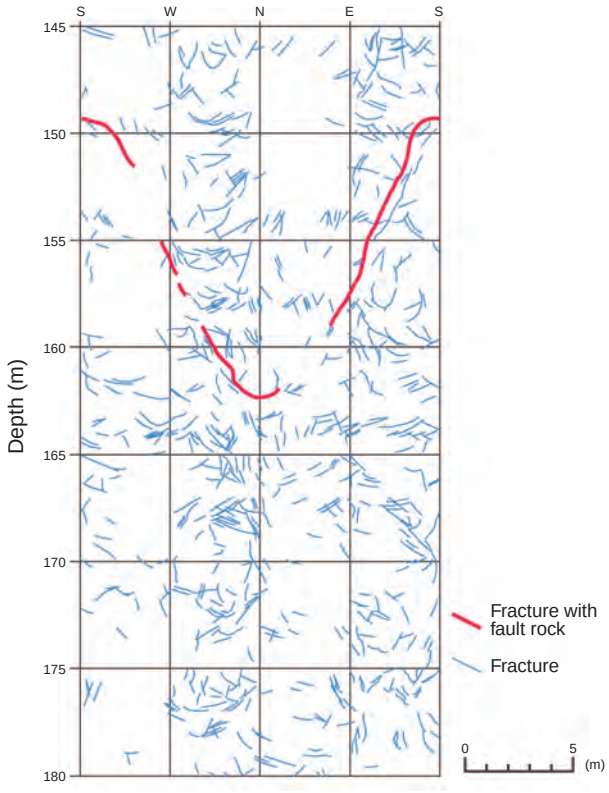

Fig.2-20 Observed fractures in shaft wall
A result of observation of the wall of the ventilation shaft (cylindrical: diameter 4.5m) currently being built near a borehole in the Koetoi Formation. The diagram indicates the fractures of over 50cm length.

In characterizing a sedimentary rock for modeling and numerical analysis of groundwater flow, it is important to assess how much highly-opened fractures connect with each other below the surface. There is a method for evaluation of connectivity of highly-opened fractures below the surface which measures the water pressure change in several boreholes unconnected to each other and one which observes the wall of an actually excavated tunnel. However, in the early stages of investigation, more information on fracture connectivity must be produced from a few boreholes drilled from the surface.

In order to examine how much the fractures connect in the sedimentary rocks of the Koetoi and Wakkanai Formations, in the Horonobe area in northern Hokkaido, we investigated the proportion of fractures which actually act as main water conducting passages of groundwater among the highly-opened fractures found in one borehole (drilling depth: 520m). Even if fractures are widely opened, in the case of rock where fracture connectivity is not high, those open fractures generally cannot be a main flow path. On the contrary, in the case of the rock where fracture connectivity is high, even if the fracture openings are not wide, those open fractures will easily conduct water.

These statistical results suggest that fractures in the Koetoi Formation are not connected at all, and fractures in the Wakkanai Formation are connected relatively more (Fig.2-19). This lack of fracture connectivity in the Koetoi Formation was indicated by observation of the ventilation-shaft wall constructed recently near a borehole, which revealed no connected fractures more than a few meters long (Fig.2-20).

Reference

Funaki, T., Ishii, E. et al., Evaluation of the Role of Fracture as the Major Water-Conducting Feature in Neogene Sedimentary Rocks, Oyo Chishitsu, vol.50, no.4, 2009, p.238-247 (in Japanese).

2-9 Findings of Long-Term Groundwater Pressure Monitoring
—Analysis of Groundwater Pressure Measurements in Sedimentary Rock—

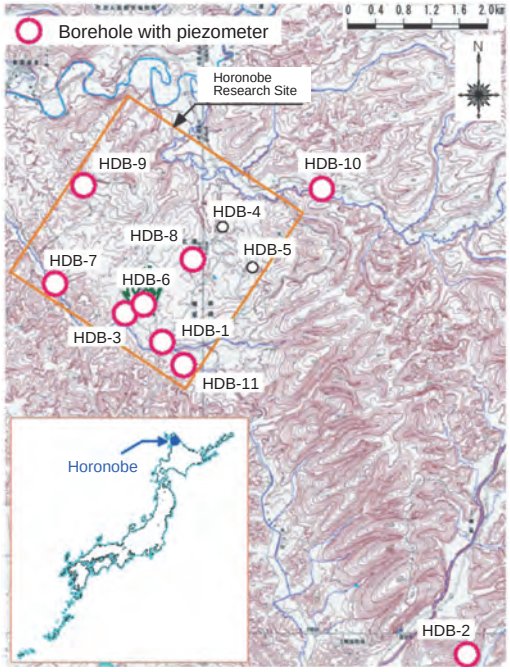

Fig.2-21 Borehole location map

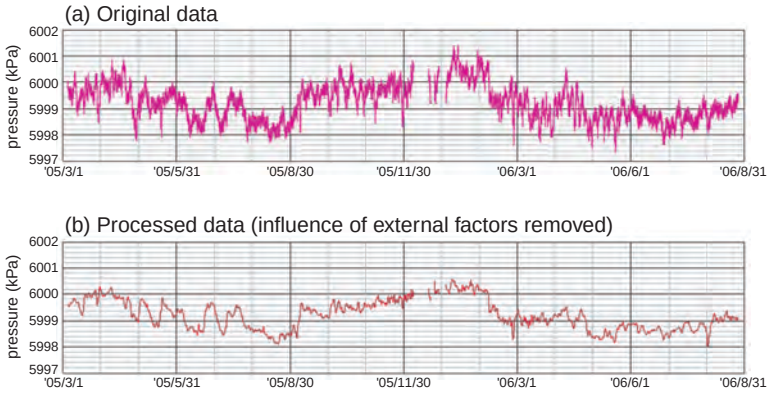

Fig.2-22 BAYTAP-G (Tamura, Y. et al., Geophysical Journal International vol.104, 1991), Example of groundwater pressure monitoring data (HDB-6: 585-620m in depth)

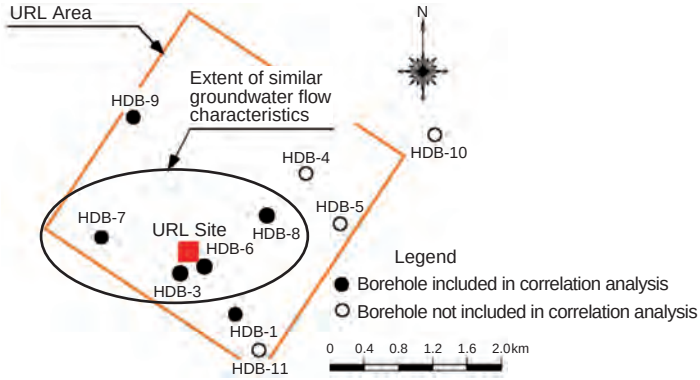

Fig.2-23 Image of area with similar groundwater flow characteristics (400m in depth)

Long-term groundwater pressure monitoring in the boreholes at Horonobe Underground Research Laboratory, Hokkaido, Japan was performed before the shaft excavation. The location of the monitoring boreholes is shown in Fig.2-21. Groundwater pressure around the shaft is expected to vary significantly due to the shaft excavation. Observation of the groundwater pressure variation will reveal the characteristics of groundwater flow and hydrogeological properties around the shaft.

An example of the groundwater pressure monitoring data is shown in Fig.2-22(a). This was collected from Mar. 2005 to Aug. 2006, before the shaft excavation. Pressure fluctuations due to atmospheric pressure variation and tidal forces were observed in the collected data. Such fluctuations can be removed by the well-known program called BAYTAP-G. Using this program, data analysis was performed for the data of 48 monitoring intervals.

Magnitude of the pressure fluctuation component due to tidal forces was from 0.01kPa to 0.08kPa, and that due to atmospheric pressure variation was from 0.05kPa to 0.6kPa. It was clear that the component of tidal forces was generally smaller than that of atmospheric pressure variation. Magnitude of the fluctuation in the groundwater pressure in the Horonobe area due to tidal forces is thought to be less than 0.1kPa. Distribution of the groundwater pressure which effects on groundwater flow can be obtained by removing such components from the observed pressure as shown in Fig.2-22(b).

Cross-correlation analysis was performed for the data sets after these components were removed. Relatively large cross-correlation coefficients were found among the HDB-3, HDB-6, HDB-7 and HDB-8 boreholes at around 400m in depth. This would imply that the characteristics of groundwater flow are quite similar around these boreholes shown in Fig.2-23.

Reference

Nakajima, M., Seno, S., Toida, M., Kunimaru, T., Sensitivity Analysis on Influence Factors of Pore Water Pressure Fluctuation in Horonobe Site, Proceedings of 36th International Association of Hydrogeologists Congress (IAH 2008), Toyama, Japan, 2008, p.1170-1178.

2-10 Estimation of Excavation Stability from Measurements
—Application of Observational Construction to Sedimentary Formations—

Table 2-2 Measurement item and use of result

observation / investigation item	use of result (item)										
	(1) construction of underground facilities				(2) research and development on advancement of tunnel design and execution technology						(3) geological feature research
	daily management		step management								
	verification of excavation surface and support selection	monitoring of existing support and evaluation of long-term stability	modification of behavior model and measurement control criterion	feedback for design and execution of later steps	verification of design technology in actual use	studies for rational evaluation of rock mass	studies for advancement of rock foundatoin model	comparative analysis on mechanical excavation disturbance due to difference of shaft excavation method / diameter	analysis of long-term behavior of rock foundation after excavation	studies for risk management of underground facilities	investigation and verification of environmental model
excavation surface observation	●	○	○	○	●	●	○	○	○	○	●
elastic wave velocity		△				●					○
schmidt hammer		△				●					○
equotip hardness test		△				●					○
needle penetration test		△				●					○
point load test		△				●					○
convergence	△	●	●	○	●	●	○	○	○	○	△
underground displacement			●	○	●		○	○	●	○	△
rock bolt axial tension		○	●	○	●		●	○	●	○	
shotcrete stress		○	●	○	●		○	○	●	○	
lining concrete stress		○	●	○	●		○	○	●	○	
steel support stress		○	●	○	●		○	○	●	○	
preceding displacement			●	○	●		●	○		○	△
borehole load test			○	○	●						○
unconfined compression test			○	○	●						○
triaxial compression test			○	○	●						○
brazilian test			○	○	●						○

● : key item ○ : taken into consideration △ : referred to in considerations

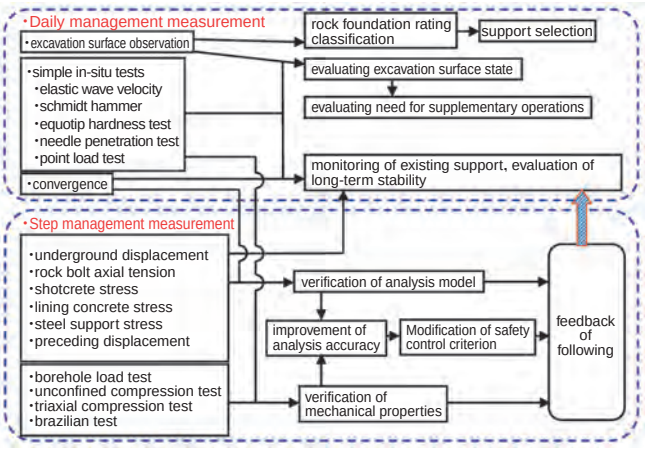

Fig.2-24 Observational construction flow

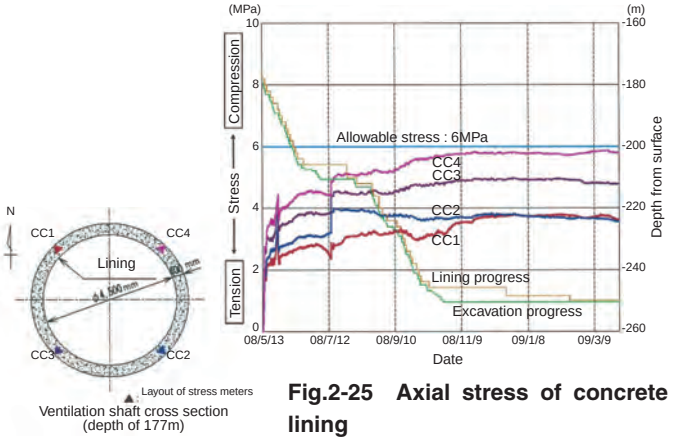

Fig.2-25 Axial stress of concrete lining

In construction of the underground facilities, it is difficult to accurately predict deep geological environmental features by surface-based investigation. Therefore, the observational construction plays an important role in achieving safe and rational construction. The stability of underground facilities is estimated by excavation surface observation and measurements of deformation and stress during construction. This estimation of stability is used as feedback for design and construction in subsequent steps.

Sedimentary formations around the underground facilities at the Horonobe URL Project are became mainly neogene sedimentary rocks (diatomaceous mudstone, siliceous mudstone). They are classified as soft rock from a strength aspect. The observational construction in sedimentary soft rocks has been uncommon. Thus, at the beginning of construction of these underground facilities, a plan for measurements and observational construction program based on the operations design was set.

The measurement plan included (1) consistency with safe and rational construction of the underground facilities, (2) feedback of measurements into design and construction of subsequent steps, (3) verification of the geological environmental model. Specific items which are being measured and utilized are shown in Table 2-2.

Also, the observational construction program being carried out is divided into two main classes. One is daily measurement that is aimed at selection of excavation support methods and monitoring of existing support, the other is step management measurement that is aimed at verification of analysis models and feedback to following steps. These are shown in Fig.2-24.

As an example, axial stress of the concrete lining at the depth of 177m from the surface in the ventilation shaft is shown in Fig.2-25. It can be seen that all lining stresses are under the allowable stress (6MPa), but the maximum stress at CC4 is almost the allowable stress and prediction analysis value. In addition, stress at CC3,4 is almost 1.3~1.5 times that at CC1,2 due to the direction of the major horizontal principal stress. It has been found to be in the east/west direction, and the minor principal stress is in the north/south direction (principal stress ratio is 1.4) from surface-based investigation. Judging from the above, the support of the underground facility is rational and underground facility is safe.

This measurement plan and the observational construction program will be continue to be carried out.

Reference

Yamasaki, M. et al., Observational Construction and Behavior Measurements for Underground Research Shaft Excavation of the Horonobe Underground Research Laboratory Project, The 12th Japan Rock Mechanics Symposium, 2008, p.305-311, in CD-ROM. (in Japanese).

3 Nuclear Fusion Research and Development

Toward Practical Use of Fusion Energy

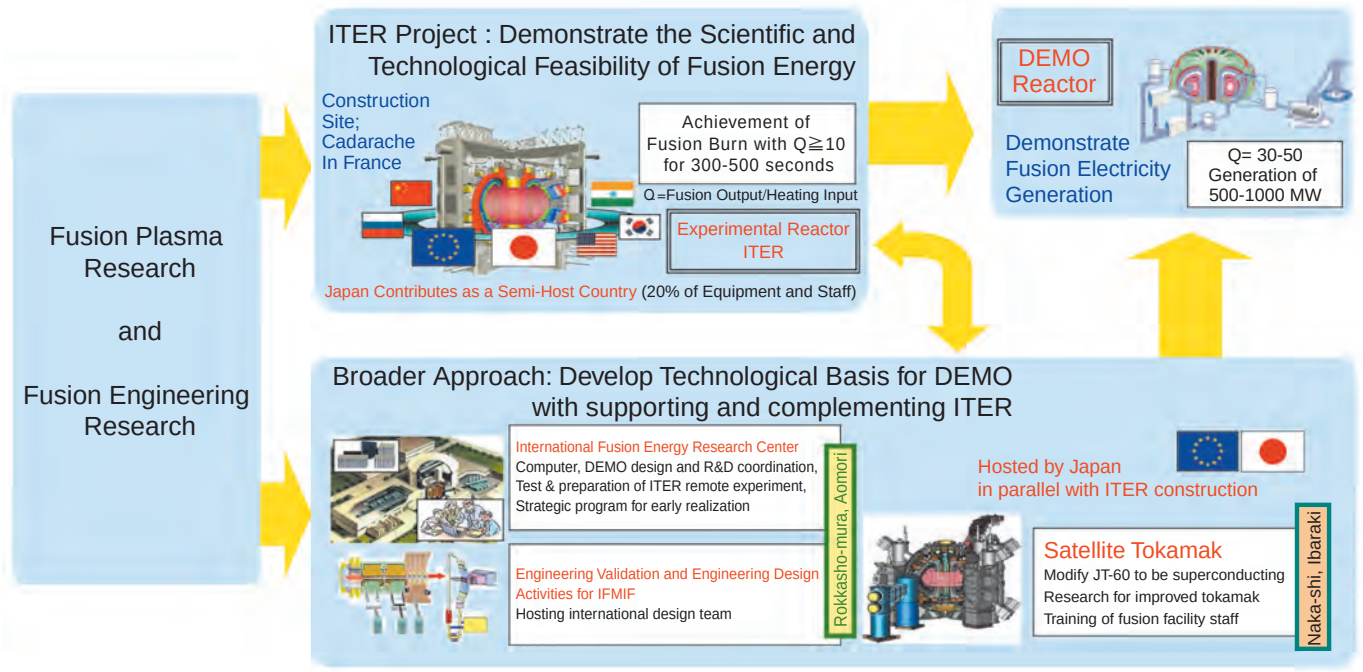

Fig.3-1 Development Steps toward the Fusion DEMO Reactor

In Fusion Research and Development Directorate, crucial R&D toward practical use of fusion energy (fusion plasma and fusion engineering R&D) has been pursued through intensive international cooperation such as International Thermonuclear Experimental Reactor (ITER) project and Broader Approach (BA) activity etc., aiming at realization of the fusion DEMO reactor (Fig.3-1).

ITER Project

The ITER project is an international cooperative project to demonstrate the scientific and technological feasibility of fusion energy through construction and operation of an experimental reactor. The ITER agreement entered into force in October 2007, and JAEA was designated as the domestic agency of the ITER project in Japan. JAEA has proceeded with the preparation of the equipment that Japan was allotted to provide, achieved technological development which leads the world, concluded a procurement agreement with ITER Organization before any other country, and has started the production of the superconducting coil conductor.

BA Activity

The BA activity is a joint project by Japan and EU, which executes the support research for ITER and the research and development for a DEMO reactor, the next step of ITER, aiming at the early realization of fusion energy. The BA agreement entered into force in June 2007, and JAEA was designated as the implementing agency of BA activity in Japan. JAEA is steadily advancing the production of the equipment that Japan was allotted to provide.

Fusion Plasma Research

JT-60 greatly contributed to fusion R&D for many years as the core device in fusion plasma research, and 23 years and 4 months of experimentation was completed on August, 2008. JT-60 achieved a lot of world records, and recently R&D to enhance the plasma pressure, aiming at improvement of the economy of the fusion reactor, was pursued aggressively with it. A world record in the time high-pressured plasma was maintained was achieved in the final fiscal year of experiments. The results of JT-60 obtained over the past years are considered highly valuable throughout the world, as was seen at the 22nd IAEA Fusion Energy Conference held in Geneva in October, 2008, where all participants stood up and respectfully applauded the completion of experiments after the overview presentation of JT-60 on the first day of the conference. The upgrade of JT-60 to JT-60SA is now in progress in a combined program of the Satellite Tokamak Project in the BA and the National Centralized Tokamak Project.

Fusion Engineering Research

The kinetic energy of the neutron generated with the reaction is converted into heat with a blanket which is situated to enclose plasma, and the heat is extracted in the fusion reactor. The R&D to develop the technological foundation necessary for the fusion reactor, such as effective method for extraction of the heat and materials that can endure irradiation with neutrons etc., is being performed.

3-1 Successful Instability Suppression by Fast Turn-On/Off of 600kW Millimeter Waves

—Demonstration of Effective Method for Instability Suppression in ITER—

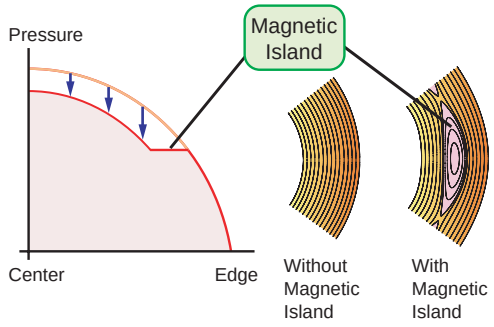

Fig.3-2 Pressure profiles with and without magnetic island

Fusion plasma is confined by nested magnetic field lines. If a magnetic island appears, heat and particles are lost, and as a result the plasma pressure decreases. The magnetic island can be shrunk and eliminated by pinpoint injection of millimeter (MM) waves in the magnetic island (Typical island width is 10cm).

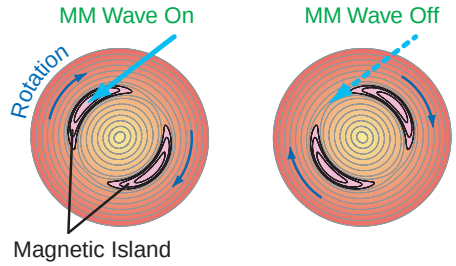

Fig.3-3 Plasma cross section with magnetic islands

Magnetic islands are rotating in the plasma. By turning on/off the MM waves very fast (typically several kHz), the waves can be injected only inside the magnetic islands.

In a fusion reactor, a high-pressure plasma needs to be sustained for a long time. However, instabilities tend to appear as the plasma pressure increases. Since the instabilities cause loss of heat and particles, and as a result, decrease of the plasma pressure, suppression of the instabilities is necessary to sustain a high-pressure plasma. Neoclassical Tearing Mode (NTM) is an instability which appears in a high-pressure plasma, and thus its suppression in ITER is a high priority. When an NTM does not exist, a plasma is confined by nested magnetic field lines. However, if an NTM appears, a structure called 'magnetic island' is formed in the plasma, and the plasma pressure decreases as shown in Fig.3-2. To suppress the NTM, it is effective to drive current locally in the magnetic island region by injecting millimeter (MM) waves. The method was previously proven effective experimentally in JT-60 using 110GHz MM waves (Wavelength is about 3mm). Current drive limited to the inside of the magnetic island (Fig.3-3) is considered more effective because current drive outside the magnetic island strengthens the NTM. However, experimental verification of this scheme was incomplete due to technical difficulties in modulating high-power MM waves at several kHz and synchronizing them with the rotation of the magnetic island.

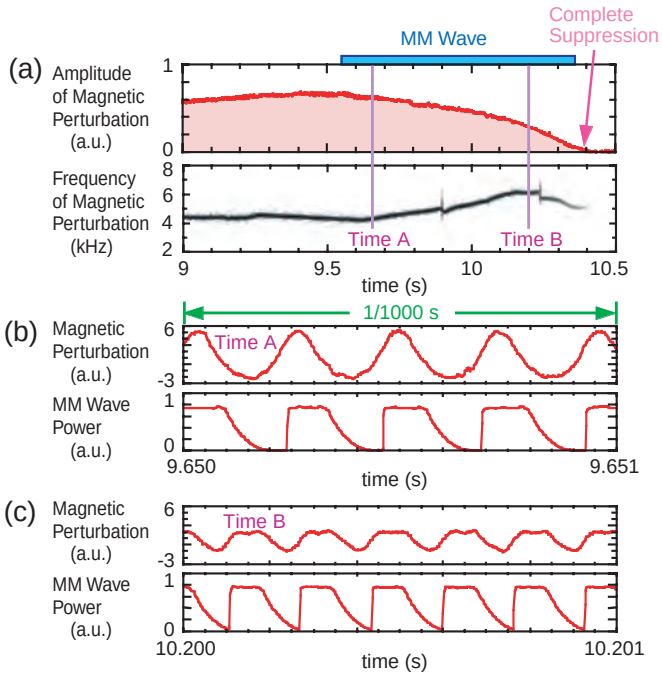

Fig.3-4 Demonstration of instability suppression

(a) Amplitude and frequency of magnetic perturbations. The frequency is increasing with time. (b)-(c) Magnetic perturbation signal and MM wave power. Although the frequency of the magnetic perturbations is changing, MM waves are turned on/off in accordance with the change. As a result, the instability (i.e. magnetic island) is suppressed completely.

To verify the effectiveness of this scheme, we have (1) upgraded gyrotrons (sources of MM waves) to modulate the output power, which is typically several hundreds to a thousand kW, at the frequency of higher than 5kHz, and (2) developed a system to generate a trigger signal synchronized with the NTM rotation by processing the magnetic perturbation signal in real time. An example of the synchronized power modulation is shown in Fig.3-4. While the frequency of the NTM rotation is about 4kHz at time A, it gradually increases to about 6kHz at time B. Figs.3-4(b) and 3-4(c) show the magnetic perturbations and the injected MM wave at time A and B, respectively. It can be seen that the period and pulse width of the modulated power is properly set according to the change in the rotation frequency. This kind of automatic optimization has never been performed in any other devices, and JT-60 is the first device to succeed in demonstrating it. It has also been clarified that the suppression effect for the modulated case is more than twice effective than that for unmodulated cases. Since NTM suppression by power modulation of a 170GHz MM wave at about 5kHz is planned in ITER, experimental verification of the suppression effect was eagerly anticipated. This result is important because it verifies the scenario for effective suppression of an NTM in ITER.

Reference

Isayama, A. et al., Neoclassical Tearing Mode Control Using Electron Cyclotron Current Drive and Magnetic Island Evolution in JT-60U, Nuclear Fusion, vol.49, no.5, 2009, 055006, p.1-9.

3-2 Improved Precision of ITER Plasma Predictions

—Parameter Determining Width of Edge Transport Barrier (ETB) Elucidated—

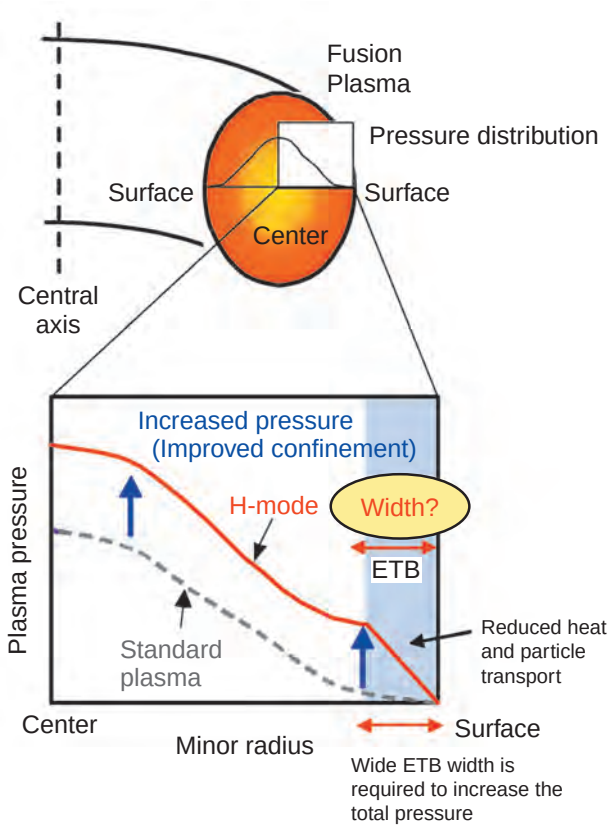

Fig.3-5 Spatial profile of plasma pressure in H-mode
Sufficiently heated fusion plasmas experience ETB formation, which increases the total plasma pressure. This state is called H-mode. It is important to predict the operational conditions where the ETB extends as wide as possible, to obtain sufficient fusion gain.

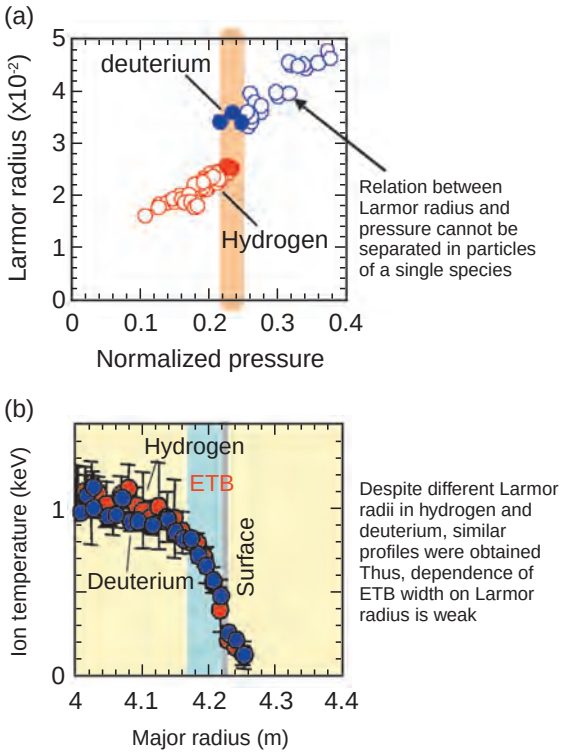

Fig.3-6 (a) Relation between normalized pressure and Larmor radius, (b) Ion temperature profiles in hydrogen and deuterium plasmas
Influences of normalized pressure and of Larmor radius on ETB width were successfully separated. Similar temperature profiles indicate that dependence of ETB width on Larmor radius is weak.

Since the fusion gain is proportional to the square of plasma pressure, sustainment of high pressure plasma in a steady state is required to realize the fusion reactor. As shown in Fig.3-5, ITER will operate in the H-mode where the edge transport barrier (ETB) is formed to reduce the heat and particle transport at the plasma edge. In particular, the edge structure in H-mode plays a role as a boundary condition for core plasma and thus strongly influences the fusion gain. Therefore, it is important to clarify the underlying physics of edge structure in H-mode. The prediction of the spatial width of ETB is one of the most crucial issues in ITER development.

Plasma characteristics can simply be expressed by three physical quantities: collisionality, Larmor radius, and normalized pressure. However, due to the existence of magnetohydordynamic instabilities, Larmor radius and normalized pressure are strongly linked. Hence, it has been hard to identify which of these parameters determined the edge structure. In JT-60U, by focusing on the difference of Larmor radius in hydrogen and deuterium, the influences of normalized pressure and of Larmor radius were successfully separated, and dependence of ETB width on these quantities was found. As shown in Fig.3-6, Larmor radius and normalized pressure are strongly linked where there is a single species of particle, but the effects of these parameters on ETB width were separated for the first time in the world by introducing hydrogen and deuterium plasmas. It was found that ETB width depends weakly on Larmor radius and strongly on normalized pressure. Since Larmor radius in ITER is expected to be smaller than in present tokamaks, this result indicates that ETB width in the future device is wide enough to obtain required fusion gain.

Reference

Urano, H. et al., Dimensionless Parameter Dependence of H-Mode Pedestal Width Using Hydrogen and Deuterium Plasmas in JT-60U, Nuclear Fusion, vol.48, no.4, 2008, 045008, p.1-9.

3-3 Study of Disruption Phenomena in Advanced Plasmas
—Clarification of Plasma Flow and Multi-Stage Phenomena—

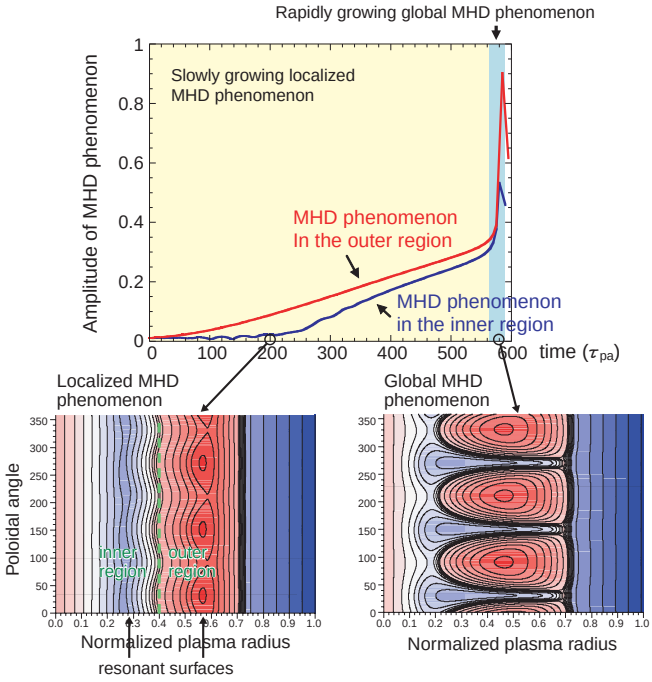

Fig.3-7 Evolution of the MHD phenomenon in advanced plasma
Time is normalized to characteristic period of the wave in the system, τ_{pa}=0.1μs. The MHD phenomenon appears in the outer region during the initial phase (t<250). In the rapid growth phase of the MHD phenomenon (t>560), a global MHD phenomenon extends in the radial direction.

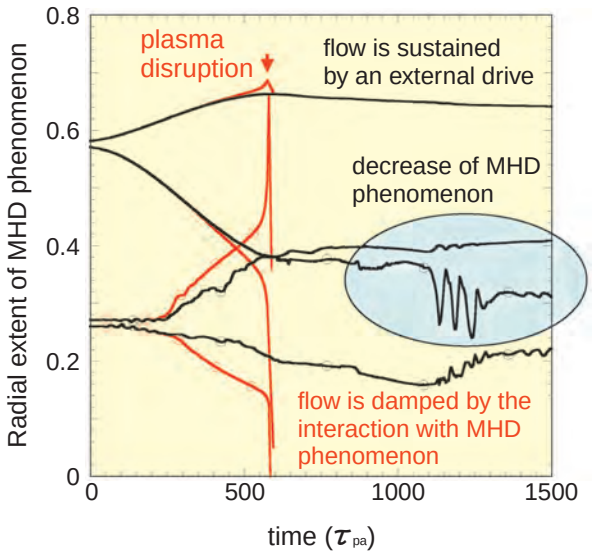

Fig.3-8 Avoidance of the low pressure disruption by the plasma flow in the advanced plasma discharge
Time is normalized by characteristic time of the wave in the system, τ_{pa}=0.1μs. When the plasma flow is sustained by the external drive, the MHD phenomenon does not lead to the plasma disruption.

Rapidly growing global magnetohydrodynamic (MHD) phenomena sometimes suppress plasma performance and damage plasma facing components in tokamak devices. It is an important research task to clarify the origin of such MHD phenomena and to find effective controlling methods. An advanced plasma discharge where the input power for the current drive can be less than in the standard plasma discharge is expected to be one of the ways to realize an economical fusion reactor. However, in these advanced plasma discharges, plasma disruptions occur in low plasma pressure regions more frequently than in standard ones. These plasma disruptions prevent realization of the advanced plasma discharge. The former linear theories could not account for the low pressure disruptions observed in the advanced plasma discharges. The low pressure disruption often has a slowly growing precursor seen before a rapidly growing disruption. Though these precursors can be utilized as a signal to predict the low pressure disruption, the causal relationship between them has not yet been clarified. In the present experiment, a series of phenomena were observed in the following order,

(1) A slowly growing localized MHD phenomenon appears at the outer or the edge plasma region.
(2) Rapidly growing global MHD phenomenon appears in a wide region including the plasma center.
(3) Low pressure disruption occurs.

In Numerical EXperiment of Tokamak project (NEXT), the plasma flow existing commonly in tokamak plasmas was focused on. The numerical simulation based on the MHD model including the plasma flow effect was executed in order to clarify the causal relationship among (1), (2) and (3). As a result, we found that experimentally observed phenomena of (1), (2) and (3) are not independent events, but one continuous phenomenon (multi-stage phenomenon) (Fig.3-7). The plasma flow plays an important role of preventing the information transfer between two regions divided by the plasma flow. In multi-stage phenomena found in this study, the originally global MHD phenomenon localizes around the outer resonant surface due to the screening effect of the flow. Such a localized MHD phenomenon, which is observed as a precursor, damps the plasma flow and extends between two resonant surfaces to trigger the low pressure disruption. Based on this finding, we propose searching for stage (1) as a precursor of the stage (3), and preventing the low pressure disruption in the advanced plasma discharge by maintaining the plasma flow (Fig.3-8).

Reference

Ishii, Y. et al., Plasma Rotation Effects on Magnetic Island Formation and the Trigger of Disruptions in Reversed Shear Plasmas, Nuclear Fusion, vol.49, no.8, 2009, 085006, p.1-10.

3-4 World Record in Longest Injection of High Power Neutral Beams above 1MW
—Towards a 100s Injection for JT-60SA—

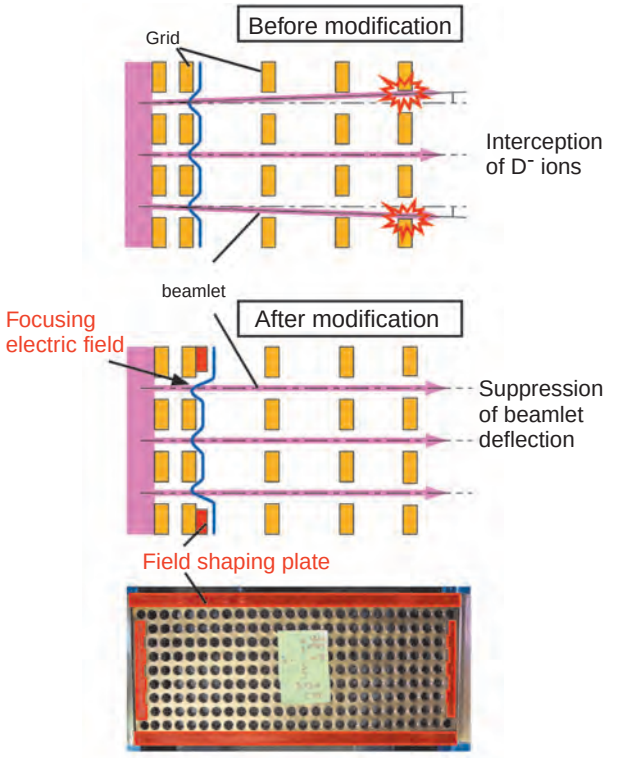

Fig.3-9 Schematic diagram of beam trajectories before and after modification
Field shaping plates (FSP), which create the focusing electric field near the outmost apertures, suppress the outward deflection of the outermost beamlets, resulting in the reduction of the grid power loading.

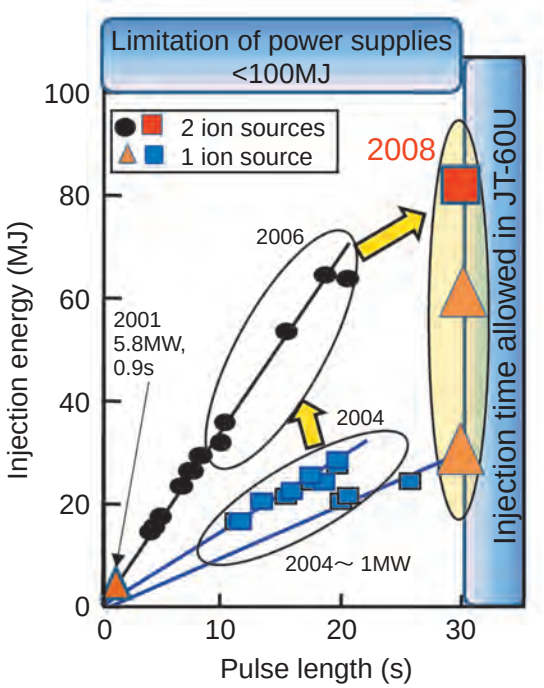

Fig.3-10 Injection energy achieved in negative-ion-based NBI (N-NBI) in JT-60U
We started long pulse injection of D^0 beams from a negative ion source in 2004, and from two ion sources in 2006. By reducing the power loadings of the acceleration grids in the ion sources, we succeeded in injecting the D^0 beams of 1MW and 2MW for 30s.

Neutral beam injection is one of the promising methods for plasma heating. Neutral beam injectors (NBI) has been utilized in many experimental fusion devices, and will be used as the primary heating method in ITER and JT-60SA. In NBI, high energy deuterium ions are produced in an ion source and converted to neutral beams in a gas cell. The residual ions are removed and dumped, and only D^0 beams are delivered into the plasma. High energy D^0 beams of 0.5-1.0MeV are required to heat the core plasma in ITER and JT-60SA. In this energy range, the NBI is required to use high energy D^- ions because neutralization efficiency of the D^- ions is much higher than that of the D^+ ions.

In ITER and JT-60SA, the injection pulse length is required to be range from 100 to 1000s which is 10-100 times longer than the rated pulse length of the negative-ion-based NBI (N-NBI) in JT-60U, 10s. To develop a long pulse N-NBI, the feasibility of long pulse injection in JT-60U was experimentally examined. One of the key requirements for long pulse injection is reduction of the power loading of the acceleration grids in the ion source.

The origin of the grid power loading was examined by calculating the beam trajectories with a 3 dimensional code. The calculation results showed that the outmost beamlets are deflected outward due to space charge repulsion and are intercepted by the acceleration grids. To suppress direct interception by the acceleration grids, a field shaping plate (FSP) was designed to deflect the outmost beamlets inward. The FSPs were installed near the outmost apertures of the acceleration grids (Fig.3-9). The use of the FSP successfully reduced the grid power loading to 500kW, an allowable level for long pulse operation. Since the ITER ion source has a structure of the accelerator similar to that of the JT-60 negative ion source, the FSP is expected to be effective for the ITER ion source as well.

The reduction of the grid power loading led to a 30s-pulse injection of 2MW D^0 beams from each ion source (Fig.3-10). This is the world record for longest injection of high power neutral beams above 1MW. In this long pulse operation, the temperature of cooling water for the acceleration grid leveled off at lower than the maximum allowable level after 25s from the onset, and thus the existing water cooling system is expected to be sufficient for ITER and JT-60SA. The long pulse injection significantly contributed to a 28s-pulse production of high-β plasma of β_N=2.6, which is equivalent to twice the output power of the ITER standard operation.

Reference

Hanada, M. et al., Development of Long Pulse Neutral Beam Injector on JT-60U for JT-60SA, Proceedings of 22nd IAEA Fusion Energy Conference (FEC 2008), Geneva, Switzerland, 2008, FT/P2-27, 8p.

3-5 JAEA's Accelerator Chosen for ITER NBI
—Comparative Test of Accelerators for Neutral Beam Injector—

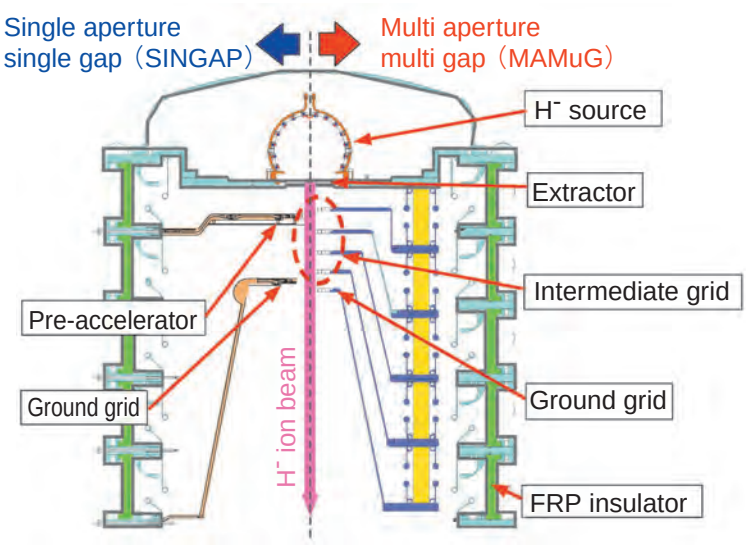

Fig.3-11 Comparison between SINGAP and MAMuG
The advantage of the SINGAP accelerator is its simplicity due to the absence of intermediate grids. However, electrons produced in the accelerator are accelerated to high energy. On the contrary, MAMuG has a complicated structure, but the electrons can be suppressed before acceleration to full energy by intermediate grids.

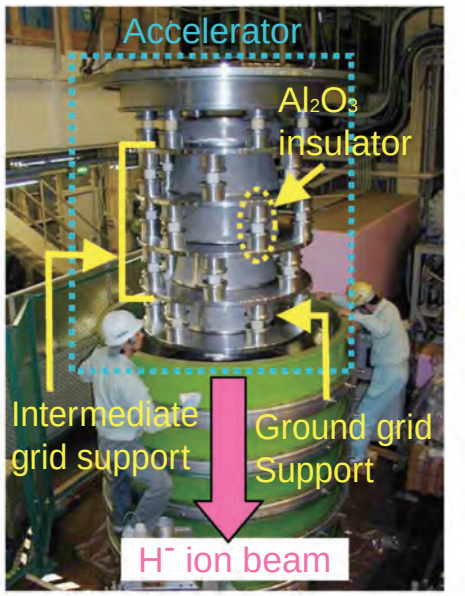

Fig.3-12 MAMuG accelerator developed at JAEA
Photograph of the MAMuG accelerator having four intermediate grids. Each grid is suspended from 1MV potential flanges supported by post insulators made of alumina.

The neutral beam injector (NBI) for ITER is required to inject 16.5MW of D^0 beams per injector. For this purpose, D^- beam current of 40A needs to be accelerated up to 1MeV by an accelerator. The required ion current is two orders of magnitude larger than conventional accelerators. To fulfill this requirement for the ITER accelerator, we have developed the "MeV accelerator" at the MeV test facility (MTF) in JAEA.

For the accelerator of the ITER NBI, two concepts have been proposed as shown in Fig.3-11. One is MAMuG (Multi-Aperture Multi-Grid) accelerator developed at JAEA (Fig.3-12) and the other is SINGAP (Single-Aperture Single-Gap) accelerator developed in EU. In order to choose the accelerator type for ITER, performance of the SINGAP and the MAMuG accelerator was tested and compared at the same test facility with the same diagnostics. For this purpose, the SINGAP accelerator was installed in JAEA's test facility and test was performed with participation of 7 scientists from EU. The results can be summarized as follows;

(1) The maximum voltage of the SINGAP was limited to 800kV, whereas the MAMuG could attain 1MV.
(2) The highest performance in the beam acceleration test of the SINGAP was 220mA at 672keV, while the MAMuG achieved 796keV, 320mA H^- ion acceleration.
(3) Co-accelerated electron current in the SINGAP was three times higher than the MAMuG, which will cause higher heat loads on beamline components.

From these results, it was concluded that the MAMuG has better performance than the SINGAP, and it has been decided to choose the MAMuG in the baseline design for the ITER NBI.

Reference

Taniguchi, M. et al., Development of 1 MeV H^- Accelerator at JAEA for ITER NB, AIP Conference Proceedings 1097, 2009, p.335-343.

3-6 Superconducting Magnet Technology in ITER
—Development of the Largest Superconducting Magnet in the World—

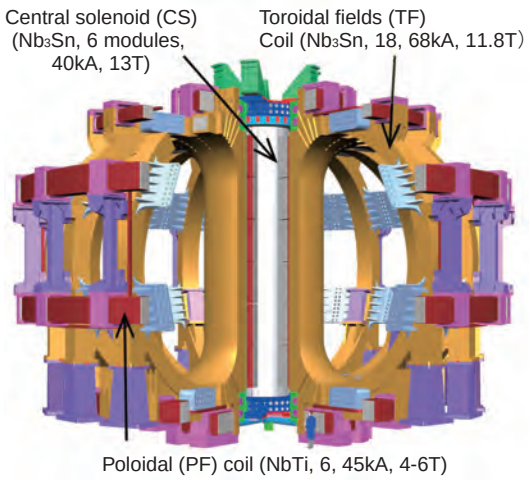

Fig.3-13 ITER superconducting magnet system

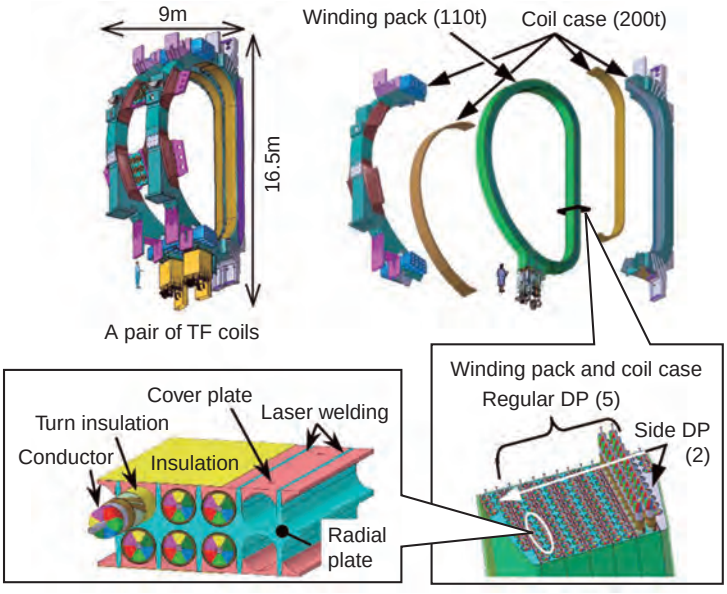

Fig.3-14 Configuration of TF coil

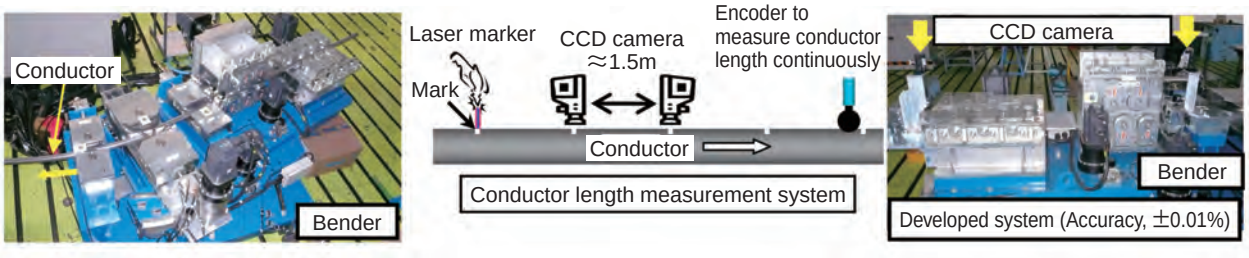

Fig.3-15 High accuracy winding system

In ITER, a joint project by China, EU, India, Korea, Japan, Russia and the US, large superconducting magnets (Fig.3-13) generating a field of more than 10 T are necessary. Japan is responsible for procuring 9 Toroidal Field (TF) coils (Fig.3-14), which are the largest superconducting coils in the world, as well as 25% of the TF conductors, whose procurement was the first contract signed in the ITER project.

In the TF coil, a winding pack (WP) is supported by a coil case, enabling it to sustain a huge electromagnetic force of 50MN/m. A WP consists of 7 double-pancakes (DP), which are fabricated as follows: (1) a 4.6km conductor is wound into a D-shape with accuracy of ±0.02% for the conductor length of each coil; (2) the conductor is heat-treated at 650℃ for 200h to generate Nb_3Sn; (3) the conductor wrapped in electrical insulation is inserted into a groove in the radial plate (RP), which provides a high degree of rigidity to support each conductor against a large electromagnetic force of 800kN/m; (4) the conductor is fixed in an RP groove by welding cover plates to the RP; and (5) the DPs are electrically insulated from each other.

A high degree of accuracy is required in the shaping of the winding. Each TF coil winding also must be made in 4 months. A highly accurate automatic winding system is a key technology to meet these requirements. We developed a highly accurate, automatic bender (Fig.3-15) that comprises a major part of the winding machine. The deformation of a conductor cross section due to bending is reduced to less than 0.2mm by optimizing the interval between the rollers. In order to measure the length of a conductor with great precision, we developed a new system in which the distance between marks scribed by a laser marker is measured with 2 CCD cameras (Fig.3-15). We have achieved a very high degree of accuracy of ±0.01% in measuring the length of a conductor and a winding speed of 3m/min. These results demonstrate the feasibility of our TF coil winding process.

Reference

Koizumi, N. et al., Critical Issues for the Manufacture of the ITER TF Coil Winding Pack, Fusion Engineering and Design, vol.84, issues 2-6, 2009, p.210-214.

3-7 Development of Diagnostics System for Divertor Plasma Control in ITER

—Creating a Highly Reliable Optical Diagnostic System for the Harsh Environment of ITER—

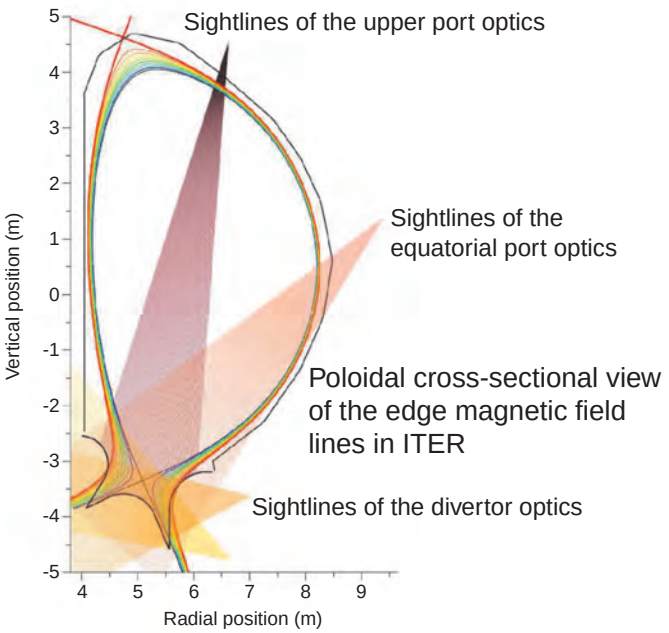

Fig.3-16 Sightlines of impurity influx monitor (divertor)
The fan arrays of the optical system emanate from an upper port, an equatorial port, a divertor port and a divertor cassette. The divertor area is measured from various directions in detail.

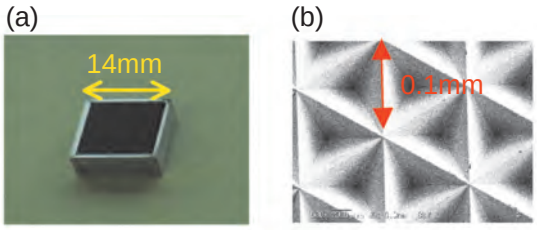

Fig.3-17 Micro retro-reflector array
(a) External view (b) Photo by SEM

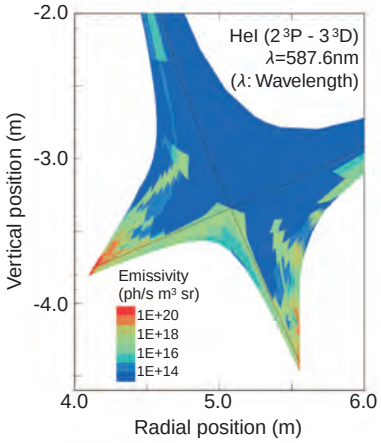

Fig.3-18 Helium atom spectral line emissivity of divertor (HeI:wavelength 587.6nm)
Red area indicates higher emissivity.

A nuclear fusion output of 500MW for 400s or longer is a primary objective for ITER. No current diagnostics systems are able to function in this harsh environment of high temperature, high radiation, and high particle flux. Such a system must be developed.

The main function of the Impurity Influx Monitor (divertor) shown in Fig.3-16 is to detect impurities and the isotopes of hydrogen (tritium, deuterium and hydrogen) in the divertor plasmas from their spectra in the wavelength range of 200 to 1000nm. The goal is to obtain valuable data indispensable for the control of impurities and of divertor plasma. To create this system, both design and R&D studies of optical systems with Mo mirrors, which are usable near the plasma, are being carried out.

A primary concern is that optical performance will deteriorate due to high temperature, high particle flux, and high radiation during operations, making it difficult to measure impurity influx to within a 10% accuracy level. Establishing an in-situ calibration method would allow the sensitivity of the optical system to be checked at any time. A new, in-situ calibration method applicable to ITER operations has been developed. Its key element is a micro retro-reflector array (MRRA) in which reflected light returns along the same optical path as incident light. The light introduced from outside passes to the further end of the optical system and is reflected by the MRRA set up there. Optical sensitivity is determined based on the strength of the light returning to the detector.

The MRRA is a compact arrangement of 0.1mm micro retro-reflectors shown in Fig.3-17. A full-scale MRRA has been constructed for the upper port optics, and testing of the array confirmed its applicability for ITER.

The helium generated by the fusion reaction flows to the divertor in ITER. The helium atom spectral line emissivity profile was evaluated using a collisional radiative model and an edge plasma model, as shown in Fig.3-18. A two-dimensional distribution can be calculated according to the observed line integration strength in the divertor region from two or more vantage points, as shown in Fig.3-16. Optimization of the positions of the side optics enables a spatial resolution of about 100mm. Results suggest that the fan array structure shown in Fig.3-16 allows an accurate determination of the complex emissivity profile shown in Fig.3-18.

Reference

Ogawa, H. et al., Engineering Design and R&D of Impurity Influx Monitor (Divertor) for ITER, Fusion Engineering and Design, vol.83, issues 10-12, 2008, p.1405 -1409.

3-8 Successful High Repetition Rate Operation of High Power Gyrotron
—Simulating ITER Gyrotron Operation—

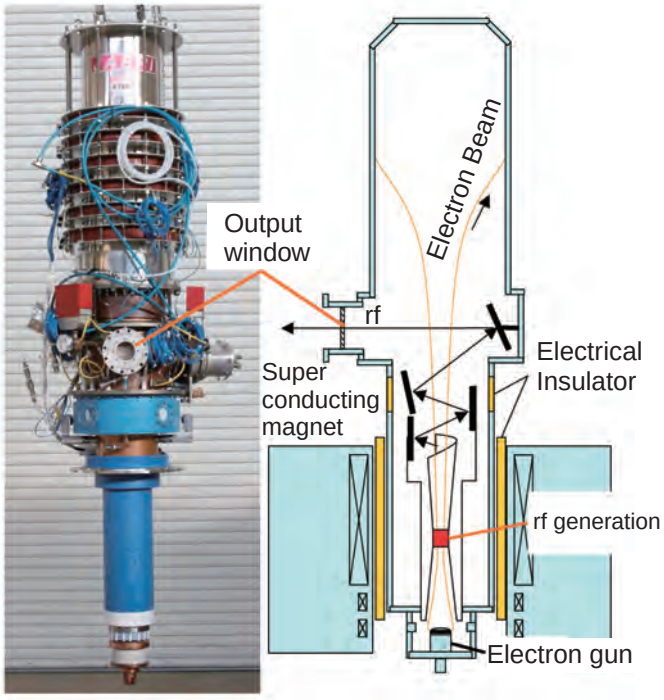

Fig.3-19 Millimeter wave plasma heating device; Gyrotron
At left is a photograph of the gyrotron. At right is a schematic cross section. The gyrotron has a 3m long rf oscillating tube. Electrons are emitted from the electron gun and generate high power rf when these electrons are go through a resonant cavity in a strong magnetic field

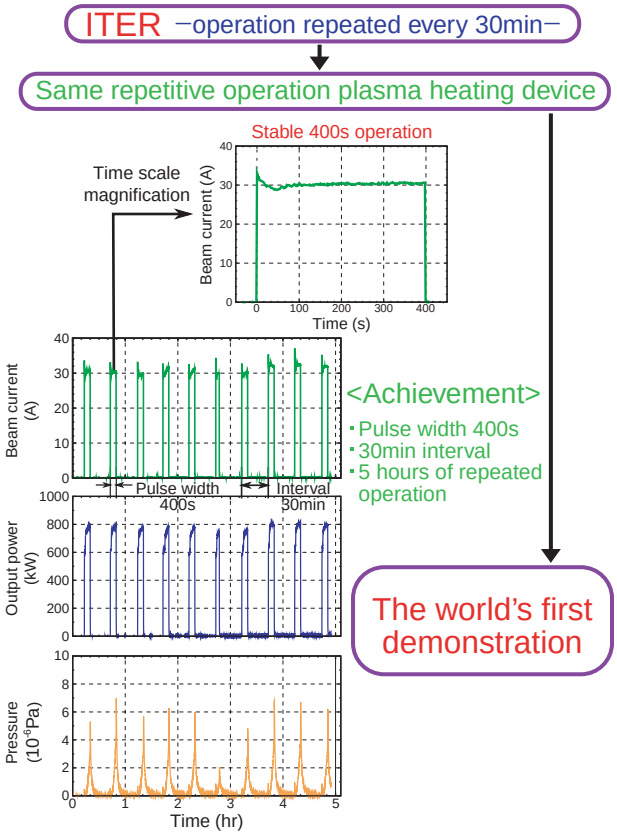

Fig.3-20 Repetitive gyrotron operation

A gyrotron is a device that can generate a high power microwave (Fig.3-19). A rotating electron beam is generated inside the gyrotron, which has a very high vacuum. The generated beam is accelerated up to 80keV and goes through a cavity in a high magnetic field region, thereby converting its energy to rf power. A 7T super conducting magnet is used in order to generate 170GHz rf power for ITER.

At JAEA, many advanced gyrotron techniques have been developed for ITER. One of the most important developments is the energy recovery technique, which dramatically improves the energy conversion efficiency. Another breakthrough is the 1MW oscillation using an artificial diamond output window.

With these advanced techniques, in 2007, we achieved the ITER requirement, i.e., 1MW oscillation, 50% energy conversion and 500s pulse width. This proves the advantages of the gyrotron as a heating device for ITER and fusion reactors in general.

We had focused on the long pulse operation (longer than 400s). However, repetitive operation becomes also important, because cyclic operation with a pulse width of 400s at 30min intervals is planned in ITER. In the repetitive operation, the operational state of the gyrotron, such as vacuum pressure and electron gun, must recover within 30min. In particular, the electron gun requires a long time to recover, because its surface temperature varies when it releases the electrons for the rf generation. Therefore, it is important to keep the temperature change as small as possible in order to shorten the recovery time. For that purpose, active control of the magnetic field, acceleration voltage and heater current of electron gun during the oscillation was performed. As a result, as shown in Fig.3-20, 5 hours of repeated operation with a 400s/30min cycle was successfully achieved. This is the world's first long pulse repetitive gyrotron operation, and proves the feasibility of ITER.

Reference

Kajiwara, K. et al., Long Pulse and High Power Repetitive Operation of the 170GHz ITER Gyrotron, Plasma and Fusion Research, vol.4, 2009, p.006-1-006-3.

3-9 ITER Divertor Prototypes Pass High Heat Flux Test
—Prototypes Fabricated by JAEA Withstand High Heat Flux—

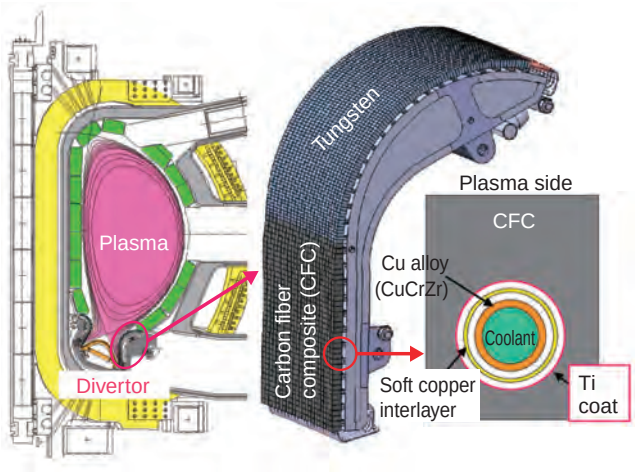

Fig.3-21 ITER divertor outer target
The divertor has the role of assisting in removing impurities from plasma. As a result of the R&D in the engineering design phase, armor materials and a cooling tube have been brazed together with a soft copper interlayer. Moreover, the quality of the brazed joint has been improved by applying metal on the carbon armor. This metallization process enables precise assembly with ±5μm accuracy.

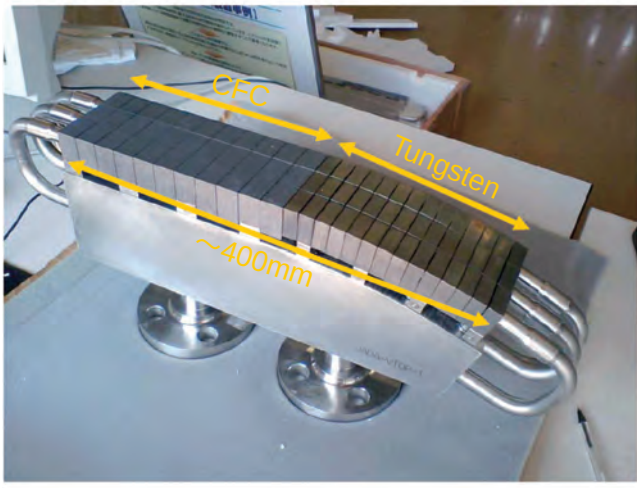

Fig.3-22 ITER divertor prototype
Our prototypes have been tested under high heat flux at Efremov institute in Russia, where they successfully withstood the required heat flux cycles. Based on these results, Japan is the first Partner whose divertors have been certified by ITER Organization.

We have been performing R&D for the divertor, one of the in-vessel components of ITER (Fig.3-21). As a preliminary step toward providing divertors for actual use, we have fabricated divertor qualification prototypes in close collaboration with Japanese companies, and they have successfully passed high heat flux tests by ITER Organization (Fig.3-22). It is necessary for the ITER divertor to withstand repetitive heat flux of 20MW/m^2 which no engineering devices have withstood up to now. To achieve robust components, we selected carbon fiber composites with higher thermal conductivity than pure copper as an armor material. The armor material is directly brazed onto a cooling tube to achieve sufficient heat removal capability.

However, it is difficult to braze armor materials with low thermal expansion coefficient onto copper alloy cooling tube. To overcome this, it is necessary to precisely control the assembly interface between the armor materials and the cooling tube. as a result of the R&D done in the engineering design phase of ITER, the armor materials and the copper alloy cooling tube have been brazed together with a soft copper interlayer to absorb the mismatch of their thermal expansion. In addition, the quality of the braze joint has been improved by applying Ti onto the carbon armor. This metallization process enables precise assembly accuracy of ±5μm.

Using the brazing technology above, we fabricated divertor prototypes. High heat flux tests were carried out at the Efremov institute in Russia under the supervision of ITER Organization. It was determined that the prototype could withstand heat flux of 20MW/m^2 for 1000 cycles which is a criterion for the ITER divertor. Thus, we are the first of the Partners (EU and Russia) whose diverter has been certified by ITER Organization as qualified to start supplying divertors for ITER.

In 2009, we are going to start the fabrication of a divertor full-scale prototype as a first step in providing divertors for ITER. After that, we are going to start quantity production of divertor components and deliver them to the ITER site by around 2011.

Reference

Ezato, K., Suzuki, S. et al., Provisional Procurement Activity and R&D's on Divertor HHF Components in JADA, Proceedings of 22nd IAEA Fusion Energy Conference (FEC 2008), Geneva, Switzerland, 2008, IT/P7-17, 6p.

3-10 Improvement of Prediction Accuracy of Neutron-Induced Heat in Fusion Reactor Materials

—Measurement of Double-Differential Cross-Sections of Charged Particle Emission—

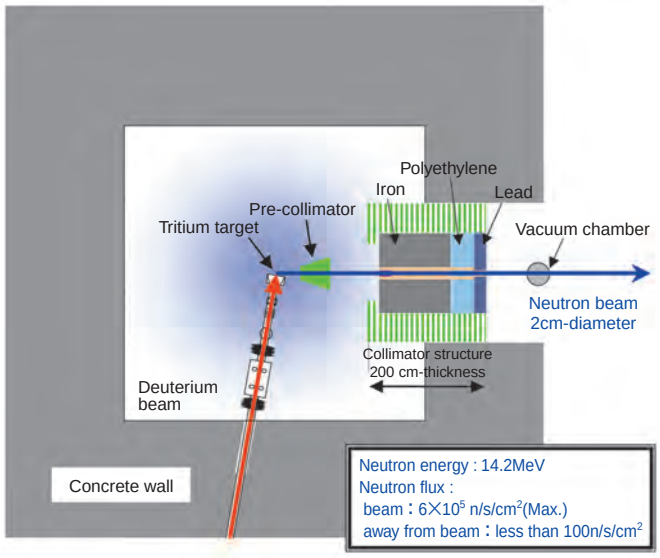

Fig.3-23 Schematic view of the charged-particle double-differential cross-section measurement system at the FNS facility
A DT-neutron pencil beam of 2cm-diameter is formed by collimating isotropically produced neutrons with a collimator. A precise measurement without background is realized with this neutron beam.

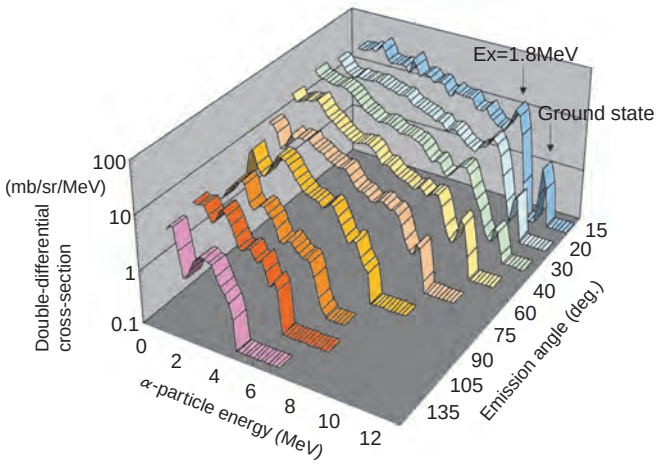

Fig.3-24 Measured double-differential cross-section of α-particle emission from beryllium
This graph shows the measured energy and angular distributions of α-particles emitted from beryllium at 14MeV neutron incidence. These data are the most detailed obtained anywhere in such a wide energy and angle range.

In a fusion reactor which uses deuterium (D) and tritium (T), neutrons carry most of the energy produced by the DT fusion reaction. Those neutrons lose their energy through various nuclear reactions with reactor devices such as the blanket, and the devices become hot. We have to accurately estimate how hot the device becomes in order to ensure the soundness of the device. Accurate prediction of generated heat is important because the heat will be also used to generate electricity in a future commercial fusion reactor.

The heat produced by nuclear reactions is called “nuclear heating” and is estimated by a simulation calculation in a reactor design. One of the essential data for such a calculation is the energy and angular distributions of charged particles like protons and α-particles emitted by a nuclear reaction. These distributions are called “double-differential cross-section (DDX) data”.

We have measured DDX of charged particles emitted from candidate materials for a fusion reactor at the Fusion Neutronics Source (FNS) facility. A schematic view of the measurement apparatus is shown in Fig.3-23. Our measurements of α-particle DDX from beryllium are more detailed than any others in the world. The measurements are shown in Fig.3-24.

Based on this measurement data, we calculated a conversion coefficient from neutron flux to the nuclear heating of beryllium. The conversion coefficient was compared with the values estimated from two cross-section databases: Japanese Nuclear Data Library “JENDL-3.3”, and Fusion Evaluated Nuclear Data Library “FENDL-2.0”, the latter used for design calculations of the ITER. As a result, it was found that the conversion coefficients estimated from these databases were smaller by around 15% than that based on our measured data. This leads to underestimation of the nuclear heating calculated for beryllium by around 15%. We found that the cause of the underestimation lay in a problem with the α-particle DDX of beryllium in these databases. In this way, our measured DDX data have been very useful for clarifying problems in the databases and for improving the prediction accuracy of the nuclear heating in a fusion reactor.

Reference

Kondo, K. et al., Verification of KERMA Factor for Beryllium at Neutron Energy of 14.2 MeV Based on Charged-Particle Measurement, Fusion Engineering and Design, vol.83, issues 10-12, 2008, p.1674-1677.

3-11 For Validation of Fusion Reactor Materials
—Research and Development of Liquid Lithium Target for International Fusion Materials Irradiation Facility (IFMIF)—

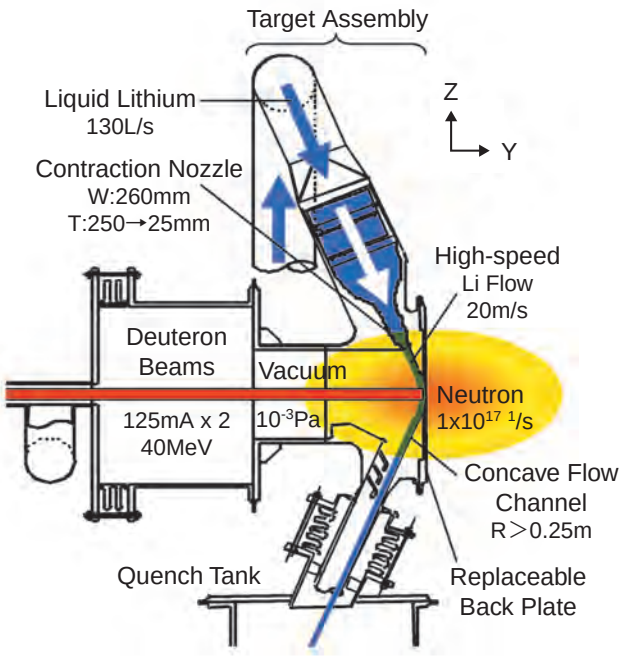

Fig.3-25 Concept of IFMIF liquid lithium (Li) target
A liquid Li is contracted through a nozzle to cause high-speed flow which is directed into a concave channel. Deuteron beams are injected into the flow to generate intense neutrons.

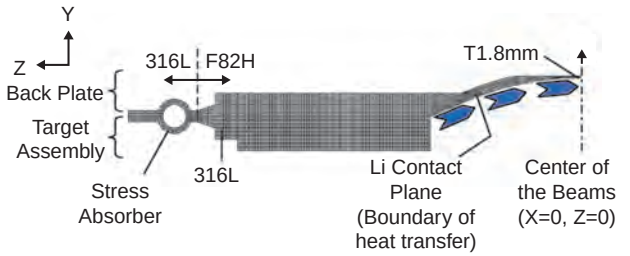

Fig.3-26 Thermal stress analysis model
The model consists of a 1/4 part of a back plate made by jointing two kinds of material and a corresponding part of a target assembly.

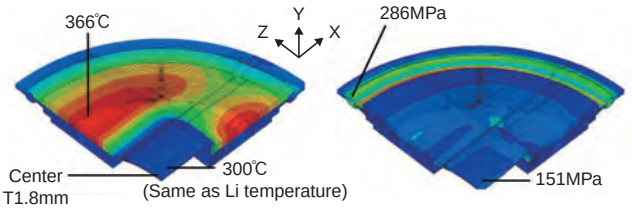

Fig.3-27 Results of thermal stress analysis on back plate under beams operation
Temperature at the center where neutron intensity was the highest was the same as that of Li, while that of the thick fringe part was higher (left). Although the temperature distribution caused thermal stress in the back plate, the stress was kept sufficiently small through deformation of the stress absorber (right).

For the development of fusion reactor materials, it is necessary to evaluate damage to the candidate materials by 14MeV neutrons generated by the deuterium-tritium fusion reaction. The International Fusion Materials Irradiation Facility (IFMIF) is designed to produce an intense high energy neutron flux for testing candidate materials to be used in the fusion DEMO reactor. At present, Engineering Validation and Engineering Design Activities (EVEDA) for IFMIF are in progress as part of the international collaboration between Japan and EU called “Broader Approach Activities”.

The concept of a liquid lithium (Li) target generating intense neutrons is shown in Fig.3-25. Deuterons (D) are accelerated up to 40MeV by accelerators and injected into a Li target. Intense neutrons with a peak energy around 14MeV are generated by the D-Li nuclear reaction. For removal of the 10MW heat power produced by the deuterium beams (40MeV, 250mA), high-speed liquid lithium flow is generated. Moreover, to avoid boiling of the liquid Li even in the vacuum condition of the accelerators, the flow channel is designed to be concave to provide centrifugal force, and boiling temperature is increased by the pressure built up by the Li flow. Because the back plate with the concave flow channel is irradiated by the intense neutrons, the back plate is made of reduced activation ferritic steel (F82H). Thickness of the back plate at a center is design to be 1.8mm to minimize attenuation of the neutrons by the wall as small as possible.

We studied the feasibility of a back plate structure intended to withstand severe conditions by thermal stress analysis of a model thereof, shown in Fig.3-26. As a result, even during beam operation with temperature distribution caused by the neutron heat as shown in Fig.3-27 left, thermal compression stress in radial directions was 286MPa at the maximum, within the acceptable range, by a circular structure to absorb thermal stress.

In the EVEDA project, in parallel with designing of actual devices for IFMIF, a Li test loop is under construction for conducting various validation tests for important technologies. The loop is to produce a Li flow hydrodynamically similar to IFMIF, in order that stability of high-speed Li flow and safety and integrity of the loop operation over a long period are validated. Techniques of flow measurement and purification using impurity traps are also to be validated with this loop.

Reference

Nakamura, H. et al., Status of Engineering Design of Liquid Lithium Target in IFMIF-EVEDA, Fusion Engineering and Design, vol.84, issues 2-6, 2009, p.252-258.

4 Quantum Beam Science Research

Development of Quantum Beam Technology

Characteristics of quantum beams

Quantum beams, which include electromagnetic waves (lasers, X-rays, γ-rays, etc.) and energetic particles (electrons, protons, neutrons, ions, etc.), possess both wave and particle characteristics. Quantum beams have a creative function, allowing us to process materials on a nanometer level (atomic or molecular level) because they interact with constituent atoms of a material to change their configuration, composition and electronic state. Such quantum beam interactions also cause changes in the beams themselves, e.g., the beam direction and energy, and sometimes generate different types of quantum beams. Thus we can get the atomic or molecular level information by observing alteration of the beam parameters, giving quantum beams a probe function as well.

Application of quantum beams

At JAEA, we are performing R&D of advanced beam technology using neutrons, ions, electrons, γ-rays, lasers and synchrotron X-rays produced in our quantum beam facility complex by research reactors, accelerators, and so on (Quantum Beam Platform) shown in Fig.4-1. By utilizing the creative and probe functions of quantum beams, we do fundamental and applied research in a wide range of fields, e.g. (1) materials science field, (2) environment and energy field, and (3) life science, advanced medicine and biotechnology field, which are listed as the 'Priority Fields to be Promoted' in the 'Science and Technology Basic Plan' of Japan. We are intensively promoting this R&D to contribute to progress in science and technology as well as for the promotion of industry.

Recent achievements

In the materials science field, we have found the collective excitation of electrons in high temperature superconductors, the Mn site dependence of the spin moment of a dilute magnetic semiconductor $Ga_{1-X}Mn_XAs$, the hydrogenation of aluminum with hydrogen fluid, and the degradation modeling of multi-junction space solar cells, which are introduced in Topics 4-1 to 4-4. In the environment and energy field, we have demonstrated breakdown of toxic organic compounds using electron-beam irradiating alumina, isotope separation by excitation of molecular vibration due to ultrashort-pulsed lasers, and isotope mapping of heavily shielded objects using laser Compton γ-rays, Topics 4-5 to 4-7. In the life science, advanced medicine and biotechnology field, we have succeeded in determining the whole atomic structure of HIV-1 protease, which is effective for developing anti-HIV drugs, Topic 4-8. We have also investigated protein dynamics using neutron inelastic scattering, found symbiotic nitrogen fixation with a positron-emitting tracer imaging system, clarified the bystander effect using heavy-ion microbeams, and developed nano-capsules opened by radiation for cancer therapy, Topics 4-9 to 4-12.

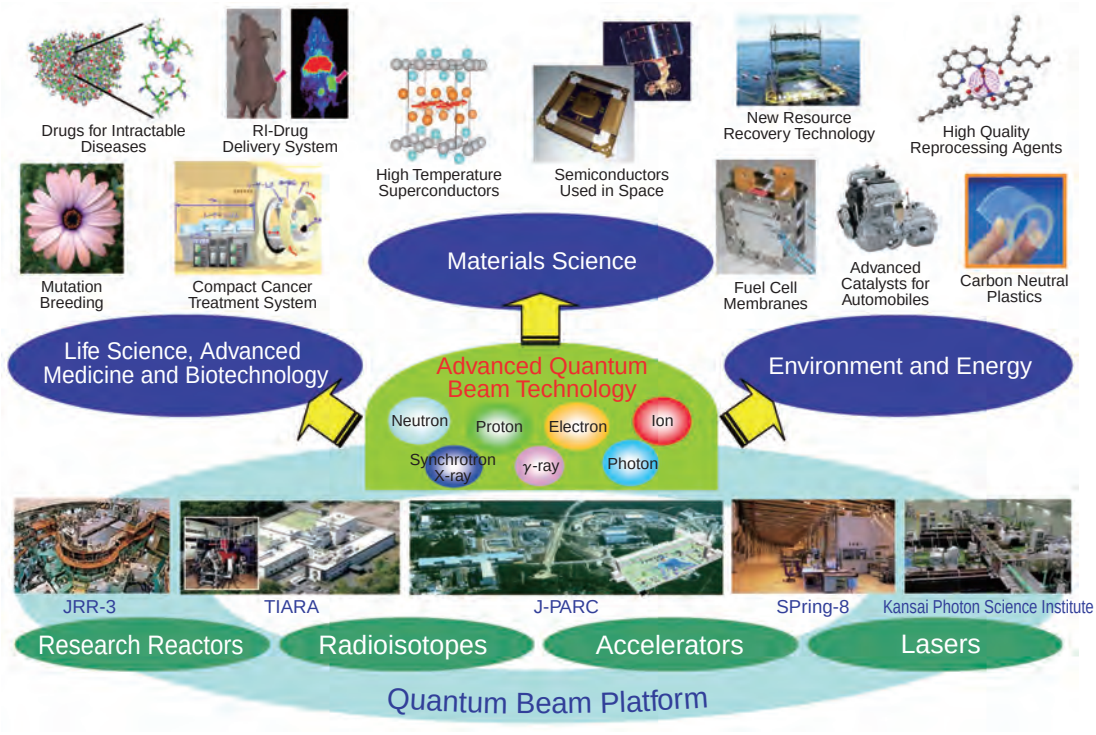

Fig.4-1 JAEA quantum beam facilities and R&D done there

4-1 Observation of Collective Behavior of Strongly Interacting Electrons
—Study of Collective Charge Excitations of Charge Stripes—

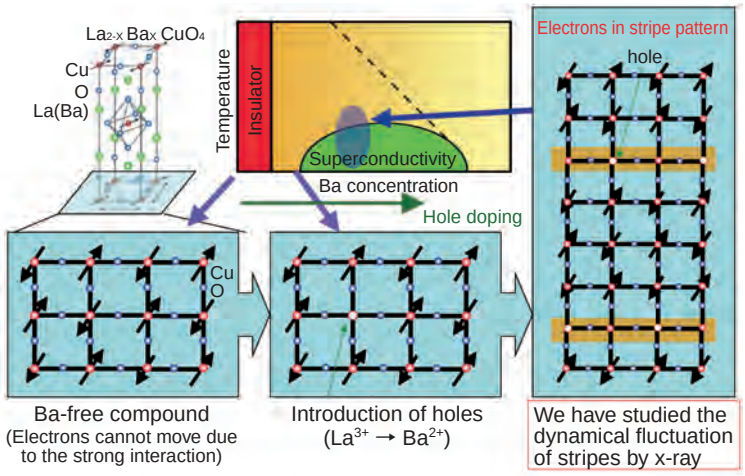

Fig.4-2 An example of strongly interacting electrons in case of cuprate $La_{2-x}Ba_xCuO_4$
The system varies from an insulator to a superconductor by the hole doping achieved by Ba substitution. The arrows represent the magnetic properties of electrons. Electrons order in the stripe form in the superconducting regime. We observed the collective excitation of the charge stripes.

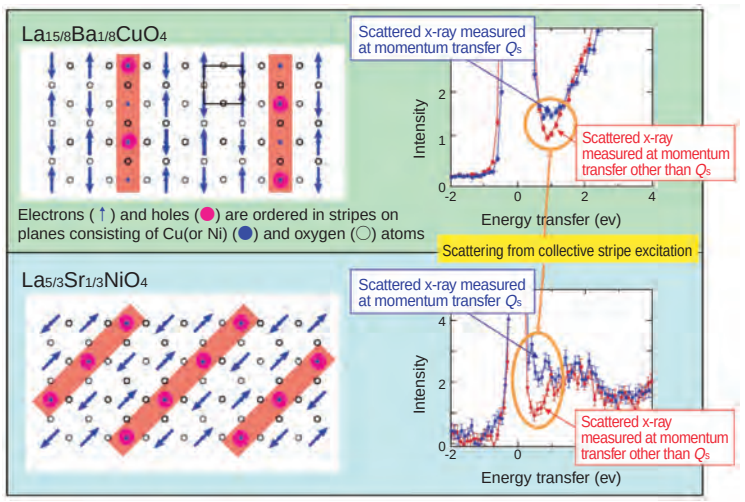

Fig.4-3 Observation of collective charge stripe excitations
Comparison between scattered x-ray intensity measured at momentum transfer Q_s corresponding to the spatial period of charge stripes (blue data) and at momentum transfer other than Q_s (red data). In both materials, additional signals of collective charge stripe excitation were observed at momentum transfer Q_s.

We succeeded in observing the collective fluctuation (collective excitation) of electrons that strongly interact with each other in a material, in collaboration with Tohoku University and Argonne National Laboratory.

In the scheme of today's physics, the behavior of electrons that do not interact with each other, such as conduction electrons in metals, is well understood, whereas the behavior of electrons that behave collectively as a result of strong interaction is not well understood because of the difficulty of theoretical interpretation. However, materials with strongly interacting electrons are known to exhibit various new functional features, notably high temperature superconductivity.

We investigated the collective behavior of electrons in high-temperature cuprate superconductor and a related nickelate compound which are typical examples of materials with strongly interacting electrons. In these materials, electrons order themselves in stripes as shown in Fig.4-2 due to their strong interaction.

In resonant inelastic x-ray scattering experiments done at the synchrotron radiation facilities "SPring-8" and "Advanced Photon Source", we succeeded in directly observing the collective charge stripe excitations in cuprate and nickelate which correspond to the periodic alignments of the electrons into a stripe pattern. As shown in Fig.4-3, the two materials used for this study have different charge stripe geometries. The charge stripes align vertically in the cuprate but diagonally in the nickelate. The observation of the collective charge stripe excitations in both materials verified the universal collective fluctuation of charge stripes, suggesting that collective charge fluctuation resulting from strong interaction between electrons is necessary for high temperature superconductivity.

This success will open up a new research field in materials science for exploration, namely, the collective excitation of electrons. It is highly expected that the mechanism behind high-temperature superconductivity of target materials will be clarified by further research in collective excitation.

Reference

Wakimoto, S. et al., Charge Excitations in the Stripe-Ordered $La_{5/3}Sr_{1/3}NiO_4$ and $La_{2-x}(Ba,Sr)_xCuO_4$ Superconducting Compounds, Physical Review Letters, vol.102, issue 15, 2009, p.157001-1-157001-4.

4-2 Study of a Dilute Magnetic Semiconductor by Observing Soft X-ray Magnetic Circular Dichroism

— Way to Improve *Spintronics* Material Performance Revealed by Synchrotron Radiation —

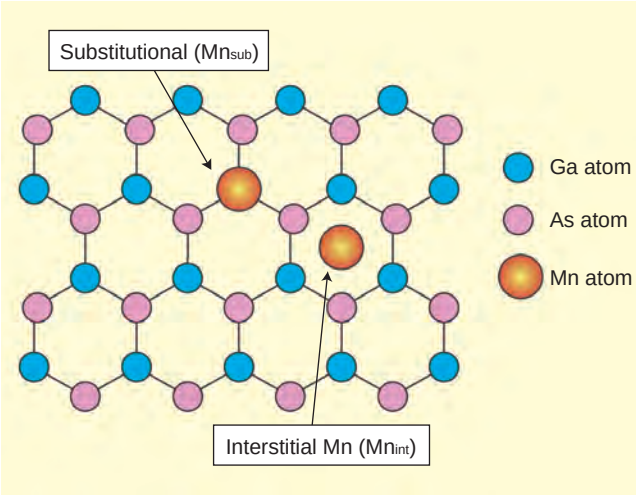

Fig.4-4 Schematic view of $Ga_{1-x}Mn_xAs$ (111) surface
Mn_{sub} and Mn_{int} represent the Mn ions replacing Ga ions and inserted in interstices, respectively.

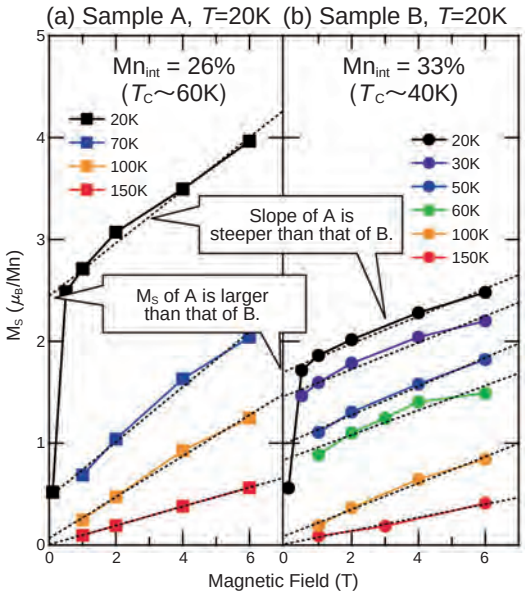

Fig.4-5 Magnetic dependence of the spin moment (M_S) of $Ga_{1-x}Mn_xAs$ at T = 20K
(a) Sample A with T_C ~ 60K, Mn_{int} / all Mn ions ~ 26% (b) Sample B with T_C ~ 40K, Mn_{int} / all Mn ions ~ 33%. The amount of Mn_{int} was estimated from our XMCD experiments.

Electrons have two characteristics, "charge" and "spin". In semiconductor electronics, we use charge only. On the other hand, *spintronics* technology utilizes spin combined with semiconductor electronics technology. For practical use of *spintronics*, a material is needed which exhibits semiconducting and ferromagnetic properties and a Curie temperature (T_C) exceeding room temperature (RT). Among dilute magnetic semiconductors (DMS's), $Ga_{1-x}Mn_xAs$ is a promising candidate, but T_C above RT has not been achieved yet. This material's ferromagnetic property is caused by Mn ions (Mn_{sub}) substituting for the Ga ions. Because $Ga_{1-x}Mn_xAs$ is grown under thermal non-equilibrium conditions, however, it is difficult to avoid the formation of the interstitial Mn ions (Mn_{int}) as shown in Fig.4-4. It has been speculated that the existence of Mn_{int} might suppress the T_C. The relation between Mn_{int} and T_C has not been revealed yet.

In order to investigate the influence of the Mn_{int} on T_C, we prepared two samples which have different T_C and amounts of Mn_{int} (Sample A: T_C ~ 60K, Mnint / all Mn ions ~ 26% and B sample: T_C ~ 40K, Mn_{int} ~ 33%) and performed soft x-ray magnetic circular dichroism (XMCD) experiments in the Mn $L_{2,3}$ absorption edge region using synchrotron radiation. From the XMCD experiment, we could extract the value of spin moment (M_S) of each Mn atom. The XMCD experiments were done at the JAEA beamline BL23SU of SPring-8.

Fig.4-5 shows the magnetic field (H) dependence of M_S estimated from the XMCD experiment at T = 20K. In the sample A, both the spontaneous magnetization ($M_{S\,H=0\ Tesla}$) and the slope of the H dependence of M_S are larger than those in the sample B. Here, the slope corresponds to the magnetic susceptibility. This indicates that the antiferromagnetic (AF) interaction between the Mn_{sub} and Mn_{int} should exist. Therefore, the M_S of the Mn_{int} is antiparallel to that of Mn_{sub}, In other words, the existence of Mn_{int} prevents increase in T_C. The present results indicate that the AF interaction between the Mn_{sub} and Mn_{int} plays an important role in the magnetic behavior of a typical $Ga_{1-x}Mn_xAs$. In addition, the amount of the Mn_{int} ions should have a strong relation to T_C.

The findings should give a valuable insight into the performance improvement of the magnetic properties of many DMS's in addition to $Ga_{1-x}Mn_xAs$.

Reference

Takeda, Y. et al., Nature of Magnetic Coupling between Mn Ions in As-Grown $Ga_{1-x}Mn_xAs$ Studied by X-ray Magnetic Circular Dichroism, Physical Review Letters, vol.100, issue 24, 2008, p.247202-1-247202-4.

4-3 Toward a Hydrogen Utilizing Society
—Hydrogenation of Aluminum with Hydrogen Fluid—

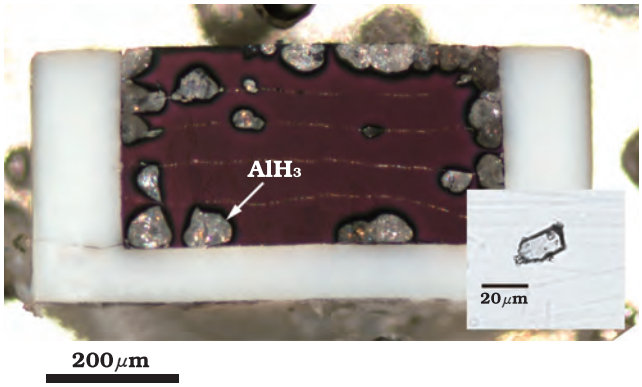

Fig.4-6 Optical micrograph of sample after treatment
The inner black portions are unreacted aluminum, and the glassy white particles are AlH_3. The grain size of recovered AlH_3 ranged from a few to several tens of microns. Inset shows a transmitting light micrograph of a single AlH_3 crystal.

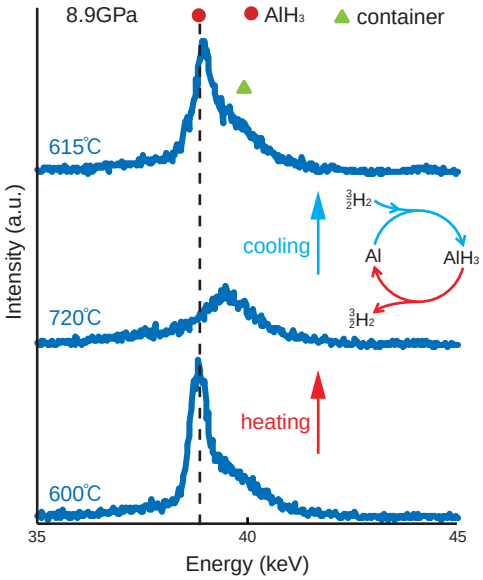

Fig.4-7 Powder X-ray diffraction profiles of aluminum sample immersed in high-pressure high-temperature hydrogen fluid
When the sample was heated from 600°C, where AlH_3 formed, at 8.9GPa, AlH_3 decomposed at 720°C. Upon subsequent cooling, aluminum was hydrogenated again at 615°C. Cyclic hydrogenation and dehydrogenation was achieved.

Hydrogen is an ideal energy carrier since it minimizes harmful effects on the environment. Development of a safe and efficient storage system of hydrogen is widely recognized as a key technological challenge which must be met to realize a hydrogen-based energy economy. Hydrogen can be stored as a pressurized gas, cryogenic liquid, and solid fuel; for example, hydrogen forms metal hydrides with some metals and alloys. These solid-state storage media provide a safety advantage over the gas and liquid storage methods.

Typical hydrogen storage alloys, such as $LaNi_5$, absorb hydrogen at relatively low pressure. In contrast to such hydrides, high pressure is needed to hydrogenate aluminum. Passivation film on the surface of aluminum also prevents the hydrogenation reaction. AlH_3 is, however, promising as a hydrogen storage material due to its large hydrogen content (10.1wt%). If the hydrogenation of aluminum is realized, it is expected to develop novel aluminum-rich alloy hydrides with moderate hydrogenation pressure.

We have succeeded in hydrogenation of aluminum and recovery of AlH_3 (Fig.4-6). The hydrogenation and dehydrogenation process was investigated by *in situ* X-ray diffraction measurement at SPring-8 (Fig.4-7). Highly reactive hydrogen fluid suppressed the influence of the chemically stable oxide layer on the aluminum surface.

In the future, we will elucidate the hydrogenation and dehydrogenation mechanism of aluminum, and develop novel aluminum-based alloy hydrides which can absorb hydrogen at practical pressure temperature conditions.

The present study was conducted as part of the “Advanced Fundamental Research Project on Hydrogen Storage Materials” commissioned by the New Energy and Industrial Technology Development Organization (NEDO).

Reference

Saitoh, H. et al., Formation and Decomposition of AlH_3 in the Aluminum-Hydrogen System, Applied Physics Letters, vol.93, issue 15, 2008, p.151918-1-151918-3.

4-4 Advanced Prediction Methods of Satellite Lifetime
—Radiation Degradation Modeling of New Outer Space Solar Cell—

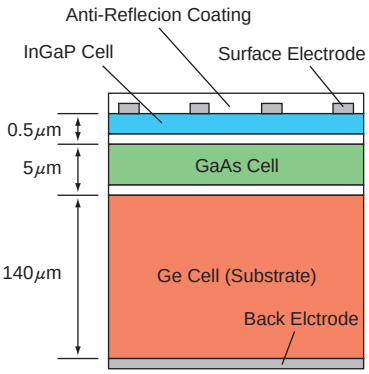

Fig.4-8 A cross-sectional diagram of InGaP/GaAs/Ge triple-junction solar cell
This solar cell consists of three layers; Indium Gallium Phosphate (InGaP), Gallium Arsenide (GaAs) and Germanium (Ge). Radiation degradation behavior of this solar cell is more complex than that of a conventional one because of the multi layer structure.

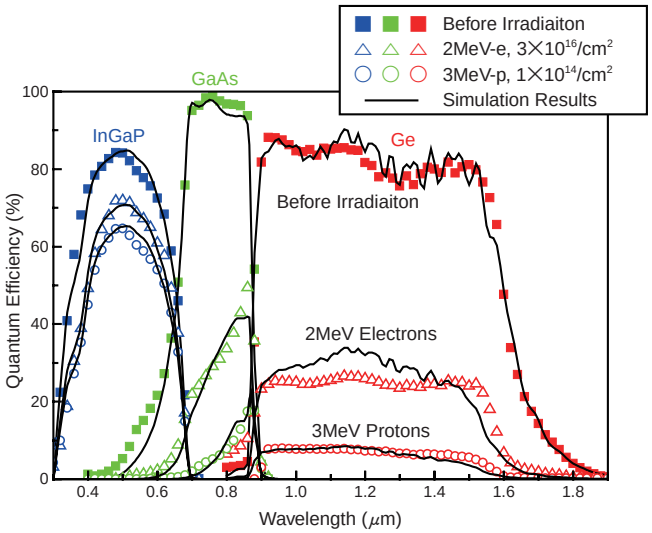

Fig.4-9 Quantum efficiencies of 3J cells irradiated with 3MeV protons or 2MeV electrons
Blue, green and red symbols denote the quantum efficiencies of the InGaP, GaAs and Ge layers, respectively. Closed and open symbols denote respectively the experimental values before and after the irradiation. Solid lines show the simulation results.

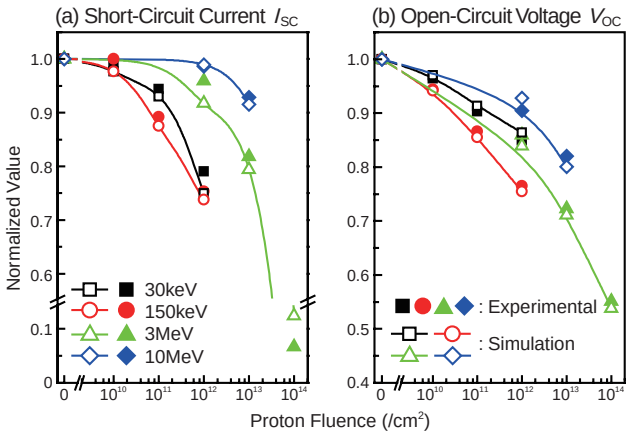

Fig.4-10 Curves of (a) I_{sc} and (b) V_{oc} for 3J cells during four levels of proton irradiation
Closed and open symbols denote the experimental and simulation results, respectively. Solid lines show the simulation results.

Since electric output from outer space solar cells mounted on satellites is degraded by space radiation (mainly electrons and protons), the amount of solar cells attached is determined considering the needed output at the end of the mission. Consequently, space solar cells are required to have both high conversion efficiency and high radiation tolerance. From the above facts, studies of radiation resistance of solar cells are carried out extensively using accelerators (ground tests). If accurate radiation degradation modeling of solar cells is developed, the number of tests for estimating the radiation degradation can be decreased and space solar cells can be developed more efficiently and economically. Recently, an InGaP/GaAs/Ge triple-junction solar cell (3J cell) as shown in Fig.4-8, which has very high conversion efficiency (~28%), has become the mainstream cell for outer space use. In this study, we clarified the radiation degradation behavior of the 3J cell by performing proton and electron irradiation experiments and by evaluating the degraded cell characteristics using an optical device simulator. We also developed a radiation degradation model on the basis of these results.

The quantum efficiency variations in the 3J cells due to 3MeV proton and 2MeV electron irradiation are shown in Fig.4-9. All the simulation results were in good agreement with the experimental results. Physical properties such as carrier concentration and diffusion length could be derived from the simulation results, and the cell performance (short-circuit current I_{sc} and open-circuit voltage V_{oc}) could be estimated from these physical properties. Fig.4-10 compares the experimentally measured I_{sc} and V_{oc} with these simulation results. The simulations nicely replicated the experimental values of both the proton and electron irradiations, though Fig.4-10 only shows the results of the proton irradiations. These results indicate that the degradation modeling proposed in this study is effective in predicting the radiation response of 3J cells.

In addition, radiation degradation behavior of the physical properties in each layer (InGaP, GaAs and Ge) can be systematically scaled using the Non-Ionizing Energy Loss (NIEL) index. Through this systematic scaling, it can be estimated how much the physical properties degrade due to space radiation exposure expected in a satellite mission. Simulating the cell performance based on the physical property degradation, we can predict the radiation degradation of 3J cells in actual space.

Reference
Sato, S. et al., Modeling of Degradation Behavior of InGaP/GaAs/Ge Triple-Junction Space Solar Cell Exposed to Charged Particle, Journal of Applied Physics, vol.105, issue 4, 2009, p.044504-1-044504-6.

4-5 Metal Oxides Become Active Catalysts When Irradiated by Electron-Beams!

— Enhancement of the Oxidation of Organic Substances with Electron-Beam Irradiated γ-Alumina —

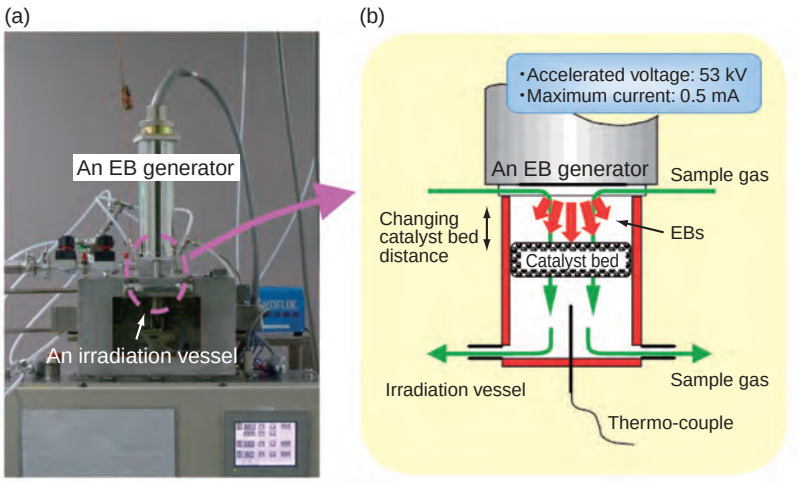

Fig.4-11 (a): An EB irradiation/catalyst system (external view), (b): an irradiation vessel for a gas stream (interior view)
This system consists of an EB generator, an irradiation vessel, catalysts, and gas analyzers. A sample gas containing organic substances was irradiated with EBs and then passed through a catalyst bed. The energy directly delivered to the catalyst bed was changed from zero to 50% of total EB energy by placing it at different distances from an EB irradiation window.

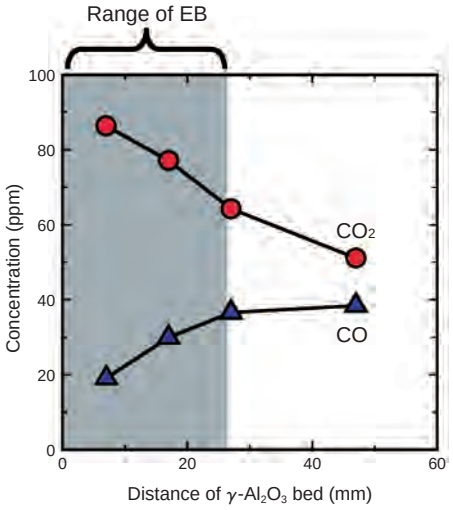

Fig.4-12 The concentrations of CO_2 and CO in 50-ppm xylene/air mixture irradiated at a dose of 10 kGy when γ-Al_2O_3 bed was placed at various distances
10-kGy EB irradiation without a γ-Al_2O_3 bed produced 28.9-ppmv CO_2 and 38.5-ppmv CO. Placement of a γ-Al_2O_3 bed at a distance of 7mm caused higher production of CO_2 with less CO production.

Emission of various organic substances from painting factories causes photochemical smog. We have developed a gas purification system that can oxidize organic substances into CO_2 and CO using electron beam (EB) irradiation. In this treatment, such organic substances should be preferentially oxidized into CO_2 without producing toxic CO. We have recently focused on the development of EB use with catalysts for this purpose and found that a γ-alumina (γ-Al_2O_3) bed exhibited the best catalytic activity together with an electron accelerator, especially when its surface is directly irradiated with EBs.

The EB irradiation involved a variety of chemical reactions. For the understanding of complicated radiation-induced catalytic reactions, we manufactured an EB irradiation/catalyst system that can irradiate a sample gas in the presence of a catalyst bed placed at various distances from an EB-irradiation window. (Fig.4-11) The catalytic oxidation of *o*-xylene in air was studied using a γ-Al_2O_3 bed as a catalyst. The results were summarized as follows;

(1) Higher CO_2 concentration was obtained by an EB/catalytic treatment.
(2) Irradiation products of xylene oxidized exclusively into CO_2 over the γ-Al_2O_3 surface.
(3) The formation of CO_2 was enhanced and the production of toxic CO was suppressed when a γ-Al_2O_3 bed was directly irradiated with EBs, namely placed in an EB-induced plasma. (Fig.4-12).

Our previous studies demonstrated that the placement of common catalysts such as TiO_2 and MnO_2 in an EB-irradiation space led to the decrease of CO_2 concentration due to suppression of gas-phase oxidation reactions. On the other hand, the placement of γ-Al_2O_3 in the EB-irradiation space caused higher-concentration of CO_2. Such catalytic oxidation activity was found to be due to the exclusive oxidation of the irradiation products of xylene over EB-irradiating γ-Al_2O_3 surface into CO_2.

In general, metal oxides, such as γ-Al_2O_3, are made into chemical catalysts by loading noble metals on the surface. The present results are important not only for an EB-gas purification technology but also for production of a new catalyst which does not load any noble-metals.

Reference

Hakoda, T. et al., Oxidation of Xylene and Its Irradiation Byproducts Using an Electron-Beam Irradiating a γ-Al_2O_3 Bed, Journal of Physics D: Applied Physics, vol.41, no.15, 2008, p.155202-1-155202-7.

4-6 Controlling Molecular Vibration to Allow Laser Isotope Separation
—Vibrational Control of Iodine Molecules by a Ultrashort-Pulsed Laser—

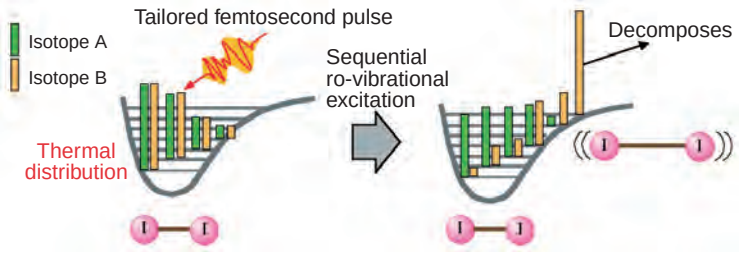

Fig.4-13 Schematic drawing of new isotope separation scheme using coherent quantum control
Using pulse shaping techniques with an ultra short pulsed laser, multiple excitation of molecular vibration can be achieved to enhance isotope shift in vibrational frequency.

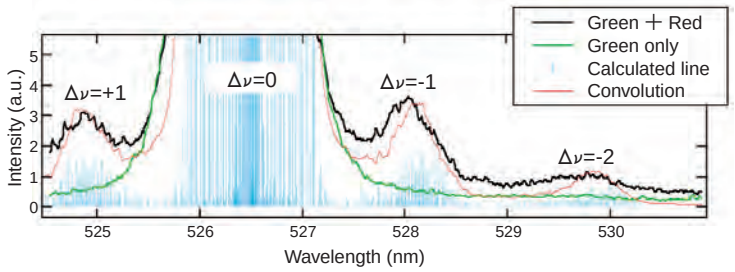

Fig.4-15 Fluorescence spectrum
Irradiation with a red ultra-short pulsed laser after the green laser formed a new sideband assigned to “Raman scattering” in the vicinity of the original band, which was formed by the green laser alone.

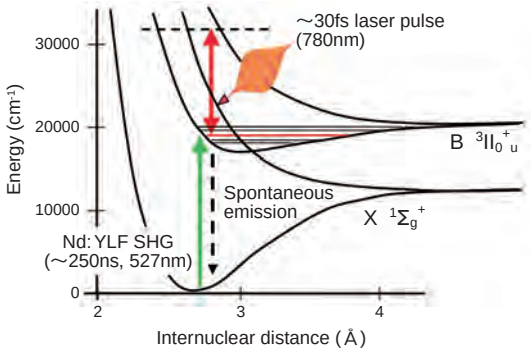

Fig.4-14 Potential energy curves of the iodine molecule and excitation scheme
The iodine molecule is excited in advance by a narrow band green laser (Nd:YLF SHG). With each ultra-short laser pulse, photo absorption and stimulated emission are induced, resulting in the vibrational energy change (impulsive Raman scattering). The amount of energy change was obtained by analyzing the fluorescence emitted by transition from the B state to the X state, and was found to obey quantum mechanics.

Isotope separation is one of the important technologies for the nuclear fuel cycle in our country. We are involved in fundamental research to develop new isotope-separation schemes using advanced laser devices. In one such recent study, we successfully demonstrated an elementary step important for the precise control of molecular vibration.

Conventional schemes of isotope separation using narrow band lasers are hard to extend to heavy elements, in which the isotope shift in the absorption spectrum is small and thus vulnerable to thermal noise. To overcome this difficulty, we are searching for new separation schemes based on broadband lasers, which can provide a strong and flexible way to control molecules with a newly developed pulse shaping technique and called “coherent quantum control”.

According to our recent theoretical studies, the isotope shift is amplified by two orders of magnitude at a sufficiently high vibrational level. To take advantage of this, we must develop the multiple excitation of molecular vibration, keeping the vibrational levels under control (Fig.4-13).

The experiment was carried out at the Kansai Photon Science Institute. Iodine molecules excited to the B state by a green laser was exposed to red ultra short laser pulses of 30fs (1fs = 10^{-15}s, Fig.4-14). The dispersed fluorescence spectrum emitted when returning from the B state to the X state was measured, and the change in vibrational energy was found to obey quantum mechanics (Fig.4-15). The process observed here, Raman scattering from the B state, had not been reported previously. In addition, we found that the direction of vibrational energy change can be controlled by chirping (temporal change of wavelength within a single pulse). In our next step, we will try to achieve multiple molecular vibration excitations and demonstrate that the isotope selectivity is thereby enhanced.

The vibration control presented here can be used for the amplification of a small isotope shift. After the amplification, conversion of chemical form and physical separation must be studied to realize a new isotope separation technique.

Reference

Matsuoka, L., Yokoyama, K. et al., Impulsive Stimulated Raman Transition on the β State of Iodine Molecules via Repulsive States, Physical Review A, vol.79, 061404(R), 2009, p.061404-1-061404-4.

4-7 Application of γ-ray Beams Generated from Laser-Electron Interaction
—Isotope-Specific Mapping of Heavily Shielded Objects—

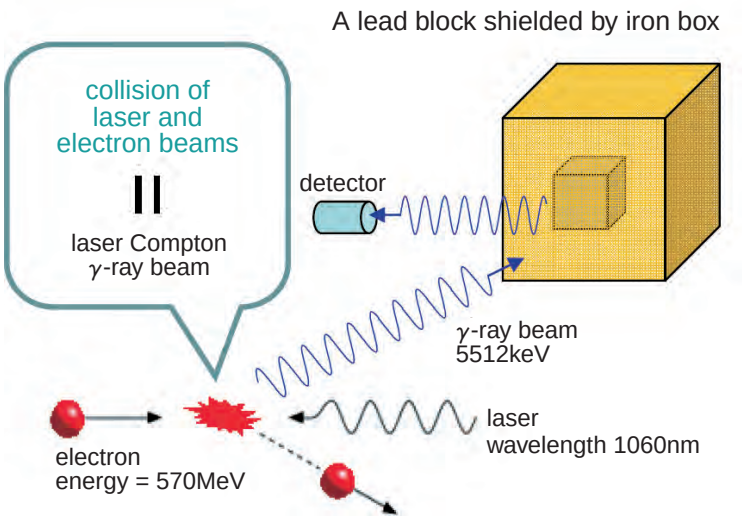

Fig.4-16 Experimental setup of isotope-specific mapping of shielded objects
A γ-ray beam generated by laser Compton scattering irradiates an iron box which contains a lead block. Position and geometry of the lead block is detected by resonant γ-rays scattered from the lead block.

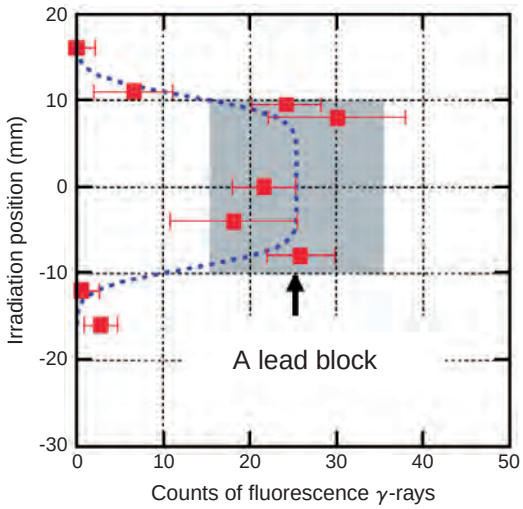

Fig.4-17 Experimental result of isotope-specific mapping
After vertical scanning with γ-ray beams, the position and geometry of the lead block shielded by iron box was detected. The gray box indicates the lead block.

Isotopic composition of materials cannot be determined with techniques of chemistry, and is particularly difficult when non-destructive and non-obtrusive detection is required as in many industrial situations. The ability to perform isotope-specific "photography" would have numerous applications. For example it would enable the detection of fissile and radioactive material of importance to development of the next generation of nuclear power systems.

We have proposed a nondestructive detection system based on nuclear resonance fluorescence (NRF) excited by laser-Compton scattering γ-ray sources (LCS) for the above purpose. This method is based on two key technologies: NRF and LCS. NRF provides a unique fingerprint of each isotope (as opposed to each atom) since the excitation energies in NRF are determined by the numbers of protons and neutrons in the nucleus of interest. Using NRF-based mapping with a tunable, monochromatic γ-ray beam, one can in principle construct a high-resolution, quantitative, isotope-specific map of the composition of any object.

We have made an experimental demonstration of NRF-based isotope mapping of deeply concealed objects. A block of ^{208}Pb was concealed in an iron box of 1.5cm thickness for this test. With irradiation from a γ-ray source tuned at the nuclear resonance energy of ^{208}Pb, we can detect ^{208}Pb in the test object as shown in Fig.4-16. In the experiment, we clearly obtained a one-dimensional image of the block of ^{208}Pb concealed in the iron box. It should be noted that the mapping is isotope specific as opposed to element specific.

The experiment was conducted at the laser Compton γ-ray beam line of TERAS, an electron storage ring at Advanced Industrial Science and Technology (AIST). A lead metal (52% ^{208}Pb) 2x2x5cm block was used as a high Z material target concealed inside an iron box. The thickness of the front and back panels of the iron box was 1.5cm. 5512keV γ-rays irradiated the ^{208}Pb, and NRF signals from the target were measured by germanium detectors.

After scanning the irradiation position vertically, we carried out one dimensional isotope mapping of ^{208}Pb concealed in the iron box as shown in Fig.4-17, which was consistent with the geometry of the lead block.

NRF-based isotope mapping can be applied to the advanced safeguard technology required for a stable and secure supply of nuclear power energy. Isotope mapping is necessary and ideally suited for the non-destructive detection of clandestine fissile materials in cargo and assays of radioactive waste from the nuclear fuel cycle. We are developing a novel type of electron accelerator, an energy recovery linac, as a future high-flux γ-ray source.

Reference

Kikuzawa, N., Hajima, R. et al., Nondestructive Detection of Heavily Shielded Materials by Using Nuclear Resonance Fluorescence with a Laser-Compton Scattering γ-ray Source, Applied Physics Express, vol.2, no.3, 2009, p.036502-1-036502-3.

4-8 Developing Effective Anti-HIV Drugs

—Success in Determination of Positions of All Atoms in HIV-1 Protease—

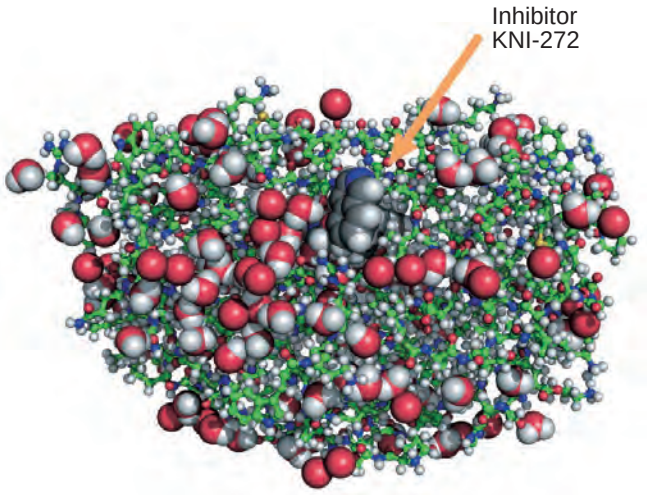

Fig.4-18 Positions of all atoms in HIV-1 protease-inhibitor KNI-272 complex
Colors represent hydrogen (white), carbon (green), nitrogen (blue), oxygen (red), and sulfur (yellow). Protein bound water molecules and the inhibitor are represented with sphere models.

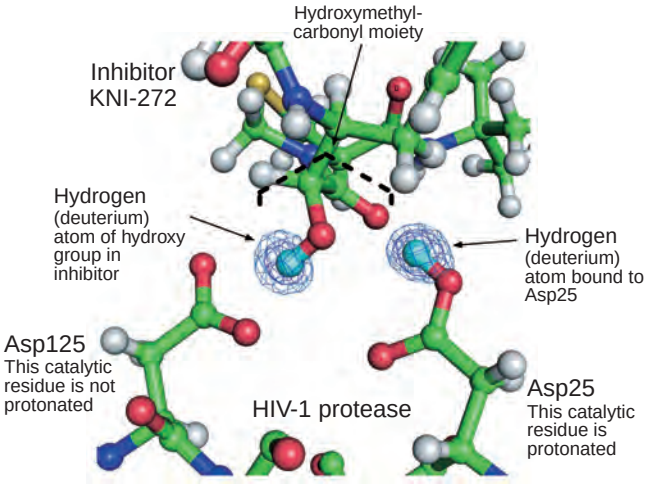

Fig.4-19 Structure in active site of HIV-1 protease
The meshes represent nuclear density, and indicate the location of hydrogen atoms. The portions in blue indicate higher density than those in cyan. The data reveal the protonation state and structure of catalytic residues, and location of a hydrogen atom belonging to the hydroxyl group in the inhibitor.

We have succeeded in determining the positions of all the atoms of an HIV-1 protease (protein)-KNI-272 (drug candidate) complex, including hydrogen atoms, by neutron crystallography.

HIV-1 protease is a dimeric aspartic protease which contains two catalytic aspartic residues (Asp25 and Asp125, defined by residue positions), and which plays an essential role in viral replication. To develop structure-based drug designs for HIV-1 protease inhibitors, it is necessary to understand the catalytic and inhibitor recognition mechanisms of HIV-1 protease. Many structural analyses of HIV-1 protease using X-ray diffraction have been reported. However, hydrogen atoms which are important for various functions have not been observed because the scattering factor of hydrogen atoms is much lower than that of other atoms. Thus, we detected those functional hydrogen (deuterium) atoms using neutron quantum beams which are effective for this purpose.

Neutron diffraction data was collected on the BIX-4 diffractometer installed at the 1G-A port of the research reactor JRR-3 in JAEA Fig.4-18 shows the positions of all the atoms, including hydrogen atoms, of the HIV-1 protease - KNI-272 complex.

Inhibitor KNI-272 used in this study contains a hydroxymethyl-carbonyl moiety that interacts with catalytic residues of HIV-1 protease. The neutron diffraction analysis directly showed that Asp25 is protonated and that Asp125 is non-protonated (Fig.4-19). Although the catalytic mechanism of HIV-1 protease has been a matter of some debate (due primarily to lack of direct visualization of hydrogen atoms in the catalytic mechanism), our results demonstrate that Asp25 provides a proton to the carbonyl group of the substrate and Asp125 contributes by activating the hydrolyzing water molecule for nucleophilic attack.

The structural information obtained in this study, including the protonation state of the catalytic residues, will provide important information for designing more effective inhibitors.

This study was performed in collaboration with Kyoto Pharmaceutical University, Osaka University and SOSHO, Inc. and published in Proceedings of the National Academy of Sciences of the United States of America.

Reference

Adachi, M. et al., Structure of HIV-1 Protease in Complex with Potent Inhibitor KNI-272 Determined by High-Resolution X-ray and Neutron Crystallography, Proceedings of the National Academy of Science of the United States of America, vol.106, no.12, 2009, p.4641-4646.

4-9 Protein Dynamics Revealed by Neutron Inelastic Scattering
—Watching Fluctuating Proteins—

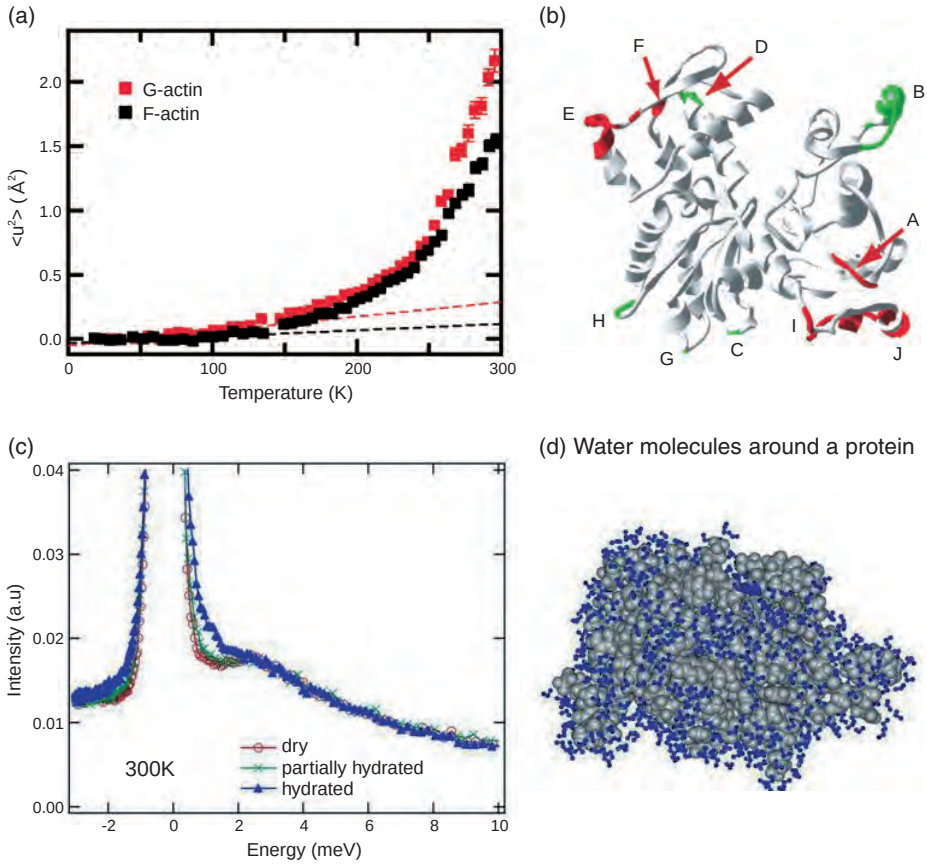

Fig.4-20
(a) Temperature dependence of the mean square displacements of actin in the monomeric state (G-actin) and polymerized state (F-actin) (b) Structure of the actin molecule. The regions shown in red or green denote the region showing large fluctuations. The fluctuations in the regions shown in green are considered to be suppressed by polymerization.

Fig.4-21
(c) Neutron inelastic scattering spectra of Staphylococcal nuclease (SNase) in various degrees of hydration. As water content increases, quasi-elastic scattering, which indicates large fluctuations, appears at 1-2meV. (d) Structure of SNase. Water molecules on the surface of the protein are shown in blue.

A living cell has various activities, the main players in which are proteins. The proteins are continuously exposed to thermal fluctuations of surrounding molecules, particularly water molecules which are most abundant, and the proteins themselves fluctuate. It is now well accepted that such thermal fluctuations (or dynamics) are important for the proteins to function. Complete understanding of protein function thus requires understanding of the dynamics of proteins with the water molecules around the protein.

Neutron inelastic scattering is the only method to directly "watch" thermal fluctuations of the proteins. We have been studying the dynamics of the proteins and the effects of the water molecules on them using various techniques of neutron inelastic scattering. Fig.4-20 shows the temperature dependence of the mean square displacements (MSD) of the protein actin, estimated from the neutron inelastic scattering experiments. The MSD is a direct measure of the amplitude of the fluctuations of the proteins. Actin has distinct structural states: the monomeric state (G-actin) and the polymerized state (F-actin). It was shown for the first time that G-actin and F-actin have different amplitudes of fluctuations. Furthermore, it was suggested that such differences arise from the different behavior of the loop regions involved with polymerization on the surface of the actin molecule. These results provide important information for elucidating the polymerization mechanism of actin.

How are such dynamics of the proteins affected by the surrounding water molecules? To investigate the effects of the water molecules, we performed neutron inelastic scattering experiments on the protein Staphylococcal nuclease (SNase), at different degrees of hydration. Fig.4-21 shows neutron inelastic scattering spectra of SNase in the dry state, the fully hydrated state (the protein is fully covered with a layer of water molecules), and a partially hydrated state. The spectra in the dry state and the partially hydrated state are similar, while the spectrum in the fully hydrated state shows inelastic scattering which indicates large fluctuations. This indicates that water molecules surrounding the protein are indispensable for the large fluctuations of the protein to occur, and thus are indispensable for the proteins to function.

References

Fujiwara, S. et al., Differences in Internal Dynamics of Actin under Different Structural States Detected by Neutron Scattering, Biophysical Journal, vol.94, issue 12, 2008, p.4880-4889.

Nakagawa, H. et al., Hydration Affects Both Harmonic and Anharmonic Nature of Protein Dynamics, Biophysical Journal, vol.95, issue 6, 2008, p.2916-2923.

4-10 Utilization of Atmospheric Nitrogen as Nutrition by Leguminous Plants

—Imaging of Symbiotic Nitrogen Fixation Using a Positron-Emitting Tracer Imaging System—

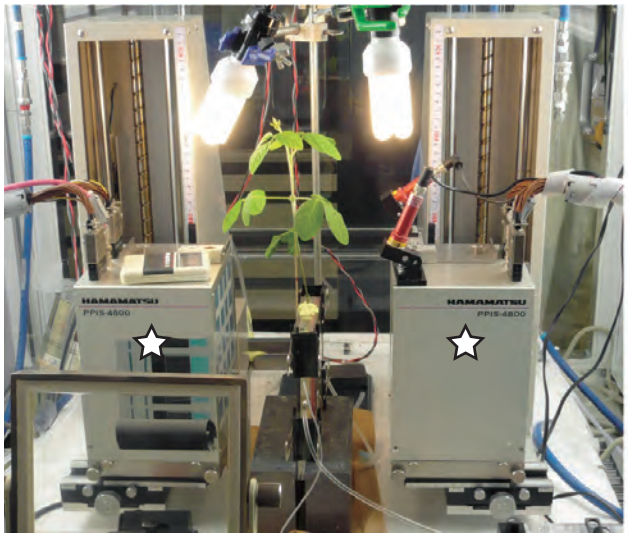

Fig.4-22 Experimental set-up (left) and a test plant (right)
A test soybean plant, whose underground part was inserted into a sealed plastic box, was placed between the detectors (star signs) of the PETIS apparatus installed in a growth chamber for plants. First, the box was filled with hydroponic solution. When the PETIS imaging was started, the level of the solution was lowered and the gaseous [^{13}N]N_2 radiotracer was introduced into the box simultaneously. Nodules were exposed to the radiotracer for 10 min and then flushed with fresh air. A static image was made every 10s, and in total 360 serial images were obtained from one experiment.

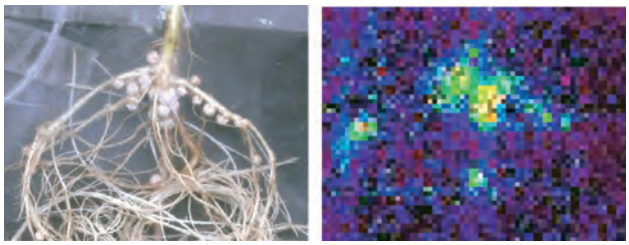

Fig.4-23 Underground part with many nodules (left) and the PETIS image of the same area (right)
Individual nodules can be identified in the PETIS image. The fixation rate of the whole nodules was estimated to be 7μg N_2 h^{-1} in this case.

Nitrogen is one of the most important nutritional elements in the soil for cultivation of plants. Although it is rich in the atmosphere as nitrogen gas (N_2), in this form it is unusable as nutrition by eukaryotes and must be converted into nitrogen compounds such as ammonium by (bio)chemical processes called “nitrogen fixation”. Symbiotic nitrogen fixation is a representative example of this process in nature, which is mainly performed in the nodules of leguminous plants in collaboration with rhizobia (soil bacteria). Industrial nitrogen fixation, another representative process, has been a foundation of modern agriculture through its role in producing chemical fertilizers. However, this process completely depends on fossil energy resources. Therefore, symbiotic nitrogen fixation is considered to be a key to realizing sustainable agriculture over the world which does not lead to overconsumption of natural resources.

We have been developing a non-invasive imaging method for plant study, the positron-emitting tracer imaging system (PETIS) which can visualize movement of various substances inside an intact plant body. In this study, we established a new production method of ^{13}N-labeled nitrogen gas tracer and successfully obtained the world’s first images of the fixed nitrogen in nodules of intact soybean plants (Figs.4-22 and 4-23). Moreover, the fixation activities of the nodules were quantitatively estimated from the PETIS images.

This non-invasive technique enables examination of the effects of various treatments on the fixation activity with the same plant. It will facilitate research into the regulation mechanism of symbiotic nitrogen fixation. Excess application of nitrogen fertilizers often results in decrease of the soybean yields due to reduction of the plant’s own symbiotic nitrogen fixation activity. Our technique may be very useful to establish the best fertilizer management with efficient symbiotic nitrogen fixation, which will lead to sustainable and environment-friendly food production, potentially doubling the soybean production in Japan. Because leguminous plants are also used as oil crops and green manure, much wider benefits are expected in the future.

Reference

Ishii, S., Suzui, N., Ito, S., Ishioka, N. S., Kawachi, N., Ohtake, N., Ohyama, T., Fujimaki, S., Real-Time Imaging of Nitrogen Fixation in an Intact Soybean Plant with Nodules Using ^{13}N-labeled Nitrogen Gas, Soil Science and Plant Nutrition, vol.55, no.5, 2009, p.660-666, doi: 10.1111/j.1747-0765.2009.00403.x.

4-11 Just 10 Heavy-Ions Induce Drastic Radiation Effect on a Million Cells
—Analysis of Bystander Effect Using Heavy-Ion Microbeam—

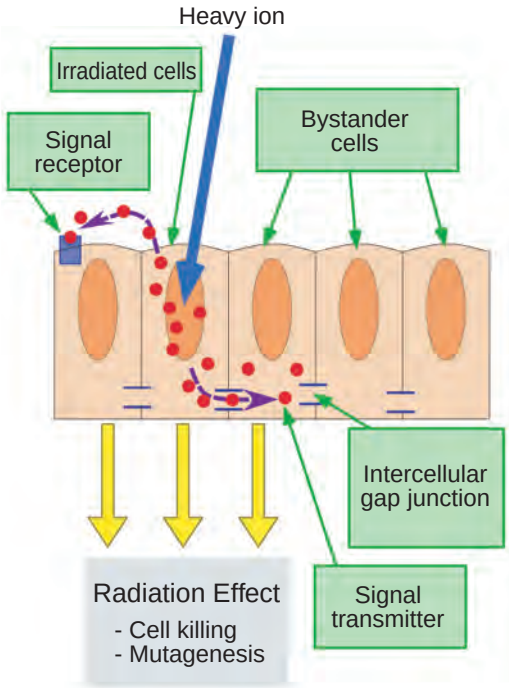

Fig.4-24 Bystander effect
Irradiated cells communicate to neighboring non-irradiated bystander cells by transmitting an irradiation signal substance, which induces radiation effect on bystander cells as well.

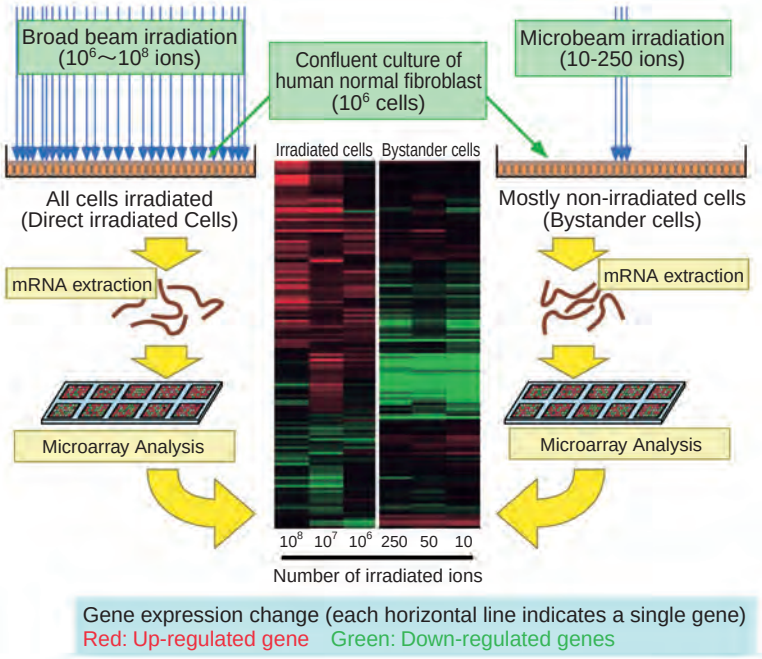

Fig.4-25 Microarray analysis of genes activated in bystander cells
The effect on bystander cells was examined by microbeam irradiation of the confluent culture containing approximately 10^6 cells with a very limited number of ions (10-250). The expression profile of the bystander cells was completely different from that of the irradiated cells.

The form and the function of living organisms are the result of the functioning of individual cells and their intercellular communications. Recently, it has become known that such intercellular communication also contributes to the response of living organisms to radiation. In the phenomenon called the "bystander effect", non-irradiated cells neighboring irradiated cells (bystander cells) exhibit radiation effect because they receive a signal transmitter substance from irradiated cells (Fig.4-24).

Heavy-ion beams are utilized for ion beam breeding and for cancer therapy because of its unique biological effectiveness. The elucidation of the mechanisms underlying biological responses to heavy-ion radiation is necessary to advance these useful applications. Analyzing the mechanisms should also contribute the assessment of health risk of space radiation, which includes low-dose heavy-ion radiation. In the cell population irradiated by low-dose of heavy-ion, the contribution of bystander effect becomes large because of an unevenness of dose distribution in the target cell population by low dose heavy-ions. Therefore, we developed a heavy-ion microbeam system in the TIARA facility of JAEA-Takasaki, and have studied the mechanism of cellular response induced by heavy-ion irradiation. This system can irradiate targeted individual cells with a desired number of heavy-ions, and distinguish irradiated cells and non-irradiated bystander cells during a post-irradiation observation period.

Biological responses of irradiated and bystander cells of human normal fibroblast were investigated using a confluent culture of these cells, which has an ability of intercellular communication through gap junctions. The effect in bystander cells was examined using a microbeam irradiation of very limited number of ions (10 - 250 ions) to irradiate the confluent culture containing approximately 10^6 cells (Fig.4-25). From the irradiated samples, mRNA was extracted and its gene expression was analyzed using a microarray. Among the gene expressions that showed more than 1.5-fold changes, the genes related to cell cycle or death and cell communication were up-regulated in irradiated cells. On the other hand, a completely different set of genes was up-regulated in bystander cells. Hereafter, we will analyze the roles of these bystander-activated genes in radiation induce cellular communications and so elucidate the effect of low-dose heavy-ion radiation on living organisms.

Reference

Iwakawa, M., Hamada, N., Imadome, K., Funayama, T. et al., Expression Profiles are Different in Carbon Ion-Irradiated Normal Human Fibroblasts and Their Bystander Cells, Mutation Research: Fundamental and Molecular Mechanisms of Mutagenesis, vol.642, issues 1-2, 2008, p.57-67.

4-12 New Drug for Concurre t Cancer Chemotherap and Rad otherapy
—Development of a Nano-Capsule Opened by Radiation—

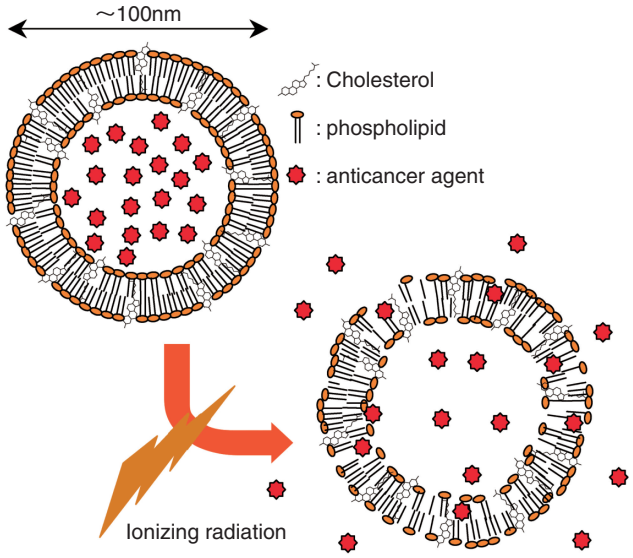

Fig.4-26 Schematic of a liposome opened by radiation
A liposome contains dilinoleoyl phosphatidyl choline (DLOPC), which is extremely vulnerable to ionizing radiation. Degradation of DLOPC by radiation makes the liposome bilayer unstable.

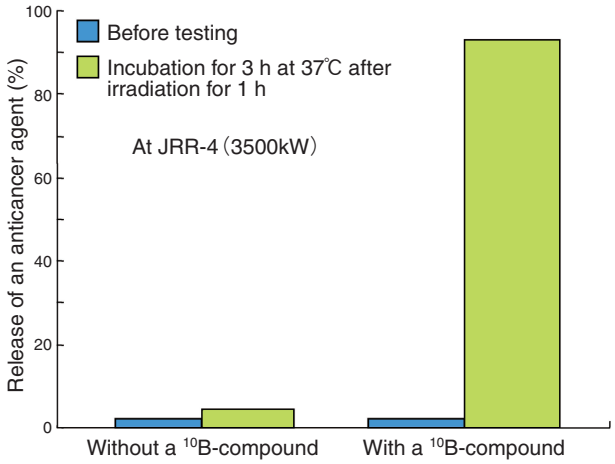

Fig.4-27 Release of an anti-cancer agent from a liposome upon thermal neutron irradiation
A liposome (DLOPC: distearyl phosphatidylcholine: cholesterol = 2 : 2 : 6) is easily broken apart by neutrons when it encapsulates a boron (^{10}B) compound as well as an anti-cancer agent.

Presently, half of all Japanese are expected to get cancer, the "national disease". Surgery, chemotherapy, and radiotherapy are generally performed to remove tumors. Actually, combinations of these therapies are usually efficient for this aim. However, chemotherapy and radiotherapy are still in the development stage because these therapies often give physical and/or mental stress to the patients. Direct administration of an anticancer agent sometimes has side effects due to undesirable influence upon normal cells. To avoid this, development of drug delivery systems (DDS) for anticancer agents which transfer them selectively to cancer cells is essential. In radiotherapy research, tumor-selective irradiation is now one of the main goals. Fortunately, heavy ion beams, whose particle energy can be controlled strictly, are expected to be a site-selective radiation. Now, we have developed a nano-capsule (liposome) that breaks when irradiated, for a new concept of DDS: concurrent cancer chemotherapy and radiotherapy (Fig.4-26).

We investigated breakability of a variety of liposomes which have different lipid compositions and different lipid compositions and different lipid content ratios, using X-rays which are easy to use in experiments. At a result, we found that the breakability can be controlled by changing the ratio of three lipid components (distearyl phosphatidylcholine, dilinoleoyl phosphatidylcholine, and cholesterol) and the lipid concentration of the liposome suspension. We also found that radiation dose-rate also influences the breakability. To date, the liposome can be degraded by several tens of Grays, which is comparable with a maximum dose at an affected part (tumor), in radiotherapy using a heavy ion beam. On the other hand, the liposome withstands thermal neutrons that are used in neutron capture therapy effective in brain tumors. However, we succeeded in making the liposome weak against thermal neutrons by co-encapsulation of a ^{10}B-compound into the liposome along with an anticancer agent (Fig.4-27).

Although more development in, e.g., selectivity to tumors is needed for clinical use, we do expect that this liposome DDS can contribute to diminish physical and mental stress during cancer treatments as a 'bridge' which offsets a demerit of one therapy with a demerit of another therapy.

Reference
Akamatsu, K., Development of a Thermal Neutron-Sensitive Liposome for a Novel Drug Delivery System Aiming for Radio-Chemo-Concurrent Cancer Therapy, Radiation Physics and Chemistry, vol.78, issue 12, 2009, p.1179-1183, doi: 10.1016/j.radphyschem.2009.07.007.

5 Nuclear Safety Research

To Support Safety Regulations and to Ensure Nuclear Safety and Confidence

NSRR for studies on reactivity accidents

RFEF for post irradiation examination of nuclear fuel

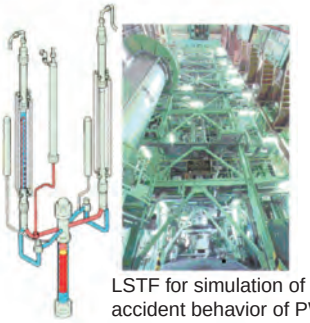

LSTF for simulation of accident behavior of PWR

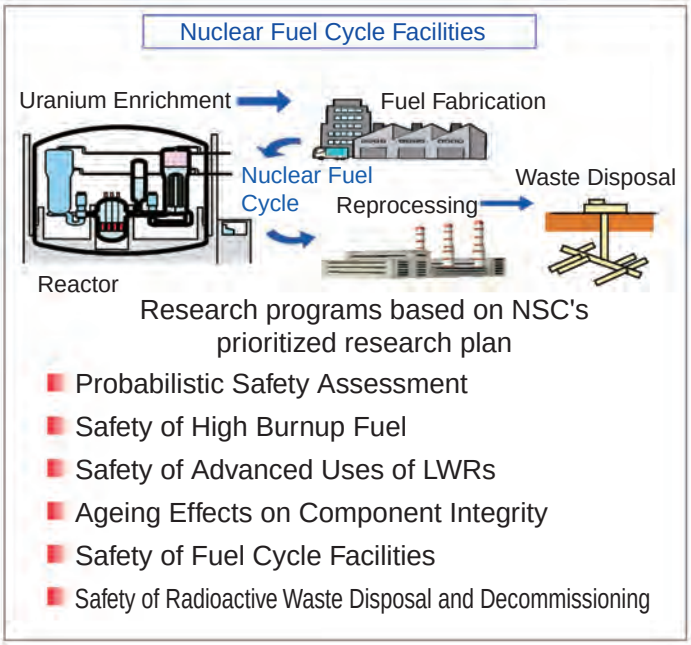

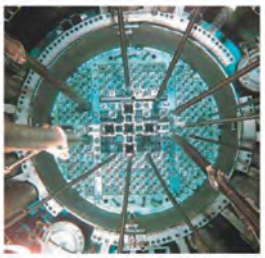

JMTR for testing material and fuel behavior

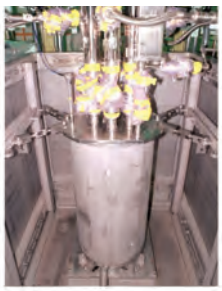

NUCEF for safety research for fuel cycle facilities

Fig.5-1 Major subjects of safety research and research facilities
In order to develop safety assessment technologies for nuclear facilities, analytical models must be developed and validated on the basis of the underlying mechanisms which come to be understood from tests that simulate phenomena in normal and accident conditions. Various large scale test facilities of JAEA are providing important data and contributing to nuclear safety in the international community.

To assure the safety of nuclear facilities, the regulatory authorities of the government perform safety examinations and inspections of the safety design and management by utilities. Safety research is essential for providing a scientific and technical knowledge base for developing guidelines and standards for regulatory decision making.

Safety research at JAEA is conducted according to the "Prioritized Plan for Nuclear Safety Research" made by the Nuclear Safety Commission (NSC), which sets priorities for safety research to be carried out based on future trends in regulation. The major subjects for us to study are shown in Fig.5-1.

Furthermore, we are supporting the regulatory body the Nuclear and Industrial Safety Agency (NISA) and its supporting organization Japan Nuclear Safety Organization (JNES) by conducting research on various technical issues in safety regulation which they have contracted us to do.

The results of nuclear safety research contribute to the maintenance and improvement of safety of the nuclear facilities and also to fostering public confidence in nuclear safety.

The following paragraphs briefly describe new results from the programs shown in Fig.5-1.

In the program on probabilistic safety assessment (PSA), a computer code for accident consequence analysis was validated by field data obtained in the area affected by the Chernobyl accident. (Topic 5-1).

For the study of high burnup fuel safety, a series of tests were conducted to measure the oxidation rate of fuel cladding which had been used for a long time when there are loss-of-coolant accident conditions (Topic 5-2). Furthermore, a study provided understanding of mechanisms behind change in the microstructure of fuel pellets due to long use of the fuel (Topic 5-3).

In the study of safety assessment of advanced uses of light water reactors, an experimental study on the heat transfer at the fuel surface under post-boiling transition conditions provided a new model for safety assessment with higher accuracy (Topic 5-4).

For the structural integrity assessment of reactor components, a detailed analysis was done of the effect of seismic loading on the crack growth in a reactor which was assumed to have stress corrosion cracking in the piping or internal structure (Topic 5-5).

In the research on safety evaluation of nuclear fuel cycle facilities, a rapid dose evaluation method was developed for use in a criticality accident in a nuclear facility (Topic 5-6).

For the safety assessment of radioactive waste disposal, a new analytical model was developed for prediction of the performance of the bentonite clay material that covers the steel container of high level radioactive waste in geological disposal (Topic 5-7). Furthermore, for the development of methods to analyze migration of radionuclides in groundwater, analysis of ground water system observations on a regional scale were performed for validation of a conceptual representation of a flow system (Topic 5-8).

5-1 Testing Environmental Assessment Models Using Chernobyl Data
—Validation of OSCAAR Models for Assessing Accident Consequences—

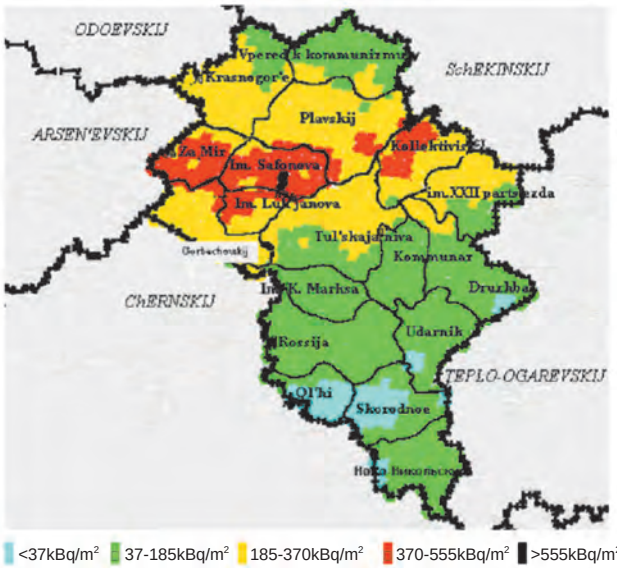

Fig.5-2 Soil contamination of ^{137}Cs in the Plavsk region
The model validation exercise was carried out with environmental data available on the Chernobyl accident in the Plavsk district about 200km south of Moscow. Although no measurements of ^{131}I concentrations in air and soil were made, the levels of ^{137}Cs soil contamination in all the settlements as well as meteorological data and information on inhabitants' lifestyle and food habits were available for testing model calculations. Soil contamination of ^{137}Cs was heterogeneous, ranging from 20 to 600kBq/m^2 due to rainfall during the movement of the radioactive cloud. Participants in this exercise were requested to estimate the contamination of ^{131}I in soil, transfer of ^{131}I in the food chain and thyroid dose to the residents.

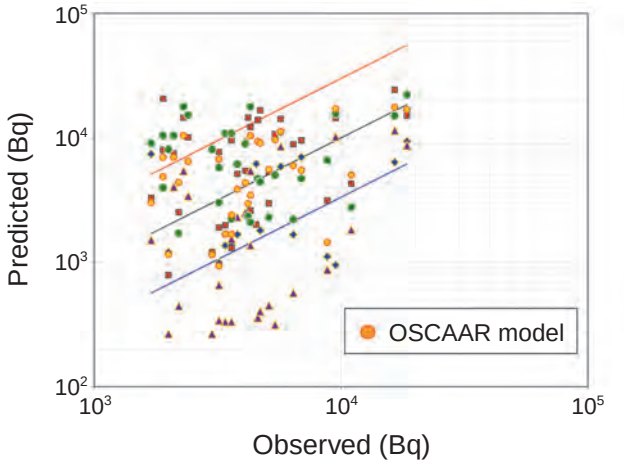

Fig.5-3 ^{131}I contents in thyroid of residents in the Plavsk region
This shows the predicted versus observed data of ^{131}I contents in thyroids of individuals from 15 settlements and Plavsk town. The results from five models including OSCAAR were shown in this figure. The blue and red lines indicate the range of 1/3 to 3 times the observed value. About 70% of the model predictions of ^{131}I contents in thyroid were within a factor of three of the observed values. The main uptake routes of radioiodine were inhalation of contaminated air and ingestion of contaminated food. This exercise showed that the iodine metabolic model which most participants used reasonably predicted the ^{131}I content in thyroids if the intake of radioiodine through the air-pasture-milk pathway was correctly inputted. The contribution of inhalation to ^{131}I content in thyroids was less than 10% of the total content.

Various kinds of mathematical models are used to assess the transport of radionuclides in the environment and to predict the potential pathways and levels of human exposure to the radionuclides. These models are used primarily to estimate the consequences to the public and the environment in which complete sets of measurements cannot be obtained: safety analysis of routine operations and accident situations of nuclear installations in a regulatory process, or dose reconstruction from past releases of radionuclides. When decisions on safety or acceptable levels of contamination for regulatory purposes are based on model results, it is essential to establish a degree of confidence in these results for the sake of scientific and public credibility.

In this regard, JAEA is conducting the research on validation of transport models of radionuclides in the environment using field measurements of various kinds of exposure situations, environmental media, and radionuclides through participation in international exercises aimed at the testing and validation of such models which have been conducted since the Swedish sponsored BIOMOVS program started in 1986.

In the BIOMASS and EMRAS programs organized by IAEA, particular attention was given to ^{131}I and ^{137}Cs which are important radionuclides for environmental assessment that are products of operation of nuclear power plants and fuel cycle facilities. We have tested the predictive capabilities of biosphere transport and exposure models in the OSCAAR computer code developed by JAEA for the probabilistic safety assessment of nuclear installations. Examples of model predictions compared with observed data are shown in Figs.5-2 and 5-3 for a test in which the transport models of radionuclides from air to plants, pasture to animal products and the metabolic model of radioiodine in human body were validated using observed data of ^{131}I and ^{137}Cs in media of the environment such as air, soil, plants and animals. Such exercises provided good opportunities for testing the predictive capabilities of models, evaluating the uncertainty in models and parameters, and improving the credibility of environmental assessment models.

Reference

Homma, T., Validation of Environmental Assessment Models and Assessment of Effectiveness of Protective Measures Using Data from Chernobyl ^{131}I Releases; IAEA EMRAS Programme, Hoken Butsuri, vol.43, no.3, 2008, p.234-245 (in Japanese).

5-2 Oxidation Behavior of Fuel Cladding Used for a Long Time
—Influence of High Burnup on Oxidation Kinetics in LOCAs—

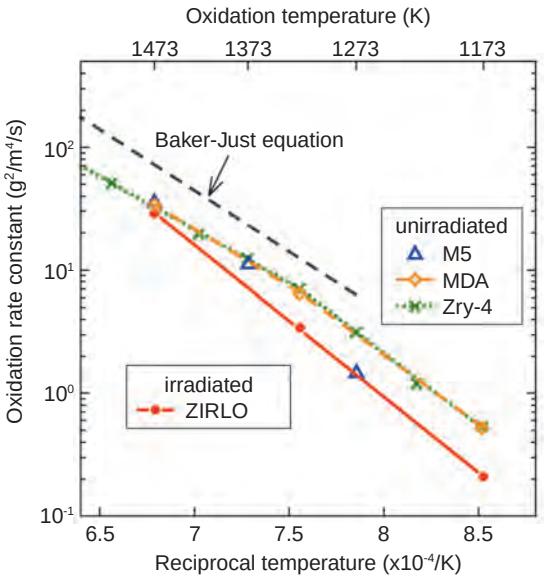

Fig.5-4 Temperature dependence of the oxidation rate constants, calculated from mass increase
Cladding used for a long time (irradiated ZIRLO) exhibits equivalent or smaller oxidation rates in comparison with unirradiated cladding. The rate constants of improved alloys (M5 and MDA) are equivalent to those of the Zircaloy-4 in its unirradiated condition.

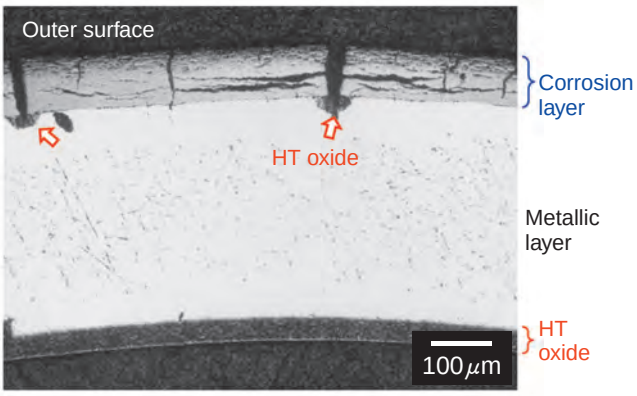

Fig.5-5 Radial cross section of the irradiated ZIRLO cladding after high-temperature oxidation test
On the cladding outer surface, high-temperature (HT) oxidation initiated at cracking positions of the corrosion layer. On the other hand, the oxidation layer is uniform on the inner surface. Growth of the inner-surface oxide is similar to that in the unirradiated cladding. Consequently, influence of hydrogen absorption and radiation damage on the high-temperature oxidation is small over the examined range, the corrosion layer having a protective effect.

Extension of the utilization period of reactor fuel, i.e. burnup extension, is being promoted worldwide for efficient use of natural resources etc. We performed experiments under simulated accident conditions to investigate the effects of long-term irradiation on fuel behavior during accidents and confirm fuel safety.

A loss-of-coolant accident (LOCA) is one of the postulated accidents considered in the safety design of a nuclear power plant. In LOCA conditions, fuel cladding is oxidized due to zirconium - steam reaction at high temperatures, and loses ductility when severely oxidized. Accordingly, it is very important to evaluate the oxidation kinetics precisely for the safety analysis. As burnup is extended, the corrosion layer grows and hydrogen absorption becomes more significant in fuel cladding, which may affect the high temperature oxidation under LOCA conditions. On the other hand, advanced alloys are being developed to improve corrosion resistance and help achieve higher burnup. It is necessary to investigate fuel behavior with the newly developed cladding under accident conditions. Hence, we performed isothermal oxidation tests with cladding that had been irradiated for a long time in European power plants in order to investigate the effect of high burnup and alloy composition on the high temperature oxidation.

The oxidation rates calculated from mass increase are summarized in Fig.5-4. The rate constants of high burnup ZIRLO cladding are lower than those of the unirradiated cladding at relatively low temperatures, while thedifference is small at 1473K. Fig.5-5 shows the microstructure in a radial cross section of an irradiated ZIRLO specimen after the high-temperature oxidation test. A thick corrosion layer that formed during the reactor operation is seen at the outer surface. The high temperature oxidation (HT oxide) appears to initiate at the positions where cracks are seen in the corrosion layer. It is generally accepted that the mechanism which governs the high-temperature oxidation of Zirconium alloy cladding is the diffusion of oxygen anions through the oxide layer. It is considered that the pre-formed corrosion layer suppressed the high-temperature oxidation by preventing the diffusion of oxygen to the surface of the metallic layer. On the other hand, increase in hydrogen absorption and changes in alloy composition had very little influence on the oxidation rate. The Baker-Just oxidation kinetics equation was found to still be applicable to the safety analysis of the high burnup fuel cladding in a LOCA.

The present study was conducted in FY2007 as part of the “Advanced Light Water Fuel Performance and Safety Research Program” commissioned by the Nuclear and Industrial Safety Agency (NISA) of the Ministry of Economy, Trade, and Industry (METI).

Reference

Chuto, T. et al., High Temperature Oxidation of Nb-Containing Zr Alloy Cladding in LOCA Conditions, Nuclear Engineering and Technology, vol.41, no.2, 2009, p.163-170.

5-3 Why Does the Microstructure of Fuel Pellets Change during Irradiation?

—Relationship between the Crystal Lattice Strain and Microstructural Change in UO_2 Pellets—

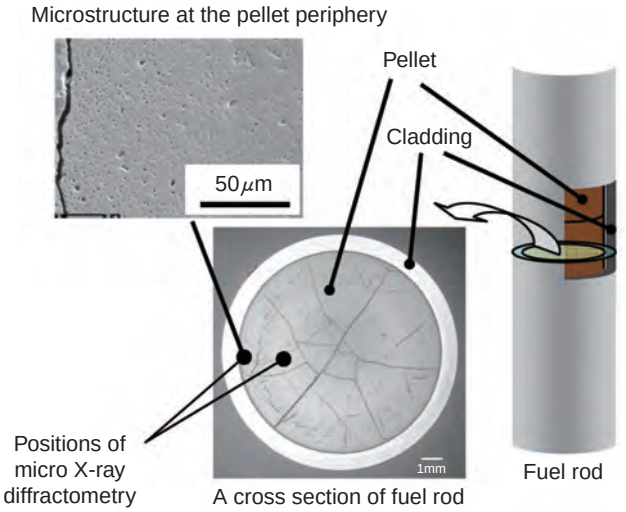

Fig.5-6 Ceramographs of high burnup fuel pellet
A cross section of high burnup fuel pellet was observed by an optical microscope and scanning electron microscope (SEM). Comparing the microstructures in the center and mid radius of the pellet, fine fission gas bubbles precipitated densely at the pellet periphery, and the microstructure changed significantly from that at fabrication.

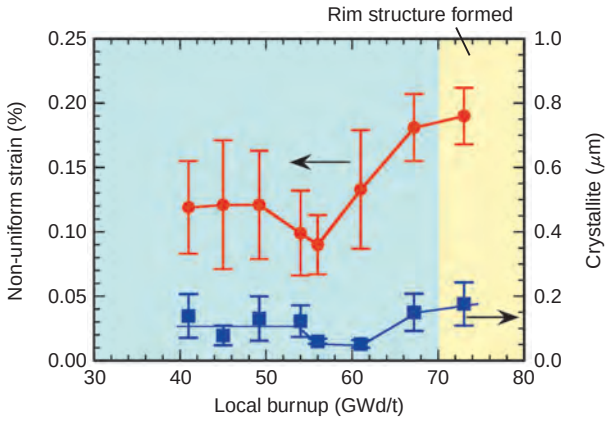

Fig.5-7 Local burnup dependence of non-uniform strain and crystallite size in the irradiated fuel pellets
Non-uniform strains and crystallite sizes in the irradiated fuel pellets were measured by means of micro X-ray diffractometry. It is considered that the decrease in the non-uniform strain at about 50GWd/t is mainly due to a tangle of dislocations (the formation of dislocation wall). The measured crystallite sizes were comparable with that of the subdivided grain in the rim structure.

Extending the utilization period of reactor fuel, i.e. burnup extension, is being promoted step by step for the efficient use of natural resources and the reduction of fuel cycle cost. With increase in fuel burnup, fission products accumulate in fuel pellets, and cladding corrosion progresses. Accordingly, in order to promote burnup extension, it is necessary to confirm fuel safety at high burnup.

At the periphery of a high burnup fuel pellet, fine fission gas bubbles precipitate densely and the crystal grains formed at the time of pellet fabrication are subdivided into fine grains was observed (Fig.5-6). A microstructure like this is called “rim structure”, and the fine bubbles in this region contain high-pressure fission gas. If the fission gas in this region is released during a reactivity initiated accident (RIA), pellet temperature increase and the cladding deformation would occur due to the degradation of the heat conduction between pellet and cladding which is caused by the additional fission gas release. These phenomena may affect fuel rod safety. Consequently, the investigation of rim structure formation conditions is an important subject of study.

Micro X-ray diffractometry was carried out at the peripheral and mid-radius regions of the fuel pellets which had different burnups. The lattice parameter was calculated from the angles of diffracted peaks, and the non-uniform strain and crystallite size were calculated from the broadening of diffracted peaks. The lattice parameter increased monotonously with increase in burnup, and exhibiting a peak at about 70GWd/t. The lattice parameter slightly decreased above 70GWd/t. The non-uniform strain decreased in the burnup range of 50-55GWd/t and increased above this burnup range (Fig.5-7). The strain energy densities stored in the crystal lattice were evaluated based on the lattice parameters and non-uniform strains. The strain energy densities were constant in the burnup range of 50-55GWd/t. From these results, it is suggested that the main cause of grain subdivision is the tangle of dislocations which forms during irradiation, and that the grain subdivision begins in the vicinity of 50GWd/t. The conditions for formation of rim structure can be understood by investigating the process of microstructure change in high burnup fuel, and this understanding will make it possible to evaluate fuel safety in the high burnup region in further detail.

The present study was conducted in FY2005 with funds for nuclear research from the Ministry of Education, Culture, Sports, Science, and Technology of Japan (MEXT), allocated based on evaluation by the Atomic Energy Commission.

Reference

Amaya, M. et al., Measurement of Crystal Lattice Strain and Crystallite Size in Irradiated UO_2 Pellet by X-ray Diffractometry, Journal of Nuclear Science and Technology, vol.45, no.3, 2008, p.244-250.

5-4 Exploration of Droplet Cooling Effect on Superheated Fuel

—Developing Models Estimating Post-BT Heat Transfer Coefficient and Rewetting Velocity—

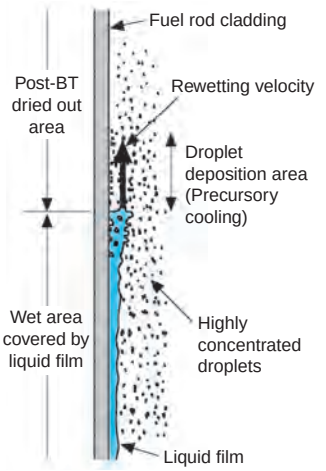

Fig.5-8 Rewetting influenced by droplet flow
Rewetting is a process to return HTC to acceptable levels by wetting the dried-out surface again and thus restarting water boiling. High mass flow rate, characteristic of AOOs, significantly enhances the rewetting because there is highly concentrated liquid droplet flow.

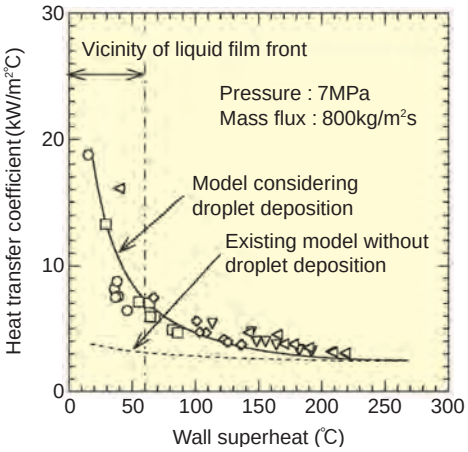

Fig.5-9 Comparison of measured and calculated HTC
Direct contact cooling by droplet deposition on dried surface is effective when the droplet density is high. This effect becomes significant on a surface heated much less than that needed for stable film boiling. The present model greatly improves the prediction, in particular in the low wall superheat range.

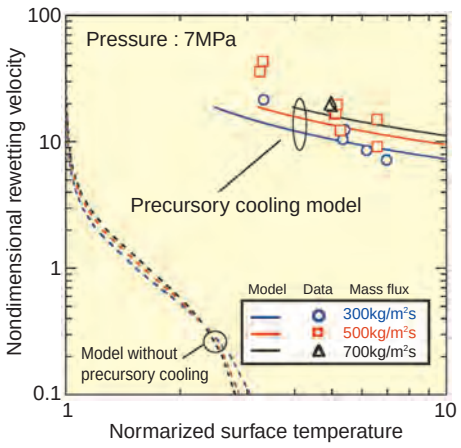

Fig.5-10 Comparison of measured and calculated rewetting velocities
The precursory cooling model shown by the solid lines predicts well the rewetting velocities, which are much larger than those predicted by the previous model (dashed lines). The wall temperature reduction near the rewetting front is enhanced by the precursory cooling effect of direct liquid droplet deposition.

In the Boiling Water Reactor, the fuel rod surface is covered with continuous liquid film for heat transfer. Depletion of the liquid film causes heat buildup. Such a deteriorated heat transfer is called boiling transition (BT), and these reactors have been required to have a design which does not allow this to occur even during Anticipated Operational Occurrences (AOOs). Results of recent studies, however, indicate that even if BT takes place, the rise in fuel cladding temperature could be small that it does not become any threat to fuel integrity, as long as the BT event terminates within a short period of time. Based on this new knowledge, the Atomic Energy Society of Japan (AESJ) proposed a new standard, the so-called post-BT standard, which allowed occurrence of BT if the dryout duration and peak cladding temperature (PCT) were kept within certain limits. We are conducting various experiments and analysis to confirm the technological appropriateness of the employed models to evaluate the dryout duration and the PCT in the post-BT standard.

The rewetting process shown in Fig.5-8 is important in the post-BT period, and it is difficult to predict. The rewetting velocity, defined as the propagation velocity of the liquid film front along the dried-out surface, is one of the key factors to determine the termination of the post-BT state. There is however little experimental data for AOO conditions. We performed experiments over a broad range of power, water flow rate and temperature of dried-out cladding, including the ranges allowed in the post-BT standard, using a round pipe test section that simulates the fuel cladding. Prediction models for the heat transfer coefficient (HTC) and the rewetting velocity were developed based on the obtained data.

From these experiments, it was found that large cooling water flow enhances generation of droplets that cool the dried-out surface just ahead of the rewetting front where they come into direct contact as shown in Fig.5-8, thus improving heat transfer. Fig.5-9 shows the comparison of the developed and existing models with data of the HTC. The predictions for the low wall superheat range were significantly improved.

The effective heat transfer by the droplet deposition causes great increase in the rewetting velocity. This effect of direct contact of droplets on the HTC has been called “precursory cooling” in the previous studies. We integrated this effect into our prediction model. The comparison shown in Fig.5-10 indicates that the present model considering the precursory cooling effect reproduces the experimental data well. It is concluded that the precursory cooling plays a predominant role in the liquid film propagation during rewetting phase in an AOO situation when there is highly concentrated droplet flow.

Reference

Sibamoto, Y. et al., Measurement and Analysis for Rewetting Velocity under Post-BT Conditions during Anticipated Operational Occurrence of BWR, Proceedings of 17th International Conference on Nuclear Engineering (ICONE 17), Brussels, Belgium, 2009, ICONE17-75287, 10p., in CD-ROM.

5-5 Assessing the Structural Integrity of Reactor Piping in Large-Scale Earthquake
—Effect of Weld Residual Stress and Excessive Loading on SCC Growth—

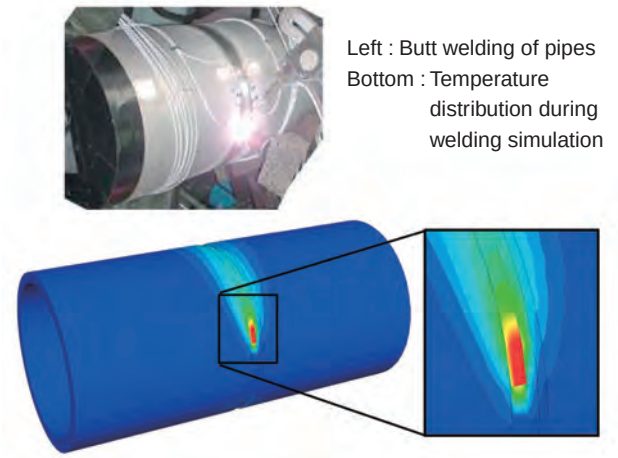

Fig.5-11 Overview of welding simulation
To increase the accuracy of weld residual stress evaluation, welding simulation has been improved by comparison with the results of experiments on butt-welds of various sizes of pipes. The moving heat source and the adhesion of metal being welding were simulated, as shown in Fig.5-11.

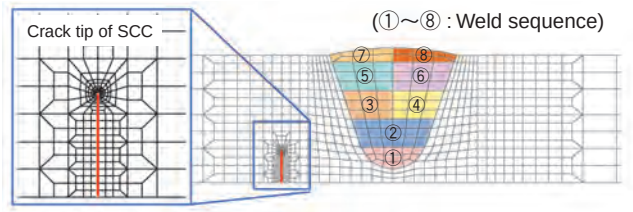

Fig.5-12 2D FEM model for welding simulation and SCC

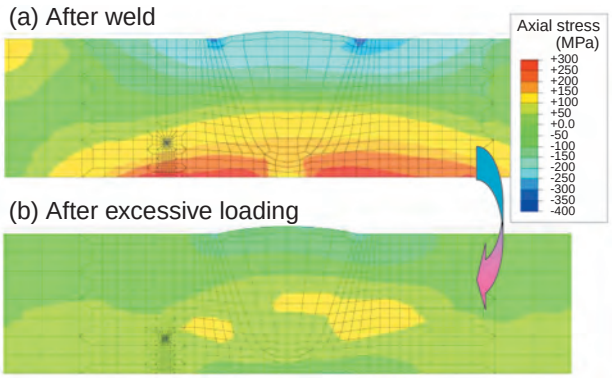

Fig.5-13 Effect of earthquake on weld residual stress
Multi-pass welding simulation was conducted using the model illustrated in Fig.5-12. After the welding, tensile stress at the inner surface of pipe was produced as shown in Fig.5-13(a). After applying a prescribed axial displacement of 0.2% simulating the excessive-loading, a relaxation of residual stress was found around the welded region as can be seen in Fig.5-13(b).

The regulatory guide for reviewing seismic design was revised in September 2006 to redefine new range of envisioned earthquake ground motions and incorporate the concept of residual risks into the design framework, so as to reflect recent findings. Also, the July 2007 Niigata-ken Chuetsu-Oki earthquake ground motion exceeded the motion which were used in the design. Both of these events have made us aware of the need to assess the effect of large-scale earthquakes beyond the design basis of reactor components regarding seismic structural integrity. On the other hand, stress corrosion cracking (SCC) has been observed around the welds of reactor piping. Residual stress produced by welding is one of the most important factors influencing structural integrity, particularly SCC, because high tensile stresses at the inner surface and through the thickness around a pipe weld affect the initiation and growth behavior of SCC. It is, therefore, important that the structural integrity assessment take into account the effect of excessive loading, caused by a large-scale earthquake beyond the range envisioned in the design, on the weld residual stress in the pipe. However, the evaluation of residual stress distribution requires expertise and special skills for detailed weld simulation and experiments.

We have developed a welding simulation technique with excellent accuracy to evaluate the weld residual stress based on a finite element method (FEM) as shown in Fig.5-11. Using this simulation technique, weld residual stress around a butt weld for stainless steel piping was evaluated (Figs.5-12 and 5-13(a)). Since a large-scale earthquake may affect the weld residual stress distribution, the effect of excessive loading simulated by prescribed axial displacements on redistribution of the weld residual stress around piping weld was also evaluated as shown in Fig.5-13(b). From these results, it was clearly indicated that excessive loading caused residual stress relaxation, i.e. tensile stress at the inner surface of pipe decreased as applied seismic load increased. Similar relaxation behavior on residual stress was also observed in the case where there was an SCC near a weld. Therefore, there is a suppressive effect of large-scale earthquake on SCC growth and hence the evaluations of the structural integrity of reactor piping due to earthquakes are too conservative from the viewpoint of mechanical stress.

The effect of scattering of residual stress due to welding on structural integrity is now being investigated by application of a probabilistic fracture mechanics analysis method.

Reference

Katsuyama, J., Onizawa, K., Analytical Study of the Effect of Excessive Loading on Welding Residual Stress and Crack Growth near Piping Welds, Journal of Solid Mechanics and Materials Engineering, vol.3, no.3, 2009, p.563-571.

5-6 Development of Rapid Dose Evaluation Method for Criticality Accidents
—High Dose Measurement of Neutrons with Thermo-Luminescence Dosimeter—

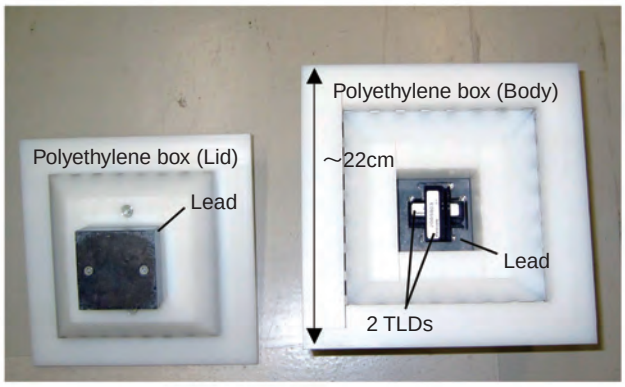

Fig.5-14 TLD outlook
The TLD is used in a polyethylene box of a cubic shape. Irradiation was performed with the box installed in the TRACY reactor room.

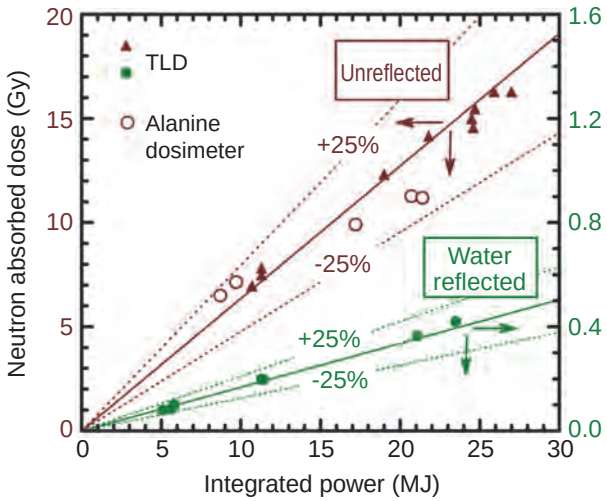

Fig.5-15 Measurement results
Neutron dose measurements had error less than 25% over the dose range (100mGy ~ 10Gy) stipulated by the IAEA. Results agreed with results of the other measurement method (alanine dosimeter).

The JCO criticality accident with the death of two workers which occurred in the autumn of 1999 is still fresh in our memory. Such an accident must not happen again. It is, however, also necessary to develop impact evaluation methods and counter action techniques in case of unlikely accidents.

The International Atomic Energy Agency (IAEA) provided technical guidelines for treatment of injuries due to heavy irradiation in a criticality accident, and in particular stipulated technical performance standards for the dosimetry. The guidelines require ➢appropriate medical care for heavily irradiated persons, ➢sufficient communication to the public, and ➢assuring those not significantly irradiated. Technical requirements are thus made that ➢the dose can be measured in terms of dose absorbed in the body, ➢in the range from 100mGy to 10Gy, and ➢ total radiation measurements be within 50% uncertainty in the first 48 hours, separate measurements for neutrons and γ-rays be within 25% uncertainty for the first week.

To demonstrate that these technical goals are achievable, first, widely utilized dosimetry methods were reviewed, and then, a thermo-luminescence dosimeter (TLD) (Fig.5-14) suitable for easy neutron dosimetry was employed. Experiments were performed in the Transient Critical Experiment Facility (TRACY) to irradiate the TLD with strong radiation as in a criticality accident. Radiation doses were varied by changing the distance between the TLD and the TRACY core or by reducing neutron leakage with a water reflector installed around the TRACY core. Another kind of dosimeter and computer simulation were used together, to obtain the correct irradiation dose. It was also confirmed that it was feasible for the measurement results to be obtained within 48 hours after the experiments. The TLD was originally designed to measure the dose equivalent instead of the absorbed dose, so a calculation method with a computer using conversion coefficients between those doses was established as well.

Fig.5-15 shows the neutron doses measured with the TLD; measurement error was within 25%. This not only satisfies the IAEA requirements but also demonstrates the capability for more rapid neutron dose measurement.

The intensity and characteristics of the radiation used in these experiments simulated a criticality accident well. To put the TLD to practical use, it is, however, still necessary to investigate if this measurement method is applicable in actual nuclear fuel facilities, and if the TLD can be handled appropriately under the extreme conditions of a real critical accident.

Reference

Murazaki, M., Tonoike, K. et al., Measurement of Neutron Dose under Criticality Accident Conditions at TRACY Using TLDs, Journal of Nuclear Science and Technology, vol.46, no.2, 2009, p.193-203.

5-7 Verifying Safety of Coastal Radioactive Waste Disposal Site

—Modeling of Mass Transport upon Chemical Reaction with Saline Groundwater—

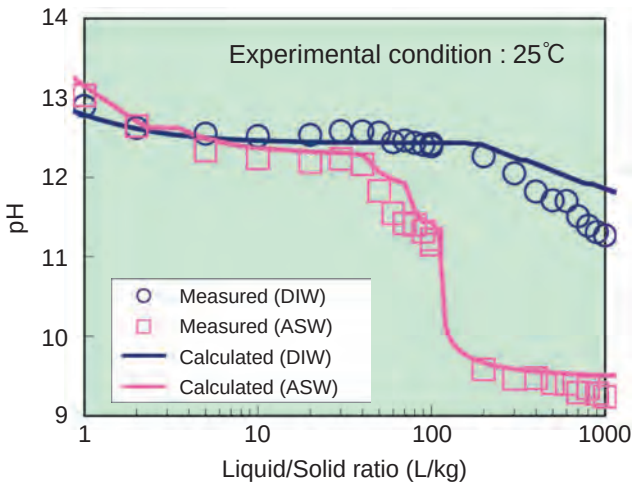

Fig.5-16 Verification of mineral model by alteration experiments
To simulate cement alteration by fresh and saline groundwater, granulated cement was immersed repeatedly in deionized water (DIW) and artificial seawater (ASW), respectively. Liquid/solid ratio represents volume of liquid immersing 1kg of cement, a higher ratio simulating larger amounts of groundwater immersing for a longer period. The two solid curves show calculations using the mineral model; there is good agreement with the measurements.

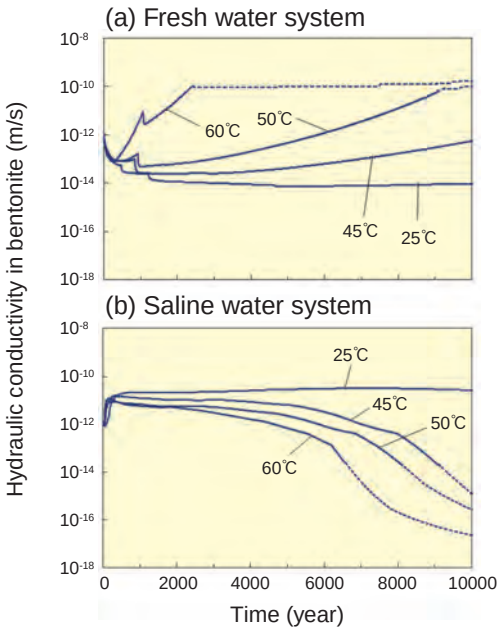

Fig.5-17 Change of hydraulic conductivity in bentonite-cement barrier system
The mineral model was used to calculate changes of hydraulic conductivity in bentonite in contact with cement in (a) a fresh water system and (b) a saline water system over a 10000 year period. The temperature is influences the hydraulic conductivity in both systems. The trend in the difference observed between (a) and (b) may be due to the systems generating different minerals.

In the Japanese high-level radioactive waste (HLW) disposal program, vitrified HLW is encapsulated in a steel container called overpack, and placed in a repository surrounded with bentonite clay material in a stable underground site. Bentonite prevents groundwater from intruding into the waste, and so it is necessary to estimate the long-term changes in the properties of bentonite, since it confines long-lived radionuclides.

The cement used in the repository likely generates an alkaline groundwater which dissolves montmorillonite, the main constituent of bentonite. Because the radionuclide confining property of the bentonite arises from montmorillonite, modeling the alterations of cement and montmorillonite is necessary to predict deterioration of the confinement performance. We performed laboratory experiments on alkaline components generated during long-term alteration of cement material and montmorillonite dissolution in those alkaline solutions, using compacted bentonite simulating the repository conditions, and then proposed models based on the results.

To verify safety of the repository, chemical reactions of cement-bentonite-groundwater systems were calculated using the models. Concurrent calculations of mass transport in cement and bentonite are needed because the parameters in the calculations are linked to each other. Verification is very important for such a coupled calculation model; we have been verifying it by comparing results of the model calculation with observations from laboratory experiments.

Groundwater is probably mixed with seawater at a repository in a coastal area in Japan. We focused on that situation and considered possible minerals generated in cement alteration by seawater in a secondary mineral generation model. The model was verified through alteration experiments with cement (Fig.5-16).

In addition, the model was used to predict the alteration of cement-bentonite systems over a 10000 year period. Searching into the calculation results revealed the great influence of temperature on the degree of alteration, and the complex effect of salinity concentration upon alteration behavior (Fig.5-17). This knowledge establishes key issues for long-term analysis of alteration.

Reference

Yamaguchi, T., Yamada, F., Negishi, K., Hoshino, S., Mukai, M. et al., Development and Verification of a Reactive Transport Model for Long-Term Alteration of Bentonite-Cement-Seawater Systems, Physics and Chemistry of the Earth, vol.33, suppl.1, 2008, p.S285-S294.

5-8 Determining Groundwater Flow on a Regional Scale

—A Study of a Regional Groundwater Flow System in a Sedimentary Rock Area—

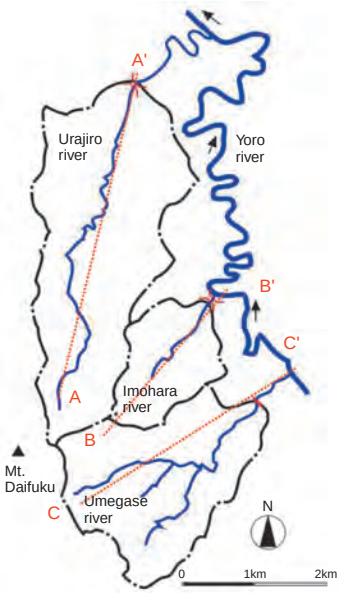

Fig.5-18 Map of position of 3 rivers (Urajiro, Imohara and Umegase River)
Flow rate and chemical compositions of water are investigated in 3 rivers. These 3 rivers flow down from Mt. Daifuku in the north, northeast, and east direction.

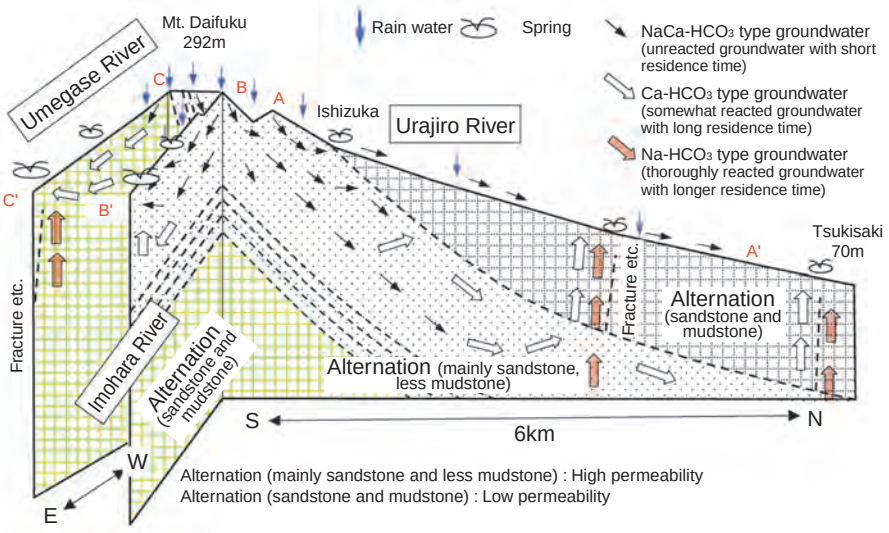

Fig.5-19 A conceptual representation of a three-dimensional groundwater flow in a research area
Groundwater is recharged at Mt. Daifuku which consists of a highly permeable sandstone. The groundwater flows through a shallow stratum and flows out at a relatively early stage into the Umegase and the Imohara rivers.

In the safety assessment for geological disposal of long-lived radioactive waste, it is important to estimate radionuclide migration to human environments through groundwater flow. We are studying regional groundwater flow systems.

In order to understand a regional groundwater flow system on a 10-100km scale, it is necessary to validate a conceptual representation of flow system from the recharged area to discharged area comparing with the observed data. Therefore, we investigated a sedimentary rock area in the Yoro river basin (Fig.5-18) and constructed a conceptual flow model of the region using the observed data of flow rate, chemical composition of groundwater, and isotopic ratios of hydrogen and oxygen in water samples collected from wells, rivers and springs.

From the observed flow rates, analyzed results of water samples and Mt. Daifuku's spatial characteristics, it is found that the groundwater recharged at Mt. Daifuku flows toward the east-northeast which is the direction in which the sandstone and high permeability mudstone strata run, and is discharged in the Imohara river and the Umegase rivers. In addition, it is estimated that a part of groundwater flows down deeper than 100m where the stratum tilts, and then flows out to the surface layer basin through fractures in a sandy-mudstone stratum with low permeability (Fig.5-19).

Chemical composition and isotopic data indicated that most of the groundwater is precipitation recharged at Mt. Daifuku, and that the groundwater is of the $NaCa\text{-}HCO_3$ type which is chemically unreacted groundwater with short residence time or of the $Ca\text{-}HCO_3$ type which is reacted groundwater with long residence time. The groundwater discharged into the downstream of the Urajiro river and the Umegase river was found to include the $Na\text{-}HCO_3$ type groundwater which has been reacted to a great extent, and which rose from a deep stratum.

Considering the above results, we conclude that a hydrological approach (measuring the flow rate of river and estimating underground flow) combined with a geo-chemical approach (analyzing the groundwater composition including isotopic ratios) is a useful method for evaluating the relationship between surface water, shallow groundwater and deep-seated groundwater which needs to be determined in order to establish a regional groundwater flow model.

The present study was conducted in FY2006 as part of the "Study of Influence of Hydrologic/Geological Changes Related to Geological Disposal" commissioned by the Nuclear and Industrial Safety Agency (NISA) of the Ministry of Economy, Trade, and Industry (METI).

Reference

Sakai, R., Munakata, M. et al., Study on Groundwater Flow System in a Sedimentary Rock Area (Part 2): Case Study for the Yoro River Basin, Chiba Prefecture, JAEA-Research 2007-083, 2008, 38p. (in Japanese).

Advanced Basic Research Making Pathways to the Future

In the Advanced Science Research Center, new frontier research of nuclear energy and ionizing radiation which is expected to bear fruit in the future is conducted to discover new principles and phenomena, and furthermore to create new materials and technologies. In order to achieve these aims, we have four basic policies; (1) to pursue research for which the high level research capability (researchers and facilities) in JAEA is effectively used and which is difficult to do in other research organizations, (2) to achieve results before the rest of the world does, (3) to nurture a new basic research area until it becomes fruitful, (4) to explain and apply the research, thus fulfilling our responsibility to society, in conformity with the Third Science and Technology Basic Plan.

The following research is being pursued: nuclear physics and nuclear chemistry of superheavy elements including elucidation of their nuclear shell structure, reaction dynamics and electrochemistry using heavy-ion beams of accelerators; synthesis of uranium and transuranium compounds, and measurement of their macroscopic quantities and electronic structure, clarification of magnetic structure, magnetic excitation, and the mechanism of superconductivity using NMR, μSR, neutron scattering, and theoretical methods; search for novel materials using mega-gravitation and nano-particle deposition, topmost surface studies using high-intensity coherent positron beams; elucidation of the interaction between molecules in supramolecular systems as a biological model by neutron scattering and X-ray spectroscopy, and studying fundamental physico-chemical processes in the interactions of ionizing radiation and heavy elements with living cells and substances (Fig.6-1).

In order to promote this research, we are collaborating with other research sections in JAEA, and several international collaborations are ongoing. In addition, we take on new research subjects based on public suggestions within the framework of the Reimei Research Promotion project of JAEA.

Science of Superheavy Elements

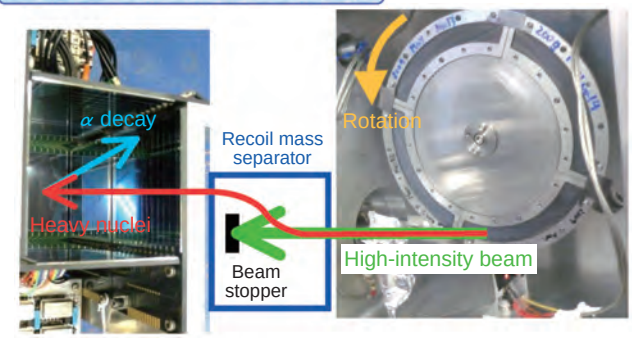

Physical and chemical properties of unknown heavy nuclei are investigated. Nuclei are synthesized in fusion reactions when a rotating target (right) is bombarded by high-intensity heavy-ion beams, separated from the incident beam by a recoil mass separator, and then implanted into a silicon-strip detector (left) which observes the α-decay chain.

Extreme Environment and Substance Science

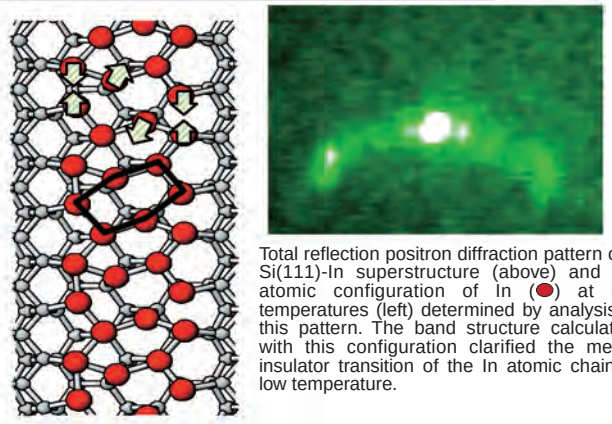

Total reflection positron diffraction pattern of a Si(111)-In superstructure (above) and the atomic configuration of In (●) at low temperatures (left) determined by analysis of this pattern. The band structure calculation with this configuration clarified the metal-insulator transition of the In atomic chain at low temperature.

Actinide Material Science

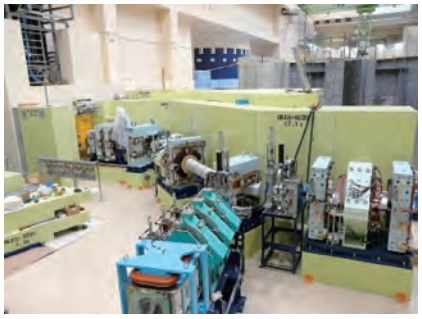

μSR spectroscopy system installed at J-PARC Muon Facility.
The system is able to detect the extremely small magnetic field to elucidate physical properties of materials, behavior of hydrogen atoms, etc., in substances.

Material and Life Sciences

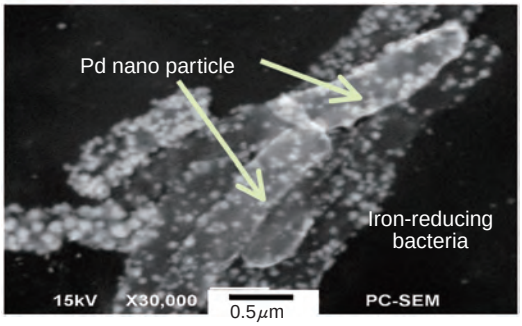

The ability of some bacteria to accumulate TRU elements from aqueous solution on their cell surface was studied.

Nano particles of Pd precipitated on the cell surface of iron-reducing bacteria (elongate ellipsoids). It was discovered that these nano particles have excellent catalytic ability.

Fig.6-1 Four research fields and collaborations in Advanced Science Research Center

6-1 Electronic Origin of Giant Magnetoresistance Effect in C_{60}-Co Films

—Spectroscopic Examination of Spin States in Organic-Transition Metal Materials—

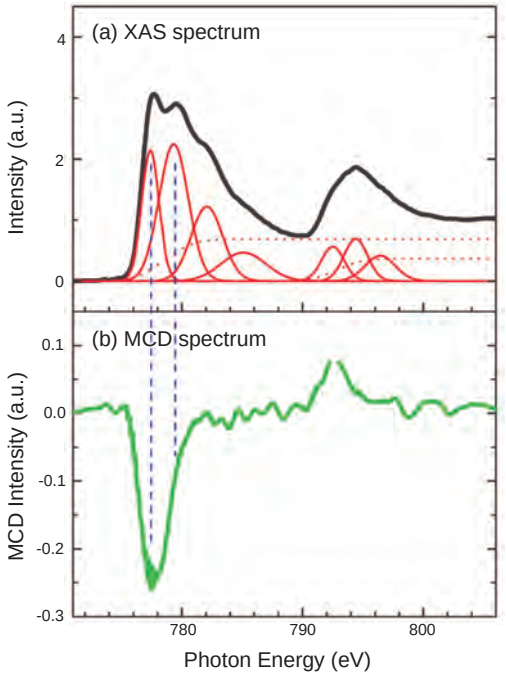

Fig.6-2 X-ray absorption and magnetic circular dichroism spectra of the C_{60}-Co compound

(a) X-ray absorption spectrum of the C_{60}-Co compound in the Co 2p→3d excitation region.

(b) Magnetic circular dichroism spectrum of the C_{60}-Co compound measured under a high magnetic field (H=50kOe) and low temperature (T=6K).

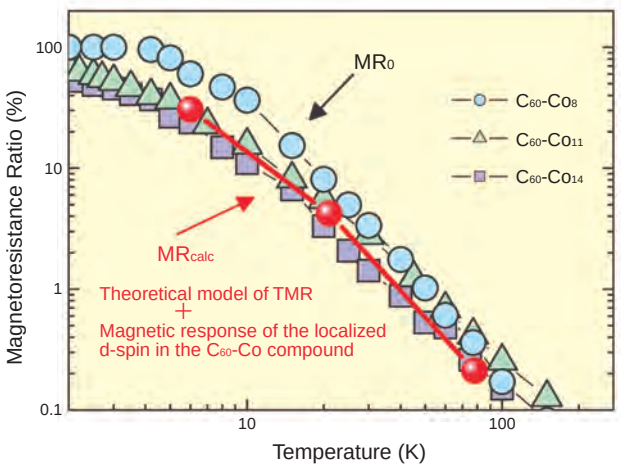

Fig.6-3 Temperature-dependence of the magnetoresistance ratios

Magnetoresistance ratios measured under the high magnetic field of H=50kOe (MR_0), and calculated magnetoresistance ratio with the theoretical model of the TMR effect and the magnetic response of the localized spins in the C_{60}-Co compound. The symbols (○, △, □) are correspond to MR_0 of the C_{60}-Co films with the different Co content, respectively.

A technology in which both electronic charges and spins are employed as information carriers has emerged recently. This technology is called "spintronics", and has been investigated actively in order to realize spintronics devices with a variety of new features. One of the important principles in the spintronics devices is the influence of magnetic field on electronic resistivity in these devices, i.e. magnetoresistance. Such phenomenon is caused by the different conductance of the electron carriers depending on the direction of the spin (up / down). Recently, we have found the C_{60}-Co films exhibit a much larger tunnel magnetoresistance (TMR) effect than previously used inorganic materials. In the present study, we investigated the electronic and spin states of the C_{60}-Co films by X-ray absorption (XAS) and magnetic circular dichroism (MCD) spectroscopy, and found that the magnetic response of the localized spins in the C_{60}-Co compound is an important factor in its giant TMR effect.

Fig.6-2(a) is a typical XAS spectrum of the C_{60}-Co compound in the C_{60}-Co films. Several multiplet structures (red curves) can be distinguished in the absorption spectrum. These structures are attributed to the different electronic states of the Co atoms due to their bonding in the C_{60}-Co compound. Moreover, a clear MCD signal (green curve) which indicates the presence of the spin-polarization can be distinguished clearly in the C_{60}-Co compound (Fig.6-2(b)). The observed MCD signal can be assigned to two major peak positions in the XAS spectrum of Fig.6-2(a). This indicates the presence of the spin-polarized states of electrons localized in the C_{60}-Co compound.

Fig.6-3 shows the temperature-dependence of the magnetoresistance ratio (MR_0) measured in the C_{60}-Co films, together with magnetoresistance ratio calculated with the theoretical model of the TMR effect (MR_{calc}). In the present study, we assumed that the localized spins in the C_{60}-Co compound affect the spin states of the electrons tunneling in the C_{60}-Co films so that their spin-polarizations (P) are enhanced to nearly P = 100%, in other words, completely spin-polarized states. It was found that in this case, the temperature-dependence of MR_{calc} agrees well with that of MR_0. This suggests the direct influence of the localized spins in the C_{60}-Co compound on the observed giant TMR effect.

Reference

Matsumoto, Y. et al., X-ray Absorption Spectroscopy and Magnetic Circular Dichroism in Codeposited C_{60}-Co Films with Giant Tunnel Magnetoresistance, Chemical Physics Letters, vol.470, issues 4-6, 2009, p.244-248.

6-2 New Fission Channel Opened in Reaction Using Deformed Nucleus ^{238}U
—Fission of Super-Heavy Nucleus ^{274}Hs—

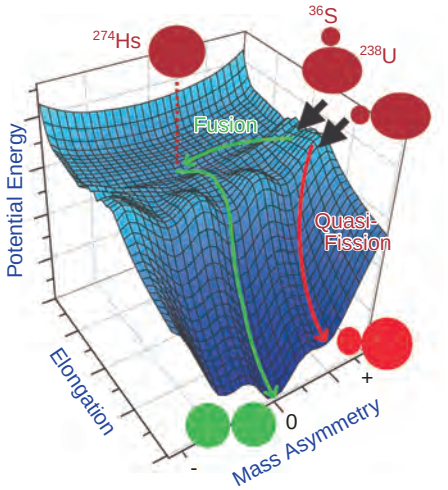

Fig.6-4 Potential energy surface for ^{274}Hs
The green curve is the fission channel from the compound nucleus, and the red curve is the quasi - fission channel. Competition between fusion and quasi-fission occurs, which depends on the colliding angle of ^{36}S with the symmetrical axis of ^{238}U.

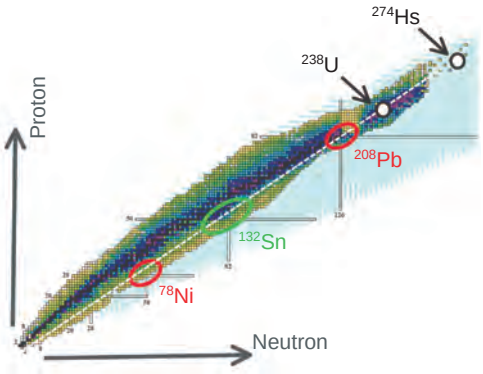

Fig.6-5 Chart of nuclei plotted according to neutron and proton number
In the fission of ^{274}Hs, asymmetric fission channel appears because of double closed shell nuclei, ^{208}Pb and ^{78}Ni. The symmetric fission channel is due to the closed shells of ^{132}Sn.

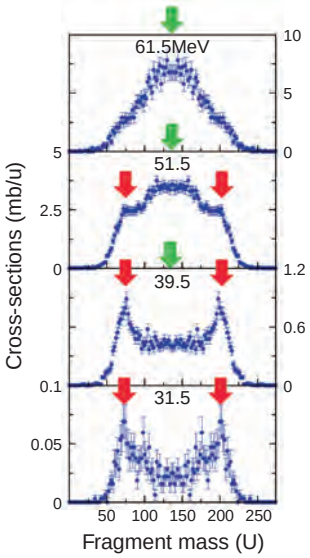

Fig.6-6 Fission fragment mass distributions in the reactions of ^{36}S + ^{238}U
Fragment yields centered at the green and red - arrows are associated from fusion-fission and quasi-fission, respectively.

Nuclear fission is a fundamental phenomenon for the use of nuclear power. The fragments of neutron-induced fission of uranium-235 (^{235}U) exhibit mass asymmetry. Even modern theory cannot predict this mass distribution, demonstrating that fission is still an unknown phenomenon.

Fission is considered to proceeds through a valley (channel) in the potential energy surface of the nucleus. In potentials calculated with the classical nuclear model, there are only mass-symmetric channels, which contradicts observations. A microscopic property (shell effects) must be taken into account to explain the mass-asymmetry.

In this work, fission of super-heavy nucleus hassium-274 (^{274}Hs, atomic number 108) was studied in order to investigate the effects of nuclear-shell on fission. In the potential energy map for ^{274}Hs in Fig.6-4, two distinct fission valleys are evident. One is the channel with mass-symmetry, occurring due to the shell around tin-132 (^{132}Sn), as indicated in Fig.6-5. The other is the mass-asymmetric channel of nickel-78 (^{78}Ni) and lead-208 (^{208}Pb), formed by double closed shells which appear only in super-heavy nuclei. To investigate this channel, we measured ^{274}Hs fission fragment mass distributions.

The ^{274}Hs was produced by bombarding sulfuer-36 (^{36}S) on uranium-238 (^{238}U). The experiment was carried out at the JAEA tandem accelerator at the Nuclear Science Research Institute. Two fission fragments produced by the reaction were detected simultaneously to determine the fragment masses. The results are shown in Fig.6-6. The upper figures show the results from higher bombarding energies. At the low energies, the distribution changes to mass asymmetry with peaks at 200/74 u. The results proved the presence of the new fission channel.

The energy dependence of the mass distributions in Fig.6-6 arises from the lemon-like deformation of ^{238}U as seen in Fig.6-4. At the high energies of ^{36}S, reaction occurs from every colliding angle. Symmetrical fission occurs after the compound nucleus is formed by fusion. At the low energies, reaction starts only from polar collisions and the system easily fissions through the asymmetric channel. Quasi-fission, i.e. fission without formation of a compound nucleus, was observed, proving the presence of the new fission channel.

Reference

Nishio, K. et al., Effects of Nuclear Orientation on the Mass Distribution of Fission Fragments in the Reaction of ^{36}S + ^{238}U, Physical Review C, vol.77, no.6, 2008, p.064607-1-064607-5.

6-3 Identification of Magnetic Fluctuations Inducing Unconventional Superconductivity
—Mechanism of Superconductivity Revealed by Nuclear Magnetic Resonance—

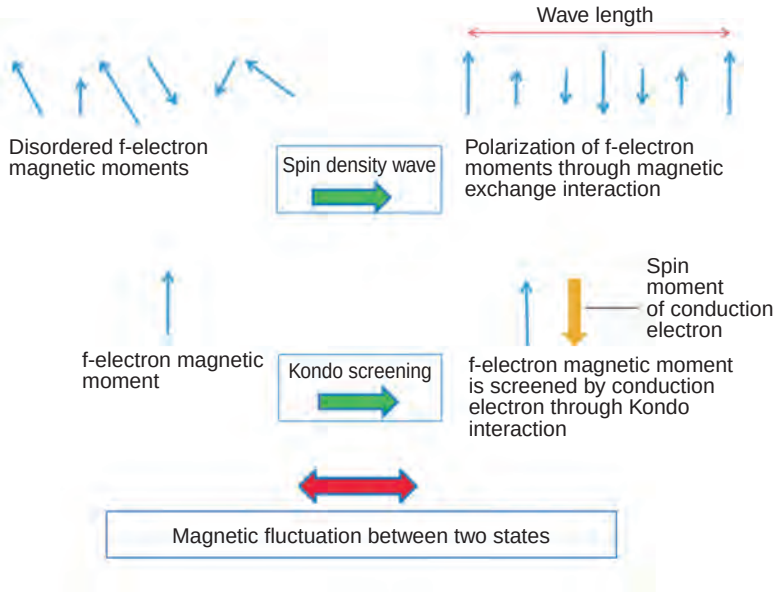

Fig.6-7 Two proposed (spin density wave and Kondo screening) models for magnetic fluctuations which may induce the unconventional superconductivity
These fluctuations can work as "glue" for inducing superconducting pairs.

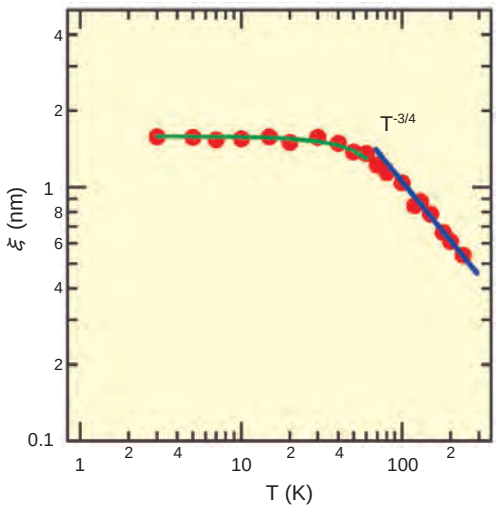

Fig.6-8 Temperature dependence of magnetic coherence length ξ in USn_3
NMR results (●) coincide well with curves calculated with the spin density wave model (blue line, green line). This indicates that the spin density wave is the origin of magnetic fluctuations.

In the superconducting state, two electrons form a pair (Cooper pair) due to attractive force. For conventional superconductors, lattice vibration (phonon) is the origin of attractive force. In contrast, for unconventional superconductors, magnetic fluctuations are believed to induce the Cooper pairs.

Recently, two different theoretical models (spin density wave and Kondo screening models) have been proposed to describe the magnetic fluctuation. However, no definitive experimental evidence has been obtained to determine which is the proper model so far. In this study, we have obtained clear experimental evidence which supports the spin density wave model in the uranium compound USn_3, using the nuclear magnetic resonance (NMR) method.

In f-electron systems such as uranium compounds, local magnetic moments due to f-electrons have magnetic exchange interactions with each other, and at the same time, interact with conduction electrons through the Kondo interaction. As illustrated in Fig.6-7, if the magnetic exchange interaction is dominant, the local magnetic moments have a tendency to be polarized, making possible determination of the magnetic exchange energy (spin density wave state). On the other hand, the local magnetic moments would be screened by conduction electron spins if the Kondo interaction is dominant (Kondo screening state). In the present work, temperature dependence of magnetic coherence length is determined in USn_3 from NMR relaxation measurements. Obtained experimental results (●) coincide well with those calculated from the spin density wave model (green and blue lines) as clearly seen in Fig.6-8, indicating that the spin density wave is dominant in uranium compounds.

The present study suggests that the unconventional superconductivity in uranium compounds is caused by the spin density wave fluctuation. A future new superconductor with higher T_c (superconducting critical temperature) is thought to be realizable in a magnetic-fluctuation-mediated superconducting system, since T_c of phonon-mediated superconductors has reached its peak already. This study suggests that a search for materials possessing enhanced spin density wave fluctuation would be effective for finding new high T_c superconductors.

We will be investigating actinide compounds to clarify the mechanism of superconductivity in detail.

Reference

Kambe, S. et al., Crossover from the Quantum Critical to Overdamped Regime in the Heavy Fermion System USn_3, Physical Review Letters, vol.102, issue 3, 2009, p.037208-1-037208-4.

6-4 Probing Interstitial Hydrogen States Using Positive Muons
—For Detailed Understanding of Rare-Earth-Based Hydrogen-Absorbing Alloys—

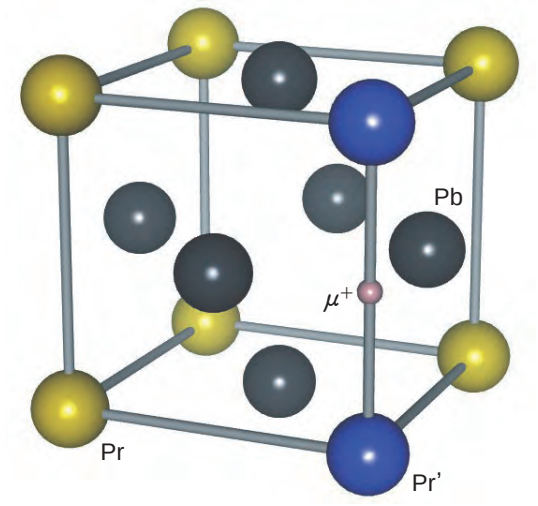

Fig.6-9 Crystal structure of $PrPb_3$ and μ^+ site
The implanted μ^+ stops at the midpoint between two Pr ions (Pr') and influences the f-electronic state of those ions.

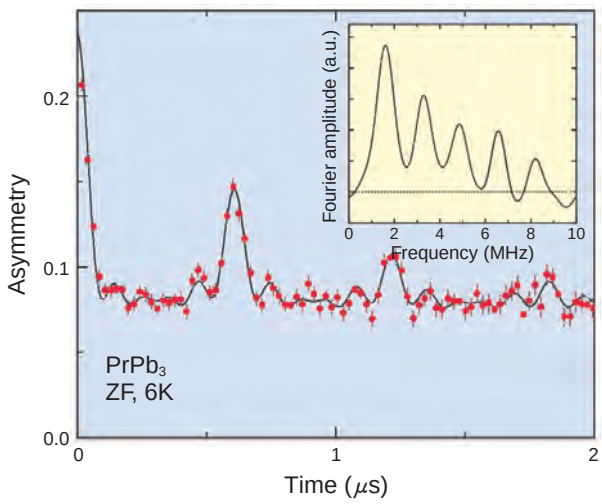

Fig.6-10 μ^+SR spectrum of $PrPb_3$ at 6K in zero magnetic field
The horizontal and longitudinal axes indicate time from arrival of the μ^+ and asymmetry of the positron emission relative to the μ^+ spin polarization, respectively. The inset shows a result of Fourier transform.

In recent years, much interest has been focused on hydrogen-based energy systems. The key of this technology is high-density storage of hydrogen, and hydrogen-absorbing (HA) alloy is useful for this purpose. The HA alloy absorbs the hydrogen to form metal hydride. In this process, the hydrogen molecule is dissociated into H atoms and these are stabilized at an interstitial site of the lattice. Detailed understanding of the interstitial H state is thus important for further improvement of HA properties.

We studied the interstitial H state in a material related to the HA alloy using positive muons (μ^+). The μ^+ can be regarded as a light isotope of ^{1}H since it possesses charge $+e$ and mass $\sim 1/9 m_p$, where m_p is the mass of a proton. Therefore, chemical properties of the μ^+ in condensed matter are considered to be identical to those of ^{1}H except for isotope effects. The μ^+ implanted into materials stops at the interstitial site and decays into a positron and two neutrinos. The positron is preferentially emitted in the direction of the μ^+ spin, which evolves via magnetic interactions with surrounding electron and nuclear spins. Detailed analysis of the time evolution of the μ^+ spin provides us with information on the magnetic environment at the μ^+ site.

We launched this research project with investigation of the interstitial H state in a rare-earth-based intermetallic compound $PrPb_3$, related to the typical HA alloy $MmNi_5$ (Mm: mixture of light rare-earth elements). First, the μ^+ site in $PrPb_3$ was determined to be the midpoint between two Pr ions (Pr') as shown in Fig.6-9, using the μ^+ spin rotation and relaxation method (μ^+SR) in a high magnetic field. μ^+SR measurements in zero magnetic field were also performed, and the characteristic spectrum shown in Fig.6-10 was obtained in the paramagnetic state. This spectrum indicates quantization of the magnitude of a hyperfine field that is generated at each μ^+ site. From detailed analysis, it was clarified that coupling between Pr' and μ^+ spins is anisotropically enhanced as a result of deformation of the *f*-electron state owing to the μ^+ charge. The quantum character of the hyperfine field strongly supports this conclusion.

The present result suggests the importance of the electrostatic interaction between the *f*-electrons and the interstitial H in HA alloys. We plan further μ^+SR studies in HA alloys which have commercial promise, to clarify the relation between this interaction and the HA properties.

Reference

Ito, T. U. et al., Quantized Hyperfine Field at an Implanted μ^+ Site in $PrPb_3$: Interplay between Localized *f* Electrons and an Interstitial Charged Particle, Physical Review Letters, vol.102, issue 9, 2009, p.096403-1-096403-4.

7 Nuclear Science and Engineering Research

Formation of Basis for Nuclear Energy R&D, and Creation of Innovative Nuclear Energy Utilization Technology

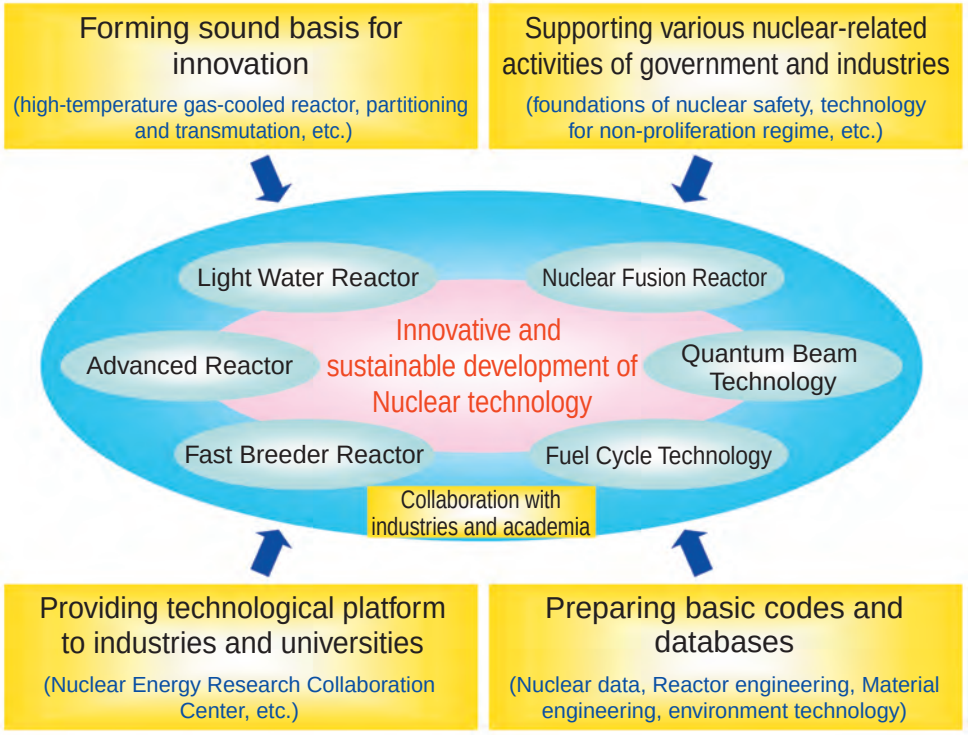

Fig.7-1 Roles of nuclear science and engineering research

The nuclear science and engineering research being conducted at the Japan Atomic Energy Agency has the four roles shown in Fig.7-1. In order to fulfill these roles, research in nuclear data and reactor engineering, fuels and materials engineering, environment and radiation science, and nuclear applied heat technology is being conducted.

Nuclear data and reactor engineering

Various types of research are being performed to investigate the feasibility of advanced nuclear systems and to establish the basic technology for these systems. Topic 7-1 is development of a prediction uncertainty evaluation method of neutronic design without full-scale mock-up critical experiments. Topic 7-2 is development of a high-accuracy measurement method for nuclear data of minor actinides (MA) e.g. Np, Am, Cm, and results obtained thereby.

Fuels and materials engineering

Basic studies on advanced nuclear fuel and cycle technology and the degradation of nuclear power plant materials are being carried out. Topic 7-3 is the publication of “Handbook on Process and Chemistry of Nuclear Fuel Reprocessing Ver. 2”, in which data comprising the technical basis for spent nuclear fuel reprocessing are complied. Topic 7-4 is the corrosion mechanism of stainless steel used in containers for spent fuel reprocessing plants, studied for safety analysis of nuclear materials. Topic 7-5 is the mechanism of thermal property changes in Am-containing oxide fuels, needed for MA. recycling technology.

Environment and radiation science

Research on movement of radionuclides in the environment and dose assessment is being carried out. Topic 7-6 is the completed development of WSPEEDI - II to predict atmospheric dispersion of radionuclides accidentally released anywhere in the world (Fig.7-2). Topic 7-7 is analysis of organ doses using Japanese voxel phantoms to evaluate the effects of body posture on dose.

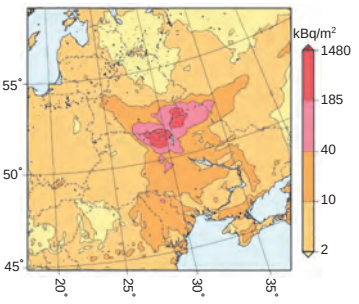

Fig.7-2 Deposition of ^{137}Cs during the Chernobyl accident predicted by WSPEEDI - II

Nuclear applied heat technology

To expand nuclear energy applications to heat utilizing industries, we are continuing extensive R&D for high-temperature gas-cooled reactor (HTGR) technology and for a HTGR-heated hydrogen production system. Topic 7-8 is efficient hydrogen production by a thermochemical IS process. Topic 7-9 is safe hydrogen use in HTGR, specifically to prevent the hydrogen from being contaminated by radioactive material.

7-1 Validation of Accuracy of Prediction of Neutronic Behavior in a Design without Full-Scale Mock-Up Critical Experiments

— Development of a Prediction Uncertainty Evaluation Method Using Results of Critical Experiments —

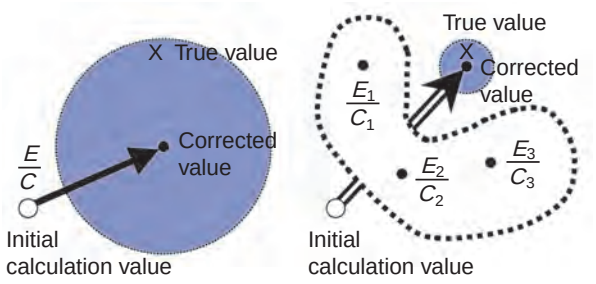

Fig.7-3 Characteristics of extended bias factor method
The conventional bias factor method which utilizes a single experiment is inaccurate if the facility of that experiment is different from the mock-up facility. The extended bias factor method which has been created constructs a facility similar to the mock-up from a number of experiments at existing facilities.

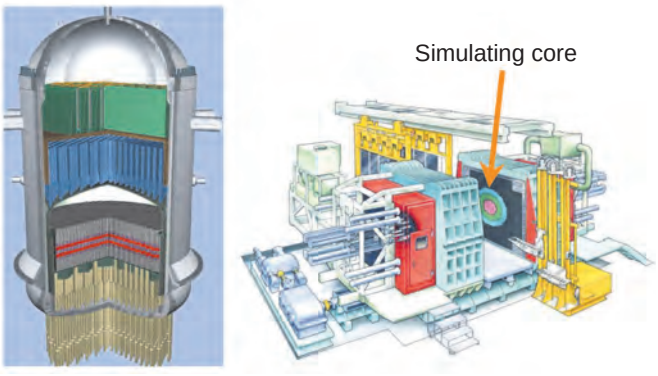

Fig.7-4 Application of FCA critical experiments to a new type reactor core design
An innovative light water reactor (FLWR) is a new type reactor which will breed fuel due to a greatly changed coolant void fraction in the core. We systematically obtained critical experimental data at FCA for the FLWR cores with various void conditions, and applied the extended bias factor method, using this FCA data to evaluate FLWR designs. We could evaluate the core performance more accurately than the conventional method.

To develop a new type reactor, accurate prediction of core performance is required. This is done with calculation codes to analyze neutron behavior based on evaluated nuclear data. With a full-scale mock-up experiment very similar to the planned core, the prediction accuracy can be validated by a comparison between the analysis value of the simulation model and the experimental value. However, comparisons are often limited to experiments with existing experimental facilities. Therefore, they may not properly simulate the planned core and it is difficult to validate the prediction accuracy. However, a full-scale mock-up experiment with new experimental facilities is costly. Thus, it is very difficult to conduct full-scale mock-up experiments.

To overcome such difficulties, we created a new method named the extended bias factor method. The method can evaluate the prediction uncertainty without a full-scale mock-up experiment, based on an original concept: utilize experimental results from a number of existing facilities in place of a mock-up facility. Taking the variance of experimental results into consideration, it utilizes the covariances arising from the nuclear data and the analysis method in the design values and the experiment analysis values of the planned core and each of the utilized existing cores which are caused by cross section and analysis method errors, and maximizes the correlation between the planned core and the experimental results. By this method, the prediction accuracy can be properly evaluated and improved (Fig.7-3).

To apply the extended bias factor method to a real group of experimental results, we developed new methods to practically evaluate covariance between experimental values and between experiment analysis values and constructed a system to evaluate covariance between different experimental results and between different cores. Based on this system, we applied this method to a new type reactor core design using the experimental results systematically measured with several simulating cores constructed in an existing facility, Fast Critical Assembly (FCA). The application results demonstrated that the method is valid for the evaluation and improvement of the prediction accuracy of core performance of the target core (Fig.7-4).

By evaluating sources of error in prediction with the extended bias factor method, we can identify necessary new critical experiments, and the experiments and the analysis method by which uncertainties can be reduced. The present R&D results can be utilized to contribute to planning of effective R&D, saving time and cost for development of the new type reactor.

The present R&D was honored with an award for distinguished technology by the Atomic Energy Society of Japan in March, 2009.

Reference

Kugo, T. et al., Prediction Accuracy Improvement of Neutronic Characteristics of a Breeding Light Water Reactor Core by Extended Bias Factor Methods with Use of FCA-XXII-1 Critical Experiments, Journal of Nuclear Science and Technology, vol.45, no.4, 2008, p.288-303.

7-2 Improving Accuracy of Nuclear Transmutation Data
—Measurement of Fast Neutron Capture Cross Sections—

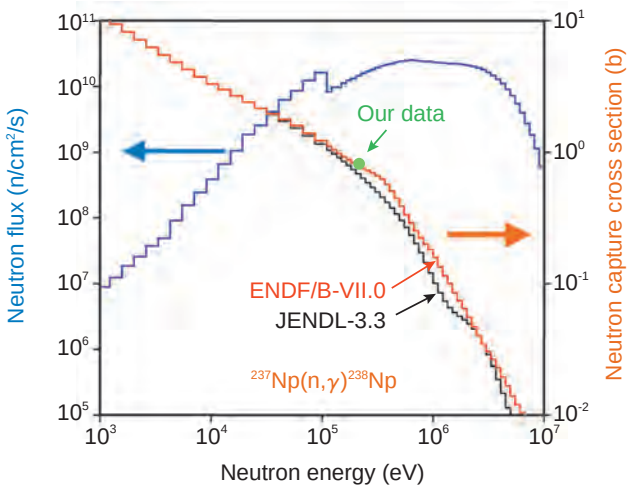

Fig.7-5 Neutron flux at the center core of the Yayoi reactor and the evaluated neutron capture cross section of ^{237}Np in two libraries, JENDL-3.3 and ENDF/B-VII.0

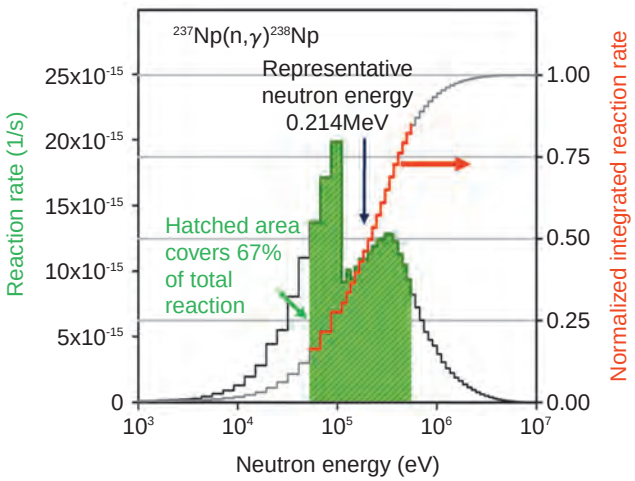

Fig.7-6 Energy dependence of the reaction rate of ^{237}Np and of normalized integrated reaction rate

Accurate data of the neutron cross sections of minor actinides (MA) such as Neptunium (Np), Americium (Am), and Curium (Cm) over a wide neutron energy range from thermal to MeV regions are required for development of innovative nuclear systems capable of nuclear transmutation of minor actinides.

However, there is an apparent discrepancy among current nuclear data on MA's. As an example, the neutron capture cross sections of ^{237}Np of JENDL-3.3 and ENDF/B-VII.0 are shown in Fig.7-5. There is a large gap above 100keV (10^5eV).

We have utilized the activation method to measure accurately the capture cross sections of MA using fast neutrons supplied by the Yayoi reactor. Since the neutron flux is very high at the reactor core in the fast neutron region, a small sample of the order of 0.1mg is sufficient. This fact is important to eliminate experimental difficulties inherent in measuring the capture cross sections of radioactive samples.

However, it is difficult to obtain point wise data by the activation method using fast reactor neutrons, since the Westcott convention established for thermal neutrons is not applicable. To overcome the problem, the new convention is proposed, in which the "representative neutron energy" is defined; the capture cross section corresponding to that energy can be determined. Fig.7-6 shows the energy dependence of the reaction rate of ^{237}Np, and of the normalized value of the integrated reaction rate, which can be used to determine the representative neutron energy analytically.

Our data is plotted in Fig.7-5. It is shown that the activation method using fast reactor neutrons is a very powerful tool to determine neutron capture cross sections for fast neutrons. The developed activation method together with the time-of-flight method under development at the J-PARC MLF neutron-nucleus reaction instrument will be used to systematically and accurately determine the neutron capture cross sections of radioactive samples such as MA.

Reference

Harada, H. et al., Measurements of Neutron Capture Cross Section of ^{237}Np for Fast Neutrons, Journal of Nuclear Science and Technology, vol.46, no.5, 2009, p.460-468.

7-3 Completion of Database Supporting Technological Basis for Spent Nuclear Fuel Reprocessing

—Handbook on Process and Chemistry of Nuclear Fuel Reprocessing Ver.2—

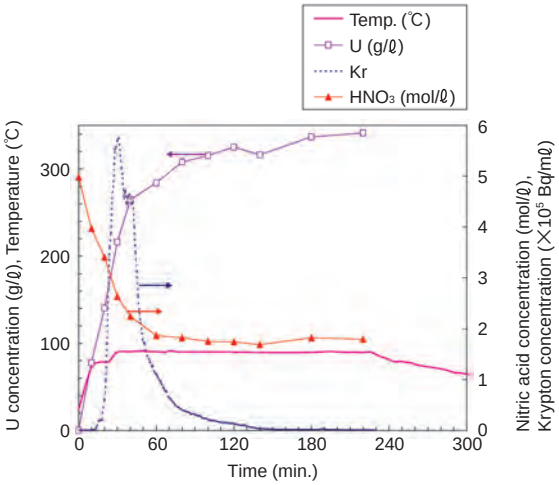

Fig.7-7 Results of dissolution tests of spent MOX fuel (41GWd/tHM)
The increase of uranium concentration and decrease of nitric acid concentration were observed as dissolution progressed. Good correlation was confirmed between krypton discharge and uranium concentration.

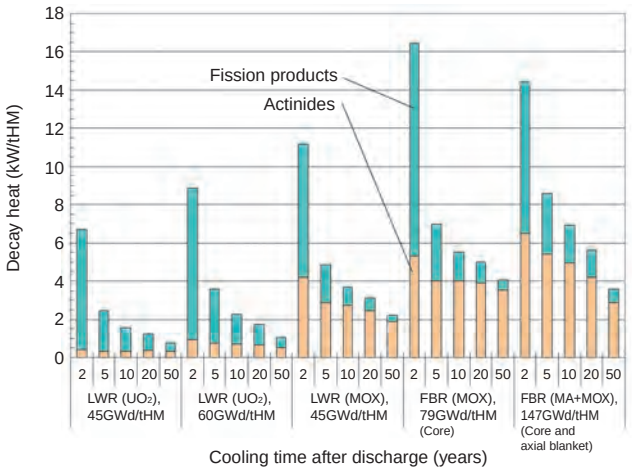

Fig.7-8 Decay heat from various kind of spent fuels
This figure shows decay heat generation from spent fuel discharged from LWR(UO_2 , MOX) or FBR (MOX or MOX with minor actinides).

In the future, high burn-up fuel and mixed oxide (MOX) fuel should be reprocessed. Since these fuels contain large quantities of fission products and plutonium, it is important to examine their influence on the dissolution of spent fuel and extraction process used in reprocessing. Furthermore, in order to improve economy and to reduce volume of radioactive waste, further research and development of reprocessing technology will be of great importance. In these efforts, a comprehensive survey and compilation of the basic data of reprocessing technology that has been determined will be of great use.

We have been studying the solution chemistry and chemical processes of actinides and fission products to find a basis for development of advanced fuel reprocessing. Experiments in fuel dissolution and extraction processes using actual spent UO_2 and MOX fuels were carried out at Nuclear Fuel Cycle Safety Engineering Research Facility (NUCEF). These experimental results and basic data collected by literature survey were compiled and published as "Handbook on Process and Chemistry of Nuclear Fuel Reprocessing Version 2" in 2008.

In the first section of this handbook, basic data, such as solution density, viscosity, absorption spectra of actinide ions and etc. are given.

The next section describes results of dissolution experiments (Fig.7-7) and off-gas treatment tests using spent fuels of several burn-ups. Concentration changes of uranium and nitric acid during the dissolution were compared with our simulation model. Results of dissolution residue analysis are also given here.

Distribution behavior and redox reactions of important elements such as uranium, plutonium, neptunium etc. during the extraction process are reviewed, and our simulation code PARC, developed for solvent extraction studies, is explained. The results of NUCEF experiments and calculations with PARC given here agreed well with each other.

In addition to these data, we summarized fission product compositions and decay heat from various kinds of spent fuels (Fig.7-8), and plutonium polymerization and solvent degradation, which will become more important with regard to safety in the future.

It is expected that this handbook will be widely utilized as one technological basis for smooth and safe operation of plants and for research and development toward the next generation of nuclear plants, since it is a useful compilation of knowledge about reprocessing.

Reference

Research Group for Aqueous Separation Process Chemistry, Handbook on Process and Chemistry of Nuclear Fuel Reprocessing Version 2, JAEA-Review 2008-037, 2008, 702p. (in Japanese).

7-4 Elucidation of Corrosion Mechanism of Stainless Steel for Spent Fuel Reprocessing Plants
—Study of Corrosion Mechanism of Nitric Acid Solution Containing Neptunium—

Fig.7-9 Appearance of corrosion testing apparatus
A corrosion testing apparatus was set in a hot cell - a room with thick concrete walls. A manipulator was also installed, which carries out corrosion tests under strong radiation.

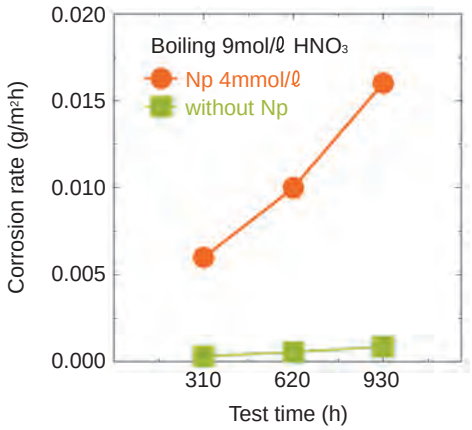

Fig.7-10 Corrosion rate of stainless steel in boiling HNO_3 solution at 70℃
Stainless steel was immersed in boiling HNO_3 solution at 70℃. It corroded greatly when there was a small amount of Np. The corrosion rate of stainless steel increased with time.

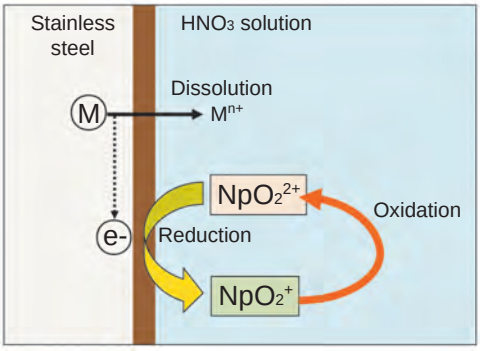

Fig.7-11 Schematic illustration of corrosion mechanism in HNO_3 solution with neptunium
On stainless steel, metal (M) is dissolved into M^{n+} by Np^{6+} (NpO_2^{2+}) which is reduced to Np^{5+} (NpO_2^{+}). In boiling HNO_3 solution, Np^{5+} is re-oxidized to Np^{6+}. This cycle is repeated during corrosion. This cycle promotes the corrosion of stainless steel.

Usable nuclear fuels (uranium and plutonium) are left in spent nuclear fuels from a nuclear power plant. A plant which chemically collects usable nuclear fuel from spent fuel, separates fission products, and safely treats radioactive wastes is called a spent fuel reprocessing plant. In Japan, there are two such plants, in Tokai-mura and Rokkasho-mura. Uranium is a limited fuel like oil. The recycling of nuclear fuel is very important for sustainable production and utilization of nuclear energy.

A very corrosive boiling nitric acid solution is used to dissolve nuclear fuel in a reprocessing plant. The solution contains plutonium and ruthenium which are dissolved from spent nuclear fuel. It has been known that these elements strongly corrode commercial grade stainless steel, and special corrosion-resistant stainless steels are used in reprocessing plants. Recently, it has been reported that a small amount of neptunium (Np) also promotes the corrosion of the stainless steel. The mechanism of corrosion acceleration by Np was investigated. The tests were conducted in the Waste Safety Testing Facility (WASTEF) that could handle radioactive materials such as spent nuclear fuel. Fig.7-9 shows the appearance of the corrosion testing apparatus set in a hot cell in WASTEF.

Fig.7-10 shows the corrosion rate of stainless steel which was immersed in boiling nitric acid (HNO_3) solution at 70℃ under reduced pressure. The solution contained a small amount of Np (ca.4mmol/ℓ), and the concentration of HNO_3 was 9mol/ℓ. The corrosion rate of stainless steel in the HNO_3 solution with Np was about 10 times higher than that without Np. This corrosion acceleration by Np was investigated using electrochemical and spectrochemical analyses that could examine the influence of ionic species in solutions. As shown in Fig.7-11, Np^{6+} (NpO_2^{2+}) caused the dissolution of a metal in the stainless steel and itself was thereby reduced to Np^{5+} (NpO_2^{+}). The Np^{5+} was re-oxidized to Np^{6+} in the HNO_3 solution. It was found that this cycle led to the increase in the corrosion rate of stainless steel in HNO_3 solutions with Np. We have been developing the new stainless steels, which are very corrosion-resistant to boiling HNO_3 solutions with corrosive ionic species such as Np.

The above knowledge is being utilized as basic data for the safe operation of Rokkasho reprocessing plant.

Reference

Motooka, T. et al., Corrosion Behavior of Stainless Steel in Nitric Acid Solutions Including Neptunium, Zairyo-to-Kankyo, vol.57, no.12, 2008, p.536-541 (in Japanese).

7-5 Elucidating Thermal Change in Am-Containing Oxide Fuels
—Investigation of Thermodynamic Properties of Nonstoichiometric Am Oxides—

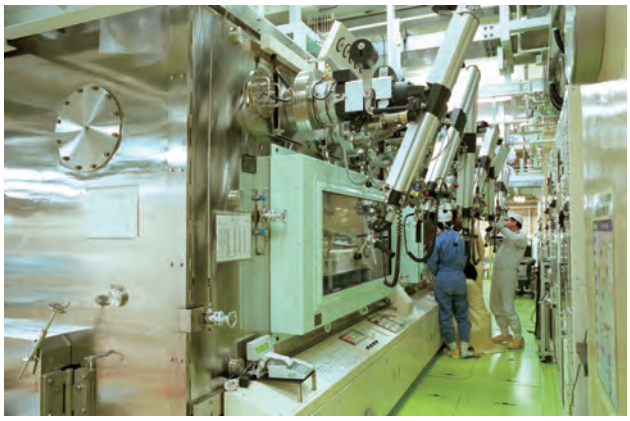

Fig.7-12 Module for TRU high temperature chemistry
The module is composed of three hot-cells and a glove-box filled with inert atmosphere.

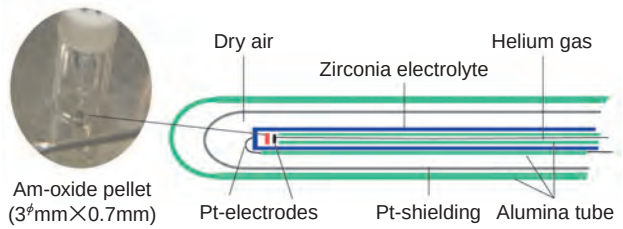

Fig.7-13 Electrochemical cell with a zirconia electrolyte
The reference gas for the cell is air. The oxygen potentials of Am oxides are calculated from the potential difference between two Pt-electrodes.

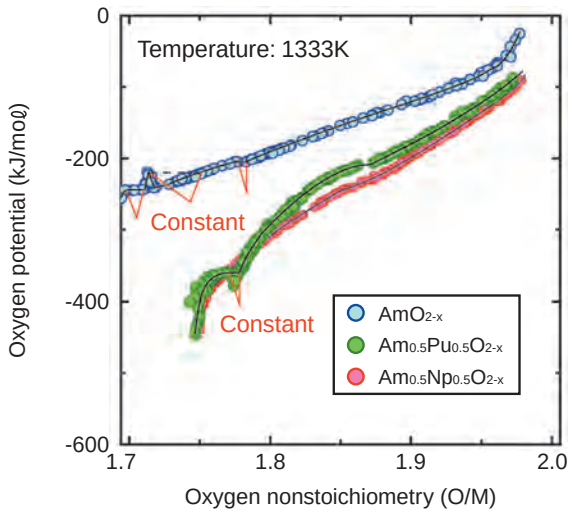

Fig.7-14 The relation between the oxygen potentials and oxygen nonstoichiometry (O/M) of Am oxides
This figure shows the comparison of the oxygen potentials of AmO_{2-x}, $Am_{0.5}Pu_{0.5}O_{2-x}$, and $Am_{0.5}Np_{0.5}O_{2-x}$ at 1333K. The oxygen potentials for each Am oxide decrease with decreasing O/M. For AmO_{2-x}, and $Am_{0.5}Pu_{0.5}O_{2-x}$, however, the oxygen potentials keep constant over some O/M ranges. This reveals that AmO_{2-x} and $Am_{0.5}Pu_{0.5}O_{2-x}$ have a mixture of phases over these O/M ranges.

For future nuclear fuel cycles, we are developing the technology of recovering minor actinides (MA: Np, Am and Cm) from spent fuels and transmuting them by fast reactors. MA recycling can reduce the long-term hazard and the area of the site needed for disposal of the high-level radioactive waste. To burn MA effectively and safely, it is necessary to develop the MA-containing oxide fuels and get a reasonable understanding of their oxygen potentials to predict their compatibility with fuel-cladding and their thermal behavior during irradiation.

Therefore, we installed a module for TRU high temperature chemistry (Fig.7-12) in NUCEF of JAEA, in order to study MA-containing fuels. We investigated the relation between the oxygen potentials and oxygen nonstoichiometry (O/M) of Am oxides by an electrochemical method (Fig.7-13). In this study, we could test a sufficiently large amount of Am, and electrochemically control O/M of the samples with sufficient accuracy to get data with good precision (Fig.7-14). We found that the thermodynamic properties of Am oxides exhibit a systematic change. This study indicates a method for prediction of the thermal behavior of Am-containing oxide fuels, enabling the evaluation of technological feasibility of MA recycling.

This study includes the results of the collaborative research program “TRU (transuranium elements) Behavior in Oxide Fuels” with Tohoku Electric Power Company, Tokyo Electric Power Company and the Japan Atomic Power Company, and the results of “Development of Common and Fundamental Technologies for Evaluation of Nuclear Fuel Behavior in MA recycling” entrusted to the Japan Atomic Energy Agency by the Ministry of Education, Culture, Sports, Science and Technology of Japan (MEXT).

Reference

Otobe, H. et al., Oxygen Potential Measurement of Americium Oxide by Electromotive Force Method, Journal of the American Ceramic Society, vol.91, issue 6, 2008, p.1981-1985.

7-6 Prediction of Atmospheric Dispersion of Radionuclides by Accidental Discharge in the World
—Development of WSPEEDI-II: Worldwide Version of System for Prediction of Environmental Emergency Dose Information 2nd Version—

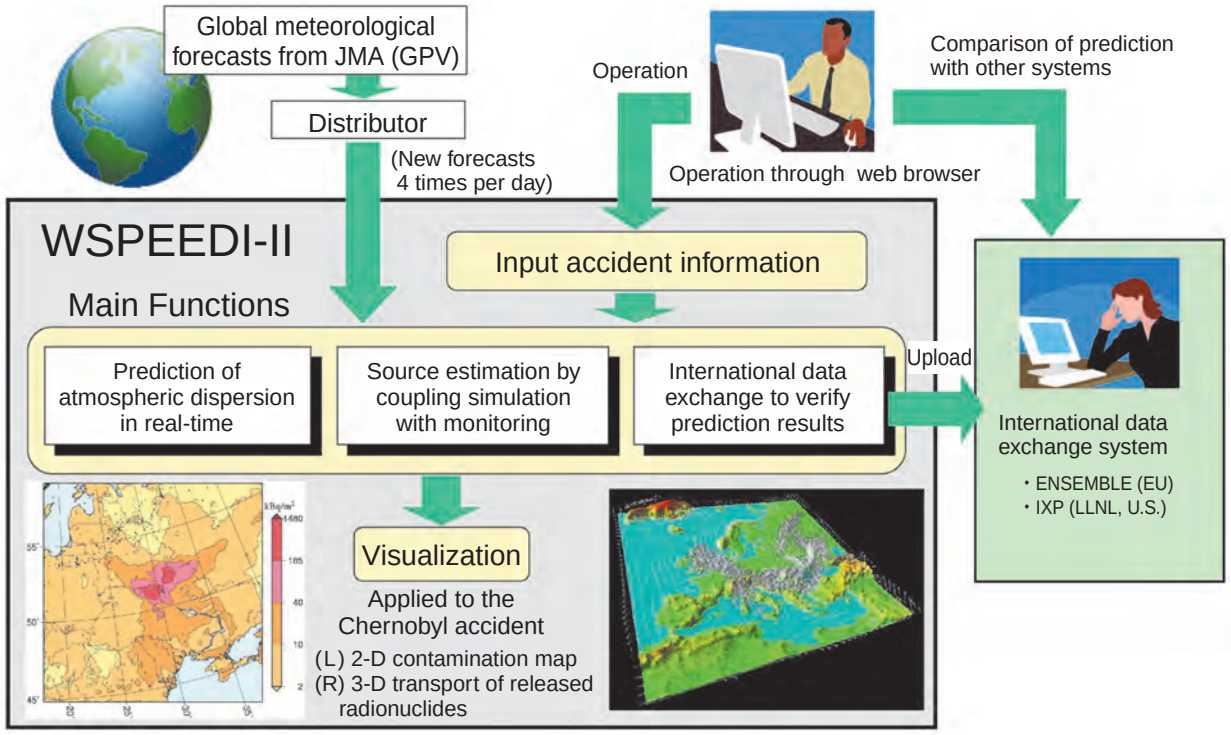

Fig.7-15 Overview of WSPEEDI-II

Due to the increase in the demand for energy and the global warming problem, it is expected that the number of nuclear power plants will increase in China, India and other countries. In the worst case when a large-scale nuclear accident like the one at Chernobyl occurs, radionuclides would be transported to other countries in addition to the environmental contamination around the accident site.

To prepare for such an accident, the computer-based emergency response system "WSPEEDI-II: Worldwide version of System for Prediction of Environmental Emergency Dose Information 2nd Version" has been developed. It is capable of predicting the atmospheric dispersion of radionuclides discharged from an accident site quickly, estimating the location of the source, and exchanging prediction information internationally (Fig.7-15).

The development of the 1st version of WSPEEDI was started after the Chernobyl accident in 1986, and was completed in 1997. As a result of successive improvements based on operation experience, the 2nd version with high-performance functions has been completed.

The new functions of WSPEEDI-II are as follows:(1) It can predict the atmospheric dispersion and the deposition on the ground precisely in areas ranging from several tens of km square around an accident site to a hemisphere by computational simulation, (2) It can predict the source conditions, e.g., release point, release time, discharged amount, by coupling simulation with monitoring, in the case when air dose rates increase at domestic monitoring points before the accident information is acquired, and (3) It can exchange its prediction results with other emergency response systems in the United States and Europe to evaluate the accuracy of predictions.

The prediction capability of WSPEEDI-II has been evaluated using monitoring data of the Chernobyl accident and of a field tracer experiment in Europe in 1994, ETEX, and it was shown that the capability of WSPEEDI-II is one of the highest in the world.

By the practical operation in future, WSPEEDI-II is expected to play important roles supporting emergency measures for public safety, airplane monitoring, etc. in case of nuclear accidents. It will also be utilized for research on atmospheric environments.

The development of WSPEEDI-II was honored with an award for distinguished technology by the Atomic Energy Society of Japan in March, 2009.

Reference

Terada, H. et al., Development of Worldwide Version of System for Prediction of Environmental Emergency Dose Information: WSPEEDI 2nd Version, Nippon Genshiryoku Gakkai Wabun Ronbunshi, vol.7, no.3, 2008, p.257-267 (in Japanese).

7-7 Effects of Body Posture on Dose Assessment
—Analysis of Organ Doses Using Japanese Voxel Phantoms—

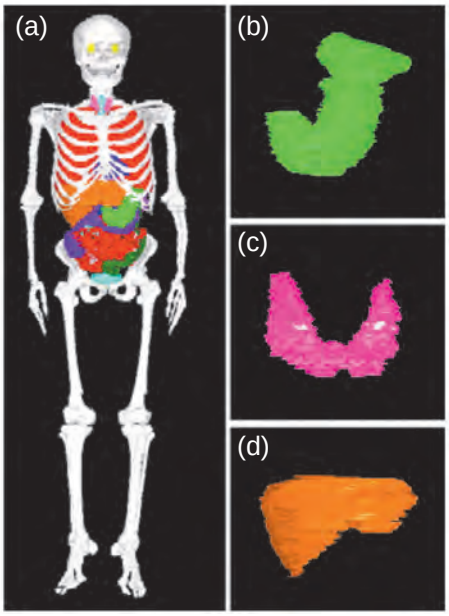

Fig.7-16 Three dimensional anterior views of (a) whole body, (b) stomach, (c) thyroid and (d) liver of Japanese voxel phantom in upright posture

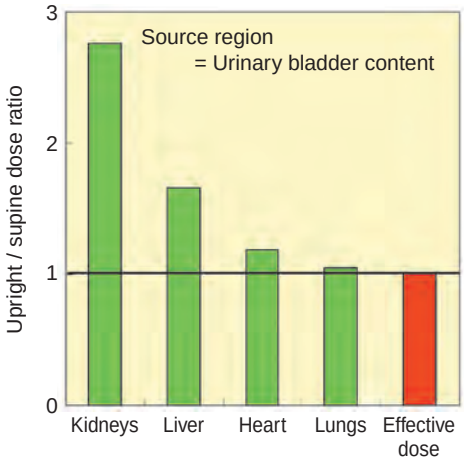

Fig.7-17 Comparison of organ doses and effective doses due to the intake of ^{131}Cs when upright and when supine

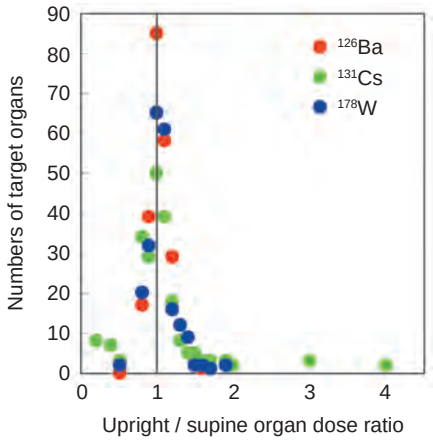

Fig.7-18 Distribution of the upright/supine organ dose ratios due to the intake of ^{126}Ba, ^{131}Cs and ^{178}W

In order to estimate the health effects in humans due to radiation exposures, organ dose needs to be calculated using human models which reproduce body sizes and shapes and elemental compositions of organs. In recent years, voxel phantoms (phantoms), which consist of small rectangular block units called 'voxel', have been developed on the basis of medical images of actual persons of various races, ages and body sizes, and are used for dose assessment. The reference phantoms adopted by the International Commission on Radiological Protection (ICRP) have been constructed on the basis of Caucasian anatomical data. The ICRP reference phantoms will be used to calculate organ doses for the purposes of radiation protection.

During radiation work, the posture is usually upright. However, the posture of previously developed phantoms is supine only. This is because the medical images are usually obtained from supine subjects. Therefore, it was impossible to clarify the variation in organ doses caused by changes in posture. We developed a Japanese adult male voxel phantom with upright posture on the basis of CT images of upright subjects for the first time in the world (Fig.7-16). The CT images in upright were again obtained from a subject for the phantom in supine previously developed by JAEA. Therefore, it is possible using these two phantoms to compare directly organ doses and to analyze the effects of posture on dose assessment. The voxel size of these phantoms is about 1mm^3, which enables us to accurately represent e.g. the thyroid with its complicated shape.

Fig.7-17 shows examples of organ doses calculated using upright and supine phantoms. The upright/supine ratio of doses in the kidneys and liver were about 270% and 170%, respectively, larger than those of heart and lungs. This result was due to the differences in the movement distances of organs when changing posture; the movement distances of kidneys and liver due to the changes of posture were longer than those of heart and lungs. The organ doses were changed by the changes in posture, but differences in the organ doses are within a factor of 2 in most cases (Fig.7-18). These results indicate that the impact of posture on the organ doses is not significant. Therefore, it can be concluded that there is no problem in using ICRP reference phantoms which have been developed from tomographic images obtained in the supine posture for the calculation of dosimetric quantities in radiation protection. The knowledge obtained from this study was reflected in the ICRP Publication 110 dealing with adult reference computational phantoms.

Reference

Sato, K. et al., Analysis of Effects of Posture on Organ Doses by Internal Photon Emitters Using Voxel Phantoms, Physics in Medicine and Biology, vol.53, 2008, p.4555-4572.

7-8 Toward Efficient Hydrogen Production by Thermochemical IS Process
—Measurement of High Pressure Vapor-Liquid Equilibrium of Hydriodic Acid—

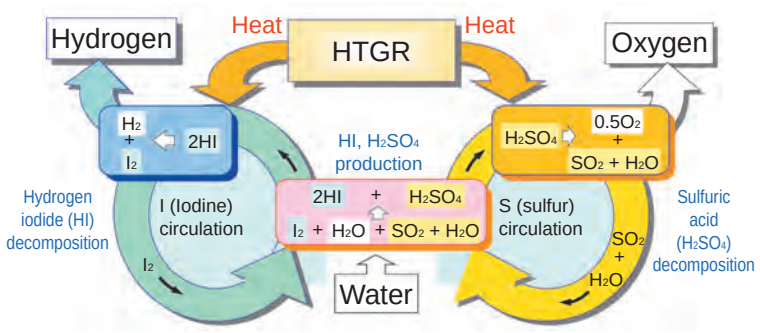

Fig.7-19 IS process
HI and H_2SO_4 should be separated from $HI+I_2+H_2O$ mixture and $H_2SO_4+H_2O$ mixture, respectively, before decomposition.

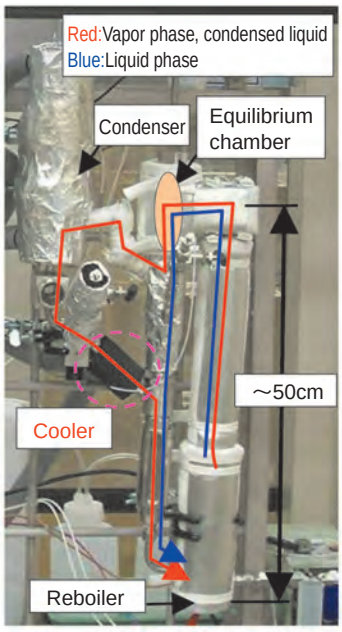

Fig.7-20 VLE measurement device
Vapor-liquid mixture flows up from the reboiler to the equilibrium chamber, where the equilibrium state is realized. Vapor is separated and condensed in the condenser. Vapor condensate and liquid phase are returned to the reboiler. After reaching steady state, the liquid phase and the vapor condensate are sampled and analyzed.

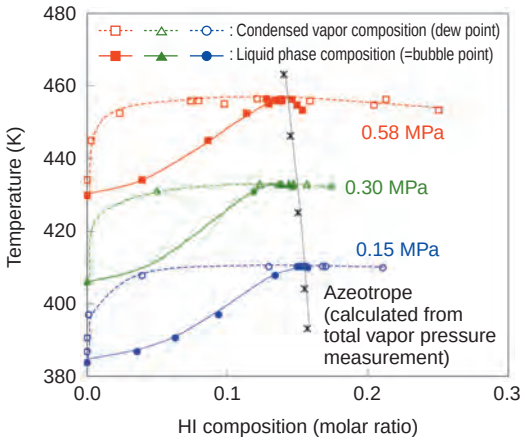

Fig.7-21 VLE data of $HI+H_2O$ mixture
The point where dew point curve and bubble point curve contact is the azeotropic point where equilibrium compositions of vapor phase and liquid phase are the same.

We are conducting R&D of thermochemical iodine-sulfur (IS) process, which can produce massive amounts of hydrogen from water without CO_2 emission, using the heat supplied by High Temperature Gas-cooled Reactors (HTGR). Fig.7-19 shows the scheme of IS process. Water (H_2O) reacts with iodine (I_2) and sulfur dioxide (SO_2) to produce hydrogen iodide (HI) and sulfuric acid (H_2SO_4), which are then thermally decomposed, producing hydrogen and oxygen, respectively. One of the difficult technical requirements of the process is efficient separation of HI from $HI+I_2+H_2O$ mixture. Distillation under elevated pressure is the promising candidate. However, little is known about the relevant vapor-liquid equilibrium (VLE).

Therefore, we have started the acquisition of VLE data. Our first target was the VLE of hydriodic acid, the two component system of $HI+H_2O$. At first, the materials for measurement devices which can be used in the highly corrosive $HI+H_2O$ solution were screened. Next, using the selected materials, a measurement device was constructed as shown in Fig.7-20. Here, in order to avoid the re-boiling of vapor condensate in the recycle line due to the large difference of boiling points of the vapor condensate and the liquid phase, a cooling system was added.

Fig.7-21 shows the obtained VLE data. $HI+H_2O$ is known to exhibit azeotropy, where compositions of the two phases of $HI+H_2O$ are identical. The measured azeotropic points were well in accord with those estimated from the former data of total vapor pressure measurement, which demonstrated the reliable accuracy of the developed measurement system. The equilibrium composition data of vapor and liquid phases newly acquired in the present study will enable precise design of the distillation column with smaller redundancy.

The acquisition of high pressure VLE data of three component system of $HI+I_2+H_2O$ system is under study. The VLE database will enable the compact and efficient design of the key separation apparatus of IS process.

Reference
Hodotsuka, M., Yang, X., Okuda, H., Onuki, K., Vapor-Liquid Equilibria for the HI + H_2O System and the HI + H_2O + I_2 System, Journal of Chemical & Engineering Data, vol.53, no.8, 2008, p.1683-1687.

7-9 Toward Safe Hydrogen Production Utilizing High-Temperature Gas Cooled Reactor
—Preventing the Hydrogen from Being Contaminated by Radioactive Material—

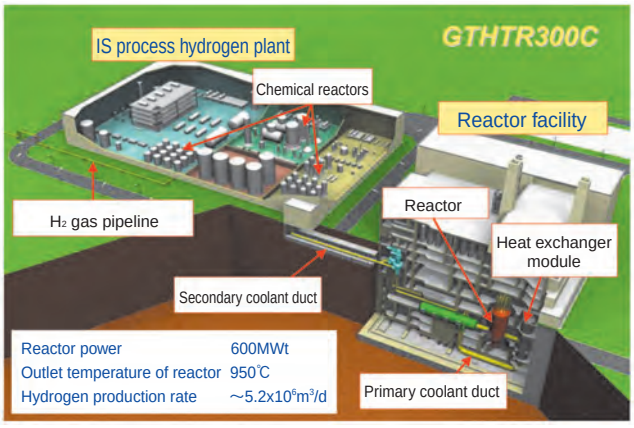

Fig.7-22 Bird's eye view of GTHTR300C

The primary coolant (helium gas) heated up to 950℃ in the reactor core transfers heat to the secondary coolant (helium gas) through the Intermediate Heat Exchanger (IHX). The secondary coolant is utilized as the heat source of the hydrogen production in the IS process hydrogen plant. A key difficult technical requirement is to prevent the tritium, which is a radioactive material produced in the reactor core, from migrating to the hydrogen by the permeation through the heat transfer tubes in the IHX and the hydrogen-producing chemical reactors.

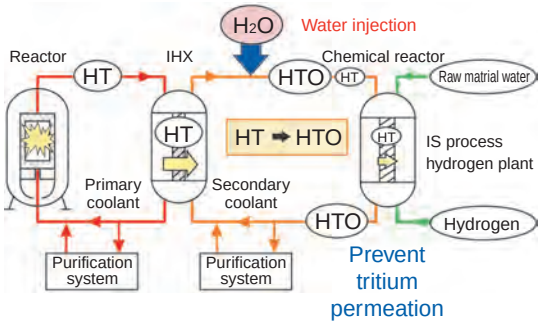

Fig.7-23 The water injection method to prevent tritium permeation

The tritium can slightly permeate through the metallic heat transfer tubes, because the main chemical form of the tritium is HT. In order to prevent the tritium permeation, we have proposed the water injection into the secondary coolant, by which the tritium is converted from HT to HTO.

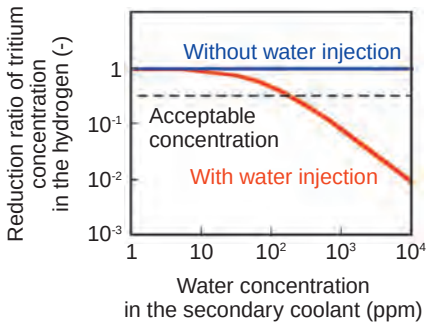

Fig.7-24 The effect of water injection on tritium concentration in the hydrogen

The numerical analysis results show that the tritium concentration in the hydrogen can be reduced to lower than the maximum acceptable concentration by the water injection method.

We have been developing the Gas Turbine High Temperature Reactor 300 for Cogeneration (GTHTR300C) (Fig.7-22), which produces hydrogen from water by a thermochemical Iodine-Sulfur (IS) process without CO_2 emission, using high-temperature heat (950℃) from a High Temperature Gas Cooled Reactor, for the realization of a low carbon society. One of the difficult technical requirements of this system is to prevent tritium, a radioactive material, from migrating to the hydrogen. Tritium is produced in the reactor core by fission and neutron capture reactions. Since a small amount of tritium can permeate through the metallic heat transfer tube in the heat exchanger, tritium migrates from the primary to the secondary coolants and to the hydrogen plant. Then, the hydrogen might be contaminated by tritium. The tritium concentration in the hydrogen should be kept lower than the maximum acceptable concentration, which has no affect on the human body.

We have experimentally evaluated these permeation characteristics through the heat transfer tube, developed a computer code for the evaluation of the tritium concentration in the hydrogen, and considered methods to reduce the tritium concentration in the hydrogen. It was confirmed that the tritium concentration in the hydrogen can be reduced to lower than the maximum acceptable concentration by the increase of the capacity of a purification system installed to trap chemical impurities (e.g., CO) in the coolants. However, this would entail an unacceptable increase in the construction cost. Therefore, we propose an alternative countermeasure: water injection into the secondary coolant, to reduce the tritium concentration in the hydrogen. Tritium in the secondary coolant (HT) is converted to HTO, which is less permeable through the metal, by the isotope exchange reaction with injected H_2O, in order to reduce the tritium permeation rate (Fig.7-23). This can be carried out without costly modification of the reactor facility, because the main additional equipment is only a water pump. Our numerical analysis results show that the tritium concentration in the hydrogen can be reduced to lower than the maximum acceptable concentration by the injection of a small amount of water, whose concentration in the coolant is so low that it does not affect the structural integrity of the reactor components (Fig.7-24).

Reference

Ohashi, H, Analytical Study on Tritium Migration in NGNP and Countermeasures to Reduce Tritium Contamination, Nippon Genshiryoku Gakkai Wabun Ronbunshi, vol.7, no.4, 2008, p.439-451(in Japanese).

Toward Establishment of Nuclear Fuel Cycle

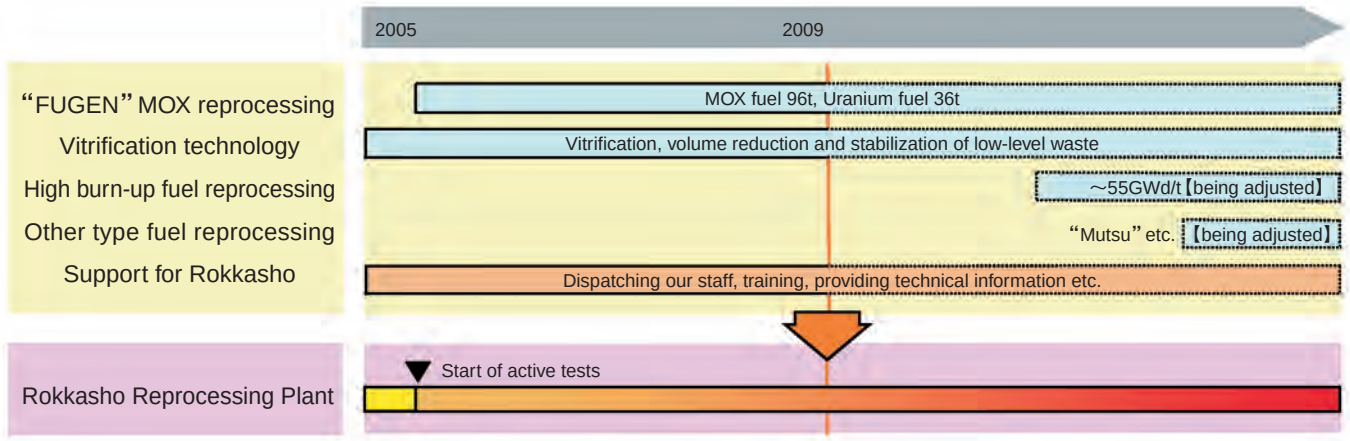

Fig.8-1 R&D to assist private enterprises' reprocessing business
To promote reprocessing of spent light water reactor fuel and usage of plutonium in light water reactors by private enterprises, we are conducting research and development of reprocessing of the "FUGEN" reactor's uranium-plutonium mixed oxide (MOX) spent fuel and vitrification of high-level waste fluid.
In response to a request by Japan Nuclear Fuel Ltd. (JNFL), we are dispatching engineers and are training JNFL staff to support their uranium enrichment, reprocessing and MOX fuel fabrication operations.

1. Development of reprocessing technology

In preparation for the reprocessing test of "FUGEN" MOX spent fuel, we are continuing basic investigations such as development of techniques for analyzing minor actinides (MA).

There now are prospects for development of a long-life glass melter for high-level liquid waste vitrification technology, thanks to experiments in reducing the erosion of the structural material (Fig.8-2).

In response to a request by JNFL, we carried out tests of glass properties and effect assessment of insoluble residue which were needed for activation tests of the vitrification facility in Rokkasho Reprocessing Plant (RRP) of JNFL.

To develop technology for volume reduction and stabilization of low-level radioactive waste, we carried out tests of cement solidification with simulated liquid waste and of nitrate decomposition of waste containing nitrates, obtaining data necessary for the facility design.

In addition, we are making arrangements with related organizations to advance reprocessing technology to treat high burn-up spent fuel (Fig.8-1).

2. Technical co-operation

We are providing technical help to JNFL for their cascade test of the super-efficient new material centrifuge for uranium enrichment, activation tests of RRP, and construction and operation of the MOX fuel fabrication facility.

RRP is in the final step of its active tests, and we have strengthened our support, especially for the test of vitrification of high-level waste fluid, by dispatching additional technicians and carrying out entrusted research and joint research with JNFL (Fig.8-1).

In addition to the above, we are carrying out training for engineers of Nuclear Fuel Chemical Analysis Co. (Limited Liability Partnership) which is conducting analysis of uranium and plutonium etc. at RRP, and of Tokyo Electric Power Environmental Engineering Co., Inc. which conducts environmental radioactive monitoring etc. Our engineers are also dispatched to the Nuclear Material Control Center and are engaged in technical support for nuclear material control at Rokkasho district.

Fig.8-2 Glass melter

8-1 Toward MOX Reprocessing

—Solvent Degradation and Its Effect on Pu Purification Cycle in Reprocessing Plant—

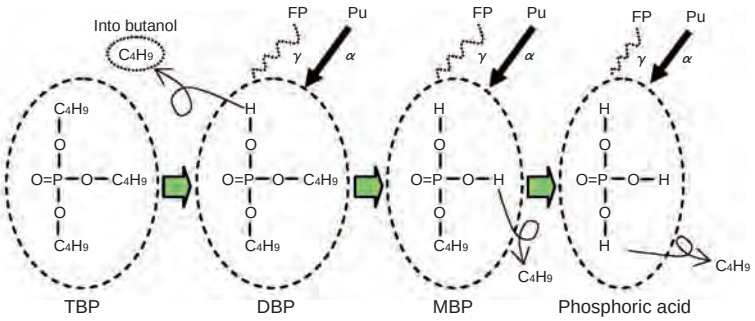

Fig.8-3 Solvent degradation
TBP is degraded to DBP by radiolysis or hydrolysis etc. Then, DBP is degraded to MBP, and MBP to Phosphoric acid. DBP is the most important compound of the three degraded materials (DBP, MBP, Phosphoric acid) because DBP produced in the extraction process is generally said to cause transfer of U and Pu to waste water.

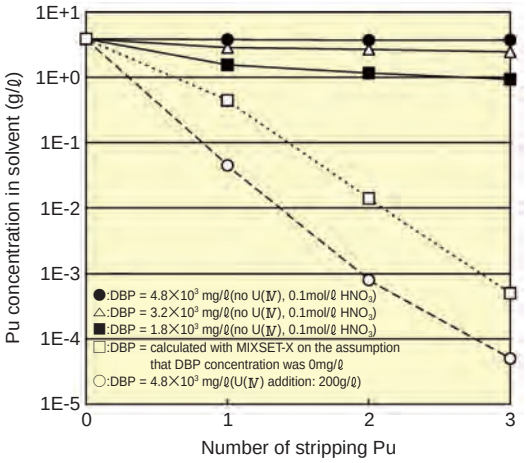

Fig.8-4 Pu concentration after stripping Pu in solvent
Pu is stripped by diluted nitric acid when there is no DBP in solvent, but the efficiency of Pu stripping was lower when there was more DBP in solvent. Pu was efficiently stripped by U(IV) even when there was DBP in solvent.

The reprocessing process in Tokai Reprocessing Plant (TRP) is PUREX process, using nitric acid and a solution of 30vol% TBP in n-dodecane.

TBP is degraded to DBP by radiolysis or hydrolysis etc. (Fig.8-3) Radiolysis depends on calorific value and hydrolysis with an ion catalyst depends on Pu concentration. We need to consider solvent degradation by the alpha rays from Pu because Pu concentration is high in the Pu purification cycle.

The Fugen spent fuel (MOX fuel) has been reprocessed at TRP since 2007. The amounts of Pu-238, Pu-240 and Pu-242 in MOX fuel are more than in LWR spent fuel. Pu - 238, Pu-240 and Pu-242 are alpha ray emission nuclides. Therefore, it is thought that solvent degradation takes place more easily when MOX fuel is reprocessed.

We sampled solvent from contactors at Pu purification cycle when MOX fuel was reprocessed in TRP, and we evaluated the alpha rays emitted from Pu-degraded solvent by measuring Pu and DBP concentration in solvent. The results are as follows.

(1) Considering that total DBP production rate depends on calorific value and Pu concentration, total DBP production rate is calculated as follows:

$$T = 51.2W + 0.06[Pu] + 0.1$$

Where T[mg/ℓ・h] is total DBP production rate, W[W/ℓ] is calorific value per unit volume and [Pu][g/ℓ] is Pu concentration. W[W/ℓ] corresponds to energy absorbed into solvent and is calculated from Pu concentration and Pu isotopic composition.

This formula enabled us to estimate DBP concentration in the Pu purification cycle from process parameters.

(2) The Pu stripping efficiency worsens when the DBP density is high, but we confirmed that there was no problem efficiently stripping Pu from solvent when U(IV) was used as the reduction reagent (Fig.8-4).

(3) We obtained the DBP concentration profile during the Pu purification step when the Fugen spent fuels were reprocessed in TRP.

In fact, we experienced a twenty day stoppage of the Pu purification cycle in TRP, during which time Pu remained in the solvent. After restarting Pu purification, we had no problem with stripping Pu from solvent, though DBP concentration was increased up to about 2.2×10^3mg/ℓ. From the results of our investigation, we think the reason for this is that U(IV) was used as the reduction reagent for stripping Pu from solvent in the Pu purification step.

These results will be utilized as basic data for research into reprocessing MOX spent fuel.

Reference
Kawaguchi, Y., Morimoto, K. et al., Study of Solvent Degradation in Reprocessing MOX Spent Fuel —Solvent Degradation and Its Effect on Pu Purification Cycle—, Nippon Genshiryoku Gakkai Wabun Ronbunshi, vol.8, no.3, 2009, p.221-229 (in Japanese).

8-2 System for Stable Operation of Rotating Equipment
—Monitoring Conditions by Shock Pulse Method—

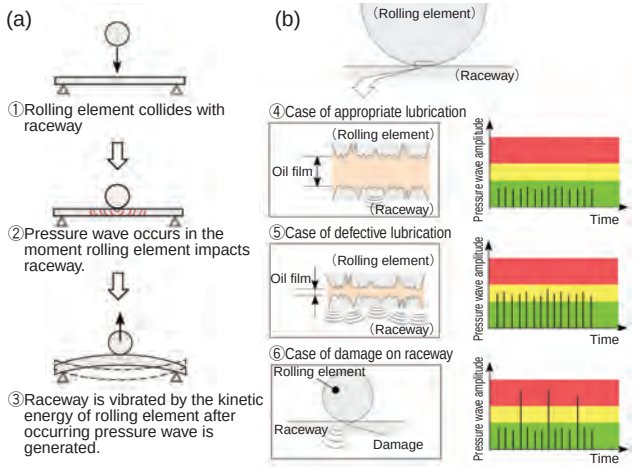

Fig.8-5 Generation of pressure wave, relation between strength of pressure wave and oil film thickness
Figure (a) shows generation of pressure wave and vibration in bearing. Figure (b) shows that the change in the pressure wave intensity, number, etc. is caused by change in the oil film thickness in the bearing.

Table 8-1 A example of measurement result in bearing
In diagnosis of a bearing by the VM and SPM, the amplitude measured by the VM was about 85μm, lower than the 120μm. However, SPM diagnosed that the bearing needed replacement, because LP value was higher than the replacement threshold value by about 10dB.

		Amp (μm)		Vel (mm/s)		Acc (m/s^2)	
		Horizontal	Vertical	Horizontal	Vertical	Horizontal	Vertical
Vibration method	measurement value	85	65	2.8	2.3	1	1
	normal value	45		2.3		1.1	
		LP(dB)※1		SP(dB)※2			
Shock pulse method		31		-2			
Specification		Type : 6313Z Rotational speed : 858rpm					

Amp: Amplitude, Vel: Velocity
Acc: Acceleration
※1: Large pulse
※2: Small pulse

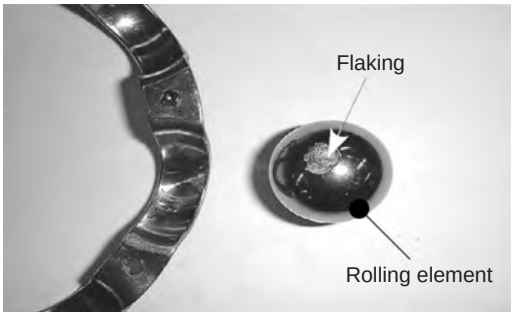

Fig.8-6 State of rolling element in bearing

In the Tokai Reprocessing Plant, lots of blowers are used to keep radioactive materials in a controlled area, and pumps are used for cooling water circulation to maintain appropriate temperature in high-level radioactive liquid waste vessels. This rotating equipment plays an important role in safety maintenance of the nuclear facilities. It is very important for stable operation of the rotating equipment to monitor the bearing damage caused by inadequate lubrication as well as imbalance and misalignment.

In the Tokai Reprocessing Plant, the bearings were diagnosed by a vibration method (VM), because measuring instruments for management of rotating equipment needed to be portable and easy to operate. However, it is difficult to determine the state of a bearing by the VM when there is vibration of other parts of the rotating equipment. Troubles in bearings are caused by defective lubrication, but it is very difficult to quantitatively measure oil film thickness during the monitoring for lubrication of bearings by the VM. Therefore, it is very important to improve the bearing condition monitoring system. We examined new diagnosis methods, by measurement of operation sound or pressure waves, to solve the problem with VM. As a result, diagnosis by pressure wave was adopted.

Pressure wave and vibration are generated by rolling elements hitting the raceway in a bearing. The strength and number of pressure waves generated are changed by oil film thickness or damage to the bearing, as shown in Fig.8-5. The shock pulse method (SPM), which uses this characteristic, is a new technique which is starting to be used widely, and is well suited to quantitative management of lubrication in bearings.

Table 8-1 shows an example of use of the SPM to diagnosis of a bearing in the rotating equipment. The bearing was diagnosed as being able to keep operating by VM. However, the bearing was diagnosed as faulty by SPM. When the state of this bearing was examined, the flaking was found to have occurred on the rolling element as shown in Fig.8-6.

SPM is well suited to bearing management, because this method has high response to changes in the state of a bearing. However, SPM has a possible problem, that it may demand excessive replacement because it is based on indirect conditions caused by faults, so it is necessary to obtain data on bearings which have replacement threshold values.

Bearings should be managed by the diagnosis of VM as well, because in the case of bearings which have been appropriately lubricated for a long period, there is a possibility that a fatigued or worn-out bearing does not generate a high pressure wave. Such maintenance for bearings will enhance understanding of the state of bearings. It is possible to improve maintenance function by combining SPM and conventional VM.

Reference

Takeuchi, K. et al., Development of Maintenance Technology for Rotation Equipments in the Tokai Reprocessing Plant II —Equipment Diagnosis by Using the Shock Pulse Method—, Japan Society of Maintenology, The 5th Science Lecture Meeting, 2008, p.353-358 (in Japanese).

Executing Decontamination & Dismantling and Radwaste Treatment & Disposal

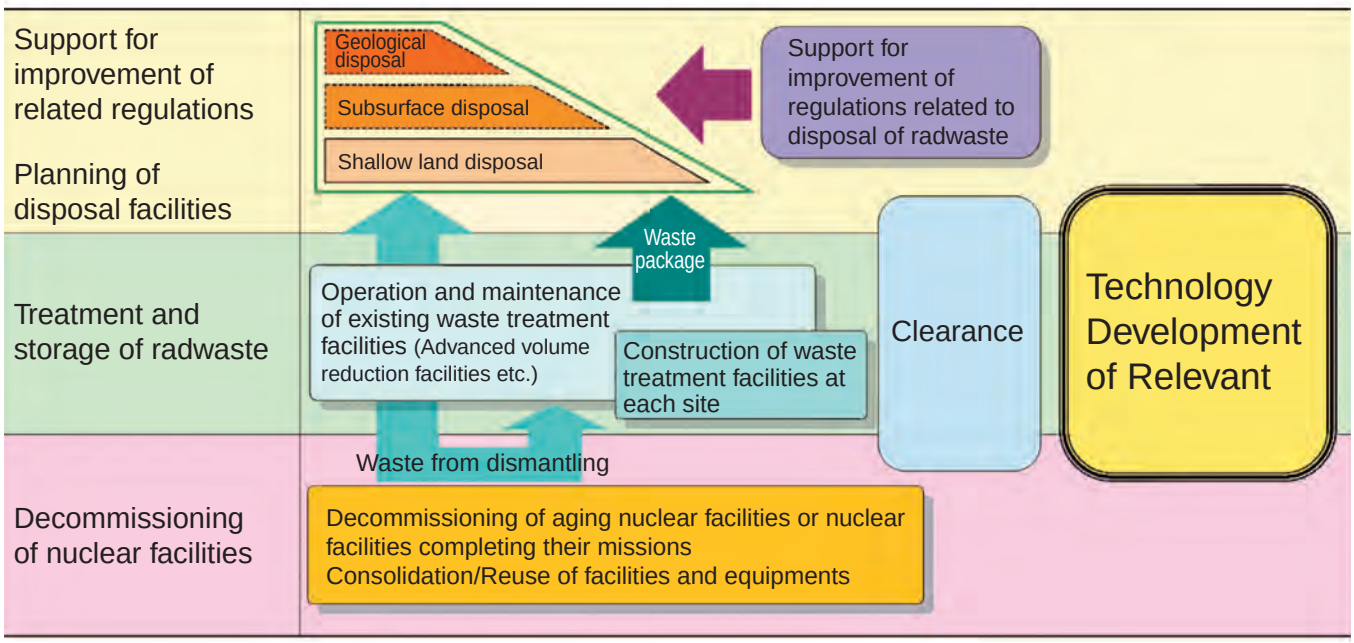

Fig.9-1 Outline of measures for decommissioning and radwaste treatment/disposal

Decommissioning and radwaste treatment/disposal are two of our major missions. In these missions, we will be disposing of radwaste arising not only from our research activities but also those of universities, institutes, industrial facilities, etc.

We are setting up systems for the decommissioning of nuclear facilities and for radwaste management, through related technology development, planning and construction of radwaste treatment/disposal facilities, and support for improvement of related regulations (Fig.9-1).

R&D for Decommissioning

We are developing a decommissioning engineering system and a waste/scrap material clearance verification/evaluation system.

To develop this decommissioning engineering system, a method for evaluating decommissioning cost efficiently which is applicable to various types of nuclear facilities has been constructed (Topic 9-1).

R&D for Waste Treatment

In order to dispose of radwaste in a cost effective manner, research in the following waste treatment techniques is being conducted: a nitrate degradation method for low level effluent, a cement solidification technique for incineration ashes, and a decontamination technique using supercritical carbon dioxide fluid to remove plutonium from radwaste.

Furthermore, we have developed a waste management system which is used for systematic management of the radwaste data acquired through various operations from generation to disposal of the wastes. This management system supplies the data needed for safety assessment of disposal of radwaste etc. (Topic 9-2).

R&D for Waste Disposal

Studies on rapid measurement of various radionuclides are underway to establish practical methods to evaluate the radioactive inventory in waste packages.

By literature review and actual measurements of natural uranium concentration, the contribution of uranium to natural background radiation has been estimated (Topic 9-3). This result will be applied to conceptual design of a clearance and disposal system for uranium bearing waste, taking into consideration the existence of natural uranium.

As for study on a subsurface disposal system for uranium-bearing waste, exposure dose in the case of “less-likely scenarios” was preliminary calculated to be less than “standard dose value” recommended by Nuclear Safety Commission.

In addition, radioactivity concentrations in radwaste generated by reactor facilities were characterized. This date will be used for safety assessment which will be applied during the implementation of disposal.

9-1 Rational Approach to Decommissioning of Nuclear Facility
—Developing a Fast Method for Evaluating Decommissioning Cost—

Table 9-1 Relationship between dismantling methods chosen according to facility characteristics and evaluation items

	Dismantling method	Evaluation item	Reactor	Nuclear fuel facility					Research facility			General facility
				Uranium treatment facility	Reprocessing related facility	MOX treatment facility	Waste treatment facility		Hot laboratory	Accelerator	Unsealed source treatment facility	
							β・γ	TRU				
Decontamination before dismantling		System decontamination			○							
		Cell decontamination			○				○			
Dismantling of equipment (Metal)	of general equipment	Uncontaminated	○	○	○	○	○	○	○	○	○	○
		β・γ/U contaminated	○			○	○		○	○	○	
		TRU contaminated		○	○	○		○				
	by heavily equipped	High radiation area	○		○			○	○			
		Low radiation area	○		○		○	○	○		○	
	of special equipment	Lining	○		○			○	○			
		Centrifuge		○								
		Large scale glove box				○						
		Small scale glove box			○	○		○				
		Block (metal)								○		
	by remote control	Dismantling in cell by robot			○				○			
		Dismantling in air	○							○		
		Dismantling in water	○									
Dismantling of building and structures (concrete)	Structures	by remote control	○									
		Removal of block					○		○	○		
	Building	Removal by workers	○				○		○	○		
		Removal using heavy machine	○				○		○	○	○	
		Reinforced concrete	○	○	○	○	○	○	○	○	○	○
		Steel-frame slate		○								○

The mark ○ denotes cost evaluation items for dismantling methods at nuclear facilities

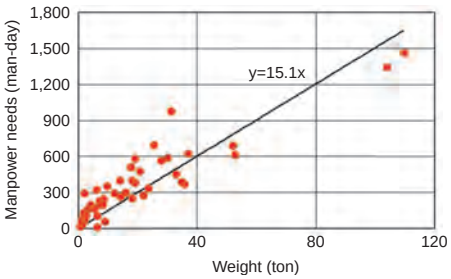

Fig.9-2 Relationship between manpower need and weight of equipment (General equipment (β-γ/U))

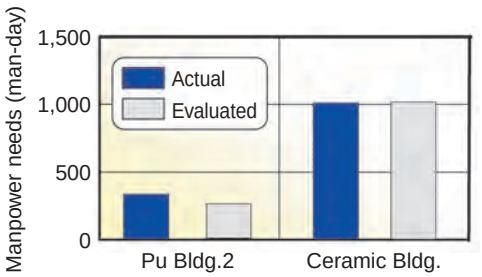

Fig.9-3 Comparison of evaluated and actually used labor

We have various types of R&D nuclear facilities which will be eventually decommissioned with their missions completed. To implement decommissioning of these facilities, it is important to make a rational decommissioning plan from a long-term point of view.

The decommissioning cost of the facilities needs to be estimated in advance to develop such a long term plan. In evaluating decommissioning cost, detailed facility information is required in general such as weight of the equipment and contamination distribution in the facility, and the specific procedure of dismantling. However, it will take much time and effort to get such detailed plant information and to determine the procedure. Therefore, a method for evaluating decommissioning cost efficiently, even if the detailed information has not been obtained, needs to be developed. Here, one important issue is how to estimate the manpower required to dismantle the facility and equipment. Once the manpower need is evaluated, it will be possible to evaluate the cost of dismantling operations using unit labor cost, and other cost of decommissioning planning and work management.

Manpower need depends on the dismantling method, which is chosen according to the type of facility. Thus we classified nuclear facilities into reactors, nuclear fuel facilities, research facilities, etc., and made the relationship between the dismantling method and each type of facility (Table 9-1). Manpower need depends on the weight of equipment to be removed, size of the operation area, and the dismantling method. Considering that there is a correlation between weight of equipment or floor area of building and manpower need, we constructed conversion coefficients from weight or area to manpower need by analyzing experienced real data of JAEA operations (dismantling of Japan Power Demonstration Reactor and partial remodeling of Reprocessing Plant). Fig.9-2 shows an example of analysis results of the relationship between manpower needs and weight of equipment. Then, we developed a method for rapidly evaluating decommissioning cost which would be applicable to various types of facilities and dismantling methods.

To verify this method, we applied it to two facilities using unsealed sources, Plutonium Research Building 2 (Pu Bldg.2) and Ceramic Research Building (Ceramic Bldg.). Fig.9-3 shows a comparison of evaluated results and actual data. There was good agreement between them, verifying the accuracy of this method.

Reference

Shiraishi, K., Tachibana, M., Ishigami, T. et al., Study on Cost Evaluation Methods for Decommissioning of Nuclear Facilities, JAEA-Technology 2007-057, 2007, 46p. (in Japanese).

9-2 Preparing Reliable Waste Data Needed for Disposal

—Development of Waste Management System Covering from Generation to Disposal—

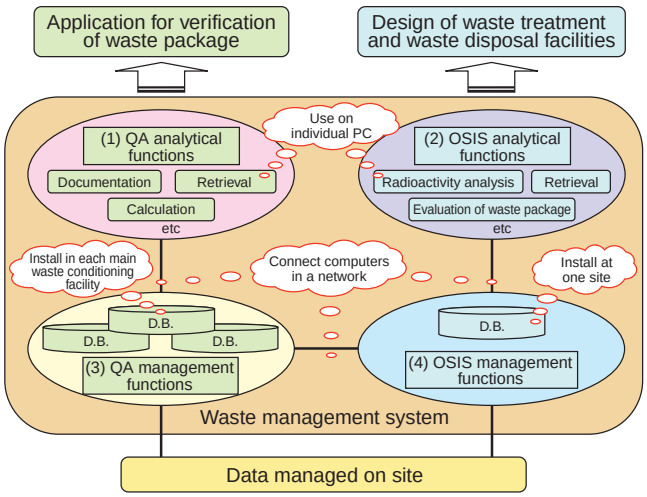

Fig.9-4 Conceptual organization and functions of "Waste Management System"
QA data and OSIS data have separate functions for data management and analysis. (QA: Quality Assurance, OSIS: Optimization Study and Information Service).

Table 9-2 Sample of QA data managed in this system
Ca. 400 items in 43 stages are to be managed

Disposal stage	Data items to be managed
Waste enclosing	generation place, enclosing date, waste ID, amount of harmful materials, mass, container class, waste classification, nuclide, radioactivity, surface dose rate, etc
Segregation	work manual ID, worker's name, educating record ID, check sheet ID, campaign No., waste ID, separating test record ID etc
Compaction	work manual ID, compaction pressure, container No., periodic inspection record ID, treatment date, device No., treated waste ID, compaction test record ID, etc
Incineration	incinerated temperature, holding time, input interval, treatment manual ID, device No., campaign No., tray No., periodic inspection record ID, ash ID, etc
Cementation	cement input, solidification manual ID, solidified date, waste batch No., waste input, mixing revolution, curing time, solidified matter ID, container No., etc
Acceptance of cement	delivery record ID, certificate of analysis of cement ID, acceptance amount, campaign No., etc
Unconfined compressive strength measurement	ultrasonic propagation velocity, measurement date, unconfined compressive strength, device No., periodic inspection record ID, solidified waste ID, etc
Sample analysis	nuclide, activity, detection limit, device No., analytical date, sample No., analytical manual ID, analytical record by third-party ID, etc
Non-destructive assay	nuclide, activity, lower detection limit, device No., measurement date, measurement manual ID, etc

For safe disposal of radioactive waste, we have to verify that waste packages meet the acceptance criteria of disposal facilities. Various data needed for this verification has to be managed systematically, retrievable for a long period of time according to their relation to other data ranging from generation to disposal. Also, this data is needed for the design of treatment and disposal facilities. Therefore, we are developing the "Waste Management System" to manage all waste data with traceability and to analyze and count the data.

We have to prepare a large amount of data for quality assurance (QA data) of the waste packages used at stages from waste generation to final conditioning for disposal, such as generation status, waste treatment methods (incineration, compaction, etc.), materials used for solidification, calibration certificates of measurement instruments, records of worker's training and so on. Examples of the data to be managed in this system are listed in Table 9-2.

In addition, we have to handle the waste data to be used for design of waste treatment and disposal facilities and for considering waste disposal systems. These data are managed as "Optimization Study and Information Service data (OSIS data)" in this system.

The Waste Management System consists of following four functions working upon the QA data and the OSIS data as shown in Fig 9-4.

(1) QA analytical function: Supporting technical documentation for quality assurance of each waste package by analyzing characteristics of each waste material.
(2) OSIS analytical function: Supporting estimation of radioactivity in each waste package and total waste package volume, design of waste treatment and disposal facilities, and so on.
(3) QA management function: Managing QA data of each waste package so as to have traceability.
(4) OSIS management function: Managing the OSIS data.

In our conception, the "Waste Management System" has data management functions and analytical functions that are connected through networks to PC & servers.

In the future, we will construct the concrete "Waste Management System" to be used for verification of actual waste packages, applying each of the above functions to actual QA and OSIS data. This system will be incorporated in the individual waste management systems in each of our R&D sites.

Reference

Kuroki, R. et al., Development of Waste Management System I —Concept Construction of the System—, JAEA-Technology 2009-016, 2009, 124p. (in Japanese).

9-3 Establishing Rational Clearance and Disposal System of Uranium-Bearing Waste
—Understanding Natural Uranium Contribution to Natural Background Radiation—

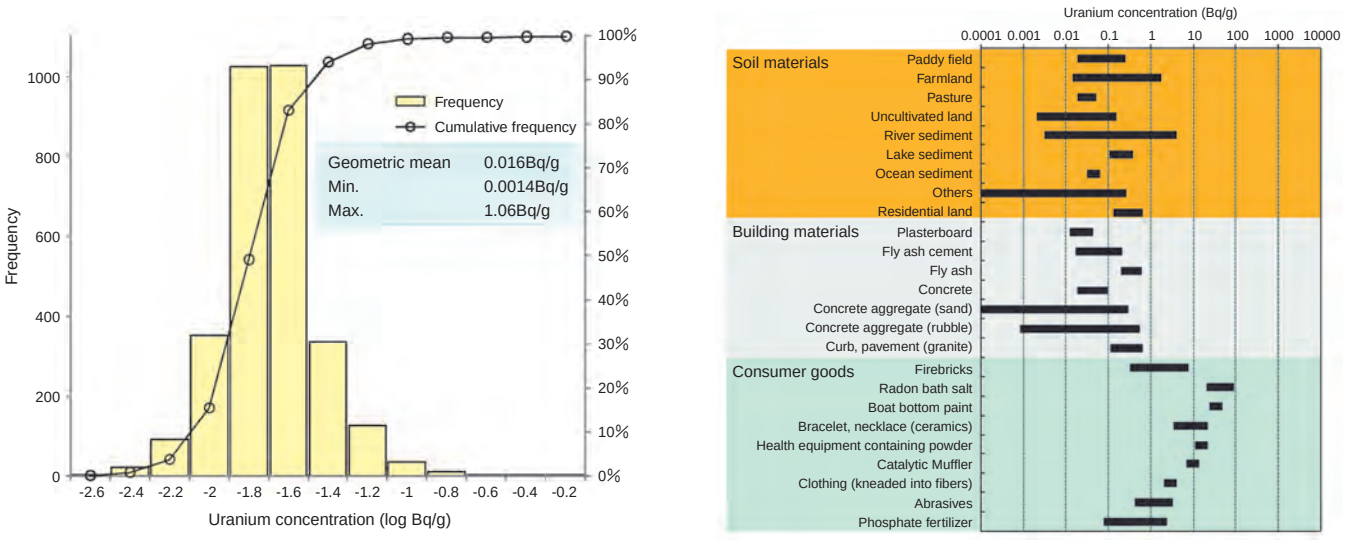

(a) Frequency distribution of various radioactivity concentrations of uranium (U-238) in surface soil/rock in Japan

(b) Radioactivity concentration of uranium in soils, building materials and consumer goods

Fig.9-5 Distribution of uranium in environment and artifacts in Japan

Table 9-3 Estimated dose contribution of radionuclides in U-238 series to annual dose in Japan

Source			Total dose (mSv/y)		Dose from U-238 series (mSv/y)[3]		
			Range	Mean	Range	Mean	Dominant nuclides
External exposure	Cosmic ray		0.22 - 0.44 [1]	0.26	-	-	-
	Terrestrial dose		0.14 - 0.44 [2]	0.30	0.026 - 0.095 [2]	0.06	Bi-214, Pb-214
Internal exposure	Radon inhalation		0.38 - 1.3 [1]	0.59	0.38 - 1.3 [1]	0.59	Rn-222 [4]
	Food ingestion	U, Th	0.13 - 0.23	0.18	0.13 - 0.23	0.18	Po-210, Pb-210
		K, etc.	0.20	0.20	-	-	-
Total			About 1.1 - 2.6	About 1.5	0.54 - 1.7	0.83	Rn-222 [4], Po-210

1) Range of mean values of each prefecture
2) Range from 10 percentile to 90 percentile
3) Dose contribution of U-235 series nuclides is small
4) Include contribution of dose from radon and its progeny

Clearance of uranium treatment facilities for uranium refining, conversion, enrichment, and fuel fabrication, and disposal of radioactive waste generated from those facilities (so-called uranium-bearing waste) has been under discussion among governments and companies.

Uranium is widely distributed in natural environmental materials such as soil, rock, river water and groundwater. Moreover, some building materials and consumer goods also contain uranium. We have carried out a review of literature to estimate uranium distribution in the environment. We also measured some samples which with high uranium concentration for confirmation of their concentration range. As a result, it was confirmed that the radioactivity concentration of uranium (U-238) in surface soil/rock in Japan ranges from 0.001Bq/g to several Bq/g (Fig.9-5(a)). Furthermore, it was found that some consumer goods have high uranium concentration, and that concentration of uranium in building materials falls inside the range of soils (Fig.9-5(b)).

We also estimated the external and internal dose contribution of radionuclides in uranium series to annual dose caused by natural background radiation by using mean values of uranium concentration in environment (Table 9-3). It was revealed that their average contribution is about 0.8mSv/y, whereas the total annual radiation dose in Japan is about 1.5mSv/y.

These results will be useful as basic information for discussion of clearance of uranium bearing materials arising from uranium treatment facilities, and of disposal of uranium-bearing waste in Japan.

Reference

Sato, K. et al., Uranium Distribution in the Environment and Its Contribution to Environmental Radioactivity, Dekomisshoningu Giho, vol.38, 2008, p.2-10 (in Japanese).

10 Collaboration on Basic Nuclear Engineering

Promotion of R&D to Meet the Demands of Industry and Academia

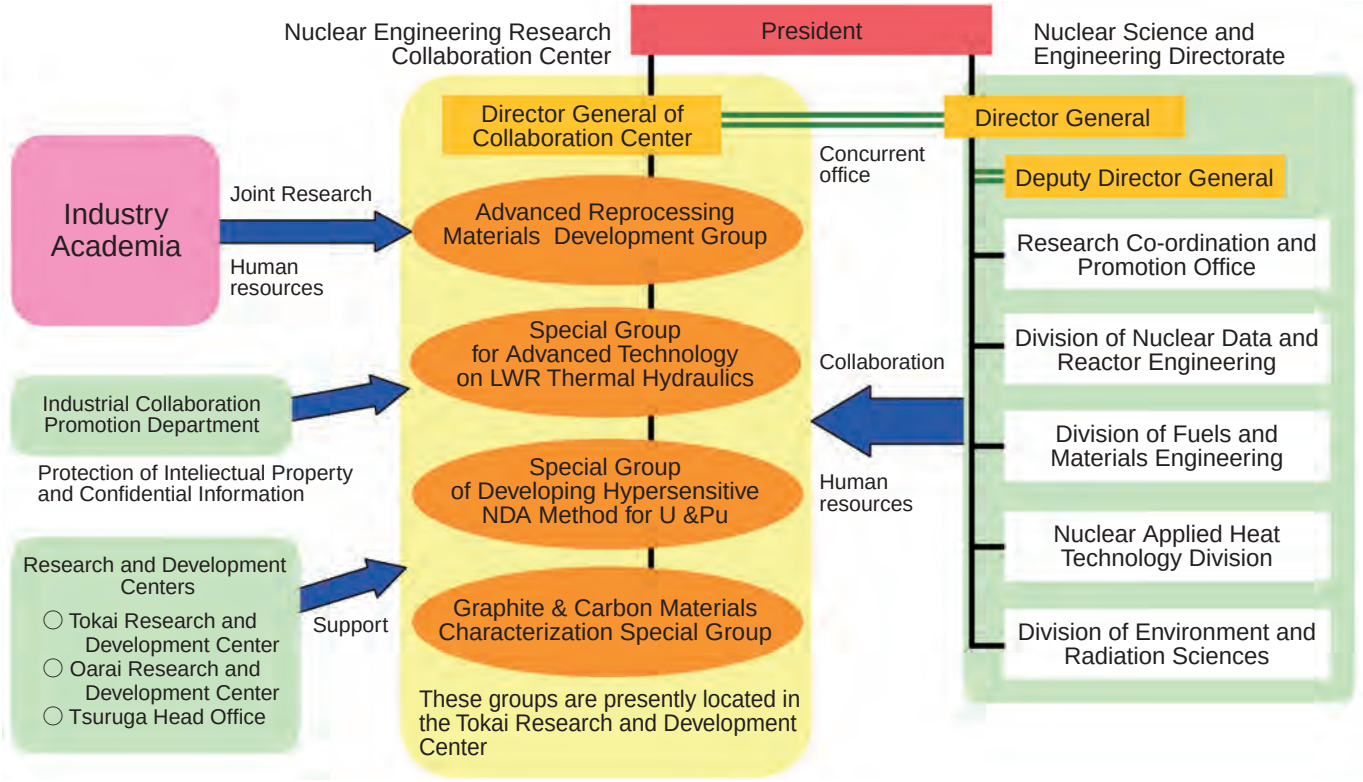

Fig.10-1 Nuclear Engineering Research Collaboration Center and Related Organizations

JAEA has been promoting joint research and development with industry and academia and has made its nuclear facilities and experimental apparatuses available to meet their needs. This collaboration is under the auspices of the Nuclear Research Collaboration Center (NRCC) established in 2005. and supported mainly by the Nuclear Science and Engineering Directorate, as shown in Fig.10-1. NRCC manages specific technology groups established through collaboration agreements. Presently there are four active technology groups, comprising researchers and experts from universities, industries, and JAEA.

The Advanced Reprocessing Materials Development Group has succeeded in cooperation with Kobe Steel, Ltd. in making original extra high purity (EHP) alloys by cold crucible induction melting (CCIM) coupled with a Ca/CaF reduction method and electron beam cold hearth refining (EB-CHR). These EHP alloys have demonstrated excellent resistance against grain boundary corrosion in severe reprocessing environments. A trial melting of several hundred kg has revealed conditions which make it possible to limit harmful impurities of the EHP alloys to less than 100ppm, even if nuclear grade clippings are used as raw material.

The Special Group for Advanced LWR Thermal-hydraulics Technology is conducting mock-up tests in collaboration with a private industry partner, incorporating improved information management. The Special Group for Nondestructive Hypersensitive Detection of U&Pu has invented a fast neutron direct interrogation method, by which distributions of U and Pu in the interior of waste material can be measured with more than 100 times higher sensitivity than conventional methods (Topic 10-1). Also, an ongoing R&D collaboration with IHI Ltd. and Tokyo University aims to apply this method to detection of nuclear material hidden in personal luggage.

The Graphite & Carbon Materials Characterization Special Group developed an evaluation method of irradiation-caused change in materials in cooperation with Toyo Tanso Co. We succeeded in the determination of pore distribution in fine-grained graphite IG-110 of 20μm grain size by 3D- X-ray CT (Fig.10-2).

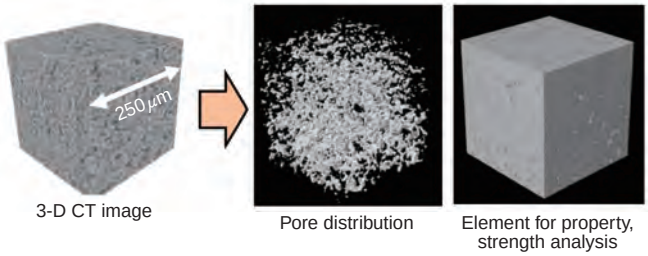

Fig.10-2 Preparation of element suited for strength and property analysis by X-ray CT

10-1 Struggling with Background in Fissionable Nuclide Detection

—Development of Hypersensitive Detection Method of a Trace Amount of Fissile Material—

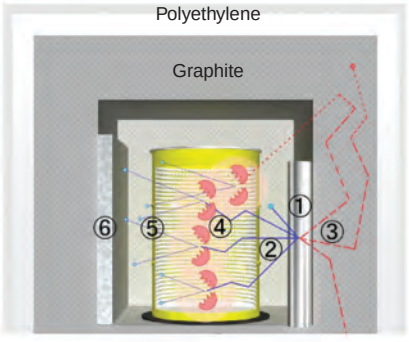

Fig.10-3 Concept of measurement
Interrogation neutrons from 14MeV neutron generator ① are slowed down to thermal neutrons ② & ③ by the moderation effect of the measurement system material (graphite) and the measured material (concrete etc.). Then, nuclear fission ④ is induced by these thermal neutrons ② & ③, and nuclear fission neutrons ⑤ are generated. These nuclear fission neutrons ⑤ are detected by a detector bank ⑥ that is surrounded with a cadmium sheath.

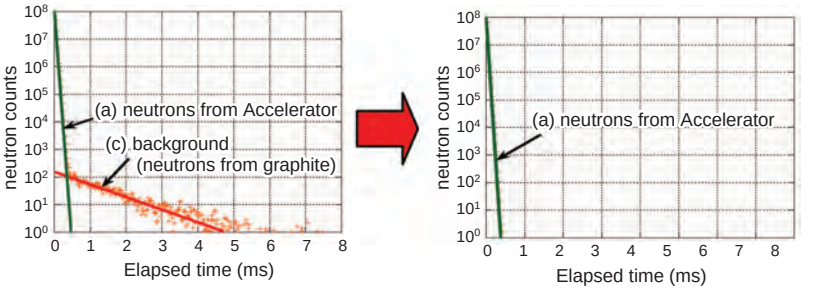

Fig.10-5 Improvement of background
A spectrum of the graphite detecting system (A) has 2 components of neutrons, from the accelerator (a) and background (c). Analytical study has shown that the source of (c) is the graphite of the detecting system. Search for the optimum material by Monte Carlo simulation revealed that (c) can be eliminated by using stainless steel instead of graphite.

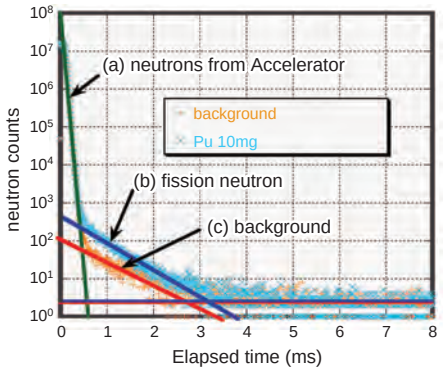

Fig.10-4 Measurement spectrum
The measurement spectrum denoted by light blue is the nuclear fission neutron component (b), generated when a nuclear material (plutonium, about 10mg) is at the center of the drum filled with paper waste. The measurement spectrum denoted by orange is the background when there is no fissile material.
In order to determine the amount of fissile material, the net count of nuclear fission neutrons is calculated by subtracting the background (c) from the nuclear fission neutron component (b). In this case, the detection limit is the deviation of the background count (c).

The 14MeV neutron direct interrogation method detects neutrons generated by nuclear fissions of the fissile material in nuclear waste which are induced by irradiation with neutrons from outside. This method has the advantage that it can detect a trace amount of the fissile material in a short time with position-independent sensitivity.

As is schematically shown in Fig.10-3, the gist of this method is to measure the nuclear fission neutrons generated by the interrogation neutrons.

First of all, the 14MeV interrogation neutrons from the generator tube are slowed down to thermal neutrons by the moderation effect of the measurement system and the materials themselves. These thermal neutrons induce nuclear fissions and generate the nu-clear fission neutrons effectively.

Next, in order for the He-3 detector to detect only the fast neutrons selectively, we use a detector bank that is surrounded with a cadmium sheath. The thermal neutrons cannot reach the detectors because of cadmium shield, and only the fast neutrons (14MeV neutrons and nuclear fission neutron) are detected.

Then, the nuclear fission neutron can be identified by sorting the time distribution of detected neutron data. The time spectra in Fig.10-4 were measured with this detector system, both when the nuclear material was present and was not present. The target of the measurement is the nuclear fission neutrons, component (b), and the background count, component (c).

A troublesome characteristic of the background neutron is that it is not easy to discriminate it from a nu-clear fission neutron. Because the spectrum (b) and (c) have a similar time inclination, the component (c) and the component (b) cannot be separated. Therefore, the detection limit of nuclear fission neutron component (b) is decided by the deviation of the back ground (c). Thus, we realized that great improvement of the detection accuracy requires elimination of background (c).

Research using computation simulation shows that the detection limit can be improved by 2 digits. The background (c) disappears as shown in Fig.10-5, if the moderator (reflection material) is changed from graphite to stainless steel.

This will enable us to perform clearance measurement of uranium waste, and to determine if there is transuranic contamination. As a result, reduction of the disposal cost of waste is expected.

It is an important task to secure safety when disposing of nuclear waste, and to suppress the cost. We wish that our research will help bring about the security and lowered cost of waste disposal.

Reference

Haruyama, M., Takase, M. et al., Improvement of Detection Limit in 14MeV Neutron Direct Interrogation Method by Decreasing Background, Journal of Nuclear Science Technology, vol.45, no.5, 2008, p.432-440.

11 Photo-Medical Research Cooperation

Toward Development of a Compact Ion Beam Apparatus for Cancer Treatment

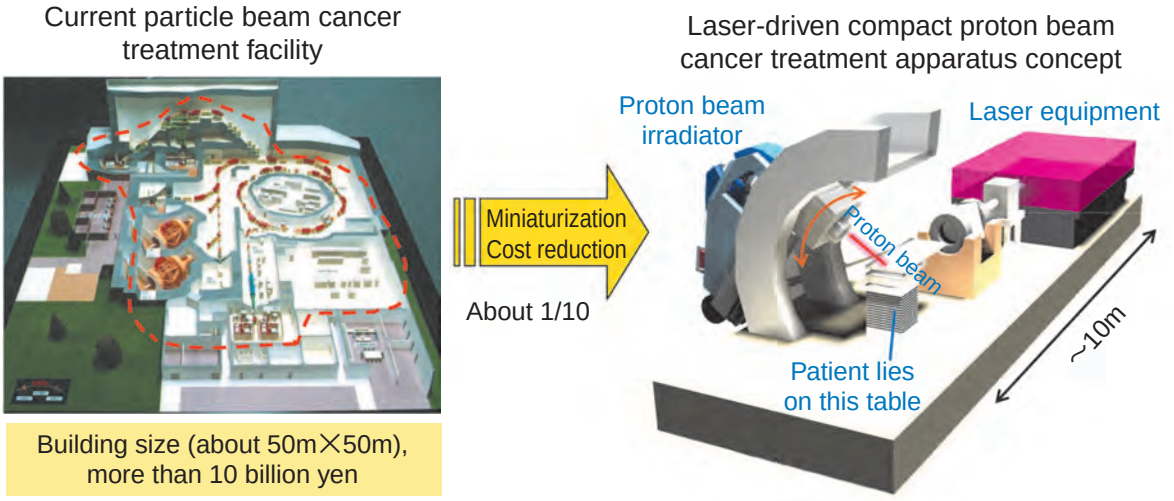

Fig.11-1 Current ion beam medical facility and outline of a compact cancer treatment apparatus

The Photo Medical Research Center (PMRC) of JAEA is promoting the innovative development of a more compact cancer treatment apparatus based on laser-driven ion beams (Fig.11-1). This is in contrast to the present conventional accelerator-based facilities that are typically larger and more costly. Our goal is for this innovation to facilitate wider access to ion beam cancer treatment (Fig.11-2). We conducted the following activities in fiscal 2008. (Cf. http://wwwapr.kansai.jaea.go.jp/pmrc_en/)

1. An Innovative Operating System

This PMRC project is being pursued in collaboration with ten partners (clinical research: Hyogo Ion Beam Medical Center (HIBMC), laser development: Hamamatsu Photonics K.K. and Ushio Inc., irradiation technology development: Toshiba Corporation, monitor device development: the Shimadzu Corporation, activation device development: Toyota Central R&D Labs., Inc., minimally invasive medical device development: HOYA Corporation and Fujikura Ltd., human resource development: Nippon Advanced Technology Co., Ltd. and HOC). We are associated with the JAEA Research Common Initiative and receive cooperation from organizations such as the Keihanna New Industry Creation and Interactive Community Center and twenty-one medical device/facility companies (members of the ITBS Research Society) and thirteen laser technology companies (members of the Society for Study of Laser Microfabrication).

2. Treatment Apparatus and Diagnostics

To advance development of a laser driven compact irradiation device, we carried out research and development to increase the number of protons accelerated by a laser and improve beam quality. To increase proton energy we made tests with various target materials and laser-irradiation parameters. In separate gas cluster target studies we also verified acceleration of heavier ions to a maximum energy of 18MeV per nucleon. We also began a study of proton irradiation effects on human cancer cells.

Using a conventional accelerator source of protons at

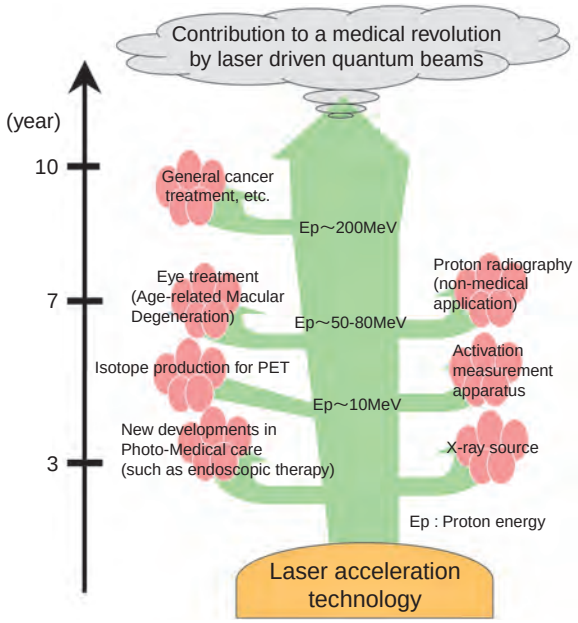

Fig.11-2 The path of medical innovation and specific technologies developed

HIBMC we have fabricated an irradiation chamber for phantom target tests and animal experiments.

As part of our industrial applications efforts, we examined application of proton-induced radio-activation to studying wear on metal surfaces. We also fabricated a minimally-invasive fiber-based medical device was and used it in animal experiments. Furthermore, we developed a technique for focusing light to a small radius and a technique for measuring blood flow. We have also considered collaborative research with the Fukui Prefectural Hospital, and have started research in preparation for clinical tests.

We have begun development of a prototype compact ytterbium-doped YAG laser system. We aim to achieve high-power and high-repetition rated operation that is stable and reliable.

11-1 DNA Double-Strand Breaks of Human Cancer Cells by Irradiation with Laser-Accelerated Protons —Toward Cancer Therapy by Laser-Driven Accelerators—

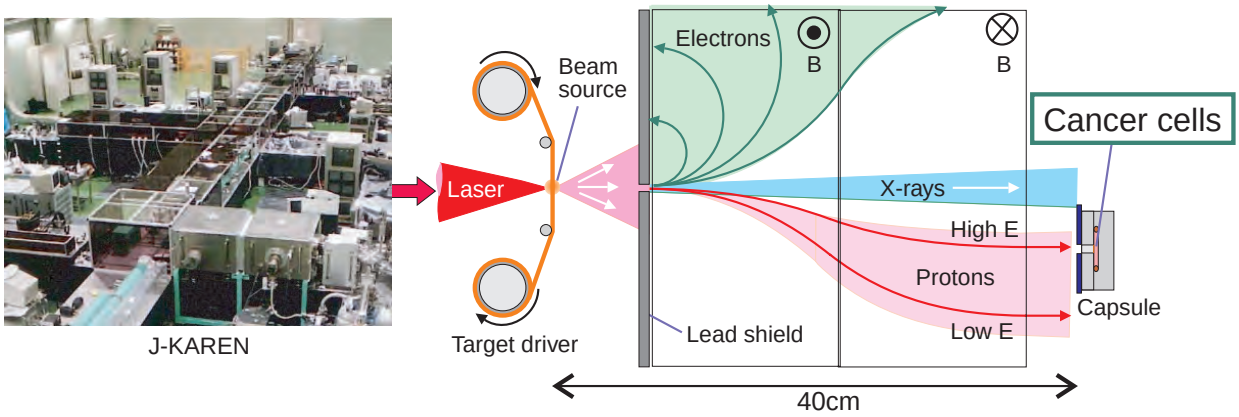

Fig.11-3 Newly-developed laser-driven proton irradiation system for radiobiological studies
High-intensity laser pulses are generated by J-KAREN laser system and focused onto thin plastic foil successively shifted by a target-driver. The laser focal spot is a "micron-sized" proton accelerator. The proton beams are separated by magnetic fields and irradiate cancer cells cultured in a capsule.

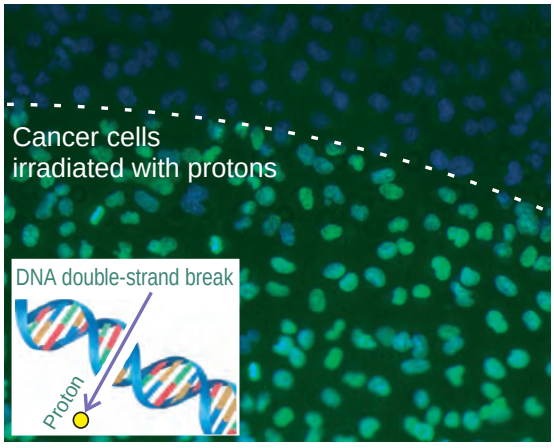

Fig.11-4 Result of laser-accelerated proton irradiation of in-vitro human lung cancer cells
Cancer cell nuclei irradiated with the protons are stained with green color indicating the generation of DNA double-strand breaks.

During these past several decades, high-frequency ion accelerators have been used for ion-beam cancer therapy. Recently, high-intensity lasers have been suggested as a potential cost-saving alternative to conventional ion accelerators for this radiotherapy. A unique feature of laser acceleration is the extremely high peak current given to a single proton bunch for a short duration. However, technical problems have prevented production of such high-current, short-duration laser-driven ion beams suited for investigating biological effects.

We have developed a laser-driven ion irradiation apparatus for biological studies that causes the desired fundamental interactions between laser-accelerated protons and human cancer cells in a vacuum (Fig.11-3). This apparatus delivers ~2.5×10^4 laser-driven protons onto a $1mm^2$ cultured (in-vitro) cell layer within a time interval of only 15ns. We estimated the proton flux to be ~$10^3 mm^{-2}\ ns^{-1}$. The peak current was seven times that in ion beam therapy by conventional accelerators. The DNA double-strand breaks of in-vitro human lung cancer cells (A549) are shown in Fig.11-4. These results indicate that laser-driven protons are applicable to ion-beam cancer therapy. This laser-driven table-top ion-irradiation apparatus will open a new field of radiobiological science, and many applications should be forthcoming.

This work was supported with Special Coordination Funds for Promoting Science (SCF) managed by the Ministry of Education, Culture, Sports, Science and Technology of Japan (MEXT).

Reference

Yogo, A. et al., Application of Laser-Accelerated Protons to the Demonstration of DNA Double-Strand Breaks in Human Cancer Cells, Applied Physics Letters, vol.94, no.18, 2009, p.181502-1-181502-3.

11-2 A Novel Compact and High Intensity Laser System
—Development of Laser-Driven Particle Accelerator for Cancer Therapy—

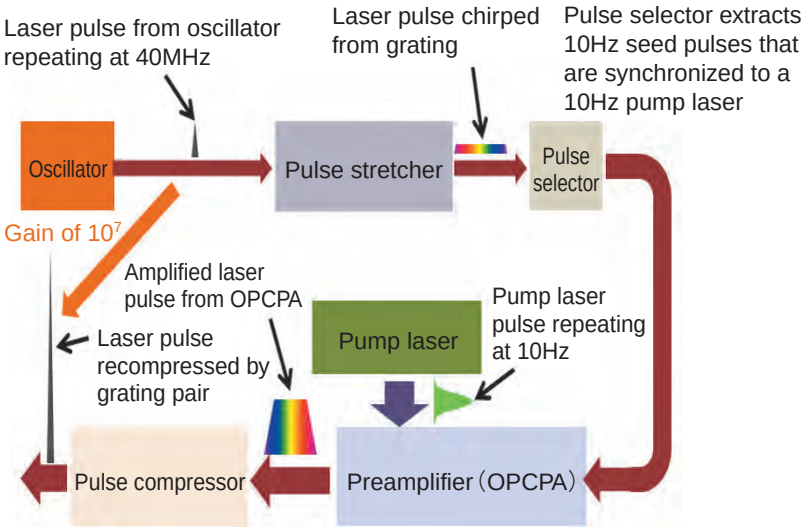

Fig.11-5 Block diagram of new laser system
Pulses from an oscillator source are stretched in time, amplified, and subsequently recompressed after amplification using a pair of diffraction gratings.

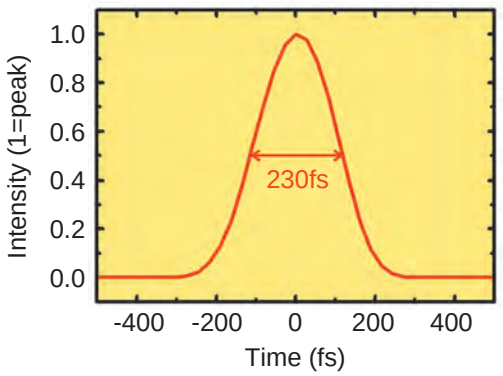

Fig.11-6 Recompressed pulse wave form
The recompressed laser pulse width of 230fs was obtained with an OPCPA gain of 10^7.

At the JAEA Photo Medical Research Center (PMRC) we are developing a compact ion accelerator for cancer therapy using a laser-driven plasma point source of ions. The high energy ions needed to treat cancerous tissue at a typical depth from the human body surface (~20cm) requires repeated short and intense laser pulses. Systems meeting these requirements are typically of the "chirped pulse amplification" (CPA) type which means that the pulses are temporally stretched or 'chirped' to reduce intensity during amplification and finally recompressed. High laser repetition rates (100Hz or more) are desirable, in order to deliver sufficient total dose within 10min. The limited ability of laser materials to dissipate heat has limited the acceleration of high energy ions to large systems (~100m long) with low repetition rates (a few shots a day). Also, though these recompressed laser pulses are of short duration (< 1ps), they may be preceded by lower power emissions (largely from amplified spontaneous emission) that can reduce ion acceleration, especially if preamplifiers are of the regenerative type (RA). A compact laser system that is suitable for cancer treatment has not yet been developed. To increase repetition rate and reduce the prepulse energy, we are developing a new laser design (emission at 1030nm) which will be pumped by high power 940nm laser diode (LD). As a first stage of this new development, we have demonstrated the feasibility of a CPA system that uses a different kind of preamplifier called an optical parametric chirped pulse amplifier (OPCPA).

Fig.11-5 is a diagram of our novel CPA laser system with which we have achieved amplification of laser pulses of short duration at a wavelength of 1030nm. 10Hz low energy 'seed' pulses from an Yb doped oscillator source were amplified in a single pass through the OPCPA preamplifier unit to over 6.5mJ, representing a net energy gain of 10^7, achieved with crystal of 56mm total length. Then, these high gain laser pulses were recompressed to a 230fs duration as shown in Fig.11-6. Formerly, under these conditions the recompressed pulse amplitude using a regenerative preamplifier would have been limited to about 1.5-2 times larger than that of the laser seed pulse from the oscillator, a well-known effect of gain narrowing. For laser-driven ion acceleration the amplified laser pulse from the OPCPA unit (not yet recompressed) will be further amplified in the next stage in a thin Yb:YAG crystal pumped by a high power LD at a 100Hz repetition rate.

This work was supported by the Special Coordination Fund (SCF) for Promoting Science and Technology managed by the Ministry of Education, Culture, Sports, Science and Technology of Japan (MEXT), and was done in collaboration with Central Research Laboratory, Hamamatsu Photonics, K.K..

Reference

Suzuki, M. et al., Multi-Millijoule, Nonlinear Preamplifier for High Intensity Femtosecond Yb:YAG Chirped-Pulse Amplification Lasers at 1030 nm, Applied Physics B, vol.97, no.2, 2009, p.379-382, doi: 10.1007/s00340-009-3741-3.

Innovation in Atomic Energy Research through Advanced Computational Science and Technology

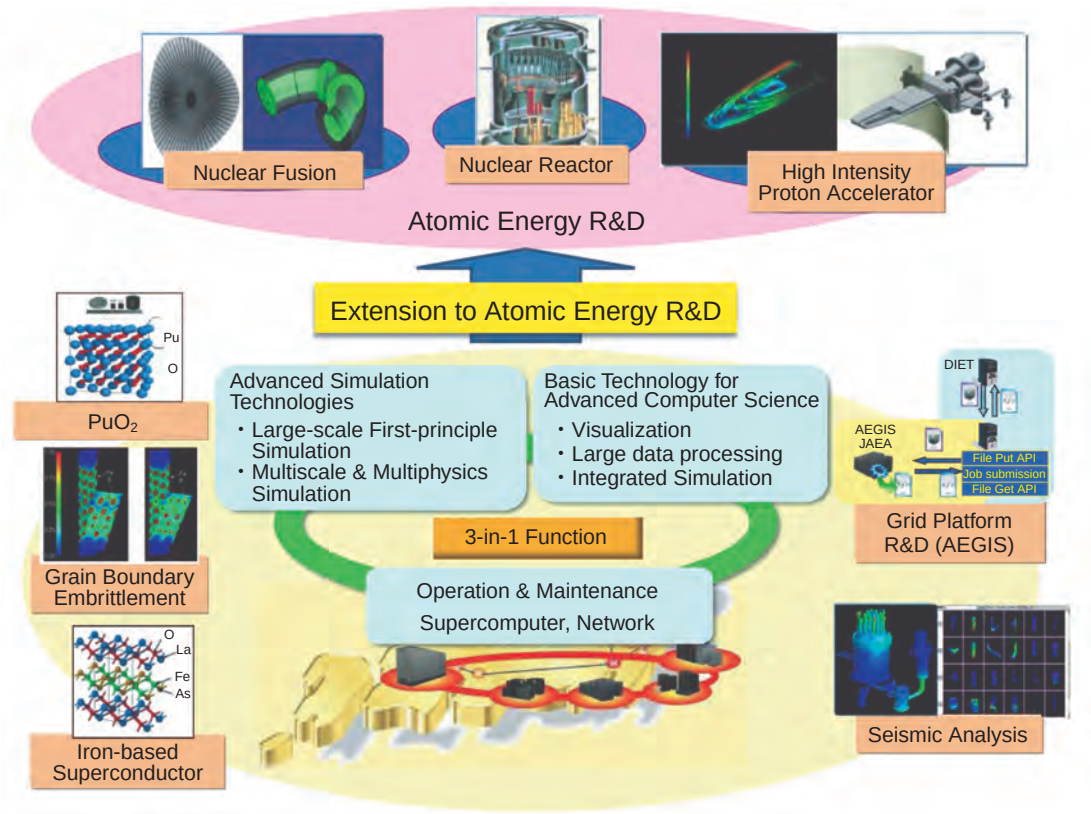

Fig.12-1 Role and achievements of computational science in atomic energy R&D
CCSE leads and supports development of computer science for the atomic energy field by promoting three missions, "Development of basic technology for computer science", "Development of advanced simulation technologies" and "Support for operation & maintenance of computer systems". Our achievements in 2008 include the development of Grid middleware, the elucidation of the mechanism of the grain boundary embrittlement, and the discovery of strong-lattice coupling in iron-based superconductors.

Computational science has made remarkable progress since the computer was invented in the 1940's. At present, computer simulation is a third method by which to pursue R&D together with "theory" and "experiment". Computer simulation especially has an important role in the atomic energy research, because experiments are difficult to perform due to budget and safety considerations. This being the case, the Center for Computational Science and e-Systems (CCSE) carries out three missions, "Development of basic technology for computer science", to promote use of supercomputing in atomic energy research, "Development of advanced simulation technologies" to perform realistic simulations, and "Support for operation & maintenance of supercomputer systems" as depicted in Fig.12-1. We believe that the combination of these three missions is the course of R&D making the most effective use of the latest supercomputers. Two typical issues taken up by CCSE R&D in 2008 were as follows.

One was R&D on AEGIS (Atomic Energy Grid Infrastructure), which is Grid middleware for atomic energy research. We connected AEGIS to DIET (Distributed Interactive Engineering Toolbox), which is the Grid middleware in France, through the Internet. The interoperable system we developed enables us to efficiently utilize the computer resources in both Japan and France. Details are reported in Topic 12-2.

The other is a first-principle study by computer simulation of the electronic properties of iron-based superconductors, which were discovered in 2008. We calculated the electronic structures of various iron-based superconducting compounds. Moreover, we compared these structures with measurement data obtained by SPring-8, and confirmed that the magnetic order and the lattice vibration cooperatively contribute to achieve superconductivity. Details are reported in Topic 12-3.

In the future, CCSE will explore more advanced simulation technologies to make more effective use of the latest supercomputers. Furthermore, we will extend these technologies to significantly contribute to the advance of atomic energy R&D.

12-1 Elucidation of Embrittlement of Iron by Sulfur and Phosphorous

—The Mechanism of Grain Boundary Embrittlement Elucidated by First-Principle Calculations—

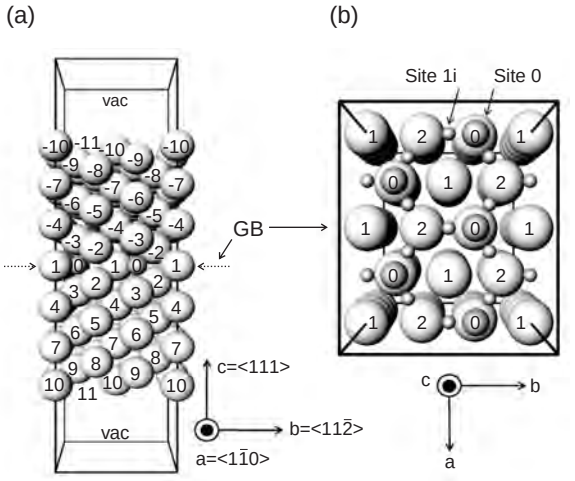

Fig.12-2 Unit cell including grain boundary (GB)
Iron slab is placed in vacuum region (vac). The largest sphere is an iron atom. The positions of atoms are labeled by numbers. (a) Side view. (b) Top view of the cross section at the grain boundary (GB) plane. Site 0 is a hole. Site 1i is an interstitial site.

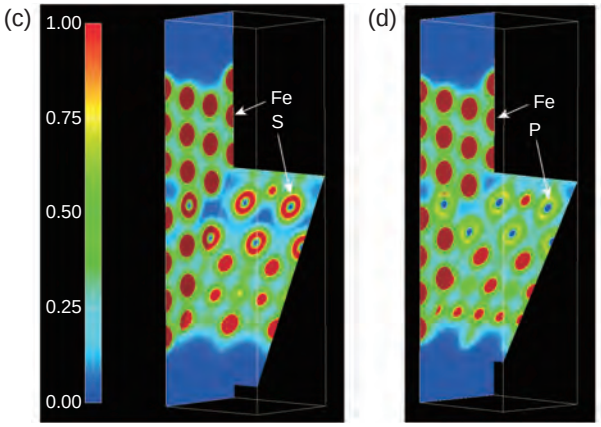

Fig.12-3 Electron distribution map at the grain boundary when sulfur (S) or phosphorus (P) atoms are segregated
(c) S. (d) P.

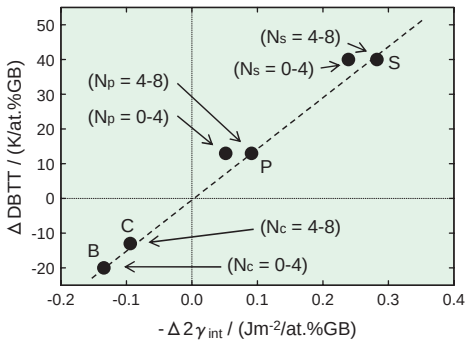

Fig.12-4
The correlation between relative change in temperature of ductile-to-brittle transition due to segregation of boron (B), carbon (C), phosphorous (P), or sulfur (S) at grain boundaries (ΔDBTT) and the segregation-caused change in the calculated cohesive energy between atoms at the grain boundary ($\Delta 2\gamma_{int}$).

Metallic materials are usually polycrystalline, consisting of crystal grains the size of which is about several ten micrometers. The boundaries between the grains are called "grain boundaries". The impurity or alloying atoms which are included in metals can move and be trapped at grain boundaries when the temperature of metals is high. This trapping is called "grain boundary segregation". Grain boundary segregation is known to bring about a large change in the mechanical properties of metals. A famous example is tempering embrittlement of low alloy steels, which is caused by phosphorous segregation. It is well known that sulfur has a much stronger embrittlement effect than phosphorous, and that boron and carbon have a strengthening effect on the grain boundary.

It is already known that grain boundary segregation occurs only in the first few atom layers, as verified by Auger electron spectroscopy. Thus, grain boundary embrittlement is considered to be caused by the change in the cohesion of metal atoms at the grain boundary caused by the segregated atoms. However, why and how the cohesion of metal atoms is changed has been a mystery for many years.

We performed first-principle calculations to simulate this phenomenon on the supercomputer in JAEA. First-principle calculation investigates the properties of materials by solving the relevant Schröinger equations numerically on computer. We made great efforts to reduce the computational time, because this calculation is very time-consuming, and so were able to perform calculations simulating the grain boundary segregation (Figs.12-2 and 12-3).

From our calculations, we found that the cohesive energy of the grain boundary is reduced by the phosphorous and sulfur segregation, and that the energy is increased by the boron and carbon segregation. These results are consistent with the experimental results. Moreover, we found an excellent correlation between the calculated cohesive energy and the experimental ductile-to-brittle transition temperature (Fig.12-4). This demonstrated that the cohesion of the atoms at grain boundaries can be understood from first-principle calculations.

Reference

Yamaguchi, M. et al., Decohesion of Iron Grain Boundaries by Sulfur or Phosphorous Segregation: First-Principles Calculations, Physical Review B, vol.76, no.3, 2007, p.035418-1-035418-5.

12-2 Cooperation of the World's Supercomputers for Nuclear Engineering Simulation —Development of Atomic Energy Grid Infrastructure AEGIS—

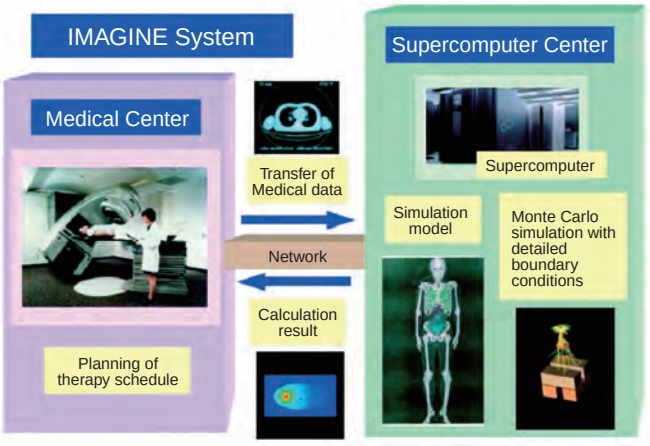

Fig.12-5 Illustration of IMAGINE system
IMAGINE calculates the dose to be given a patient using Monte Carlo simulation on separate supercomputers based on data on the patient. This calculation speeds up the planning of an X-ray cancer therapy schedule.

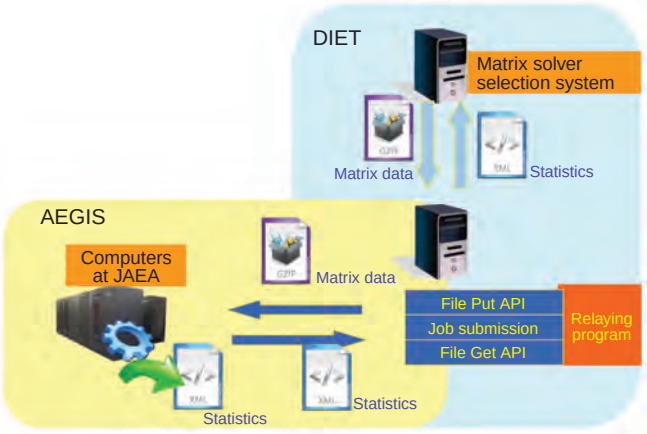

Fig.12-6 Outline of matrix solver selection system
AEGIS and DIET work together through our relaying program, which was developed using API. The solver selection system can be used in this collaborative environment. Consequently, the solver selection system allows the solvers installed in the AEGIS computers to be used, so that there is a wider choice of solvers than before.

We have developed the Atomic Energy Grid Infrastructure (AEGIS), which allows us to carry out large-scale numerical simulations in the atomic energy field, e.g. seismic analysis of an entire nuclear power plant, since it enables supercomputers situated all over the world to work together. In this study, we developed an application programming interface (API) which allows us to run programs on other supercomputers with just a small modification of the program. Here we introduce two case examples of AEGIS use.

IMAGINE (IT-based Medical Aiding Gear for Instantaneous Numeration of Energy Deposition Distribution System)

IMAGINE (Fig.12-5) is a dose calculation system being developed by the Nuclear Science and Engineering Directorate of JAEA, for X-ray cancer treatment. To decide the best irradiation point and strength considering the influence on both cancer tissue and normal organs, IMAGINE performs Monte Carlo computation. Since the size of the Monte Carlo calculation can be large, we attempted to use several supercomputers located far from each other, to shorten the total calculation time, using our API.

We won an incentive award from FUJITSU user forum on this study.

International Matrix Solver Selection System Development

In this study, we are developing the matrix solver selection system that selects the most appropriate linear equation solver for one's problem from among those in Japanese and French computers (Fig.12-6). Since a linear equation solver usually the part of a simulation consuming the most time and memory, we must select a solver suited to the specific task for speed up or accuracy improvement of simulation. Since the selection system finds the linear solver best suited to solve the equations in question, increasing the number of available linear solvers will tend to result in a more suitable solver. In order to achieve this increase, we established collaboration between AEGIS and DIET, which is the French grid infrastructure. Consequently, many solvers installed only in Japan or French computers become available to the other country through this selection system.

The present study was conducted as one of the activities promoting strategic international cooperation in science and technology of the Japan Science and Technology Agency (JST).

Reference

Saito, K. et al., Gridization of IMAGINE, Dose Calculation System, for the Remote Assistance of Radiation Therapy, Fujitsu User Forum, 2008, 20p. (in Japanese).

12-3 Search for the Superconducting Mechanism of Iron-Based Superconductors
—SPring-8 X-ray Measurements Compared with First-Principles Calculations—

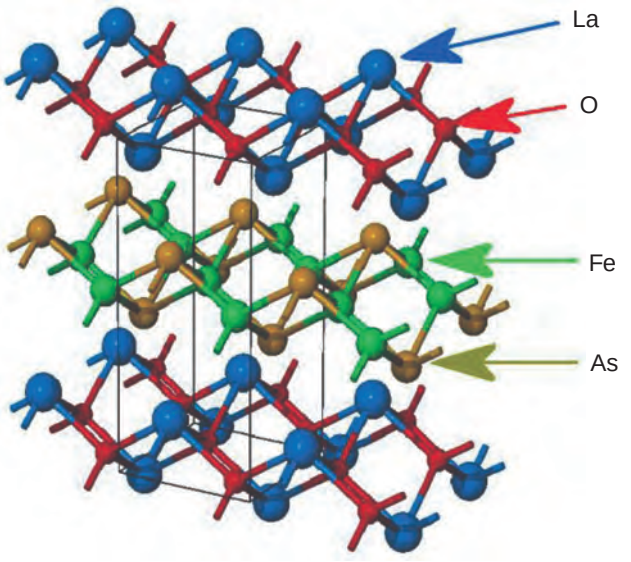

Fig.12-7 Crystal structure of the first iron-based superconductor LaFeAsO
This material becomes a superconductor below 26K when oxygen (O) is partly substituted for fluorine (F). When lanthanum (La) is replaced by samarium (Sm), the transition temperature rises up to 55K. The structure is characterized by layers, and superconductivity occurs at the layer composed of iron (Fe) and arsenic (As).

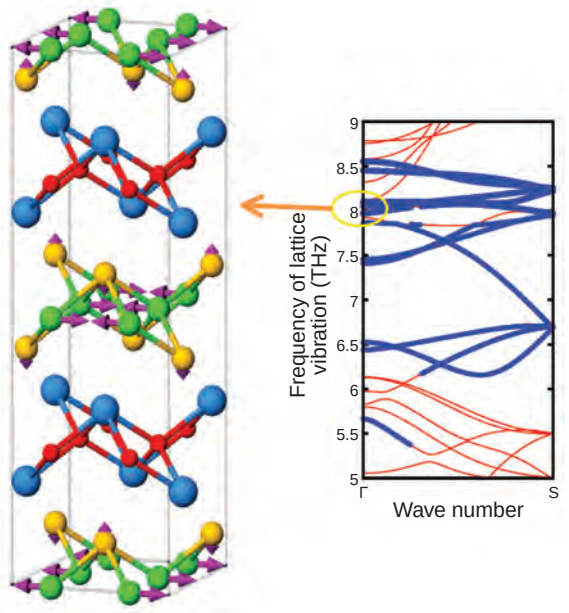

Fig.12-8 Visualization of the lattice vibration in the iron-based superconductor LaFeAsO and its dispersions
The right side panel is a dispersion graph showing the relation between the vibration frequencies of the lattice of LaFeAsO and wave number. Iron's vibration dominates in the lattice vibration drawn by blue thick curves. In the left side panel, the lattice vibration at the frequency 8.1THz is visualized. The purple arrows show the direction and strength of the vibrations. The arrows on iron atom (green sphere) are longer, showing that the vibrations of iron atoms are larger than those of the other atoms.

Superconductivity is a phenomenon characterized by disappearance of electric resistance at very low temperature. Until 1980, it had been believed that this phenomenon did not occur above 30K. However, cuprate superconductors whose superconducting transition temperatures rise above 100K were discovered in 1987. This discovery encouraged many to search for room-temperature superconductor. Unfortunately, room-temperature superconductors have not been discovered yet, and moreover no materials that deserve the name of high-temperature superconductor have been found except for cuprate superconductors.

In 2008, when the dream of room-temperature superconductors was fading away, iron-based superconductors (Fig.12-7), which exhibit superconducting transition above 50K, were discovered. Since then, many researchers all over the world have been enthusiastically trying to discover higher-temperature superconductivity in iron-based materials.

To achieve higher-temperature superconductivity, it is necessary to understand its superconducting mechanism. It is known that the mechanism of cuprate and iron-based superconductors is different from that of metals whose superconductivity occurs at considerably lower temperature. However, no one has elucidated this mechanism yet. To make progress in this situation, we evaluated electronic states of iron-based superconductors by numerical simulations and compared them with experimental data, aiming to shed light on the superconducting mechanism.

It is well known that lattice vibration, that is, vibration of atoms, plays an important role in the superconductivity of metals. We evaluated lattice vibration by numerical simulation (Fig.12-8) and compared it with measurement data obtained at "SPring-8". We found that our simulation of lattice vibration agrees well with the measurement, if one takes into account iron magnetism which was not detected experimentally. This result implies that in this superconducting material there is hidden magnetism which has an inseparable relation with the lattice vibration. Thus, we revealed that both magnetism and lattice structure play an important role in the superconducting mechanism.

This comparison between simulations and measurements is aiding our investigation of the superconducting mechanism, which is still however far from completed. We hope that effective coordination of numerical simulations and experiments will clarify this mechanism and help make the dream of room-temperature superconductors come true.

Reference

Nakamura, H. et al., First-Principle Electronic Structure Calculations for Iron-Based Superconductors: An LSDA+U Study, Journal of the Physical Society of Japan, vol.77, suppl.C, 2008, p.153-154.

12-4 Supporting Evaluation of Tera- to Petabyte Scale Data
—Proposal of Novel Data Analysis Method for Large Scale Simulation—

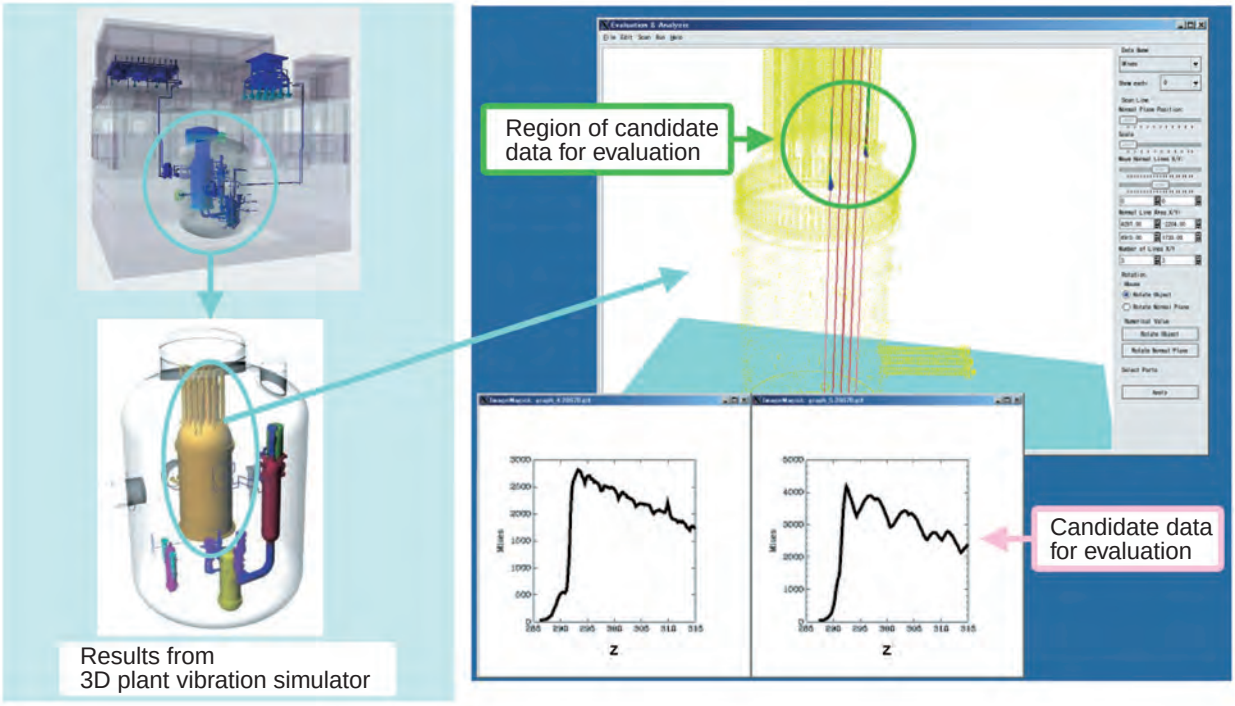

Fig.12-9 Example of application of the novel data analysis method to results from 3D plant vibration simulator
We applied our data analysis method to the results obtained from a 3D plant vibration simulator with which the behavior of a nuclear plant in an earthquake larger than the design anticipated is simulated. As a result, we succeeded in the automatic extraction and visualization of candidate data for evaluation by sensing changes of physical quantities such as stress distribution, and thus identified the regions of potential damage.

We carried out computer science research aiming at establishing a novel data analysis method to evaluate tera to peta byte scale data output from simulations in the nuclear energy field.

In a traditional evaluation of results of large scale simulation, the following processes need to be repeatedly carried out: (1) extracting and visualizing portions of data, (2) extracting and visualizing data of a cross-section, (3) extracting and visualizing distribution information, and (4) evaluating these results. Problems here are the exertions required for extracting relevant information from visualized results by human judgment, and the time required for extraction and visualization. For example, it takes more than one hour just for data-transfer to the computer for the evaluation of just the time data obtained from 3D plant vibration simulator.

To deal with the problem with extracting data, we have developed a function which calculates the rate of change of physical quantities and classifies successive changes according to certain characteristics in order to selectively extract and visual only a portion of the data. Here, we have solved the problems with traditional analysis methods such as the derivation and difference method, where errors of recognition readily occur and uniform analysis is difficult. Analogous to the way persons recognize a spatial profile as a pattern, we utilized a neural network method, which is an information processing method able to develop pattern recognition capability. As a result, we were able to uniformly analyze global and local rate of changes and to classify these characteristics according to a user's instruction.

To deal with the problem of excessive time requirements, we have developed a function which makes computers process with simple operations such as extraction of cross-section. We have realized pattern recognition in a parallel and distributed manner and have reduced data transfer time to a few seconds, by using the grid computing technology for nuclear research which we have developed, the Atomic Energy Grid Infrastructure (AEGIS).

We have succeeded in reducing the effort and time required to analyze data output from the 3D plant vibration simulator, thus helping make it possible to analyze this data (Fig.12-9).

As a result of this R&D, at the International Conference for High Performance Computing, Networking, Storage and Analysis (SC07, SC08) our innovative methodology we proposed was highly regarded, we won prizes two years in a row (Analytics Challenge Finalist).

Reference

Kino, C., Suzuki, Y. et al., Concept Design of Cognitive Methodology Based Data Analysis System —Application to Seismic Analysis Using Finite Element Method—, Transactions of the Japan Society for Computational Engineering and Science, vol.2008, no.18, paper no.20080018, 2008, 8p. (in Japanese).

13 Scientific & Technical Development for Nuclear Nonproliferation

Development of Technology for Nuclear Nonproliferation to Support Peaceful Use of Nuclear Energy

Policy research and study

With the goal of promoting confidence building and transparency in nuclear nonproliferation field, we planned concrete activities to help Vietnam and Thailand in their introduction of atomic power generation, as nuclear nonproliferation policy studies based on our technical knowledge. Also, we have started to analyze past U.S. nuclear nonproliferation policy, including the process of enactment of the nuclear nonproliferation law, in regard to its influence on Japanese nuclear fuel cycle policy.

Development of technology for nuclear nonproliferation

We studied concepts of advanced safeguards systems to provide effective and efficient safeguards/nuclear material accountancy in the future FBR cycle system.

We are promoting cooperation with the Korea Institute of Nuclear Nonproliferation and Control in remote monitoring technology development as a mean of building confidence and achieving transparency in peaceful use of nuclear energy in nuclear nonproliferation.

Also, we studied methods for evaluating the nuclear proliferation resistance of future nuclear fuel cycle systems.

Support of denuclearization

We have been developing technology to convert surplus weapons plutonium into MOX vipac fuel for fast breeder reactors. This technology was demonstrated in the Russian fast breeder reactor BN600. The U.S. and the Russian Federation stated that application of this method has been approved in a joint statement issued November, 2007. Consequently, the U.S. requested us to transfer to them the results of this Japan-Russia cooperative study, and also the Russia Federation requested us to provide Japanese FBR fuel cladding (PNC-316). JAEA is still discussing these issues with the U.S. and Russia, respectively, in particular the conditions of provision by Japan.

For the establishment of a global verification regime in the framework of the CTBT (Comprehensive Nuclear Test Ban Treaty), we continued operation of Takasaki and Okinawa radionuclide monitoring stations, and have made detailed analyses of filter samples, delivered from monitoring stations around the world, at our Tokai laboratory.

We have been operating the National Data Center (Tokai) provisionally since April, 2009 based on the results of data analysis software development, and currently receive, analyze and evaluate data on a daily basis from monitoring stations around the world (80 stations as of March of 2009).

Nuclear material management

We have been making technical contributions to IAEA safeguards implementation by conducting several technical development projects in cooperation with the U.S. Department of Energy. We have also cooperated in domestic and international personnel training.

In the field of physical protection, we are continuing operation and environmental durability tests of intruder automatic detection systems.

In the field of nuclear material transportation, we made preparations for safety tests of a prototype container for MOX powder transportation.

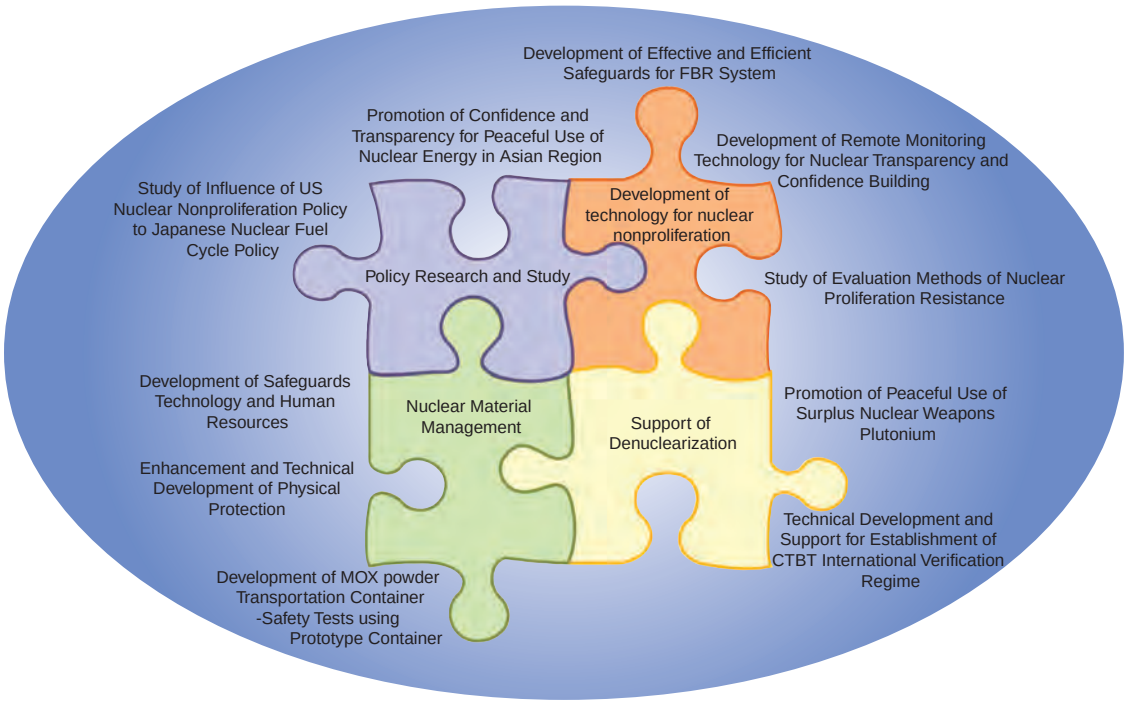

Fig.13-1 JAEA Activities in Scientific and Technical Development for Nuclear Nonproliferation
We have two primary missions regarding nuclear nonproliferation: to support the government in developing nonproliferation policies through research and study, and to support government and international organizations by developing nuclear nonproliferation technology. Other important missions of JAEA are to support denuclearization in Russia, nuclear material control in JAEA facility, and human resource development.

13-1 Continuous Monitoring of Nuclear Material
—Advanced Algorithm of Process Monitoring—

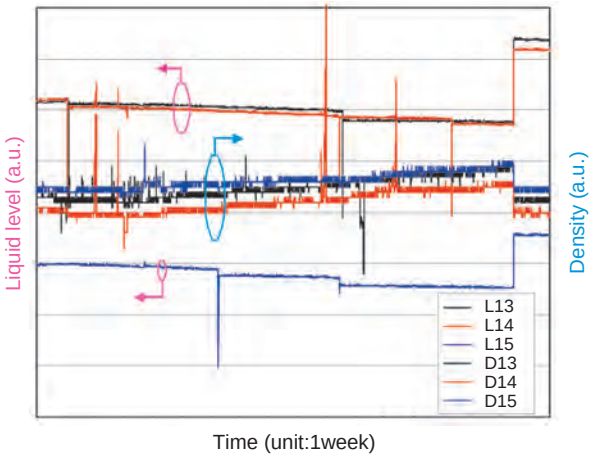

Fig.13-2 TRP Tank Data
Liquid level and density of tanks no.13, 14, and 15 without the solution transfer. With the level decrease due to evaporation, the density increases gradually.

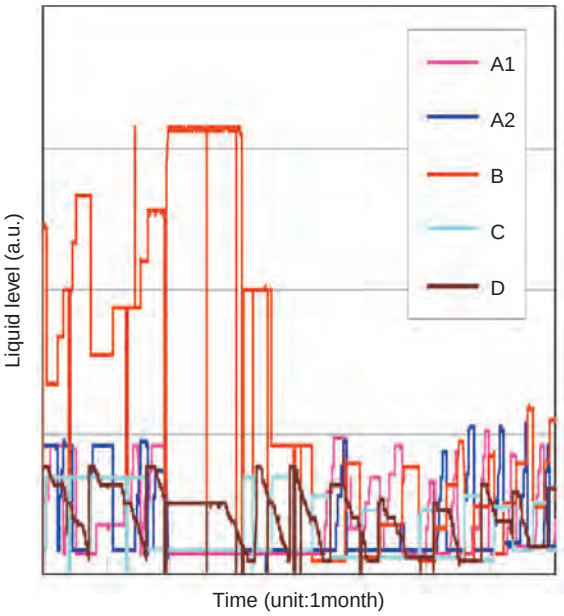

Fig.13-3 SRS Tank Data
Liquid levels of tanks A1, A2, B, C, and D. The solution is taken in batches from tanks A1 and A2 alternately and transferred to the tank B. The solution goes from tank B to C and from C to D in batches, but the tank D outputs the solution continuously.

In contrast to the handling of operation data for maintenance of safety, safeguards against deliberate unauthorized transfer of radioactive material by facility staff are insufficient. Process monitoring (PM) to detect malicious diversion and misuse started in the 1970's, and introduction of PM into IAEA safeguards has been proceeding with caution.

The objective of IAEA safeguards is to detect a significant quantity (SQ) (=8kg Pu) loss in a timely fashion (within 30days). Since a statistical test depends on a known probability distribution, the most sensitive such detection of material unaccounted for (MUF) in a specified period cannot identify the time of loss within that period. Some sequential tests have been developed to meet the timeliness target even when throughput increases. Although the most powerful test for any type of loss lacks precision, a near-real-time accounting (NRTA) method is widely accepted for the interim accounting.

A solution monitoring system (SMS) with liquid level, density, and temperature in the solution tank in a reprocessing plant being measured is a typical example of PM. Real data of Tokai Reprocessing Plant (TRP) is shown in Fig.13-2 and data of Savannah River Site (SRS) in USA in Fig.13-3. A consistency check comparing the declared and the actual levels and recognizing any abnormalities during the solution transfer is an important role of SMS. Currently SMS is installed in Rokkasho Reprocessing Plant (RRP) to complement the IAEA safeguards.

In this study, we intend to demonstrate the benefit of PM quantitatively and to pursue its application as a NRTA substitute. To avoid more frequent accounting to meet the timeliness constraint even if the measured MUF exceeds 1 SQ without waiting 30days, several candidates such as quantified C/S, loss accounting by PM, and less frequent NRTA were investigated.

Because the PM study was started first in the U.S. and some researchers there had been already working on this in accordance with internal DOE and NRC regulations, we are studying SMS application and evaluation using TRP and SRS data in a two-year joint project with Los Alamos National Laboratory (LANL). Up to now it has been found that after simulating a hypothetical removal of liquid with real tank data, multivariate statistical analysis considering loss due to evaporation accurately determines the amount of the removal based on level decrease and density increase. Moreover, we demonstrated that the event monitoring detects wait and transfer modes, and investigated the effect of time variation on detection probability of abnormal changes in the nuclear material quantity. We are striving for results that will be useful for future IAEA safeguards.

Reference

Suzuki, M. et al., Study on Loss Detection Algorithms Using Tank Monitoring Data, Journal of Nuclear Science and Technology, vol.46, no.2, 2009, p.184-192.

14 Development of Experimental Techniques / Facilities at JAEA R&D Centers

We have been promoting a wide range of R&D activities by systematically coordinating the R&D Directorates for each of the research themes which have been described in the previous chapters, and R&D Centers in 12 locations throughout Japan.

The R&D Directorates of JAEA are promoting R&D for their respective purposes with experimental equipment/facilities at relevant R&D Centers. The R&D Centers have not only been operating and managing various types of equipment/facilities but have also been working on innovations and improvements for them, and in addition have themselves been developing experimental techniques, management techniques and equipment/facilities necessary for the various R&D projects of JAEA.

This chapter introduces the developments which have been made recently at each R&D center.

Tsuruga Head Office

The Entire System Function Test (ESFT) of "MONJU" was completed in August 2009, after overcoming troubles found in 2008 including false alarms by sodium leak detectors and corrosion holes in an outdoor exhaust duct. At present, repairs and inspection are being carried out in order to begin the System Start-up Test (SST) in fiscal year 2009.

"FUGEN" was reorganized from the Fugen Nuclear Power Station into the Fugen Decommissioning Engineering Center after the approval of a decommissioning plan in February 2008. This Center aims to incorporate useful innovations in decommissioning projects, and is currently dismantling facilities and equipment with relatively low-level radiation or without contamination. The Center also collects and ships out heavy water in accordance with careful plans.

Confirmation of data from the fuel damage detector during the ESFT

Tokai Research and Development Center, Nuclear Science Research Institute (NSRI)

NSRI has safely and successfully operated research reactors, accelerators, criticality testing facilities, nuclear fuel handling facilities, and post-irradiation testing facilities (hot laboratories), which are used for various kinds of nuclear research.

The Facility of Radiation Standards (FRS), one of the largest calibration facilities in Asia, is equipped with reliable devices for calibrating detectors of radiation and radioactivity. FRS is used for calibration and performance tests of radiation measuring instruments for radiation protection, such as survey meters, installed monitors, and personal dosimeters, used in nuclear facilities. Calibration fields of mono-energetic neutrons using a 4MV Van-de-Graaff accelerator and of high-energy γ-rays are being developed and R&D on dosimetry is being carried out, to contribute to radiation protection in large accelerator facilities such as J-PARC (Topic 14-2).

Outside view and calibration devices of Facility for Radiation Standards

Tokai Research and Development Center, Nuclear Fuel Cycle Engineering Laboratories

At the Plutonium Fuel Development Center, an engineering scale test for an advanced FBR fuel fabrication method named the "Simplified Pellet Fabrication Process" is being carried out. The obtained pellets satisfy specifications of the "MONJU" fuel, are used as fuel for "MONJU".

Various other R&D are being executed, for technology such as advanced reprocessing by an aqueous method and by a pyrochemical method, and low level rad-waste treatment methods.

At the Reprocessing Technology Development Center, evaluation of the seismic safety of Tokai Reprocessing Plant is being carried out.

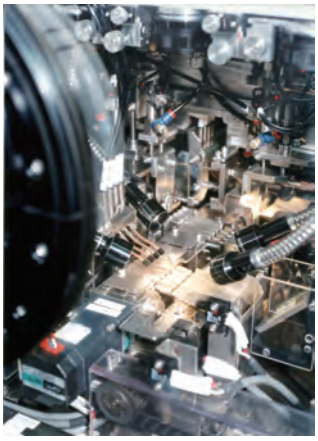

Mixed oxide fuel pellet inspection by remote control automated equipment

J-PARC Center

Construction has been completed for facilities defined as Phase-I of the J-PARC project in 2009. In the last fiscal year of 2008, on-beam tests of 3GeV synchrotron was conducted to achieve a stable operation increasing beam current with a stable beam injection from the linear accelerator. In May, 2008, beams were successfully injected to both the Materials & Life Experimental Facility (MLF), and the 50GeV synchrotron. Beam operation with more than 100kW power was demonstrated in December, 2008. The 100kW power was one year early achievement of the milestone we have set as the goal during the intermediate term of research framework. In MLF, a high performance of pulse neutron source was assured in terms of neutron intensity and pulse resolution.

Since December 2008, we have started a user operation with six neutron instruments and one muon port.

Engineering Materials Diffractometer TAKUMI (BL19, MLF)
Full view (lower left) and internal view of TAKUMI
This instrument is expected to contribute to the development of industrial products through its ability to evaluate structural integrity in such equipment as automobile engines and gas turbines of power plants by atomic-level residual stress analysis using pulsed neutrons.

Oarai Research and Development Center

One of the experiments needed in the Fast Reactor Cycle Technology Development Project "FaCT", the post irradiation examination of FBR high burn-up fuel and minor actinide-containing fuel, was conducted. Experimental research at water and sodium test facilities was also carried out.

The investigation of the cause of the trouble of the obstacle on the in-vessel storage rack in the experimental fast reactor JOYO (occurring in November 2007) and development of a strategy for prevention of this problem continued.

The refurbishment of the Japan Materials Testing Reactor (JMTR) for restart in JFY2011 progressed, and JMTR held the 1st International Symposium on Material Testing Reactors from July 16 to 17, 2008. The High Temperature engineering Test Reactor (HTTR) had its annual inspection, and preparations for 50 days of HTTR full power operation with 950°C outlet coolant temperature in JFY2009 proceeded.

Commemorative photograph of the "1st International Symposium on Material Testing Reactors" attendees (July 17, 2008)

Naka Fusion Institute

Towards the goal of creating "a sun on Earth", Naka Fusion Institute has been promoting research and development for the realization of fusion energy together with the Fusion Research and Development Directorate.

In August 2008, the JT-60, the tokamak device in Naka Fusion Institute, completed its experimental operation, which had continued for 23 years since its first plasma in April 1985. On the other hand, the Satellite Tokamak JT-60SA (Super Advanced) Programme has been commenced in cooperation with EURATOM based on the Broader Approach Agreement, under which the JT-60 is being upgraded, for the purpose of providing support and supplemental research for the International Thermonuclear Experimental Reactor (ITER), as well as conducting research in core plasma and reactor engineering.

As part of this Programme, 2 buildings for the manufacturing of JT-60SA superconducting coils (Superconducting Twisted Strands Jacketing Building and Superconductor Winding Building) were completed in March 2009. With this and other developments, this Programme is progressing to its next stage.

Superconducting Strands Jacketing Building and Superconductor Winding Building and their interiors

Takasaki Advanced Radiation Research Institute

The four ion accelerators so-called Takasaki Ion Accelerators for Advanced Radiation Application (TIARA), the electron accelerator, and the gamma irradiation facilities at Takasaki Advanced Radiation Research Institute can be used both by researchers in JAEA and in other organizations to perform R&D on new functional and environment-friendly materials, biotechnology, radiation resistance of materials, or quantum beam analysis. Development of three dimensional in-air PIXE analysis technology (Topic 14-10), three dimensional microbeam writing technology, and technology for uniform wide area irradiation by a cyclotron is in progress. In fiscal 2008, fast single-ion hits of heavy ion micro beams of several hundred MeV at a rate of 1,500 hits per min or more were achieved by the cyclotron, which allow to start studies such as evaluation of radiation resistance of semiconductors and evaluation of effects of radiation on living cells.

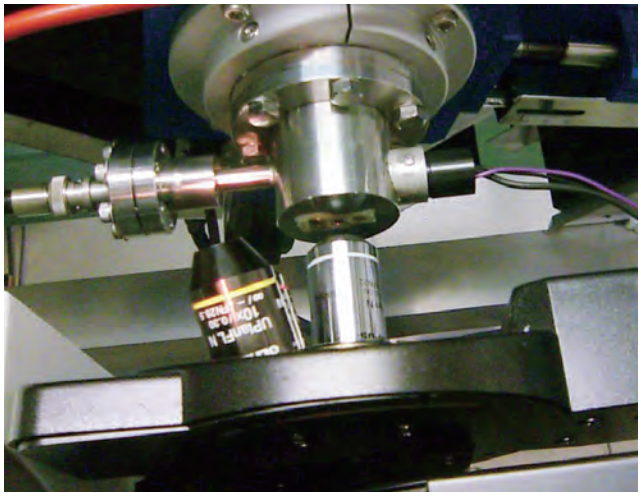

Extraction window for a micro ion beam from the cyclotron (upper portion) and a part of the microscope to observe ion-irradiation sample position (lower portion)

Kansai Photon Science Institute

At our facility in the Kizu district outside Osaka, we are making improvements in advanced lasers, such as improved beam quality of high-energy lasers and increased repetition rate of an X-ray laser, and are using these lasers for various research projects.

Also, the Photo-Medical Research Center is promoting a project to create a "Photo-medical Industrial Valley", which was included in the "Formation of Bases for Innovation by Integrating Frontiers of Research" program adopted by the Ministry of Education, Culture, Sports, Science and Technology (MEXT) of Japan in 2007 and funded by the Special Coordination Funds for Promoting Science and Technology. (Topic Chapter 11: Photo-Medical Research Cooperation)

Plasma X-ray Laser apparatus

Another new project "Consortium for Photon Science and Technology (C-PhoST)", which had been proposed in the scheme of "Photon Frontier network", consisting of universities and institutes (including JAEA) for pioneering photon research, was established in fiscal 2008. The Center for Photon Science and Technology was set up in August as the core institute of this consortium.

In the Harima area near Himeji, we carry out various material science research projects, for example, a study on superconductivity of uranium compounds, using synchrotron radiation from SPring-8. In addition, JAEA provides four beamlines in SPring-8 not only for in-house but also outside researchers.

Horonobe Underground Research Center

As part of our research and development for geological disposal of high-level radioactive waste (HLW), the Horonobe Underground Research Center, a division of the Japan Atomic Energy Agency (JAEA), is implementing the Horonobe Underground Research Laboratory Project (Horonobe URL Project).

The ventilation shaft and the east shaft were excavated to depths of 250m and 140m, respectively, and horizontal tunnels were excavated at the bottoms of these shafts. The waste water drainage facility to deal with underground water entering new excavations was expanded. Construction of an international exchange facility allowing interaction with researchers all around the world and with residents in Horonobe town was started, and this will be opened in October, 2009. Next year, excavation of the east shaft to the depth of 200m and of a new tunnel at 140m, and surveys to aid in underground water control will be carried out.

Current Underground Facilities

Tono Geoscience Center (TGC)

TGC's task is to provide the scientific and technical basis for safe geological disposal of high-level radioactive waste. This involves research on long-term stability of the geological environment, and researches on development and improvement of techniques for characterization of deep geological environment and a wide range of engineering for deep underground application at an underground research laboratory in crystalline rock, referred to as the "Mizunami Underground Research Laboratory (MIU)". As of March 2009, the Main and Ventilation Shafts had reached depths of 300.2m and 331.2m, respectively. A horizontal tunnels of Measurement Niche off Ventilation Shaft (about 20m long) and an Access/Research Gallery (about 100m long) were excavated at a depth of 300m Stage (Topic 14-11).

Geological mapping at "-300m Access / Research Gallery"

Ningyo-toge Environmental Engineering Center

The Ningyo Toge Environmental Engineering Center has been developing the nuclear material measurement apparatus "Ningyo Waste Assay System (NWAS)" to be used in safeguard measures and nuclear material management. During the decommissioning of a refining and conversion facility, this system will be tested.

Because dismantling this refining and conversion facility will generate a large amount of waste and construction material contaminated with uranium, very quick measurement is needed. NWAS carries out neutron and the gamma-ray measurements simultaneously, and an estimation method comparing these measurements is adopted, allowing quick detection of even small amounts of uranium. Moreover, NWAS is portable, allowing measurement of dismantled materials at each place in the facility.

NWAS "Ningyo Waste Assay System"

Aomori Research and Development Center

In the Rokkasho area in Aomori Prefecture this March, the Administration & Research Building of the International Fusion Energy Research Center was opened for activities relating to the "Agreement for the Joint Implementation of the Broader Approach (BA) in the Field of Fusion Energy Research" between the government of Japan and the European Atomic Energy Community. The construction of three other buildings for the Center is expected to be completed by the end of next March.

In the Mutsu area of Aomori, a radioactivity database for a clearance evaluation system is being compiled and a practical decommissioning method is being considered for the decommissioning of the nuclear ship "Mutsu" reactor facility. Also, technology for ultra low level measurement of C-14 and I-129 using an accelerator mass spectrometer (AMS) are being developed, and measurements are being done.

Photograph of the participants in the opening ceremony for the Administration & Research Building of the International Fusion Energy Research Center. (30th March, 2009)

14-1 Remote Nondestructive Examination of Steam Generator (SG) Heat Transfer Tubes

— SG Heat Transfer Tubes Integrity Confirmation by Eddy Current Test, Visualization and Gas Leak Tests —

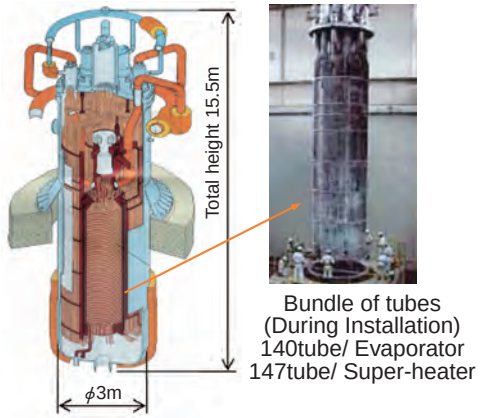

Fig.14-1 Steam Generator (Evaporator)

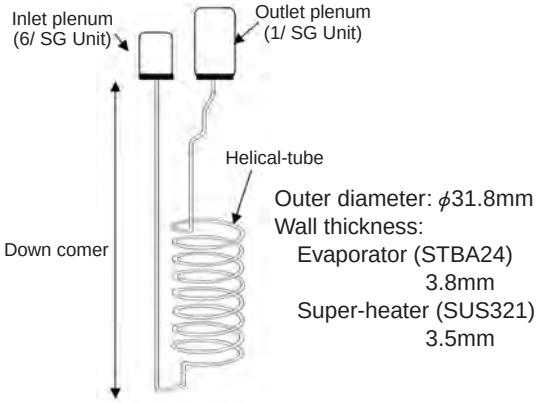

Fig.14-2 Steam Generator Tube (1 Tube)

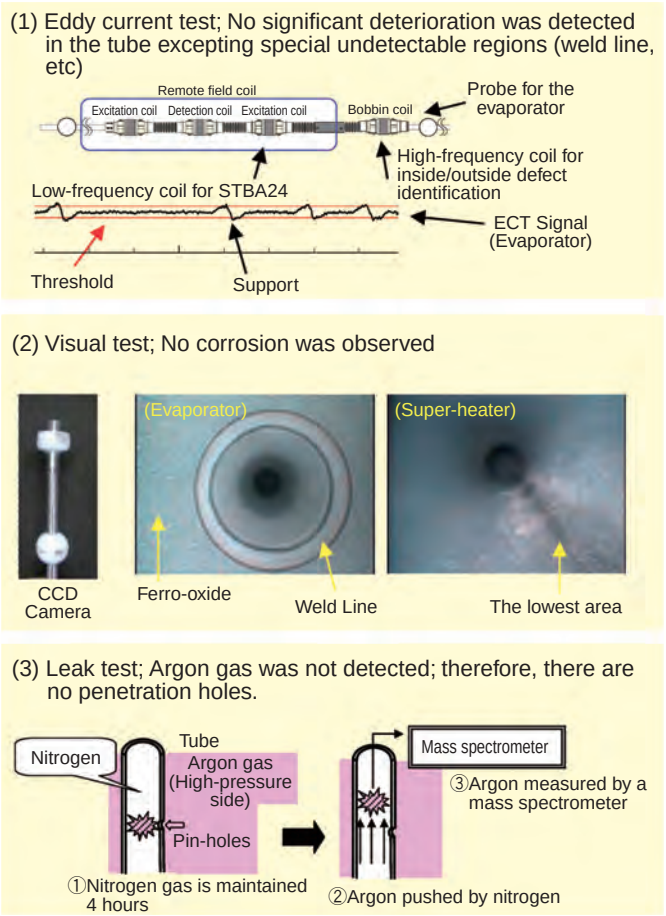

Fig.14-3 Three types of tests

The confirmation of "MONJU" system and its component integrity in preparation for the restart of "MONJU" was planned and started in 2006. Confirmation of the steam generator heat transfer tube integrity using remote nondestructive examination equipment was carried out from November 2007 to March 2008. The steam generators consist of 3 evaporators and 3 super-heaters. The evaporator is shown in Fig.14-1 while Fig.14-2 presents the heat transfer tube specifications.

The outer surface of the heat transfer tube is surrounded by a sodium inert argon gas environment. It was confirmed that corrosion of tube material in sodium and argon gas is almost negligible. However, there is water/steam inside the tube during operation, therefore to confirm both corrosion and wall thinning were carried out an eddy current test (ECT), a visual test (VT), and a leak test, as shown in Fig.14-3.

The ECT detection performance was improved using exciting frequencies optimized for evaporator and super-heater tubes using a technique based on improvements made in noise reduction tests. Also, the correlation between ECT signal and tube thickness was checked by using test pieces. By comparing test results with records of the inspection at the time of manufacture, it was confirmed that no wall thinning occurred since the last inspection.

The visual test using CCD camera was improved by increasing the camera resolution, by a better lighting, and by enhancing its insertion-ability. The CCD camera fixed speed insertion mechanism was newly developed to obtain accurate sensor location. The heat transfer tube down-comer area including welds was inspected as a typical heat transfer tube because its environment is the same as the other steam generator area. This test confirmed that there was no significant corrosion or defect.

In the leak test, the argon gas concentration in a heat transfer tube was measured by a mass spectrometer. Argon gas was not detected, showing that there were no penetration holes.

In these three tests, no significant deterioration of SG heat transfer tubes were observed, and the integrity of tubes were confirmed, taking us a step closer to restart of "MONJU".

Reference

Takahashi, K., Shiina, A. et al., Inspection of the Steam Generator Heat Transfer Tubes for FBR MONJU Restart, Proceedings of 17th International Conference on Nuclear Engineering (ICONE 17), Brussels, Belgium, 2009, ICONE17-75904, 9p., in CD-ROM.

14-2 High Precision Calibration of Neutron Detectors in keV Region

— Development of keV Region Mono-Energetic Neutron Calibration Fields Using an Accelerator —

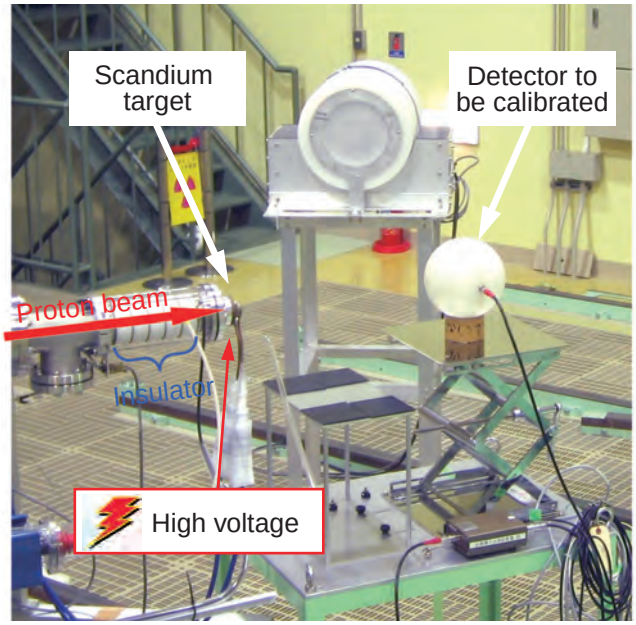

Fig.14-4 Setup in the mono-energetic neutron calibration fields
The 8keV and 27keV mono-energetic neutron calibration fields have been developed using an accelerator. Fine-tune control of the incident proton energy is achieved by a target voltage control system which can supply high voltage between 0kV and +50kV to the scandium target.

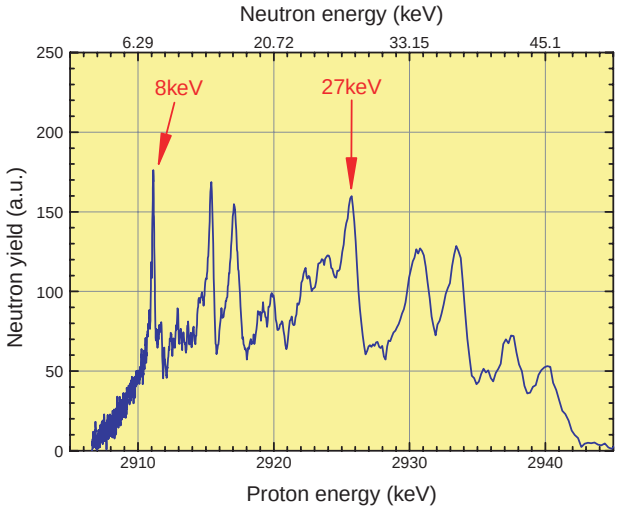

Fig.14-5 Relative neutron yield generated by the ^{45}Sc(p,n)^{45}Ti reaction as a function of the incident proton energy
The neutron yield strongly depends on the incident proton energy due to the ^{45}Sc nucleus structure. Therefore, it is necessary to fine-tune the incident proton energy to a resonance peak at which 8keV or 27keV neutrons are generated.

Neutron dosimetry is distinctive in that its measurement energy range is very wide, from thermal to a few tens of MeV neutrons. As the sensitivity of conventional neutron detectors largely depends on incident neutron energy, it is necessary to measure this energy dependency precisely using mono-energetic neutrons. Therefore, we are developing mono-energetic neutron calibration fields in the energy region from a few keV to 20MeV. There were no facilities in Japan which could measure the dependence of sensitivity on energy in the keV region, where the sensitivity of detectors varies greatly, so we developed the 8 and 27keV mono-energetic neutron calibration fields as shown in Fig.14-4. These fields are formed by bombarding a scandium target with a proton beam, causing a ^{45}Sc(p,n)^{45}Ti nuclear reaction, which has a resonance structure. Then the mono-energetic neutrons produced by this reaction are used for the calibration of the detectors.

Fig.14-5 shows the relationship of relative neutron yield and the incident proton energy. The 8keV and 27keV neutrons are generated by precisely adjusting the proton energy to correspond to one of the resonance peaks in Fig.14-5. Even if the incident proton energy diverges by only 1keV from 2911keV peak, the 8keV neutrons are not generated. The proton energy must be adjusted within an accuracy of 1keV, but such fine-tuning by controlling the acceleration voltage of the accelerator is difficult. Thus, we developed a target voltage control system which can quickly adjust the proton energy to a resonance peak by applying voltage to the target as seen in Fig.14-4. The magnitude of this voltage can be remotely controlled with a computer in the control room. This system achieves stable and reliable generation of the 8keV and 27keV neutrons.

In this way, fields of 8keV and 27keV mono-energetic neutrons making possible the finest calibration in the world have been developed. These fields will make calibration of neutron detectors in the keV region possible.

Reference

Tanimura, Y. et al., Construction of Monoenergetic Neutron Calibration Fields Using ^{45}Sc(p,n)^{45}Ti Reaction at JAEA, Radiation Protection Dosimetry, vol.126, 2007, p.8-12.

14-3 New Reprocessing Method without Organic Reagent
—Development of Uranium-Plutonium Cocrystallization Process—

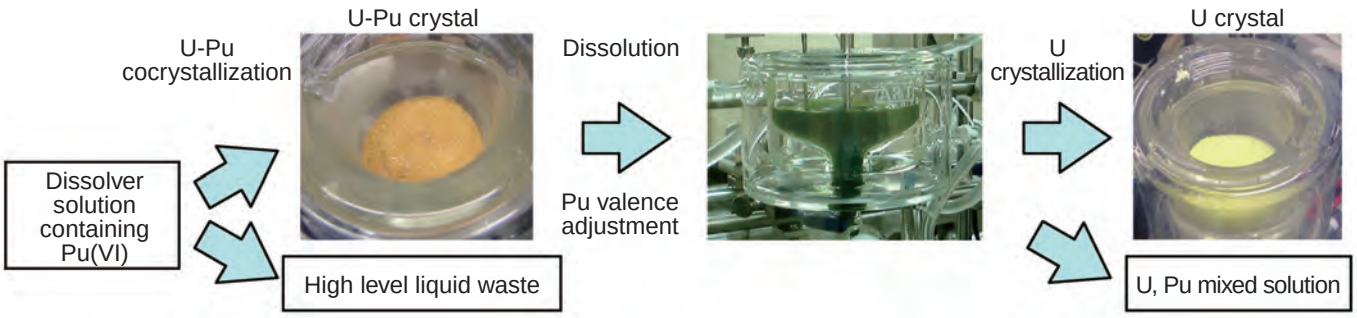

Fig.14-6 Steps in U-Pu cocrystallization reprocessing
The spent fuel dissolver solution is heated for Pu oxidation, and cooled for U-Pu cocrystallization. The U-Pu crystal (the color is orange) and mother liquor are separated by filtration. The crystal is dissolved in nitric acid solution, and Pu in the solution is reduced to Pu(IV). The solution is cooled again, resulting in U crystal (the color is yellow) and U-Pu mixed solution.

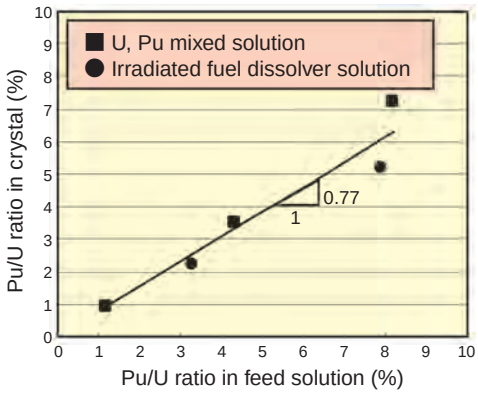

Fig.14-7 Comparison between Pu/U ratio in feed solution and Pu/U ratio in crystal
A good correlation with a linear coefficient of 0.77 is obtained. This means that the yields of Pu were lower than those of U.

Crystallization is considered to be one of the most promising methods for recovering uranium (U) and/or plutonium (Pu) in next-generation reprocessing. The principle of this method is based on the different temperature dependency of U and Pu solubility, which means no special reagent or extractant is required. Using U and Pu mixed solutions obtained by dissolution of irradiated fuel from the experimental fast reactor "JOYO" or unirradiated MOX (mixed oxide of U and Pu), fundamental experiments have been conducted in the hot laboratory named CPF (Chemical Processing Facility).

Through experiments, it has been revealed that hexavalent Pu (Pu(VI)) was co-crystallized with U even though Pu concentration was below its solubility limit. Taking advantage of this phenomenon, an innovative reprocessing process relying on crystallization alone was created (Fig.14-6), which features are;

- Pure Pu cannot be recovered.
- U/Pu ratio in the U, Pu mixed product is controllable by means of only U recovery posterior to the co-crystallization.
- Organic reagents are not used

The mechanism of U/Pu co-crystallization is considered to be similar to co-precipitation where the target element reacts with a carrier compound and a reagent additive. Usually, the carrier has a crystalline structure similar to that of the target element. The nitrate hexahydrates of U and Pu have the same type of crystal structure.

In the U-Pu co-crystallization, Pu is the target element and U acts as the carrier. U crystal is produced by temperature dropping instead of reagent addition, and Pu precipitates together with it. Conducting experiments using solutions with several kinds of U/Pu ratio, it has been confirmed that the U and Pu were co-crystallized under any conditions. It has also become clear that the U/Pu ratio in the crystal is lower than that of the feed solution (Fig.14-7).

In order to commercialize this system, methods for improvement of U/Pu co-crystallization yield and purification of resulting U and Pu must be developed.

This work was financed by the Ministry of Economy Trade and Industry of Japan (METI).

Reference

Shibata, A. et al., Experimental Study on U-Pu Cocrystallization Reprocessing Process, Journal of Nuclear Science and Technology, vol.46, no.2, 2009, p.204-209.

14-4 For Reliability Improvement of LWR-MOX Fuels
—Database of MOX Fuels Irradiated in "FUGEN" and "Halden"—

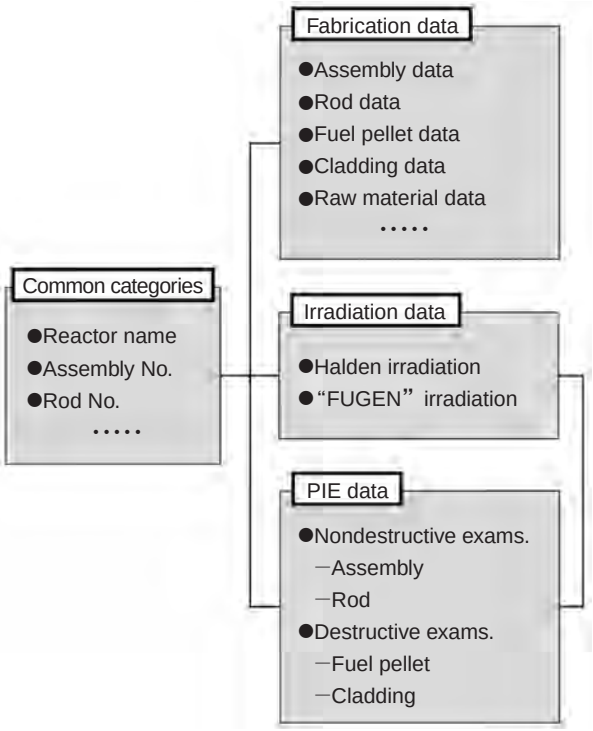

Fig.14-8 Outline of MOX fuel database
Database consists of fabrication, irradiation, and post-irradiation examination (PIE) data of mixed uranium-plutonium oxide fuels irradiated in "FUGEN" and "Halden", systematically arranged.

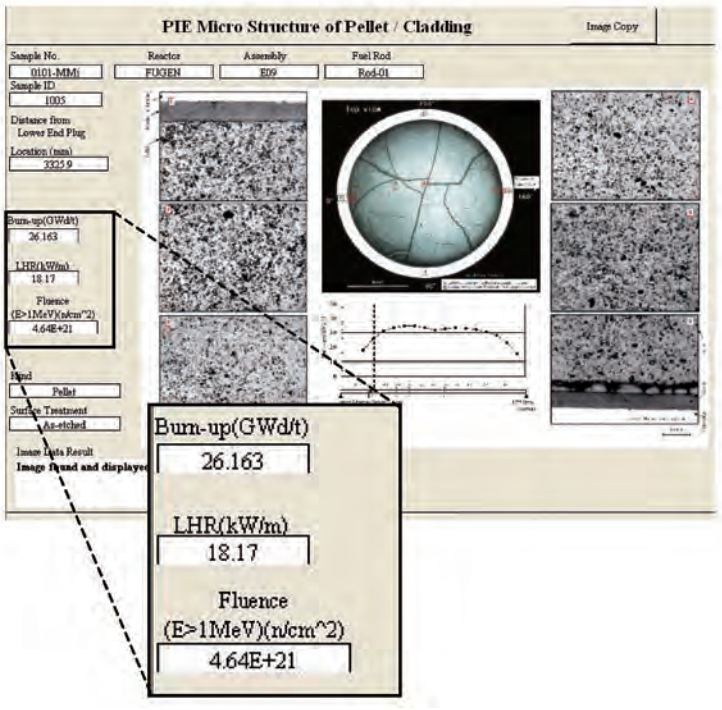

Fig.14-9 Display image of PIE data
Local irradiation conditions are displayed in the page along with transverse cross-section metallography of an irradiated fuel pellet.

For the effective utilization of energy resources, preparations are underway to recycle plutonium separated by reprocessing the spent fuels from nuclear power plants into nuclear fuels for Light Water Reactors (LWRs). In this nuclear fuel cycle, plutonium is reused as mixed uranium-plutonium oxide (MOX). In Japan, a total of 772 MOX fuel assemblies were used in "FUGEN" without any failure until the end of its operation in March, 2003, the most MOX fuel usage by a thermal reactor in the world.

We developed a MOX fuel database (Fig.14-8) to make the most of our experiences with "FUGEN" in helping improve the reliability of future MOX fuel use in LWRs. This database includes the data from not only MOX fuel assemblies irradiated in "FUGEN" but also Norway's "Halden" reactor test data of MOX fuel assemblies whose fuel center temperature, cladding elongation, rod inner pressure etc. during irradiation were measured by in-pile instruments (Fig.14-9). The post-irradiation examinations necessary to evaluate MOX fuel performance were carried out on the MOX fuel assemblies irradiated in "FUGEN", whose Pu content was ~6wt.% and whose pellet peak burn-up reached ~50GWd/t. Consequently, we were able to obtain data helpful in evaluating the irradiation behavior of MOX fuels. In the regular operation irradiation tests in "Halden", the pellet peak burn-up of MOX fuel rods reached ~60GWd/t, and MOX fuel rods used for the power ramp test in "Halden" were irradiated to the maximum linear power (~70kW/m), which was ~10kW/m higher than that of UO_2 fuel rods, without failure. In addition, as the result of the load-follow test in "Halden", we confirmed that the power changes due to load following during reactor operation had no influence on the integrity of MOX fuel rods.

In the MOX fuel database development, we systematically arranged fabrication, irradiation, and post-irradiation examination data which were obtained from several irradiation tests performed in "FUGEN" and "Halden", and organized irradiation data such as power output history to facilitate input of data for fuel behavior evaluation with computation codes.

These MOX fuel data are also included in the IFPE (International Fuel Performance Experiments) database in OECD/NEA, and are appreciated throughout the world. In Japan as well, we expect this data to contribute to improving the reliability of MOX fuel use in LWR in the future.

Reference

Ikusawa, Y., Ozawa, T., Development of MOX Fuel Database, JAEA-Technology 2007-010, 2007, 44p.

14-5 Toward a Higher Field Gradient
—Development of Magnetic Alloy Core for the RF Cavity of J-PARC RCS—

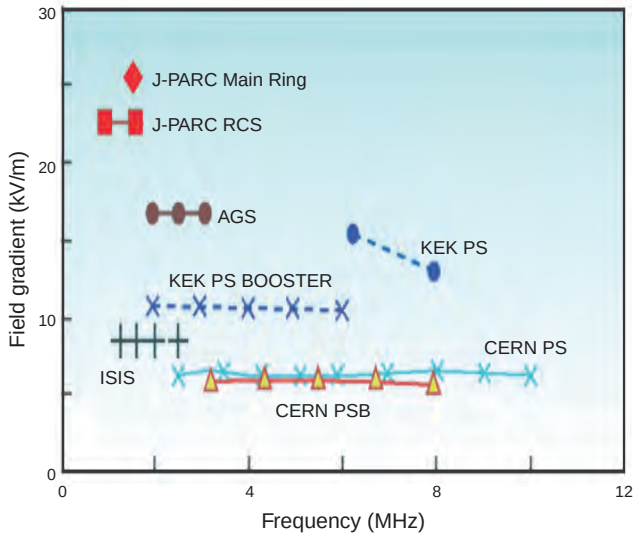

Fig.14-10 Field gradient of major proton synchrotrons in the world
This map shows the operating frequency and field gradient of major proton synchrotrons in the world. Other than J-PARC, these synchrotrons employed conventional ferrite cores and so could not achieve a field gradient higher than 20kV/m.

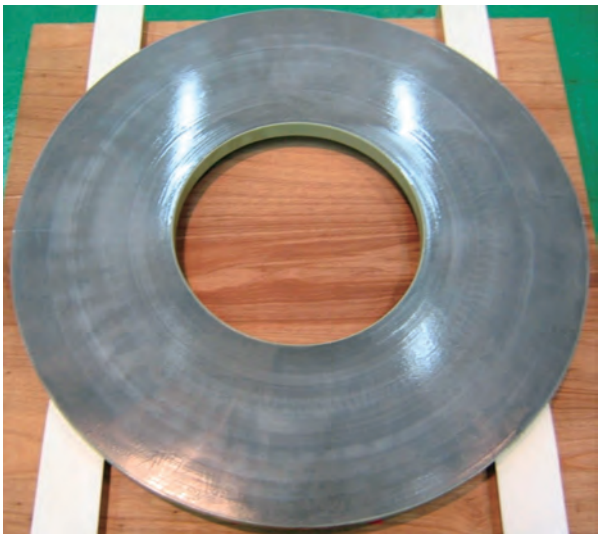

Fig.14-11 Magnetic Alloy core
The Magnetic Alloy core developed for the J-PARC RCS. The inner diameter is 375mm, the outer diameter is 850mm, and the weight is around 100kg. The core surface is covered with epoxy coating.

J-PARC Rapid-Cycling Synchrotron (RCS) is one of the core facilities in J-PARC. In the RCS, a proton beam is accelerated up to 3GeV with high repetition rate of 25Hz. One of the most difficult challenges was how to achieve a field gradient of higher than 20kV/m in order to keep the RCS to a reasonable size. It is impossible to achieve such a high field gradient with conventional ferrite cores because the magnetic flux in the ferrite core reaches saturation level (Fig.14-10). Thanks to high saturation flux density of Magnetic Alloy (MA) cores, the RF cavity loaded with MA cores can generate the required field gradient and has the potential for higher gradients.

The material we chose for the MA core was a ribbon of amorphous metal composed mostly of iron. The MA cores are produced by winding ribbons with a thickness of about 18μm and width of 35mm. A coating of SiO_2 with thickness of 2μm was put on one side of the MA ribbon to create electrical insulation (Fig.14-11).

We employ a direct water-cooling system for the RF cavity, and therefore the core surface was covered with epoxy coating to prevent rusting. The length of the rf cavity is about 2m and 18 MA cores are loaded in it.

In the development of MA core, we improved the core quality on the basis of the results of over 300 hours of high power tests. In the early stage of high power tests, we observed core damage and detachments of the epoxy coating from the core surface. Investigating the circumstances of the core damage, we found that they were caused by poor electrical insulation between ribbons. We improved the electrical insulation by optimizing the tension of the winding process of the ribbons in order to protect the SiO_2 layer. To solve the problem of epoxy coating detachment, we impregnated epoxy resin inside the core, to improve the coating adhesion. In high power tests using these improved cores, we observed no core damage and no detachments of epoxy coating. Finally, we achieved the field gradient of 23kV/m, which was higher than our development target of 20kV/m.

We installed 10 RF cavities loaded with MA cores in the RCS in May 2007 and started beam commissioning in October 2007.

Reference

Nomura, M. et al., Development of MA Core for J-PARC Ring RF Cavity, Proceedings of the 5th Annual Meeting of Particle Accelerator Society of Japan and 33rd Linear Accelerator Meeting in Japan, Higashihiroshima, Japan, 2008, p.246-248, in CD-ROM.

14-6 Toward a Breakthrough in Hydrogen Storage Technology for a Hydrogen Society
—Construction of Pulsed Neutron Total Diffractometer for Hydrogen Storage Materials—

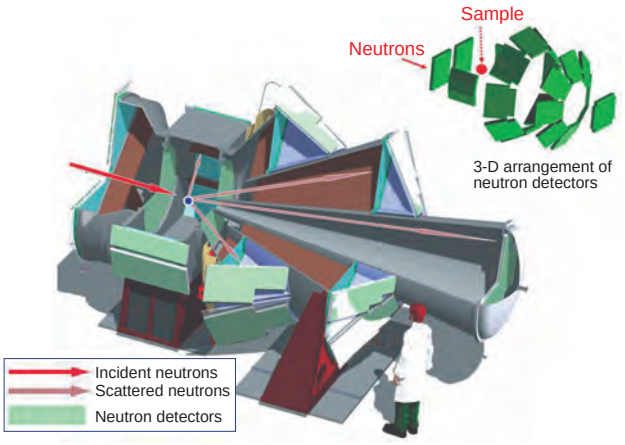

Fig.14-12 Bird's eye view of the high-intensity pulsed neutron total diffractometer (NOVA)

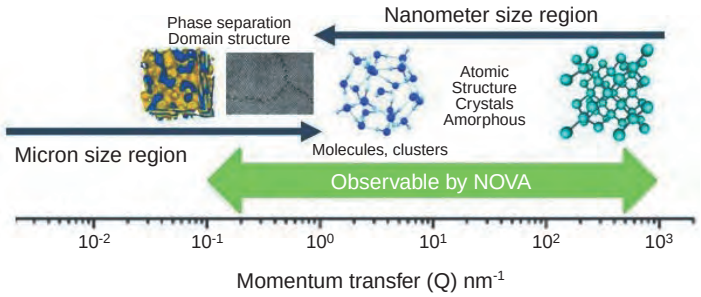

Fig.14-13 Momentum transfer (Q) range observed by NOVA

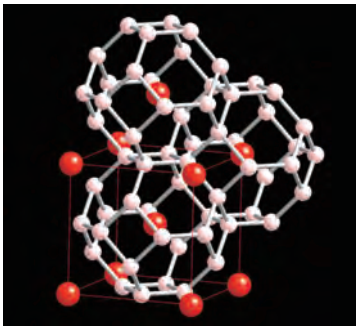

Fig.14-14 Positions of vacancies (white balls) where hydrogen can enter in a body-centered cubic lattice (red balls)

Table 14-1 Basic specifications of NOVA

Momentum transfer (Q)	0.1nm^{-1}～1000nm^{-1}
Neutron wavelength (λ)	0.012nm～0.83nm
Scattering angle (2θ)	0.8°～165°
Neutron detection area	14m^2

It is difficult to investigate the structure of the hydrogen storage materials by X-ray diffraction and other methods because hydrogen is the lightest element and because of the disordered structure of hydrogen storage materials. To analyze such a disordered structure with high accuracy, a high-intensity pulsed neutron total diffractometer (called "NOVA", Fig.14-12) was constructed at J-PARC. Hydrogen is expected to be a next-generation source of clean energy. A great increase in the capacity of the hydrogen storage materials, in which hydrogen is accumulated, is essential to achieve a hydrogen society. To enlarge this capacity, it is necessary to understand the positions of hydrogen atoms and the structural paths of hydrogen entry/discharge in the storage materials accurately within a large-scale observation range from nanometer to submicron (Fig.14-13). NOVA has a large-area (14m^2) neutron detection system (Fig.14-12, inset) at the world's highest intensity neutron source in the J-PARC Material and Life Science Facility (MLF), which makes difficult observations possible. The world's highest specifications of NOVA are listed in Table 14-1.

Typical hydrogen storage materials include hydrogen storage metals such as vanadium and niobium, which have body center cubic (bcc) lattices making free internal vacancies as shown in Fig.14-14. Not all these vacancies, however, can be occupied by hydrogen atoms at one time. There must be a mechanism (structural reason) which suppresses the proportion of vacancies occupied by hydrogen atoms in the materials. We can observe the hydrogen-hydrogen correlations (not only lattice of metal atoms) directly using NOVA. The structural factors that control the amount of hydrogen that can be absorbed are expected to be revealed by this direct observation of the structural order/disorder that hydrogen atoms form.

The construction of NOVA has been supported by new technologies developed at J-PARC for data integration, electronics, detectors, choppers and radiation shielding.

The present study was conducted under the "Advanced Fundamental Research Project on Hydrogen Storage Materials (FY2007-2011)" commissioned by the New Energy and Industrial Technology Development Organization (NEDO).

Reference

Otomo, T., Suzuya, K., Overview of the High-Intensity Total Diffractmeter at J-PARC and Structural Study of Hydrogen Absorbing Materials, Nippon Kessho Gakkai-Shi, vol.50, no.1, 2008, p.29-34 (in Japanese).

14-7 Detecting Small Amount of Sodium Less than Salinity in Atmosphere
—Sodium Leak Detector Using Laser Resonance Ionization Mass Spectrometry—

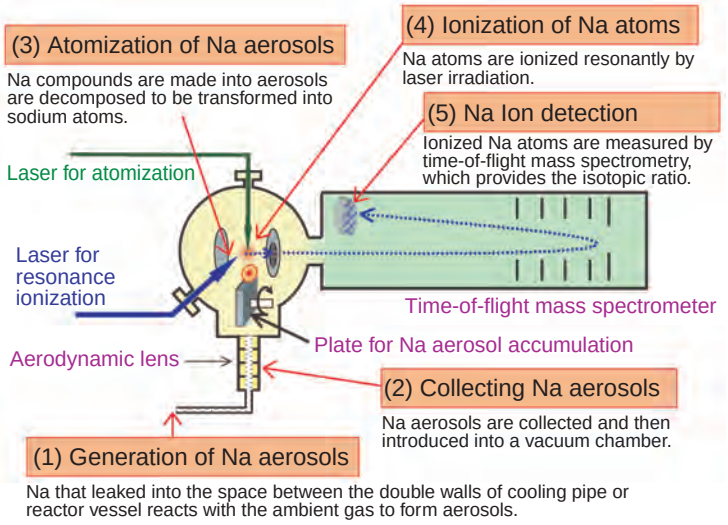

Fig.14-15 Conceptual Diagram of Fast Reactor Sodium Leak Detection System Using RIMS
Sodium aerosols are collected, atomized and detected by means of mass spectrometry using RIMS.

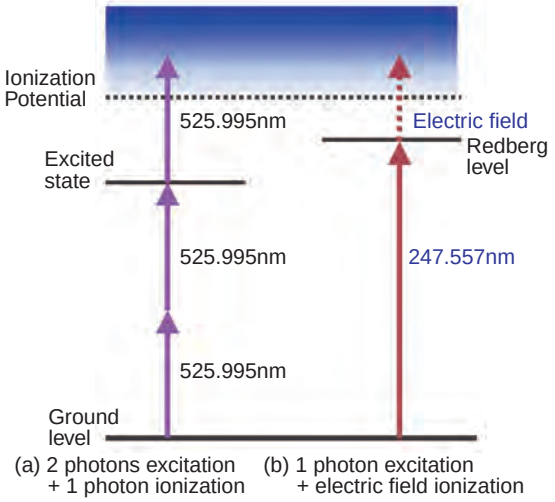

Fig.14-16 Resonance Ionization Scheme of Sodium
Scheme (a) comprises excitation by two photons (wave length: 525.995nm) and ionization by one more photon. Scheme (b) comprises excitation to Rydberg level by a single photon (wave length: 247.557nm) and ionization by an external electric field. We have selected Scheme (b) because our experiments have shown that the ionization rate of scheme (b) is 10 times larger than Scheme (a).

In a sodium-cooled fast reactor, small sodium leaks must be detected quickly, which requires a highly sensitive detector. Conventional sodium detectors have difficulty in detecting ultra-small sodium leakage, because of salinity in the atmosphere. To overcome this problem, we are developing a technology for high sensitivity isotopic analysis of sodium leaking from the primary coolant system, using laser resonance ionization mass spectrometry (RIMS).

We planned to develop this technology by investigating the detection process of the sodium aerosol by the RIMS, optimizing experimental equipment for sodium detection, and evaluating the sodium detection capability of this equipment by performance tests using radioactive sodium. Fig.14-15 outlines our conceptual process for sodium leak detection, which consists of five sub processes (1) ~ (5).

Promising methods for each of these sub-processes from the sodium aerosol sampling to the detection of ions have been selected. The selections include a sampling method using an aerodynamic lens, an atomization method using laser ablation, and an ionization method combining single step excitation by an ultraviolet laser beam and pulsed electric field ionization, shown in Fig.14-16.

In the next step, all aspects of this system will be optimized and then a prototype sodium detection system will be designed and manufactured. With this system, we will measure sodium aerosols using a radioactive test sample from the primary cooling system of Joyo to test detection accuracy. The sodium leak detection system in this study will improve the safety of fast reactors and thus contribute to realization of the fast reactor fuel cycle.

Present study is the result of "the study of highly sensitivity technique for sodium leak detection using laser resonance ionization mass spectrometry to improve fast reactor plant safety" entrusted to the Japan Atomic Energy Agency by the Ministry of Education, Culture, Sports, Science and Technology of Japan (MEXT).

Reference

Aoyama, T., Ito, C. et al., Development of Sodium Leak Detection Technology Using Laser Resonance Ionization Mass Spectrometry, Journal of Nuclear Science and Technology, suppl.6, 2008, p.43-50.

14-8 Innovative Method to Produce ^{99}Mo for Medical Diagnosis without Uranium
—Development of ^{99}Mo Production Technique with Molybdate Solution—

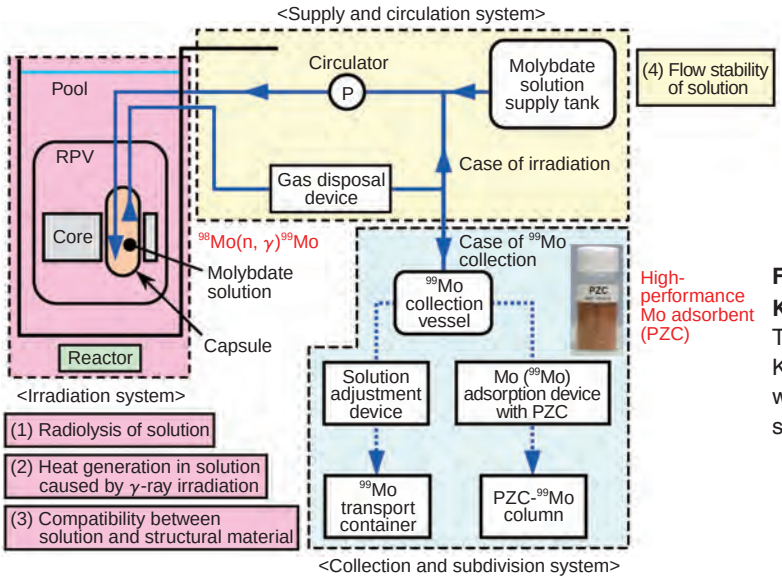

Fig.14-17 Outline of systems for ^{99}Mo production by solution irradiation method, and evaluation items
In the irradiation system, a molybdate solution in a capsule installed in a reactor core is irradiated with neutrons, and ^{99}Mo is generated. In the supply and circulation system, this solution is supplied to the capsule, and then circulated back. In the collection and subdivision system, the solution including generated ^{99}Mo is collected from the capsule, and this solution is purified and put into transport vessels. (1) to (4) are evaluation items for two of these systems.

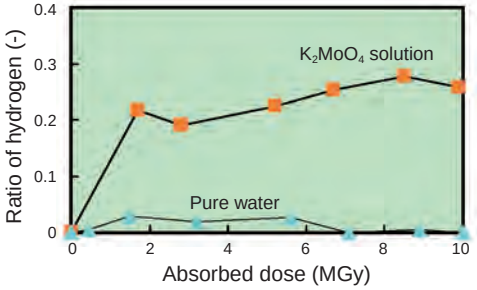

Fig.14-18 Relationship between absorbed dose of K_2MoO_4 solution and ratio of hydrogen in generated gas
The ratio of hydrogen in the radiolysis gas generated from K_2MoO_4 solution (concentration: 58wt%, temperature: 80°C) was investigated. As a result, it was found that this solution generates more hydrogen than pure water does.

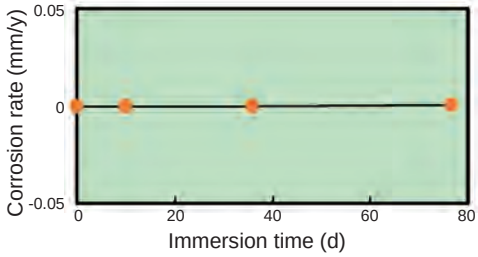

Fig.14-19 Relationship between immersion time and corrosion rate of SS304
SS304 was immersed in a K_2MoO_4 solution (the concentration: 58wt%, the temperature: 80°C), and the compatibility between SS304 and the solution was investigated. As a result, it was found that SS304 has no corrosion after 80 days of immersion.

Technetium-99m (^{99m}Tc) is the most widely used radiopharmaceutical for medical diagnosis. The raw material of ^{99m}Tc is molybdenum-99 (^{99}Mo), and all ^{99}Mo used in Japan is imported from foreign countries. However, a problem has emerged that the supply of ^{99}Mo is unstable due to aging production facilities. Therefore, the stable supply and production of ^{99}Mo is needed in Japan.

^{99}Mo has been produced mainly by the fission method using highly enriched uranium. In Japan, ^{99}Mo production by the fission method is difficult because of nuclear nonproliferation requirements and radioactive waste. Therefore, taking a hint from the shipment form of ^{99}Mo, the solution irradiation method was invented (Fig.14-17). In this method, a solution of molybdate that has high solubility is irradiated with neutrons in a nuclear reactor. ^{99}Mo is thus produced by the ^{98}Mo (n, γ) ^{99}Mo reaction and is collected with the high-performance Mo adsorbent PZC. This method has three advantages: ^{99}Mo production rate can be increased simply by increasing the volume of the irradiation target, the processes required to produce a shipment are simpler, and the amount of radioactive waste is much smaller than that of the fission method.

As the molybdate solution used in the solution irradiation method, potassium molybdate (K_2MoO_4) solution which has a high concentration of molybdenum was selected to increase the ^{99}Mo production rate. For the investigation of its suitability as the irradiation target, γ-ray irradiation tests of the solution were carried out. The test results indicated: (1) the ratio of hydrogen in the gas generated from the solution is 20 times higher than that from pure water (Fig.14-18); however, this is not a serious problem for the gas disposal device installed into the ^{99}Mo production system, (2) the increase in calorific value of the solution upon γ-ray irradiation is about the same as that of pure water, (3) the compatibility (nonreactivity) between the solution and stainless steel material of the capsule is very good (Fig.14-19), (4) the solution flows stably in a pipe 4mm in inner diameter and 30m in length without precipitation.

From the above results, it is clear that the K_2MoO_4 solution is suitable as the irradiation target for the ^{99}Mo production system by the solution irradiation method. In addition, it is evaluated that over 20% of the domestic demand for ^{99}Mo (88.8TBq/week) can be provided by this system using JMTR. Based on this obtained data, plans for the practical application of this system are to be considered.

Reference

Inaba, Y. et al., Development of ^{99}Mo Production Technique by Solution Irradiation Method; Characterization of Aqueous Molybdate Solutions, Nippon Genshiryoku Gakkai Wabun Ronbunshi, vol.8, no.2, 2009, p.142-153 (in Japanese).

14-9 Development of Technology for a Commercial High Temperature Gas-Cooled Reactor —Non-Destructive Inspection Method for Reactor Pressure Vessel—

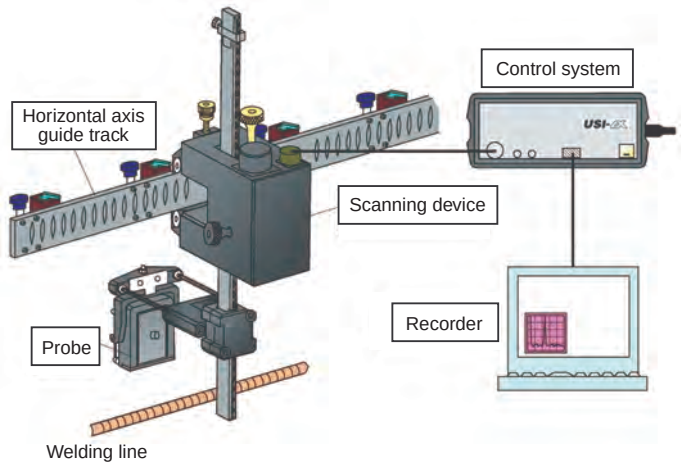

Fig.14-20 Semi-automated ultrasonic inspection system
The semi-automated ultrasonic inspection system is used for a narrow space or a large curved dome space where the automated ultrasonic inspection system cannot reach.

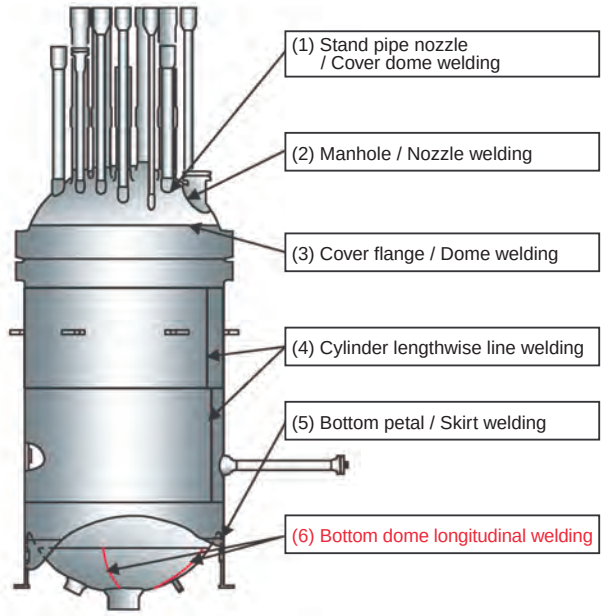

Fig.14-21 Main welding lines of the RPV of HTTR
There are six welding line regions to be given non-destructive inspection. We inspected the sixth welding line region, at the bottom of the RPV in this diagram.

The High Temperature engineering Test Reactor (HTTR) is the first high temperature gas-cooled reactor (HTGR) constructed by JAEA in Japan. HTGR is a high-safety reactor type, that can be designed to prevent severe accidents even if coolant is lost due to destruction of a pressure-bearing part. However, in-service inspections of the reactor pressure vessel (RPV) by non-destructive inspection as thorough as those for LWRs are still indispensable for safe HTGR operation.

So far, we have developed an automated ultrasonic inspection system in corporation with the Japan Atomic Power Company in order to automate the inspection of a reactor pressure vessel for HTGR and to shorten the inspection time. However, it was found that this inspection system cannot inspect the narrow spaces around the stand pipes and the curved area of the cover dome, because giving the system high performance increased its size. Therefore, we developed a semi-automated ultrasonic inspection system that can inspect any space reached by a magnet track attached to the RPV surface, as shown in Fig.14-20. Because the RPV test regulations stipulate that the weld line should be inspected from nine directions: perpendicular to the tangent plane of the weld line and from above, below, right, and left (four directions) with respect to two different weld line incident angles, we improved an ordinary ultrasonic signal processing system to be able to process ultrasonic signals in those nine directions. Besides, we gave a curvature to the magnet track which agrees with that of the RPV to allow access to any space to be inspected.

The RPV of an HTTR reaches much higher temperatures than that of a LWR, and therefore, in our design the maximum allowable working temperature was 440°C. 2.25Cr-1Mo steel, which has enough strength at high temperatures, was used as the material of the RPV. We prepared a test piece made of 2.25Cr-1Mo steel to obtain the distance-related amplitude reduction characteristics necessary for accurate detection of defects. Also, based on our determination of the sonic speed of the 2.25Cr-1Mo steel, we optimized the ultrasonic inspection conditions to allow measurement of defect positions with high accuracy. Moreover, we made a mock-up apparatus outside the reactor, and we improved the efficiency of the inspection by mock-up tests.

We executed a non-destructive inspection of the longitudinal welding lines of the dome at the bottom of the RPV shown in Fig.14-21 using the system resulting from the above R&D. The inspection confirmed that the safety and performance requirements of the RPV were met, because no echo signal which would indicate cracks or defects was detected.

By the development of this semi-automated ultrasonic inspection system, effective ultrasonic inspection of all welding lines of the RPV is possible. Therefore, a non-destructive inspection method for the RPV of the HTGR has been established.

Reference

Nojiri, N. et al., Ultrasonic Test Results for the Reactor Pressure Vessel of the HTTR —Longitudinal Welding Line of Bottom Dome— , JAEA-Technology 2008-045, 2008, 38p. (in Japanese).

14-10 Highly Sensitive Diagnosis of Asbestos Diseases Using Ion Microbeams
—Identification of Asbestos Type in a Lung Tissue Cell—

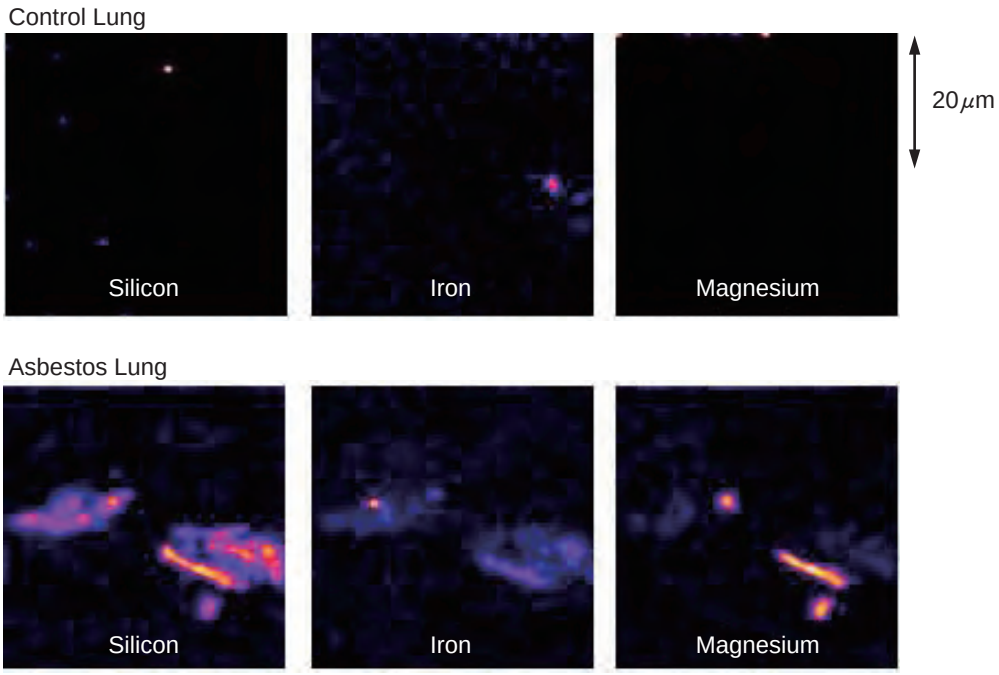

Fig.14-22 Pulmonary tissue taken from lung cancer patients with and w/o asbestos
The control lung has cancer but no asbestos; the asbestos lung has both. In asbestos lung tissue, needle-shaped distributions of silicon, iron and magnesium were clearly imaged.

Asbestos is called a "silent time bomb" because the asbestos-related symptoms appear after scores of years. Therefore, investigations of type, concentration and distribution of asbestos in lungs are very important for early recognition and treatment. However, in the present situation, surgical extraction of about 5g of lung tissue is necessary for diagnosis of asbestos-related lung diseases.

Particle induced X-ray emission (PIXE) is a powerful and nondestructive elemental analysis technique. Bombardment by ions with sufficient energy causes inner shell ionization of target atoms in a specimen. When the outer-shell-electrons drop down to the induced inner-shell vacancies, X-rays with energies unique to each element are emitted. By analyzing the energy spectrum of the X-rays, the elements in the specimen can be identified, and also the absolute concentration and distribution of each element can be measured. This method has about 100 times higher sensitivity than electron microprobe analysis (EPMA), because the electrons in the target atom are more efficiently removed by ions than by electrons. Combining these advantages of PIXE with our extremely thin (dia. less than 1μm) ion beam formation technique, a technique of in-air micro-PIXE analysis has been developed. This method can analyze distribution of about 80 elements from magnesium to uranium in a minute specimen of 100μm or less.

In this study, the position and shape of asbestos fibers in lung tissue were successfully identified through elemental analysis by in-air micro-PIXE. In addition, the type of asbestos was identified from the proportion of the elements (Fig.14-22).

This study was carried out in collaboration with Gunma University as part of its 21st century COE program "Biomedical Research Using Accelerator Technology". These results were published in an international medical journal. After this study, the correlation of the distributions of silicon, a main element of asbestos, and of the protein involved with pulmonary fibrosis was elucidated by means of in-air micro-PIXE combined with immunohistochemical staining.

Reference

Shimizu, Y., Dobashi, K., Kusakabe, T., Nagamine, T., Oikawa, M., Satoh, T. et al., In-Air Micro-Prticle Induced X-ray Emission Analysis of Asbestos and Metals in Lung Tissue, International Journal of Immunopathology and Pharmacology, vol.21, no.3, 2008, p.567-576.

14-11 Construction of Research Tunnels Deep Underground

—Reduction of Water Inflow at the "Mizunami Underground Research Laboratory"—

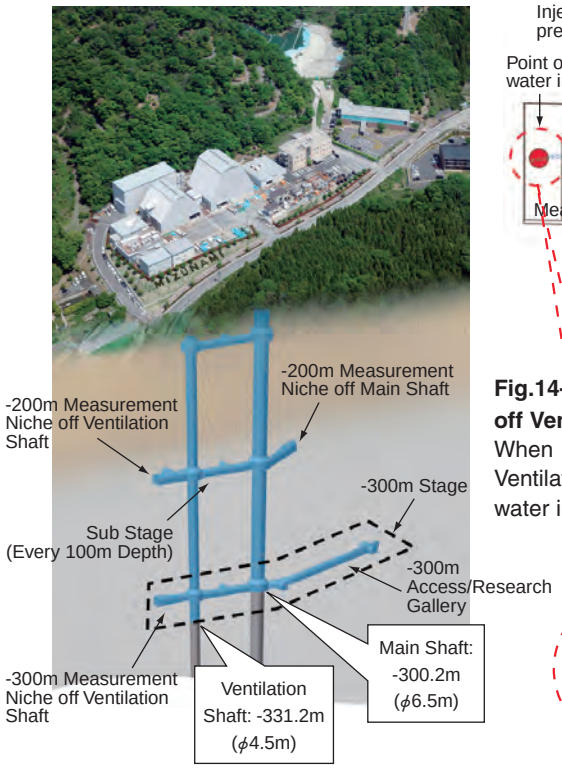

Fig.14-23 Image of the "Mizunami Underground Research Laboratory"
Depth of shafts as of March 31 2009.

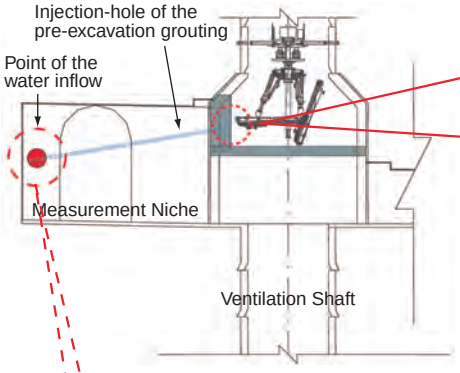

Fig.14-24 GL-200m Measurement Niche off Ventilation Shaft
When an injection-hole was drilled from the Ventilation Shaft, there was the point of the water inflow before the Niche excavation.

Fig.14-25 Water inflow from injection-hole of the pre-excavation grouting
The water inflow rate was about 500 liters per minute.

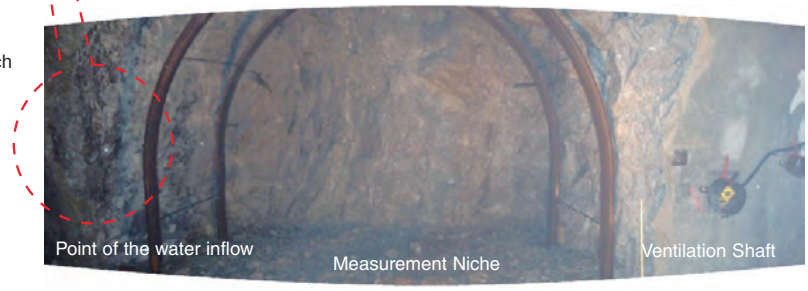

Fig.14-26 Tunnel and wall of GL-200m Measurement Niche off Ventilation Shaft
The water inflow through the grouted rock mass was quite small.

The "Mizunami Underground Research Laboratory", one of the main facilities in Japan for research and development of the technology for high-level radioactive waste disposal, is under construction in Mizunami City. As of March, 2009, the excavation of the Main and Ventilation Shafts had reached GL -300.2m and -331.2m, respectively (Fig.14-23).

In planning the construction, it was necessary to get reliable information on the bedrock conditions, specifically the rock mass stability and hydrogeology. Therefore, borehole investigations were conducted before excavations started. The results indicated that large water inflow could be expected during the excavation around the Ventilation Shaft at GL-200m. In order to mitigate water inflow, pre-excavation grouting was conducted before excavation of shafts and research tunnels. Grouting is the injection of material such as cement into a rock mass to stabilize and seal the rock.

Pre-excavation grouting injection holes were drilled from the Ventilation Shaft at GL-200m. One of these grouting injection holes produced water at an inflow rate of about 500 liters per minute (Figs.14-24 and 14-25). After tunnel excavation, water inflow through the grouted rock mass was reduced considerably. Geological mapping of the tunnel confirmed the successful injection of cement grout into the fractures (Fig.14-26).

In planning the pre-excavation grouting, a target where water inflow must be prevented was established by theoretical analysis to determine rock mass stability and hydrogeological conditions. The pre-excavation grouting was shown to be successful by subsequent excavations of shafts, in which the targeted reduction in water flow was achieved. This is a good indication that the construction of shafts and research tunnels can proceed with water inflow into the facility prevented by pre-excavation grouting.

Reference

Hara, M., Kinoshita, H., Ikeda, K. et al., Pre-Excavation Grouting in Construction of Mizunami Underground Research Laboratory, Japan Society of Civil Engineers, Proceedings of Tunnel Engineering, vol.18, 2008, p.23-30 (in Japanese).

14-12 Establishment of Traceability of Radon Measurements at JAEA

—Standardization of Our Radon Measurement Techniques and Assuring Their Accuracy—

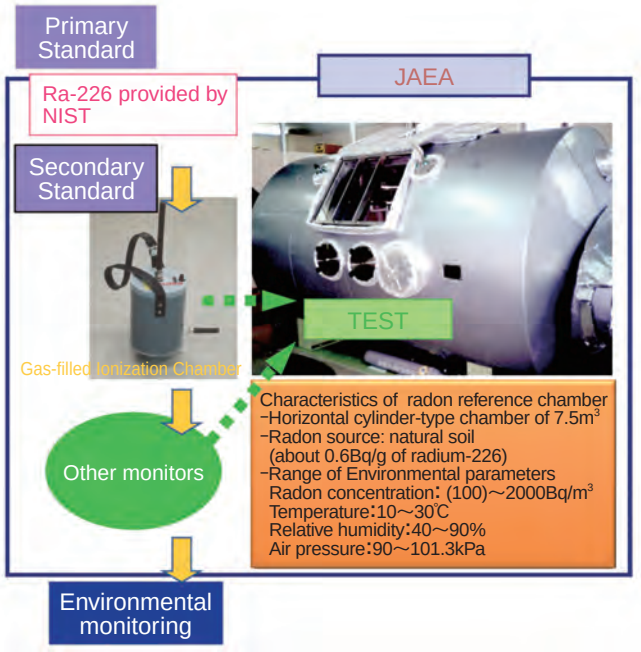

Fig.14-27 Concept of traceability of radon measurements at JAEA Ningyo-toge

Table 14-2 Radon measurement techniques used at JAEA Ningyo-toge

Method	Concentration in Atmosphere	Exhalation rate from Ground Surface	Concentration in Water
Spot measurement	Gas-filled ionization chamber method	Chamber method with a scintillation cell	Direct method with Liquid scintillator
Continuous measurement	Pulse ionization chamber method	Chamber method with a scintillation cell	
Time integrated measurement	Electro static passive method with etched track detector		

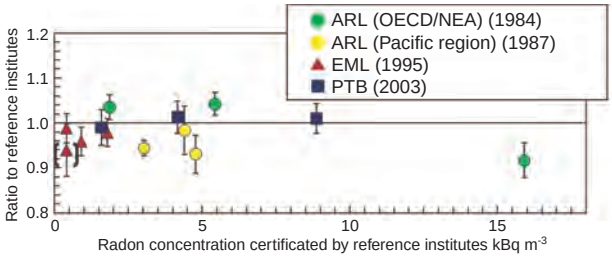

ARL: the Australian Radiation Laboratory
(presently, the Australian Radiation Protection and Nuclear Safety Agency)
EML: the Environmental Measurement Laboratory in the USA
PTB: Physikalisch-Technische Bundesanstalt in Germany

Fig.14-28 Summary of intercomparison experiments among international reference institutes

Closed uranium mine sites are managed at JAEA Ningyo-toge and JAEA Tono. Radon (radon-222), a naturally occurring radioactive noble gas, is the immediate decay product of radium-226, one of progeny nuclides of uranium-238. For environmental assessment of uranium mine sites, radon is one of the most important nuclides to monitor, due to its atmospheric dispersion.

Assurance of the accuracy expected in measurement results is realized by traceability. That is, the monitors should be relating to a national standard or an international standard by an unbroken chain of comparisons. However, there is neither the calibration method established by the Japanese Industrial Standard nor the national reference field. Thus, we are performing radon studies on measurement techniques and their traceability mainly at JAEA Ningyo-toge, to validate reliability and accuracy of measurements objectively.

The concept of the traceability system created at JAEA Ningyo-toge is shown in Fig.14-27. The primary standard is a radium solution provided by the National Institute of Standards and Technology in the US, and the secondary standard is a method utilizing gas-filled ionization chambers calibrated with this solution. Other monitors standardized as shown in Table 14-2 are related to the secondary standard. A radon reference chamber, the main facility for maintenance of traceability, was developed to provide reference atmospheres for testing of instruments, and has been operated since 1992. Major results of evaluation of these activities are as follows.

(1) It was proven theoretically and experimentally that the above method utilizing a gas-filled ionization chamber provides highly accurate and stable measurement of radon in the environment.

(2) Through intercomparison experiments among the international reference institutes, it was confirmed that the reliability and consistency of our measurement techniques has been retained since 1984 (Fig.14-28).

(3) It was objectively demonstrated that the calibration and measurement techniques at the JAEA Ningyo-toge were maintained well by the traceability system which we constructed.

Radon is widely distributed in the environment, even in residences, because radium - 226 is naturally contained in soil and in building materials. Moreover, radon is also important in the issues of naturally occurring radioactive materials and uranium waste disposal. Therefore, radon-related issues are being watched domestically and internationally with keen interest. Our systematic activities and experiences are contributing to Japanese standardization of radon measurements.

Reference

Ishimori, Y., Traceability on Radon Measurements at the JAEA Ningyo-toge, Hoken Butsuri, vol.42, no.3, 2007, p.247-254.

14-13 Search for the Migration of ^{129}I on the Earth
—Estimating Relative Sizes of ^{129}I Original Sources—

Fig.14-29 Accelerator Mass Spectrometer (AMS) at Aomori Research & Development Center
This AMS can measure ^{129}I in environmental samples which could not be measured previously.

Table 14-3 The relative sizes of sources of ^{129}I in seawater
More than 80% of ^{129}I originated from overseas reprocessing plants.

Origin	offshore from Sekine	Toyama Bay
Natural	2.2	1.8
Weapons testing	8.9 - 12.2	9.2 - 13.8
Reprocessing Plants	85.6 - 88.9	84.5 - 89.1
Total	100	100

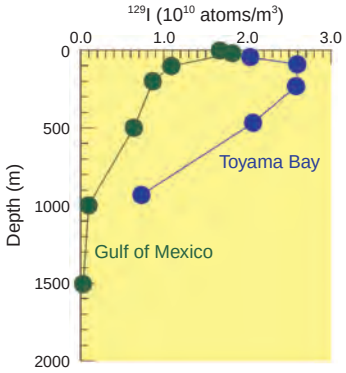

Fig.14-30 The vertical profiles of ^{129}I in seawater
The inventory of ^{129}I in the Japan Sea is three times higher than that of the Gulf of Mexico.

Iodine-129 (^{129}I) is a long-lived radionuclide with a half-life of 15.7 million years which is produced naturally by the interaction of cosmic-rays with xenon and by spontaneous fission of uranium. ^{129}I was released from nuclear weapons testing in the 1950s - 60s and is released from commercial and military nuclear fuel reprocessing plants. Because the amount of ^{129}I released from reprocessing plants is larger than that of other sources, reprocessing plants are point sources in models of iodine circulation on a global scale. The released ^{129}I from reprocessing plants, therefore, proved useful information for general studies of global circulation of substances. On the other hand, there has been no technique to measure ^{129}I in environmental samples with high sensitivity. We thus modified the Accelerator Mass Spectrometer (AMS: Fig.14-29) at the Aomori Research and Development center of the Japan Atomic Energy Agency for ^{129}I measurement, established technology to measure iodine isotopic ratios (^{129}I/^{127}I) with detection limit below 10^{-14}, and applied this technique to seawater samples.

^{129}I/^{127}I in surface seawater was measured offshore from Sekine and in Toyama bay. The ^{129}I/^{127}I ratios were fifty times higher than that of natural level. Because the excess of ^{129}I is due to the released amounts from nuclear weapons testing and reprocessing plants, the ratio of contributions of these sources was estimated. The estimated ratio was natural: nuclear weapons testing: reprocessing plants = 2 : 10 : 88 (Table 14-3). This study shows that more than 80% of the ^{129}I originated from reprocessing plants. Because large reprocessing plants are operated in England, France, and U.S.A., the ^{129}I released from those plants was transported via the atmosphere. Therefore, this study shows that the ^{129}I released from reprocessing plants are transported on a global scale and that iodine diffuses over long distances via atmospheric movement.

Next, the concentration of ^{129}I in seawater was measured vertically at Toyama Bay (Fig.14-30). The inventory of ^{129}I in Toyama bay was three times higher than that in the Gulf of Mexico. The surface seawater in the Japan Sea sinks in the winter, and the Japan Sea is largely enclosed by land; these are likely causes of this higher inventory.

This development of high sensitive ^{129}I measurement technique using AMS at Aomori Research and Development center allowed us to measure ^{129}I in seawater with higher sensitivity than ever before. This technique will be useful not only in obtaining new information about iodine migration but also in oceanographic studies using iodine as a tracer. Moreover, AMS is expected to be increasing useful various other studies in the future.

Reference

Suzuki, T. et al., Measurement of Iodine-129 in Seawater Samples Collected from the Japan Sea Area Using Accelerator Mass Spectrometry: Contribution of Nuclear Fuel Reprocessing Plants, Quaternary Geochronology, vol.3, issue 3, 2008, p.268-275.

About the Design of the Cover :

The cover is designed to envisage a hopeful future shining in the sky which is a clear blue like the color of the JAEA logo. This is accompanied with white colored hexagons similar to the pattern in a tortoise shell which symbolizes the wish of people for longer lives from ancient times in Japan. Coincidentally, this shape is the same as that of the core fuel assemblies for both the prototype "MONJU" Fast Breeder Reactor, and the High Temperature Test Reactor "HTTR".

The picture in the upper left shows 3D image of the computer-based nuclear emergency response system "WSPEEDI-II: Worldwide version of System for Prediction of Environmental Emergency Dose Information 2nd version".

The picture in the lower right shows the facilities of JAEA Horonobe Underground Research Center where we are conducting R&D activities for advanced geological science and geological disposal of high-level radioactive wastes.

R&D Centers of JAEA

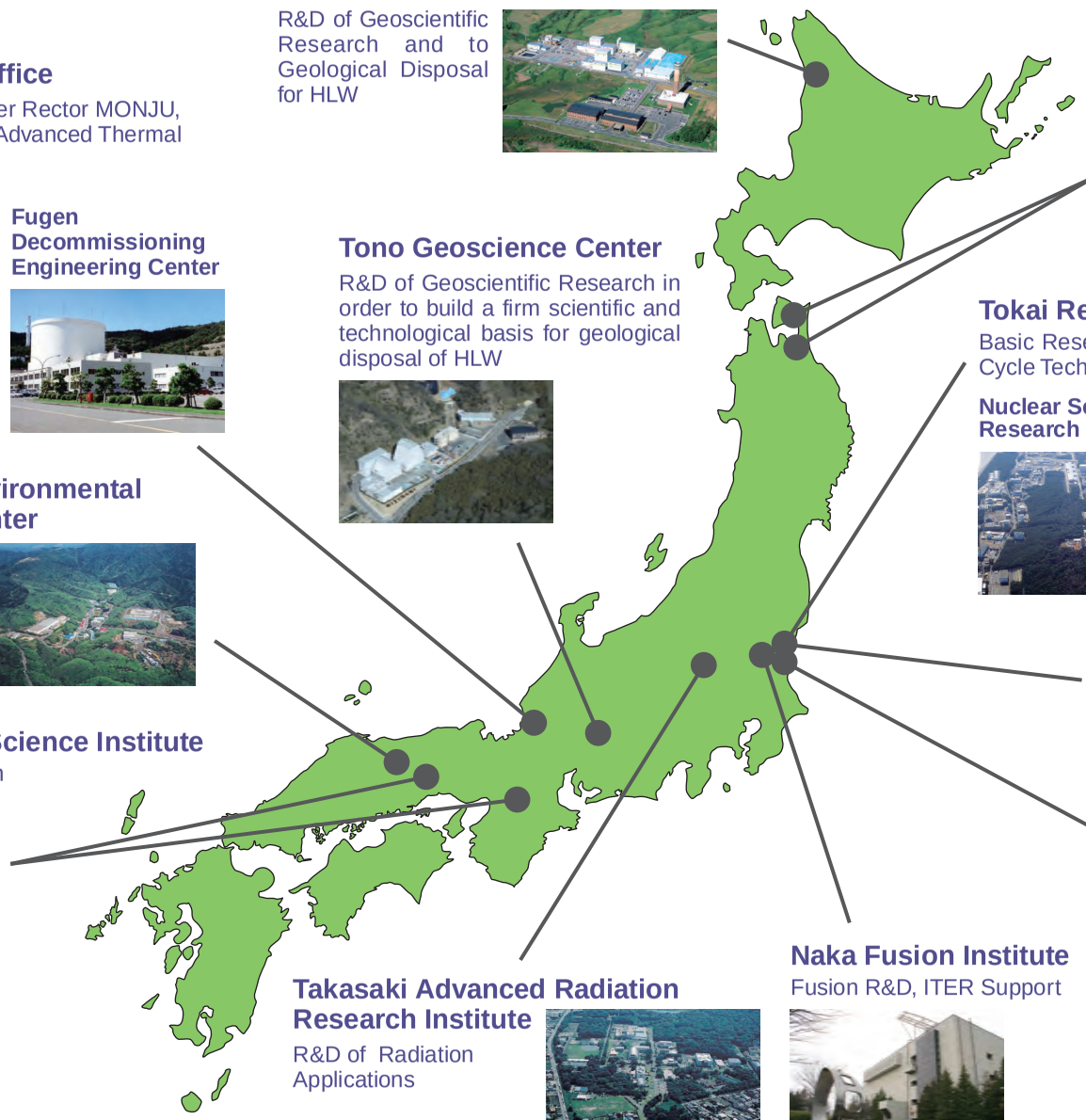

Horonobe Underground Research Center

R&D of Geoscientific Research and to Geological Disposal for HLW

Aomori Research and Development Center

Broader Approach Project, Support for Nuclear Fuel Cycle Business, Decommissioning of Nuclear Ship

Tsuruga Head Office

Prototype Fast Breeder Rector MONJU, Decommissioning of Advanced Thermal Reactor FUGEN

Fast Breeder Reactor Research and Development Center (MONJU)

Fugen Decommissioning Engineering Center

Tono Geoscience Center

R&D of Geoscientific Research in order to build a firm scientific and technological basis for geological disposal of HLW

Tokai Research and Development Center

Basic Research, Safety Studies, Neutron Science, Nuclear Fuel-Cycle Technologies, Rad-Waste Management and Disposal, etc.

Nuclear Science Research Institute

Nuclear Fuel Cycle Engineering Laboratories

Ningyo-toge Environmental Engineering Center

Decommissioning of Uranium Enrichment Plants

J-PARC Center

Japan Proton Accelerators Research Complex, Accelerators and Science

Kansai Photon Science Institute

Photon & Synchrotron Radiation Science

Takasaki Advanced Radiation Research Institute

R&D of Radiation Applications

Naka Fusion Institute

Fusion R&D, ITER Support

Oarai Research and Development Center

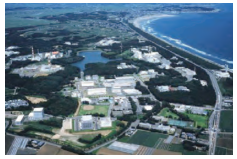

Experimental Reactors; JMTR, JOYO, and HTTR, R&D of FBR Cycle System Technology.
Irradiation Test Technology, High Temperature Gas Reactor and Hydrogen Production Technology

Japan Atomic Energy Agency —Outline of Organization—

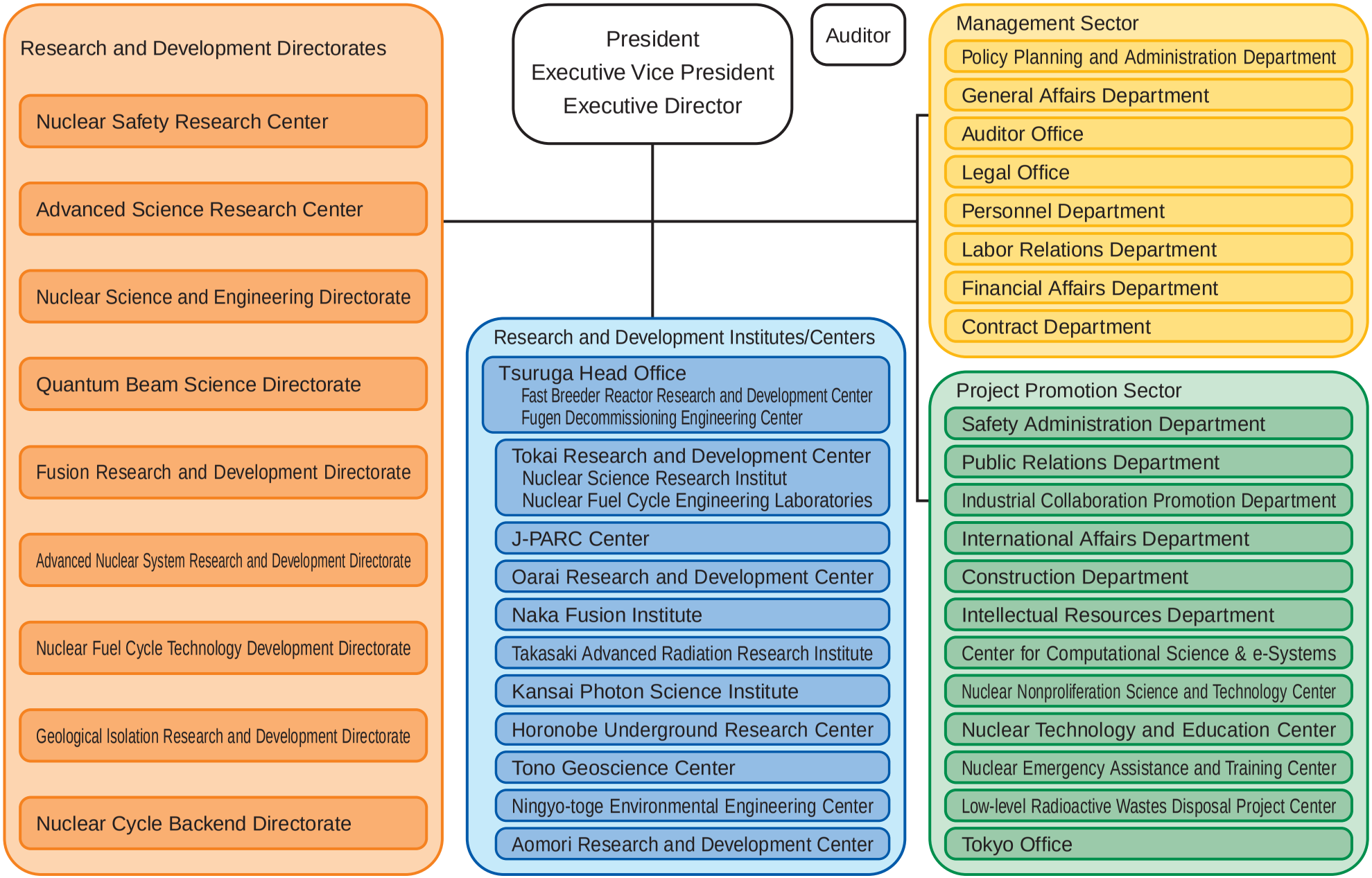

JAEA R&D Review 2009

Published by Japan Atomic Energy Agency (JAEA)
Editorial Office: Intellectual Resources Section, Intellectual Resources Department
2-4 Shirakatashirane, Tokai-mura, Naka-gun, Ibaraki-ken 319-1195, Japan
Phone: +81-29-282-6387 Facsimile: +81-29-282-5920
e-mail: ird-seika_shi@jaea.go.jp

Japan Atomic Energy Agency